Wissenschaftszentrum Weihenstephan für Ernährung, Landnutzung und Umwelt

Modeling and optimal control of enzymatic depolymerization using population balances

Christoph T. Kirse

Vollständiger Abdruck der von der Fakultät Wissenschaftszentrum Weihenstephan für Ernährung, Landnutzung und Umwelt der Technischen Universität München zur Erlangung des akademischen Grades eines Doktor-Ingenieurs genehmigten Dissertation.

Vorsitzender: Prof. Dr. Volker Sieber

Prüfender der Dissertation:

1. Prof. Dr.-Ing. Heiko Briesen

2. Prof. Dr.-Ing. Achim Kienle

3. Prof. Daniele Marchisio

Die Dissertation wurde am 15.02.2017 bei der Technischen Universität München eingereicht und durch die Fakultät Wissenschaftszentrum Weihenstephan für Ernährung, Landnutzung und Umwelt am 30.09.2017 angenommen.

Acknowledgment

First, I want to thank Professor Dr.-Ing. Heiko Briesen for giving me the opportunity to undertake the research that is presented in this dissertation. Also many discussions with him have shown me ways to improve my work. Second, I thank Professor Dr.-Ing. Achim Kienle and Prof. Daniele Marchisio for taking their valuable time to read and grade this dissertation. Furthermore, I want to thank Professor Dr. Volker Sieber for chairing my thesis committee.
I am grateful to Paul Spaunhorst, who has implemented a population balance solver which has served as the basis for the solver used in this dissertation. Furthermore, I thank Simon Weber for the discussions we had during our common stay at the Chair of Process Systems Engineering.
The work undertaken by Martin Obersteiner and Andreas Mayerhofer during their master thesis and by Ljubomir Grozdev during his internship has not been used in this work. However, their effort has given me confidence that the problems tackled by them can be solved. This has given me more time to focus on the work presented here. The work undertaken by Kai Borowiak during his bachelor thesis has sparred me the effort of trying to use the numerical method tested by him. For this I thank all of my students.
I have to thank Elsevier for the kind permission to use text and figures in Chapter 2 from the contribution Kirse and Briesen [1] and in Chapter 1, 2, and 3 from the contribution Kirse and Briesen [2]. I have to thank Springer for the kind permission to use text from the contribution Kirse and Briesen [3] in Chapter 1 and 5. Also all reviewers of these papers and the other papers written during my research leading to this thesis have contributed greatly with their helpful comments. The participants of PBM2013 in Bangalore, ProcessNet 2014 in Aachen, PSE/ESCAPE 2015 in Kopenhagen, and ESCRE 2015 in Fürstenfeldbruck have also improved the quality of this research with their insightful comments in the discussions.
All (not) mentioned (current and former) employees of the Chair of Process Systems Engineering have done their share to create a good working environment and have made me feel welcomed here in Freising. Last but not least I want to thank my family for their continuous support during my graduate work and prior to this.

This research was supported in parts by the German Ministry of Economics and Technology (via AiF) and the FEI (Forschungskreis der Ernährungsindustrie e.V., Bonn) Project AiF 16542 N.

Kurzzusammenfassung

Die modellbasierte Optimierung der enzymatisch katalysierten Depolymerisation von verzweigten Polymeren könnte die Transformation der Ökonomie in die Bioökonomie erleichtern. Um dies zu realisieren, wird ein deterministisches Modell benötigt. Im Rahmen dieser Dissertation wurde ein deterministisches Populationsbilanzmodell entwickelt. Dies ist das erste Modell, das die Denaturierung der Enzyme mittels der „Equilibrium Theory" und die Abhängigkeit der Hydrolyserate von der Anzahl der Monomereinheiten und der Verzweigungsdichte mittels der „Subsite Theory" berücksichtigt. Daher handelt es sich um ein mechanistisches Modell. Weiterhin ist es das erste Populationsbilanzmodell für die enzymatisch katalysierte Depolymerisation von verzweigten Polymeren. Eine erste vorläufige Validierungsstudie hat gezeigt, dass das entwickelte Populationsbilanzmodell sowohl experimentelle Daten als auch mittels einem stochastischen Modell simulierte Daten wiedergeben kann. Allerdings erscheint die für exo-aktive Enzyme vorhergesagte Reaktionsrate falsch zu sein, was darauf hindeutet, dass der Gültigkeitsbereich einer getroffenen Annahme nicht hinreichend groß ist.
Um dieses Modell zu lösen, wurde die „Direct Quadrature Method Of Moments" modifiziert und auf ihre Eignung getestet. Obwohl diese Modifikation die Stabilität und Genauigkeit von der „Direct Quadrature Method Of Moments" erhöht hat, wurde herausgefunden, dass die „Direct Quadrature Method Of Moments" keine geeignete Methode zur Beschreibung von Depolymerization ist, weil die Abweichung zwischen der mit Monte Carlo Technik erzielten Ergebnissen und denen mit der „Direct Quadrature Method Of Moments" erzielten zu groß war.
Deswegen wurde untersucht, ob sich die „Cell Average Technique" und die „Fixed Pivot Technique" als Lösungsverfahren eignen. Es wurde herausgefunden, dass beide Methoden Ergebnisse mit ähnlicher Genauigkeit erzielen, jedoch war die „Fixed Pivot Technique" wesentlich schneller. Die mit der „Fixed Pivot Technique" erzielten Ergebnisse wurden mit Monte Carlo Simulationsergebnissen für die Depolymerisation von einem verzweigten Polymer für eine einfache und eine realistischere Reaktionsrate verglichen. Es wurde herausgefunden, dass für stark verzweigte Polymere die Wirkung von einem zufällig Verzweigungen hydrolyisierenden und einem endo-aktiven Enzym nicht gut beschrieben werden können. Allerdings sind nicht lineare Reaktionsraten unproblematisch.
Die mechanistische Grundlage und deterministische Formulierung haben es ermöglicht, dieses Modell für Optimierung und Optimalsteuerung zu verwenden. Eine Parameterstudie für ein lineares Polymer wurde durchgeführt. Für die untersuchten Parametersätze hatten die Optimierung der Enzymmischungzusammensetzung und -menge wie auch der isothermen Prozesstemperatur die größten

Auswirkungen. Der Prozess konnte weiter verbessert werden, wenn nicht-isotherme Temperaturverläufe verwendet wurden. Es wurde herausgefunden, dass ein vereinfachtes lineares Temperaturprofil schon den größten Teil der Einsparungen realisieren könnte. Der Algorithmus wurde erfolgreich für ein verzweigtes Polymer angewendet.

Abstract

Applying model-based optimization of the enzymatically-catalyzed depolymerization of branched biopolymers would aid the transformation of the economy into the bioeconomy. To perform this, a deterministic model is required. In this dissertation, a deterministic Population Balance Model for the enzymatically catalyzed depolymerization of a branched polymer was developed. This is the first model that accounts for denaturation of enzymes by using the Equilibrium Theory and the amount of monomer units and branching density dependence of the hydrolysis rate by using the Subsite Theory. The model is, therefore, a mechanistic model. Furthermore, it is the first Population Balance Model for the enzymatically catalyzed depolymerization of a branched polymer. A preliminary validation study showed that the developed population balance model could describe experimental data as well as a stochastic literature model. However, the reaction rate predicted for end-chain scission performing enzymes appeared to be wrong which suggests that the region of validity of one taken assumption is not sufficiently large.

In order to solve this model, the Direct Quadrature Method Of Moments was modified and tested as a possible solution technique. While the modification improved the stability and accuracy of the Direct Quadrature Method Of Moments, it was found that the Direct Quadrature Method Of Moment is not a suitable technique to describe depolymerization because the deviation between Monte Carlo technique based solutions and Direct Quadrature Method Of Moment based solution was too large.

Accordingly, the Cell Average Technique and the Fixed Pivot Technique were investigated as possible solution techniques. It was found that both techniques obtained solutions with comparable accuracy, but the Fixed Pivot Technique was significantly faster. The results were compared to Monte Carlo simulation results for depolymerization of a branched polymer described using simple and more realistic reaction rates. It was found that for highly branched polymer the action of a random debranching and an endo-active enzyme together could not be described well. However, non-linear reaction rates did not pose any problem.

The mechanistic foundation and the deterministic formulation allowed using this model for optimization and optimal control. A parameter study for a linear polymer was performed. For the investigated parameter sets, optimization of the enzyme mixture composition and amount as well as the isothermal process temperatures had the greatest effect. The process could be further optimized by applying non-isothermal temperature profiles. It was discovered that a simplified linear temperature profile could already realize most of the savings. The algorithm was successfully applied to a branched polymer.

Contents

Acknowledgment iii

Kurzzusammenfassung iv

Abstract vi

Table of Content x

Notation xi

Acronyms xv

1 Introduction 1

1.1 Motivation . . . 1
1.2 Modeling enzymatic depolymerization . . . 2
1.3 Population Balance Modeling . . . 3
1.3.1 Review of solution techniques for the Population Balance Equation . . . 4
1.3.2 Solving the Population Balance Equation describing depolymerization . . . 7
1.4 Optimal control . . . 9
1.4.1 Review of solution techniques . . . 9
1.4.2 Model-based optimal control of enzymatic depolymerization . . . 11
1.5 Aims and scope . . . 11

2 Modeling enzymatic depolymerization 13

2.1 Starch . . . 13
2.1.1 Structure of starch . . . 15
2.1.2 Initial distribution . . . 15
2.2 Enzymes . . . 16
2.3 Population Balance Equation . . . 17
2.3.1 Assumptions . . . 17
2.3.2 Population Balance Equation for a branched polymer . . . 18
2.3.3 Population Balance Equation for a linear polymer . . . 19

2.4 Production rate . . . 20
2.4.1 Production rate for a linear polymer . . . 20
2.4.2 Production rate for branched polymers . . . 21
2.4.3 Product Distribution Function . . . 22
2.5 Reaction rate . . . 25
2.5.1 Michaelis-Menten kinetics . . . 25
2.5.2 Simplified validation case . . . 26
2.5.3 Equilibrium Model . . . 27
2.6 Subsite Theory . . . 29
2.6.1 Linear polymer . . . 29
2.6.2 Extension to branched polymer . . . 32

3 Solving the Population Balance Equation using the Direct Quadrature Method Of Moments 37
3.1 Direct Quadrature Method Of Moments . . . 37
3.1.1 Monovariate Population Balance Equation . . . 37
3.1.2 Bivariate Population Balance Equation . . . 40
3.2 Direct Quadrature Method of Moment for a divided domain . . . 41
3.2.1 Linear polymer . . . 41
3.2.2 Branched polymer . . . 43
3.3 Numerical implementation . . . 48
3.3.1 Initial moments . . . 48
3.3.2 Initial quadrature . . . 48
3.3.3 Solution of the resulting equations with error handling . . . 49
3.3.4 Validation with Monte Carlo simulations . . . 50
3.4 Results and Discussion . . . 50
3.4.1 Monte Carlo technique . . . 50
3.4.2 Linear polymer . . . 51
3.4.3 Branched polymer . . . 51
3.5 Conclusion and outlook . . . 56

4 Solving the Population Balance Equation using a Method of Classes 59
4.1 Theory . . . 59
4.1.1 Method of Classes for a monovariate Population Balance Equation . . . 59
4.1.2 Fixed Pivot based techniques for a bivariate Population Balance Equation . . . 63
4.2 Extension to a discrete Population Balance Equation . . . 64
4.3 Implementation . . . 65
4.3.1 Meshing . . . 65
4.3.2 Computations prior to the solution of the Ordinary Differential Equations . . . 66

4.3.3 Solving the system of Ordinary Differential Equations . . . 68
4.4 Validation . . . 69
4.4.1 Linear validation case for branched polymer . . . 69
4.4.2 Validation for linear polymer . . . 73
4.4.3 Validation for a branched polymer . . . 74
4.5 Validation of the Population Balance Model . . . 75
4.5.1 Parameters . . . 77
4.5.2 Results . . . 77
4.6 Conclusion and outlook . . . 79

5 Optimal control **83**
5.1 Necessary conditions for optimality . . . 83
5.1.1 Problem statement . . . 83
5.1.2 Derivation . . . 85
5.2 Algorithm . . . 87
5.3 Problem specification . . . 89
5.3.1 Objective function . . . 89
5.3.2 Parameters . . . 91
5.3.3 Numerical parameters and settings . . . 93
5.4 Results and Discussion . . . 93
5.4.1 Isothermal operation . . . 93
5.4.2 Maximizing yield in fixed time with fixed enzyme concentration . . . 94
5.4.3 Minimizing reaction time with a fixed yield and enzyme concentration . . . 94
5.4.4 Trade-off between reaction time and yield with fixed enzyme concentration . . . 96
5.4.5 Trade-off between reaction time and enzyme concentration at a fixed yield . . . 96
5.4.6 Necessity for optimization . . . 99
5.4.7 Effect of using the Product Distribution Function derived by Subsite Theory . . . 99
5.4.8 Effect of branching bonds . . . 99
5.5 Conclusion and outlook . . . 101

6 Conclusion and outlook **103**
6.1 Population Balance Model . . . 103
6.2 Direct Quadrate Method of Moments . . . 104
6.3 Methods of Classes . . . 104
6.4 Optimal control . . . 105
6.5 Application to cellulose . . . 105

Bibliography **107**

A Different formulations of the Population Balance Equation and production rate **131**

A.1 Formulations of the Population Balance Equation . . . 131
A.1.1 Population Balance Equation for a linear polymer . . . 131
A.1.2 Population Balance Equation for a branched polymer . . . 131
A.2 Formulations of the production rate . . . 132
A.2.1 General form for a linear polymer . . . 132
A.2.2 General form for a branched polymer for hydrolysis on linear bonds . . . 132
A.2.3 General form for a branched polymer for hydrolysis on branching bonds . . . 133
A.2.4 Product Distribution Functions for specific mechanism . . . 134

B Closure of the moments **137**
B.1 Subdomain I . . . 137
B.2 Contribution of Subdomain I to Subdomain II . . . 138
B.3 Subdomain II . . . 140
B.4 Contribution of Subdomain I to Subdomain III . . . 140
B.5 Contribution of Subdomain II to Subdomain III . . . 142

C Curriculum Vitae **145**

Notation

Indices

cat	Catalytic
end	End chain
$inact$	Inactivation
$inner$	Inner chain or monomer units
ll	Lower left corner
lr	Lower right corner
m	Mesh point
$\max$	Maximal value
$\min$	Minimal value
ul	Upper right corner
ur	Upper right corner
ECS	End-chain scission
I	Subdomain I
II	Subdomain II
III	Subdomain III
L	Type L element, which is a lower triangle
RCS	Random-chain scission
RDS	Random debranching scission
T	Type T element, which is an upper triangle
0	Initial value
$\sum$	Summation over all enzymes
$\bullet$	Equation is valid for all enzymes

Accents

$\bar{}$	Continuous or belonging to continuous domain
$\breve{}$	Discrete or belonging to discrete domain

$\hat{}$ Mixed continuous-discrete or belonging to a mixed continuous-discrete domain

$\tilde{}$ Normalized or arbitrary fixed

$'$ Summation index or mother particle

$''$ Summation index

$\dot{}$ Derivative with respect to time

$*$ Optimal

Symbols

a	Amount of monomer units released by end-chain scission
b	Amount of branching bonds or inhibition constant
b_I	Inhibition on a newly started side chain due to the branching bond starting the chain
b_{II}	Inhibition on any other branching bond towards the reducing end
b_{III}	Inhibition on any other branching bond towards the non-reducing end
c	Average chain length
d_b	Degree of branching
f	General function or factor or counting variable
f_i	Objective function for initial state
f_f	Objective function for final state
g	Constraint on final state
h	Plank's constant
i	Counting variable or order of the moment
j	Counting variable or order of the moment
k	Amount of monomer units
k_c	Critical amount of monomer units (a numerical parameter)
k	Reaction constant
k_{+1}	Reaction constant of enzyme-substrate complex formation
k_{-1}	Reaction constant of enzyme-substrate complex decay
k_{+3}	Reaction constant of enzyme folding into inactive form
k_{-3}	Reaction constant of enzyme folding into active form
k_B	Boltzmann's constant
l	Counting variable
n	Number density of polymer
n_0	Initial molar concentration of polymer
p	Parameter of negative binominal distribution
r	Parameter of negative binominal distribution
s	Binding mode or if used with index cat specificity
t	Time

t_f	Final time of reaction
u	Control variable
w	Weight
x	Variable
x_j	Mass fraction of the j-th pivot
y	Variable or distance from branching bond
z	Subsite number
z_-	The catalytic site is between subsite $\breve{z}_-$ and $\breve{z}_- + 1$
z_+	Number of subsites above the catalytic center
$\mathbf{A}$	Inversion matrix
B	Production/ birth rate
C	Constant
C_1	Weighting factor for yield in Monetary Units (M.U.)
C_2	Weighting factor for enzyme concentration in M.U.
D	Death/ hydrolysis rate
DE	Dextrose equivalent
E	Enzyme
$E_\bullet$	Total concentration of enzyme
E_{act}	Concentration of active enzyme
E_{den}	Concentration of denaturated enzyme
E_{inact}	Concentration of inactive enzyme
E_l	The l-th element
$\Delta G^\ddagger$	Activation energy
ΔG_a	Acceleration factor
ΔG_{mixing}	Cratic free energy of mixing
H	Heaviside function or Hamiltonian
$\Delta H^\ddagger_{eq}$	Enthalpy difference between active and inactive form of enzyme
$\Delta H^\ddagger_m$	Enthalpy of substrate binding
I	Inverse of Michaelis constant
J	Objective functional and for some cases the profit in Monetary Units (M.U.)
K'	Association constant
K_{eq}	Equilibrium constant
K_m	Michaelis constant
L	Lagrange function
$\mathbf{M}$	Matrix to compute the moments of the production rate from the hydrolysis rate
M_{H_2O}	Molar mass of water
N_{Glu}	Molar mass of anhydro-glucose $C_6H_{10}O_5$
N	Number of quadrature points
$\mathbf{P}$	Matrix to compute the polymer generation at the pivots due to hydrolysis

R	Universal gas constant
S	Substrate
T	Temperature
T_{eq}	Equilibrium temperature
T_{ref}	Reference temperature
α	Moment of production rate
β	Beta function
γ	Product distribution function
Γ	Gamma function
δ	Dirac delta function or Kronecker delta
ε	Small positive quantity
ϕ	Yield in %
ϕ_{des}	Desired yield in %
Φ	Objective function
$\psi_{i,j}$	Contribution due to production in the i-th bin on the j-th pivot
$\psi_{i,l,j}$	Contribution due to the i-th pivot via the l-th bin on the j-th pivot
Ψ	Lagrangian multiplier
σ	Parameter of Schulz-Zimm distribution
Θ	Parameter of Schulz-Zimm distribution
μ	Moment or Lagranian multiplier
ω	Moment of hydrolysis rate

Acronyms

CAT Cell Average Technique 12, 62, 64, 66, 67, 70, 73, 74, 79, 93, 103–105

CM Method of Classes 4, 6–8, 59, 69, 73, 104

DQMOM Direct Quadrature Method of Moments 5, 8, 12, 37, 39, 41, 51, 56, 58, 69, 103, 104, 137

ECS End-chain scission 8, 9, 24, 32, 50, 51, 56, 69, 70, 79, 90, 91, 94, 96, 99, 101, 103–105

FEM Finite Element Method 4

FP Fixed Pivot technique 12, 60–62, 64, 66, 67, 69, 70, 73–75, 79, 81, 88, 103–105

kMC kinetic Monte Carlo 2, 4, 12, 33, 50, 59, 69, 70, 73–75, 77, 79, 81, 88, 103–105

MOM Method Of Moments 4, 5, 8, 37, 42, 58, 59, 104

NDF Number Density Function 4–6, 8, 15, 16, 37–40, 42, 51, 59–63, 65, 69

ODE Ordinary Differential Equation 4, 7–11, 18–20, 38–40, 49, 60, 64, 66, 68, 75, 83, 84, 88, 89, 131

PBE Population Balance Equation 3–8, 10, 11, 17–20, 37, 38, 40–44, 46, 50, 58, 59, 64, 69, 77, 79, 87, 88, 103, 104, 106, 131, 135

PBM Population Balance Model 1, 3, 11, 12, 17, 20, 33, 77, 79, 91, 103, 104

PDE Partial Differential Equation 4, 19, 20, 87, 88, 131, 132

PDF Product Distribution Function 20–25, 31, 64, 73, 79, 91, 93, 99, 103

PSE Process Systems Engineering 1, 2, 11, 13

QMOM Quadrature Method of Moments 4, 5, 37–39, 58

RCS Random-chain scission 8, 23, 24, 50–53, 55, 56, 58, 69, 70, 79, 90, 91, 94, 99, 101, 103, 105, 134

RDS Random-debranching scission 24, 50, 54, 69, 70, 79, 103, 105, 135

Chapter 1

Introduction

This thesis is motivated by the desire to apply Process Systems Engineering (PSE) tools to the saccharification process. After giving a short overview why this process is important, the state of the art in modeling and the use of the PSE tool optimal control for this process is reviewed. Then in Chapter 2 a Population Balance Model (PBM) for the enzymatically catalyzed saccharification is derived. In Chapter 3 and 4 two simulation techniques are applied to this process and evaluated. As an example for a PSE tool optimal control is applied in Chapter 5. In Chapter 6 the results are summed up, conclusions are drawn, and further work to be undertaken is outlined.

1.1 Motivation

Several nations, including Germany, have signed the Paris Agreement [4]. In this agreement, they have expressed their desire to reduce the emission of carbon dioxide. This requires transforming the current oil based economy into a renewable resources based economy, the bioeconomy. In the bioeconomy fuels and chemicals have to be produced using biomass as a feed stock. For ethical reasons usage of this biomass should increase (or at least not decrease) food security world wide, which could be achieved by using a wide variety of different crops for biofuel production [5]. One way of utilizing biomass is to produce chemicals directly by photosynthesis which is used for fine chemicals [6]. Another way is to use vegetable or algal oil or fat as a starting material [6–8]. The last way is to use polymers or oligomers of glucose (e.g. sugar, starch, cellulose, and lignocellulose) as the feed stock [8, 9]. Sugar produced by sugarcane is directly fermented into ethanol and used as fuel in South America [7].
Because the polymers starch and cellulose are present in wide variety of crops and other plants [10, 11], utilization of them would be beneficial for the transformation. However, they need to be broken down either into sugars, which are fermented into more desirable chemicals [9], or by thermal means into syngas, which is used as the feed stock for Fischer-Tropsch synthesis [12]. The conversion into sugars, i.e., saccharification, followed by fermentation is already in industrial use [13]. Currently, the most commonly used method is the enzymatic catalyzed depolymerization into glucose [13]. This process is also quite established as this is one of the steps of brewing beer which has been performed for centuries

[14]. The economic optimization of enzymatically catalyzed depolymerization, e.g. by increasing the yield or reducing the required processing time or enzyme amount, is therefore highly desirable [9].
Accordingly, much research has been undertaken for process optimization, e.g. by improving the pretreatment step [15], combining the saccharification with the fermentation step [16], using an additional acidic catalyst to accelerate the hydrolysis [17], breeding better biomass producing plants [18], and engineering more suitable enzymes [19]. It is well known [16, 20] that the temperature profile has a great influence on process performance.
Optimizing the temperature profile using model-based optimal control is chosen as the most promising method. Other PSE tool such as process design or advanced process control (e.g. model predictive control) can also benefit from the developed model and simulation technique.

1.2 Modeling enzymatic depolymerization

A model suitable for PSE needs to represent reality sufficiently well. With data driven methods [21, 22] experimental data can be represented well. However, extrapolation to parameter combinations not used for parameter estimation might not be possible. Accordingly, in this thesis only mechanistic models are considered.
The simplest model with some mechanistic background describes the polymer as a homogeneous substance with an average amount of monomer units and models the conversion to product by a Michaelis-Menten equation [23, 24]. Several studies have extended this to also tracking the evolution of a few representative degradation products [25, 26]. However, it is well known [26, 27] that naturally occurring polymers are distributed in the amount of monomer units. Experimental results and predictions from theory [28, 29] agree that the reaction rates of enzymes depend on the amount of monomer units of a polymer. Therefore, models that do not include the distributed character of the polymers have a very weak mechanistic basis [30]. It is therefore expected that variations in the amount of monomer distribution of the starting material, e.g. because of seasonal changes or different pretreatment steps, will not be represented well by such models. This might necessitate a seasonal recalibration of the model parameters. Furthermore, studying the influence of the pretreatment step would require a significant experimental effort. Another problem is that the model parameters are measured for temperature profiles that are significantly different from the ones computed by optimal control. It is expected that the parameters of a non-mechanistic model will not describe these different conditions well. Accordingly, simple models might predict the wrong result around the optimal point, which will likely result in the identification of suboptimal process conditions.
To overcome the weak mechanistic basis, models to describe the depolymerization of cellulose [31] and starch [32–34] starting from the subsite theory of enzymes [28] have been proposed. Furthermore, models to take the structure of the substrate into account have been developed [35]. These models are so complicated that they could only be solved using the kinetic Monte Carlo (kMC) technique. However, kMC simulations are unsuitable for optimal control due to their high computational cost and stochastic

nature. Accordingly, detailed structure requiring models are not used in this work and also not further reviewed. Instead the reader is referred to the review of structure based models, non-distributed models, and data driven approaches written by Galanakis et al. [22].
The approach used in this work copes with the complexity of the distributed chain length by formulating a balance equation for each species of polymer. The earliest work found using this approach for enzymatic depolymerization was authored by Chang et al. [36]. Watanabe et al. then modeled the enzymatic depolymerization of xenobiotic polymers using a PBM [37–39]. The first work using this approach in a bioenergy context was undertaken by Hosseini and Shah [40] who modeled the degradation of cellulose by endo-cellulase. This approach was extended by the second paper in this series [41]. Several other works have focused on cellulose [42–47]. All of these approaches consider a linear polymer which is depolymerized at isothermal conditions. Except Hosseini and Shah [40] all authors consider cellulose to be an insoluble polymer which is present in a particulate form. The enzymes bind on the surface and cleave the polymer. In all works (except the one authored by Hosseini and Shah [40]) cellulose is attacked by two enzymes: one exo-active, i.e., only active on the end of the polymer, and one endo-active, i.e. active (not exclusively) on the inner part of the polymer. Besides Lebaz et al. [46] all authors assume the particles to be monodisperse and the polymer to be distributed in the chain length.
Starch is rarely modeled using population balance approaches. Only one other group has published on enzymatic depolymerization of starch using a population balance approach [48, 49]. Their work focuses on the simultaneous fermentation and saccharification. They assumed starch to be linear and soluble. It was attacked by two enzymes at isothermal conditions.

1.3 Population Balance Modeling

PBM as a term was coined by Randolph [50], but the framework was also independently derived by Hulburt and Katz [51]. Parts of the framework can be traced back to at least 1916 [52] (see Sporleder et al. [53] for a more detailed history). In short, PBM introduces further inner coordinates (e.g. chain length for polymers [54] or size and shape for crystals [55]) and formulates a balance equation for the number density for the variable of interest (here polymer amount). The theory is explained with a focus on crystallization but great clarity by Randolph and Larson [56] and with a solid theoretical foundation by Ramkrishna [57]. PBMs are used in a great variety of field (see [58, 59] for good reviews). As most polymers are distributed at least in the amount of monomer units the usage of PBM is well established in polymer modeling [54, 60–62] and even depolymerization modeling [40, 42, 63–68].
Analytic solutions of the Population Balance Equation (PBE) are only possible for some cases, e.g. [57, 69–75]. Accordingly, numerical solution techniques are necessary. A wide variety of solution techniques has been developed in the past. Only some of these techniques have already been applied to depolymerization or breakage PBEs.

1.3.1 Review of solution techniques for the Population Balance Equation

The solution techniques are presented shortly in an arbitrary order in this section.

Kinetic Monte Carlo technique

kMC techniques were developed for particle physics in the 40s [76] and have been used in many fields [77, 78]. kMC techniques are stochastic solution technique. Accordingly, noisy results are obtained. Furthermore, they are often very slow [77]. Combined this makes using them for control and optimization purposes unsuitable.
There are two approaches in using kMC for solving PBEs. The first approach, sometimes called equation free, does not formulate a PBE, but rather simulates the particles directly [33–35, 79]. This allows access to detailed information, such as molecular structure [33], but also is quite time consuming. The second approach brought to sophistication by Smith and Matsoukas [80] and Lin et al. [81] evolves a selected set of particles according to the underlying kinetics, which is described using a PBE.

Method of Weighted Residuals

The Method of Weighted Residuals is a family of solution techniques and is used for solving Partial Differential Equations (PDEs) in general. For example the popular software COMSOL® Multiphysics [82] uses the Finite Element Method (FEM) which is a subclass of the Method of Weighted Residuals. All of the techniques within this class assume the Number Density Function (NDF) to be a weighted sum of basis functions, substitute this sum into the PBE, and then derive evolution laws for the weights. The methods in the family differ in how they derive the evolution laws.
Collocation methods evolve the weights such that at certain points the error in solving PBE is minimal. The Collocation method was found to be inferior in performance for solving PBE when compared to the FEM [83].
Galerkin methods multiply the approximated PBE with a basis function and integrate over the whole domain. If this is carried out for all basis functions, one can obtain a system of Ordinary Differential Equations (ODEs) that describes the evolution of the weights. If the basis functions are defined over the whole domain, this is a spectral method [84]. And if the basis function are only defined on finite elements, this is FEM [85]. FEM has found to be inferior for solving the PBE compared to a Method of Classes (CM) [85] and Quadrature Method of Moments (QMOM) [86]. The software PARSIVAL® [87] and PREDICI® [88] use a Galerkin based method to solve PBEs.

Methods Of Moments

The Method Of Moments (MOM) is again a family of solution techniques. It appears to yield approximate solutions of PBEs at moderate computational cost [89–92]. Instead of solving for the NDF the moments of the NDF are solved for. For several systems, only a few moments have been required to provide meaningful results [89–92]. The major problem occurring, except in rare cases, e.g. [60, 93], is that

the equations for the moments are not closed. That means that in the equations for the moments not computed moments appear. For moment closure several strategies can be pursued:

Simplification of the Population Balance Equation Sometimes [94], the PBE is simplified until the moments can be closed. This results in being able to obtain a solution to a simplified and not necessarily correct model. A more rigorous way of simplifying the PBE was proposed by Yu et al. [95] with the Taylor Extension Method Of Moments. In this method the Taylor expansion of the terms in the PBE are used which allows closure. This approach was further extended by Yu et al. [96]. However, this method only works well if the terms can be described with a low order Taylor expansion [96] which cannot be guaranteed in this work.

Method Of Moments with Interpolative Closure By interpolation between known moments one can obtain the moments needed for closure [97]. This approach is only applicable to rational moments which cannot be guaranteed in this work.

Assuming a number density function If one assumes the NDF to be a certain distribution, e.g. a Gamma distribution [98, 99], a log-normal distribution [99], or a normal distribution [55] one can obtain an approximation of the NDF from the moments and compute the missing moments by this method. The parameters of the NDF are set such that the moments of the NDF are equal to the known moments. This method obviously works well if the NDF is described well by the assumed distribution shape, but fails otherwise [99]. By making the NDF to be sufficiently general this method can be made very powerful and in fact all closures mentioned afterwards are a subset of this method. As the NDF is non-negative, the reconstructed NDF should also be non-negative. If a polynomial basis [100], piecewise constant functions [101], or splines [102] are used, one can not guarantee non-negativity.

Quadrature Method Of Moments The Quadrature Method of Moments (QMOM) was first applied to a PBE by McGraw [90]. It applies a Gaussian quadrature rule of an appropriate order to the integrals defining the moments and obtains the approximated NDF as a sum of Dirac delta functions. Gaussian quadrature rules have the desirable property that they integrate polynomials up to a certain order exactly [103] which approximates most functions well. Furthermore, if the moments are realizable, the weights are positive [103]. The computation of the position and the weights of the quadrature points is problematic [104, 105]. This has motivated Marchisio and Fox [106] to develop the Direct Quadrature Method of Moments (DQMOM) which directly tracks the weights and position of the quadrature points (see Chapter 3). QMOM and Direct Quadrature Method of Moments (DQMOM) are widely used methods (see Marchisio and Fox [107] and Chapter 3 for an overview).
It was modified to the Sectional Quadrature Method of Moments [108]. This method attempts to combine the benefits of sectional methods with the MOM by dividing the domain into sections and defining the moments only in this section. By increasing the number of sections the accuracy but also the computational effort increases. It is slightly more difficult to implement than standard QMOM but more

robust [108].
Yuan et al. [109] proposed the Extended Quadrature Method of Moments which uses a sum of distributions instead of Dirac deltas. The mean and weight of the distributions are chosen as the position and weight of the quadrature points. In addition, there is one shape factor for all distribution which is chosen to satisfy one more moment. Obtaining the shape factor requires solving a non-linear set of equations. Furthermore, the distribution is not only defined at the quadrature points but rather over the whole domain. This necessitates an approximation of integrals. The main advantage is in describing behavior (such as dissolution) at boundaries. It has not been extended to multivariate cases.

Maximum entropy The distribution having maximal entropy at the given moments and being uniquely determined can be expressed as the exponential of a polynomial [110]. Because the distribution with the maximal entropy is the statistically most likely, Attarakih and Bart [111] used this closure rule to solve the PBE. The approximated NDF is defined over the whole domain which necessitates approximation of integrals but increases stability.

Methods of Classes

Method of Classes (CM) divide the computational domain into sections, also called bins or classes, and approximate the NDF in this section by one Dirac delta [112–114]. The only difference between the methods is how created particles and growth are handled. CM are very commonly used. As they are also used in this thesis, they are described in Chapter 4 in more detail.

Probability Generating Functions

Using Probability Generating Functions [115, 116] a z-Transform is applied to the PBE. The transformed equation is then solved approximately in the z-Domain. If the NDF is required, the transform is inverted. For the studied problems, this method provided good results [115, 116]. However, the usage as a numerical technique is a very new method and has only recently been used by more than one group. The usage of this method to obtain analytical solution is established [61, 117]. Currently, as a numerical method it cannot handle size dependent reaction rates [115, 116]. Therefore, it can not be used in this work.

Other methods

The PBE can also be solved efficiently and accurately using the Finite Volume Method [118, 119]. However, as the method has not been rigorously compared to modern CM, it is not known whether using the Finite Volume Method would be beneficial.
The Finite Difference method can also be used to solve PBEs. However, it requires a very fine grid and accordingly many equations [85, 98, 120].
The Method of Characteristics [121, 122] is the best method to describe process with only growth and

nucleation. However, it has never been extended to breakage.
The Lattice Boltzmann method has also been used in the last several years to solve PBEs [123]. However, it has not been used in depolymerization context and has been found to best describe growth dominated processes [124].

1.3.2 Solving the Population Balance Equation describing depolymerization

As almost all polymers are distributed in the molar mass (and therefore in the amount of monomer units) PBEs are widely used to describe polymers undergoing reactions. If the balance equation for each discrete amount of monomer units (and branching bonds, etc.) are formulated and solved directly, one does - in theory - not need a numerical technique besides the one required to integrate the resulting system of ODEs. For oligomers and small polymers [40] this is computational feasible [125]. However, the number of equations to be solved increases at least linearly with the molar mass which makes this unsuitable for the large biopolymers considered in this work. In some cases [88, 126, 127] discrete simulations were performed for validating a new algorithm. Also for some unrealistically simple cases, e.g. [69, 93, 128], analytical solutions were found. These cases can be used to validate algorithms but not to describe enzymatic depolymerization. Accordingly, numerical techniques are required. If the amount of monomer units is sufficiently high, one can regard the polymer to be continuous in the molar mass [54]. Then again for some unrealistic cases analytical solutions can be found [128, 129]. But again these cannot be used and numerical techniques are required.

PREDICI

Computing in Technology has developed PREDICI and PARSIVAL [130]. PARSIVAL is a general solver for PBEs, whereas PREDICI is developed for processes involving polymers. It uses an adaptive Galerkin method [131] and describes the polymer as being discrete. It has been used to describe degradation dominated processes [66, 132] and polymerization processes with scission present [62]. Just using the Galerkin method implemented in PREDICI allows describing linear polymers and copolymers. In order to be able to describe branching several techniques were used in combination with PREDICI: Iedema et al. [62] introduced the concept of pseudo-distributions. The amount of polymer and branching bond at a certain amount of monomer units is obtained by summation of the PBE. This converts the 2D PBE into two 1D PBEs. However, one needs to provide closure which is normally [62, 133] done by simplification. Because scission cannot be simplified with a high accuracy [66], this cannot be be used in this work. Iedema et al. [88] solved the PBEs for each amount of branching bonds which is only numerically feasible with a low amount of branching bonds. However, one could also use a CM for the branching bonds as done by Seferlis and Kiparissides [134] who combined a collocation method with a CM and did not use PREDICI. Recently, an algorithm similar to the one implemented in PREDICI has also been implemented by Yaghini and Iedema [135], extended to 2D [136], and using a pseudo-distribution approach even to 3D [133]. In the most recent work [133] good results at an acceptable computational cost were obtained.

Method of Classes

Assuming the PBE to be continuous and the polymer to be linear, several authors [36, 37, 42–44, 48, 49, 127, 137, 138] have used a CM with good results. However, for branched polymers the variation in the amount of monomer units and the degree of branching must be considered. For such bivariate cases CMs have not been used for depolymerization. However, for polymerization Krallis and Kiparissides [139] have used the fixed pivot technique with around 800 ODEs to describe bivariate polymerization. Iedema and Hoefsloot [140] have also solved a PBE for a polymerization reaction with a branched polymer using a CM. However, they did not provide any further details.

Method of moments

The Method Of Moments (MOM) has often been applied to polymerization and depolymerization. In early works simple systems were studied and the equation for the moments of the continuous PBE were closed (for polymerization [60] and depolymerization [63, 65]). Saidel and Katz [141] proposed to close the moments by approximating the NDF as a Gamma function. They used this to study a continuous-discrete 2D polymerization process. This approach was later used for polymerization [142] and depolymerization [98]. A purely continuous approach was found to not be sufficient to describe the evolution of the product. Therefore, Kruse et al. [143] tracked the product discretely, while describing the polymer with a Gamma function. In order to describe the branching of the linear polymer during depolymerization they lumped all branched polymer into one group and used a binomial distribution for branching bonds within this group. In a later work, the group used the same approach while tracking more species discretely [144].
Recently, Lebaz et al. [46, 67] used DQMOM to describe the depolymerization of linear cellulose. Even though they considered cellulose to be continuous, they still tracked the product discretely.

Other methods

The PBE has been solved by Probability Generating Functions numerically in a discrete form [115, 116, 145]. This method has also been used for a bivariate polymerization process [116]. However currently, this method cannot be used for internal coordinate dependent reaction rates, therefore it is unsuitable.
In order to solve a 2D discrete polymerization process, Kryven and Iedema [146] approximated the NDF in one coordinate as a sum of Gaussian distribution with fixed mean and standard deviation. The other coordinate was solved directly. The numerical effort for polymers with a significant amount of branching bonds would be prohibitive.

Mechanisms of depolymerization

The most well studied mechanisms for the depolymerization include Random-chain scission (RCS) and End-chain scission (ECS) [42, 63]. This two mechanisms also serve as the extreme cases for most depolymerization mechanisms. Solving RCS with high-resolution methods has been reported to be

problematic [66]. Solver for the ECS based on the method of moments are also difficult to implement [147]. Solving ECS dominated processes using high-resolution methods requires a very fine resolution [127].

1.4 Optimal control

The aim of optimal control is to find the optimal control action profile (over time and/or space) that minimizes an objective functional. This is different from normal optimization that searches an optimal scalar value (or a vector thereof) [148–151]. Optimal control as a mathematical field started in the 17th century. It was put on a solid foundation by Euler and Lagrange in the 18th century by the introduction of the calculus of variations [152]. With the advent of computers in the mid of the 20th century it started being applied to engineering problems which were at first aeronautical problems [153]. In the 60s Horn [154] introduced optimal control into the chemical engineering community. He found the spatial temperature profile that allows attaining the highest possible yield for a system with coupled reversible and for the starting material competing reactions. Later in this decade, Chou et al. [155] found the optimal spatial temperature profile for a problem with decaying catalyst. The first works derived analytical solution, but numerical solutions started being applied [156] in the 60s. In the 70s and afterwards, the amount of publications is too great to provide a comprehensive review here. But it should be noted that already in 1970 Ho and Humphrey [157] used optimal control to find the best temperature profile for an enzymatically catalyzed reaction. The interest into using optimal control for enzymatically catalyzed processes is still high, e.g. [158, 159]. Even though, only temperature was mentioned here, optimal control has been used to optimize e.g. the pH profile [159], the enzyme dosage profile [160], and the substrate feed profile [161].
The works mentioned above designed open loop control. This means that the proposed control profile is optimal if no disturbances occur. Already in the late 70s, Brisk and Barton [162] developed the first algorithm that allowed closed loop optimal control of a chemical process. Therefore, the process can react to disturbances (and model mismatches) by taking the measured values into account and updating the control action to still find the optimal profile. This model predictive control is a topic of research [163] and already applied [164–166]. Another topic of research is to find an optimal profile that is robust to uncertainty in parameters or inputs [167].

1.4.1 Review of solution techniques

The solution strategies for optimal control of systems described by ODEs can be broadly classified into three groups [151, 168]: Indirect and direct solution strategies and full discretization.

Indirect solution strategies

Indirect solution strategies try to satisfy the necessary conditions at all times. This necessitates solving the set of ODEs for the states coupled with the ODEs for the adjoint states (see e.g. [168, 169] and Section 5.1). Numerically this is tricky because one has to solve a boundary value problem which can be handled using appropriate solvers [170]. For the complicated set of ODEs obtained by approximation of the PBE having to solve a boundary value problem with double the amount of equations did not seem promising and this approach was therefore not attempted. Most analytical solutions are obtained using indirect solution strategies. Analytical solutions have been obtained for some simple problems relevant to optimal temperature control of reactors [154, 171] and more recently [172].

Complete discretization

If complete discretization is used, the states as well as the control variables are discretized in time/or space. Then one searches for the values of the states that would result in a solution of the governing equations coupled together with the optimal control variables. This results in large scale non-linear programming problem [151, 168]. This approach is used in a commercial solver based on a pseudo-spectral method [173]. However, one obtains an optimization problem with the number of states plus the number of control variables times the number of time steps as the size [151]. For the large systems of ODEs (up to 1000 ODEs with more than 300 time steps taken) studied this also did not seem promising and this approach was therefore not attempted.

Direct solution strategies

The control variable is parametrized and the optimal value of those parameters is searched. This reduce the problem to a finite dimensional optimization problem [151, 174]. The states corresponding to any parameter value can easily be obtained by integration of the ODE system using any time integrator. This is the easiest method to implement, but one is not guaranteed to obtain the true optimal solution. Rather only the optimal parametrized profile is obtained. If the parametrization is able to represent the true solution, one however obtains a true solution [175]. As very complicated profiles are unlikely to be used in industrial practice [175], this constraint is not critical and a direction solution method was used.

Parametrization One can use any parametrization for the optimal heating profile [174]. A very general approach is due to Sirisena [176] who used piecewise polynomials. The usage of high order polynomial introduces assumptions on the continuity of the profile which can be minimized if a piecewise constant approach is used.

Single and multiple shooting With single shooting the ODEs describing the problem are solved forward in time from the initial state to the final state. However, with multiple shooting the problem is divided into several subproblems. Each subproblem is solved forward in time from a guess of the

state vector at the start of the subproblem. The state vector at the start of each subproblem has to be obtained numerically. Multiple shooting can solve some problems that are inefficient or impossible to solve using single shooting [177]. However, estimating the state vector at the start of each subproblem adds the amount of state variables times the amount of evaluation of the right hand side of the system of ODEs. This would lead to a very large system of equations and, accordingly, single shooting is used.

1.4.2 Model-based optimal control of enzymatic depolymerization

Of course one does not need PSE to propose a temperature profile and experimentally test this. However, already in 1998 Einsiedler et al. [178] formulated using optimal control of the temperature as a modeling goal. Currently, a heuristical experimental approach is used to optimize depolymerization temperature ramps: First, one gains knowledge about the behavior of the enzymes by suitable experiments and then proposes to operate the process at "optimal temperatures" of the enzymes. This results in a temperature profile that can be used to handle polymer from a novel source [20]. However, a truly optimal profile is unlikely to be found by such a method and the experimental effort is large. This becomes even more of an issue if one considers that polymers from a natural source, which are subject to change [179], are to be used. Accordingly, it might be necessary to perform the optimization with every change of source and at least every season anew. This makes a model-based approach highly desirable.
Model-based optimal control has been applied to the saccharification process, though models that neglect the amount of monomer units distribution were used [16, 23] with the above mentioned deficiencies. Optimal control has been applied to polymerization, instead of depolymerization, processes described by PBEs [94, 180, 181], though. However, those studies used either a very coarsely discretized optimal profile because of computational limitations [180, 181] or were able to use simplifications not possible for enzymatically catalyzed reactions [94]. Optimal control for depolymerization processes represented by a complex PBM is challenging and has, to the best of my knowledge, not been pursued yet.

1.5 Aims and scope

PSE has been used to improve a lot of chemical processes. However, it is rarely applied in biotechnology and food engineering. Applying PSE methods such as optimal control to biotechnological process might help in establishing biotechnology. Thereby, the economy can be transferred more easily into the bioeconomy.

Thesis statement This thesis aims at showing that PSE methods (as an example optimal control of temperature) can be used to optimize the enzymatically catalyzed depolymerization process. It is the aim of this thesis to use a mechanistic model that can deal with variabilities in the starting material and the enzymes.

Formulating a Population Balance Model A PBM that takes degradation of enzymes and the distributed nature of the polymer into account is developed in Chapter 2. Furthermore, the model is on solid mechanistic foundation and is extended from linear polymers to branched polymer. The predictions of this model are compared to a stochastic model and experimental data from the literature in Chapter 4.

Solving the Population Balance Model Three techniques are evaluated for their ability to describe depolymerization of branched polymer. This is done in this dissertation by comparing the results to kMC results. The three methods are DQMOM (see Chapter 3), Cell Average Technique (CAT), and Fixed Pivot technique (FP) (see Chapter 4 for both methods). All of the methods had to be modified in order to be used for the problem studied in this work.

Optimal control of temperature Optimal control of the temperature profile is performed for enzymatic depolymerization in Chapter 5. For a linear polymer several objectives and parameters are studied. Furthermore, the effect of using a more realistic product distribution function and considering the effect of branching is investigated.

Limitations In this dissertation the developed model is not thoroughly validated with experimental data. No experiments to investigate the validity of the assumptions were undertaken. The parameters used in this dissertation are taken from literature sources and not estimated from experimental data.

Chapter 2

Modeling enzymatic depolymerization

Having a model is, obviously, a necessity for applying model-based Process Systems Engineering (PSE) methods. The model must be able to predict the state, even for conditions that were not used for calibration or parameter estimation. For example, optimal control can result in temperature profiles whereas most parameters are estimated for isothermal conditions. Therefore, a mechanistic model should be used. As the priorly derived models (see Chapter 1) are either too simplistic or too complicated for optimal control, a new model (see Figure 2.1 for a schematic drawing) to describe the enzymatic depolymerization with coupled denaturation of enzyme is derived in this chapter.

2.1 Starch

One of the most abundant polymers in the world is starch. It is so common because many plants produce it to store energy. Plants synthesize it by linking the monomer glucose by α-1-4 and α-1-6-glycosidic bonds. As the polymer is less soluble than the monomer glucose it is then deposited in granules of different radii. Nevertheless, the polymer is still soluble in water at moderate temperatures [10].

Starch has been converted into saccharides (the monomer glucose and small oligomers) for millennia as a step in brewing beer [182]. 2015 in Germany more than $467 \times 10^3\,\mathrm{ton}$ of ethanol for usage as fuel were produced via saccharification of starch followed by fermentation [13]. Accordingly, starch was chosen as the model polymer.

Starch is made up by two fractions: A linear (or almost linear) fraction, called amylose, and a branched fraction, called amylopectin. Depending on the origin of the polymer the percentage of linear polymer can be significant [10]. Amylose has a broad distribution in the amount of monomer units with a mean amount of monomer units in the order of 10×10^3 [183]. Amlyopectin is also broadly distributed but much larger with a mean amount of monomer units up to around 10×10^6 [184]. Furthermore, it is highly branched with a branching density greater than 4 % [185].

The α-1-4 bonds are linear bonds, whereas the α-1-6 bonds are responsible for branching. As starch does not crosslink the amount of branching bonds b must be less than that of monomer units k minus

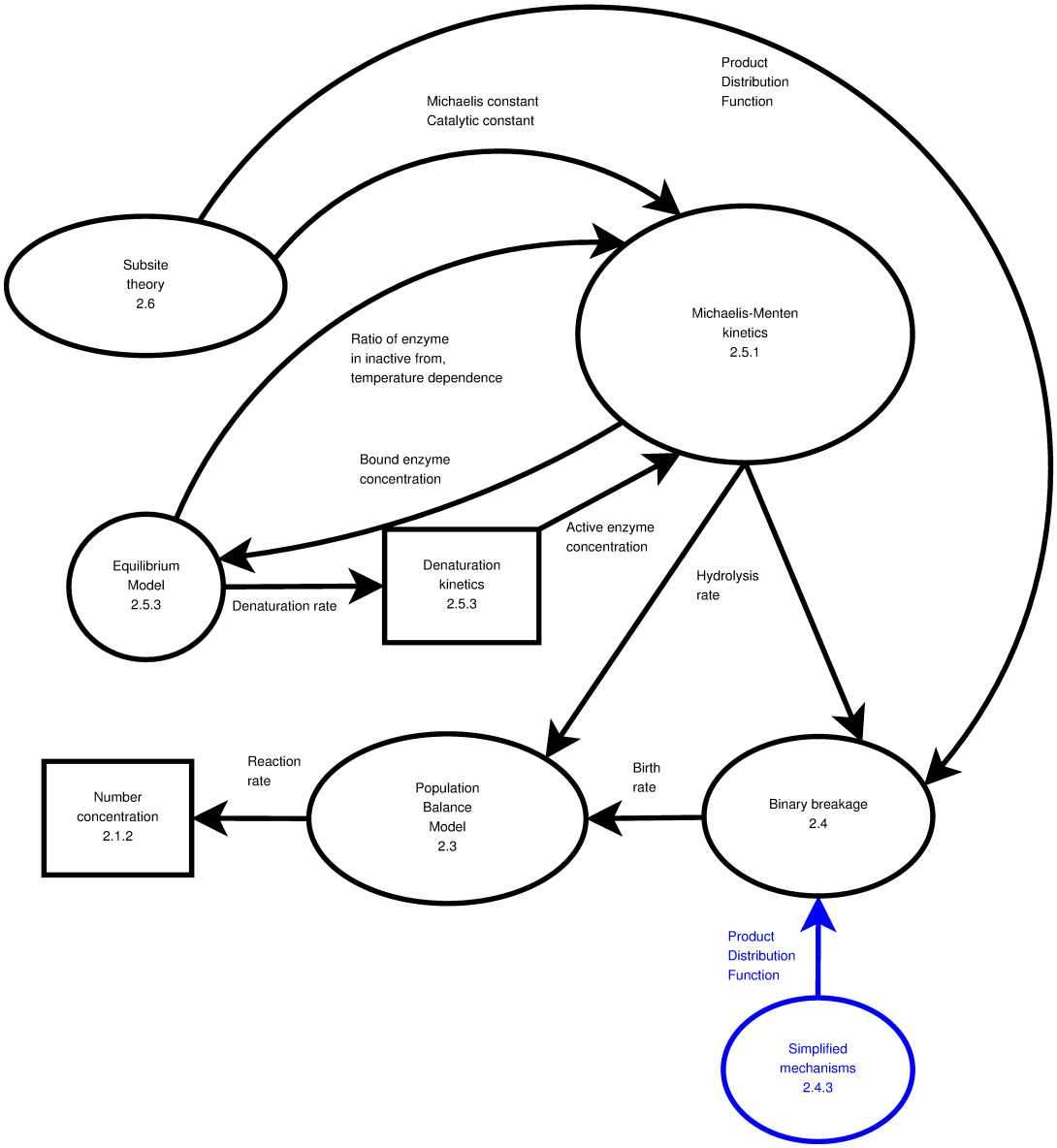

Figure 2.1: Schematic drawing of the model. The model parts (circle) provide information (arrows) to other parts of the model or ordinary differential equations (rectangles). The blue parts belongs to the simplified model. The numbers show in which section the part is explained.

one. However, two glucose units can be linked with an α-1-6 bonds. Accordingly, a branching bond is not necessarily the start of a new chain but every new chains starts with a branching bond [10]. The nomenclature of calling α-1-6 bonds bonds associated with branching would be more clearly than calling them branching bonds but rather tiresome, accordingly, in this work α-1-6 bonds are called branching bonds.

2.1.1 Structure of starch

The structure of starch is not fully known. Because detailed modeling of the structure is not possible with the approach used here, the readers are referred to Pérez and Bertoft [10] for an overview over models of the structure. For the purpose of this work a chain is defined as the α-(1-4) (linearly) connected monomers between the start of a chain at either the reducing end or at a monomer unit with a branching bond up to either the end of the polymer or to another branching bond. Accordingly, every branched starch polymer has $2 \cdot b + 1$ chains: $b+2$ chains are end-chains and $b-1$ chains are inner chains. The average amount of monomer units per chain is $\frac{k}{2 \cdot b+1}$. It is well established that there are several types of chains and that the amount of monomer units per chain[1] is distributed [10]. This cannot be modeled using the chosen approach.

2.1.2 Initial distribution

The form of the amount of monomer unit distribution of starch is not yet clear, but the commonly used Schulz-Zimm distribution [186, Ch.5] was found to fit experimental data from Rolland-Sabate et al. [187] reasonably well. The Number Density Function (NDF) for a linear polymer would be

$$\bar{n}(t=0,\bar{k}) = n_0 \cdot \frac{\bar{k}^{\sigma-1} \cdot \Theta^{\sigma}}{\Gamma(\sigma)} \cdot \exp(-\Theta \cdot \bar{k}), \tag{2.1}$$

where n_0 is the initial molar concentration and σ and Θ are parameters that are chosen such that the measured mean molar mass by weight and the polydispersity agree with the computed values. The Schulz-Zimm distribution, however, assumed that the polymer can be described as being continuous. If one wants to avoid this assumption, one can use the discrete distribution with the same shape which is a negative Binomial distribution [188]

$$\breve{n}(t=0,\breve{k}) = n_0 \cdot \frac{\Gamma(r+\breve{k})}{\Gamma(r) \cdot \Gamma(\breve{k})} \cdot (1-p)^r \cdot p^{\breve{k}}, \tag{2.2}$$

where r and p are parameters that are chosen such that the measured mean molar mass by weight and the polydispersity agree with the computed values.
It is reasonable to assume that the degree of branching is also distributed. However, no measurements

[1] In this work chain length means the amount of monomer units per chain, whereas the (total) amount of monomer units without any specifying words means the total amount of monomer units of a polymer. For a branched polymer the chain length is **not** the total amount of monomer units.

of the degree of branching distribution haven been undertaken. Rolland-Sabate et al. [184] have found that the average degree of branching is a function of the molar mass. In this work, two different functions are assumed for the degree of branching. For the continuous case it is assumed that the NDF is distributed by a symmetric Beta distribution with the shape parameter set arbitrarily to 2. This case is only used for testing the numerical solver and therefore agreement with reality is not imperative. This results in a distribution

$$\bar{n}(t=0,\bar{k},\bar{b}) = n_0 \cdot \frac{\bar{k}^{\sigma-1}\cdot\Theta^{\sigma}}{\Gamma(\sigma)} \cdot \exp(-\Theta\cdot\bar{k}) \cdot \frac{1}{\beta(2,2)} \cdot \left(\frac{\bar{b}}{\bar{k}-1}\right) \cdot \left(1-\frac{\bar{b}}{\bar{k}-1}\right). \tag{2.3}$$

For the discrete case, the simplest one parameter distribution with a limited supporting domain is used which is the Binomial distribution. This results in the distribution

$$\breve{n}(t=0,\breve{k},\breve{b}) = n_0 \cdot \frac{\Gamma(r+\breve{k})}{\Gamma(r)\cdot\Gamma(\breve{k})} \cdot (1-p)^r \cdot p^{\breve{k}} \cdot \begin{pmatrix} \breve{k}-1 \\ \breve{b} \end{pmatrix} \cdot d_b^{\breve{b}} \cdot (1-d_b)^{\breve{k}-\breve{b}-1}, \tag{2.4}$$

where d_b is the degree of branching. To better compare the model developed in this Chapter with literature data, the limitation that between two branching bonds are at least to unbranched glucose units [32, 189] was implemented. This structure imposes an upper limit on the branching bonds $\breve{b} \leq \lfloor \frac{\breve{k}-1}{2} \rfloor$. This results in a slightly different initial distribution

$$\begin{aligned}\breve{n}(t=0,\breve{k},\breve{b}) =& n_0 \cdot \frac{\Gamma(r+\breve{k})}{\Gamma(r)\cdot\Gamma(\breve{k})} \cdot (1-p)^r \cdot p^{\breve{k}} \\ & \cdot \begin{pmatrix} \lfloor \frac{\breve{k}-1}{2} \rfloor \\ \breve{b} \end{pmatrix} \cdot \left(\frac{\breve{k}-1}{\lfloor \frac{\breve{k}-1}{2} \rfloor} \cdot d_b\right)^{\breve{b}} \cdot \left[1-\left(\frac{\breve{k}-1}{\lfloor \frac{\breve{k}-1}{2} \rfloor} \cdot d_b\right)\right]^{\lfloor \frac{\breve{k}-1}{2} \rfloor - \breve{b} - 1}\end{aligned} \tag{2.5}$$

This initial distribution provides the initial value for the number concentration (see Fig. 2.1).

2.2 Enzymes

Due to their normally high specificity enzymes are desired catalysts. Enzymes are proteins and have a complicated tertiary structure which is required for the catalytic function [190]. The loss of this structure is modeled in Section 2.5.3. Here, the hydrolysis of glycosidic bonds of starch is considered. The enzyme is then a type of hydrolase (EC number top level 3) producing a type of sugar (EC class 3.2) and acting on the O- and S-glycosydic bonds (EC subclass 3.2.1 [191]). This family of enzymes is called Glycosidases. Four enzyme types are considered in this work. α-amylase (EC 3.2.1.1) is present in the mashing process [14] and during bioethanol production [48, 49, 192]. The enzyme performs endo-active attacks (i.e., not exclusively, on inner bonds) on α-1-4-bonds (linear bonds) of starch. β-amylase (EC 3.2.1.2) is present in the mashing process [14], but is rarely used in bioethanol production. It performs exo-active attack (i.e., on the ends of the polymer) on α-1-4-bonds of starch and releases

the dimer maltose. Glucan 1-4-α-glucosidase or glucoamylase (EC 3.2.1.3) is generally not held to be important in the mashing process [14, 20, 193] but is used in bioethanol production [49, 192, 194]. It also performs exo-active attack on α-1-4-bonds of starch but releases the monomer glucose. It has been reported that some glucoamylase attack α-1-6-bonds [195] which is neglected in this work as the effect is small. One can easily include this though. As an example for a debranching enzyme limit dextrinase (EC 3.2.1.142), which hydrolyzes α-1-6-bonds but not α-1-4-bonds, is considered. It performs endo-active attack on the branching bonds. The model could easily be extended to dextranse (EC 3.2.1.11) and pullulanse (EC 3.2.1.41) which also perform endo-active attack on the branching bonds.

2.3 Population Balance Equation

Starch is a branched polymer with a wide distribution in the amount of monomer units as mentioned in Section 2.1. The amount of monomer units is an important property to characterize the attack of enzymes on starch [125]. Furthermore, experimental effects of the branching bonds have been observed [196]. Accordingly, the distributed nature of the polymer and the branching should be included in a model. This is done in this work using a two dimensional Population Balance Model (PBM). The amounts of monomer units k and bonds associated with branching (called branching bonds for brevity) b are used as internal coordinates.

2.3.1 Assumptions

To describe the depolymerization process using a Population Balance Equation (PBE) some simplifying assumptions must be made. One assumption inherent in the use of population balances is that all polymers with the same internal coordinates behave identically and deterministically [57]. This assumption is only valid if the used internal coordinates are able to describe the behavior of the polymer. Furthermore, the amount of polymers must be sufficiently large that the required averaging of the (stochastic) hydrolysis rate of bonds is valid [78].
The choice of internal coordinates implies that all the polymers are ideally dissolved. One can easily adapt the population balance to not ideally dissolved polymer [36, 42]. Only having two internal coordinates prohibits knowing the chain length distribution. In addition, the reaction is assumed to occur in an ideally stirred batch reactor, and thus no spatial distribution is considered. Spatial distributions can be described using population balances, but this increases the numerical effort [107, 197, 198] and is, therefore, not considered here.
The population balance is formulated here for a pure breakage problem. This is due to the assumption that only the enzymes act on the polymer and the enzymes only break the polymer into smaller polymers (or oligomers or monomer). For some enzymes the reverse reaction (polymerization or branching) have been observed [193], but for commercially used enzymes under real process conditions this effect can be neglected. Further effects such as precipitation, chemical modification, or release by granules

is not taken into account in this work. However, release can be described easily [36] and precipitation would also not pose a problem. Because the enzymes catalyze the hydrolysis very selectively, chemical modification should not occur [193].

2.3.2 Population Balance Equation for a branched polymer

The computation domain is complicated by the fact that the amount of branching bonds must be less than that of monomer units minus one because the polymer is assumed to not crosslink. This restriction on the amount of branching bonds has not previously been included in any population balance formulation. However, the inclusion of this restriction is crucial in this work because physically impossible polymers would otherwise be created. These polymers would not be a numerical problem, but would lead to erroneous reaction patterns because the reaction mechanisms strongly depend on the presence of branching bonds. Due to this constraint the domain of valid amount of monomer units k and amount of branching bonds b is a triangular domain with $k-1 \geq b$. Furthermore, each polymer has to have at least monomer unit $k \geq 1$ and negative branching bonds are not possible $b \geq 0$. This domain is shown in Figure 2.2.
If the *degree* of branching bonds would be adopted as the second internal coordinate, a rectangular domain would be the benefit. However, subdividing the domain (see Chapters 3 and 4) would be much more complicated because the lines with a constant amount of branching bonds would not be straight. This approach is therefore not adopted in the present study.

Discrete population balance No additional assumption is required to derive a discrete PBE with the internal coordinates $\breve{k} \in \mathbb{N}$ (the accent $\breve{}$ indicates that a variable belongs to a discrete equation or is discrete) and $\breve{b} \in \mathbb{N}_0$ with the only remaining constraint $\breve{k}-1 \geq \breve{b}$. The corresponding domain is shown in Figure 2.2a. A polymer can either be destroyed by being split into smaller polymers or can be created by a larger polymer being split into this smaller polymer and other polymers. A balance equation for the number concentration $\breve{n}(t,\breve{k},\breve{b})$ of polymer, which is attacked by several enzymes, can then be derived

$$\frac{\mathrm{d}\breve{n}(t,\breve{k},\breve{b})}{\mathrm{d}t} = -\breve{D}_{\sum}(t,\breve{k},\breve{b}) + \breve{B}_{\sum}(t,\breve{k},\breve{b}). \tag{2.6}$$

Equation (2.6) defines a set of Ordinary Differential Equation (ODE)s for the concentration of polymers with $\breve{k}$ monomer units and $\breve{b}$ branching bonds (refer to Fig. 2.1). Here $\breve{D}_{\sum}(t,\breve{k},\breve{b})$ is the reaction rate on the polymer with $\breve{k}$ monomer units and $\breve{b}$ branching bonds due to all enzymes and is obtained by summing up the individual contributions of the enzymes. The individual reaction rates of the enzymes are described in Section 2.5. $\breve{B}_{\sum}(t,\breve{k},\breve{b})$ is the sum of the production rates of polymer with $\breve{k}$ monomer units and $\breve{b}$ branching bonds due to attack of all enzymes on all larger polymers. This birth rate is described in Section 2.4. All of the PBEs used in this work have the same general form of the death term being subtracted from the birth term and this being equal to the change of polymer number concentration or

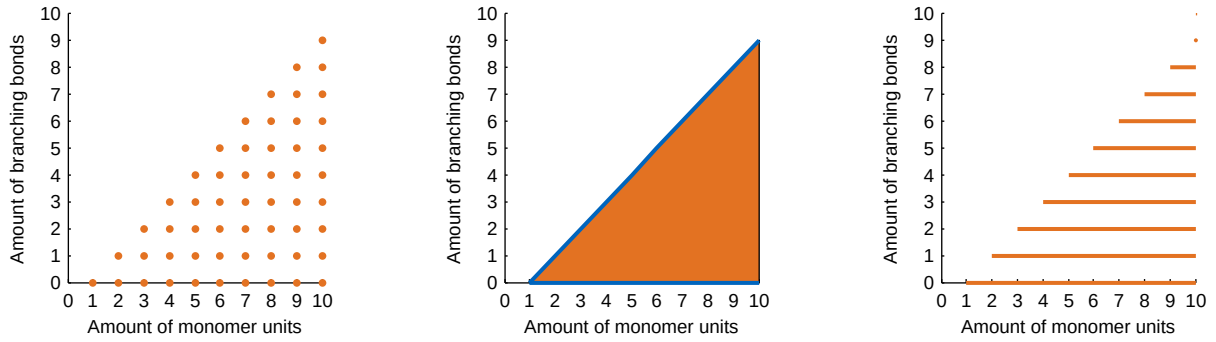

(a) Domain on which the discrete Population Balance Equation is formulated.

(b) Domain on which the continuous population balance is formulated.

(c) Domain on which the mixed continuous-discrete population balance is formulated.

Figure 2.2: The domains on which the population balance for branched starch can be formulated.

density. They are shown in Appendix A. Further on, for clarity dependency on time, amount of monomer units, and enzyme and polymer concentration are only noted if they aid understanding.

Continuous population balance For sufficiently large polymers one would obtain the same results if one uses a continuous PBE [54]. The extension to also considering the amount of branching bonds to be continuous, if the amount of branching bonds is sufficiently high, is straightforward. But this PBE would be in a form more suitable for efficient numerical population balance solvers (see Chapter 3). Instead of a set of ODEs for the concentration one obtains one two dimensional Partial Differential Equation (PDE) for the number density $\bar{n}$ (the accent $\bar{}$ indicates that a variable belongs to a continuous equation or is continuous). The amount of monomer units $\bar{k} \in \mathbb{R} : k \geq 1$ and branching bonds $\bar{b} \in \mathbb{R} : b \geq 0$ is then continuous and the second coordinate for the PDE. The domain is still triangular and shown in Figure 2.2b.

Mixed continuous-discrete population balance As the amount of branching bonds is less than the amount of monomer units (see Section 2.1) the assumption of large amount of branching bonds is questionable. Accordingly, a mixed continuous-discrete PBE, discrete in the amount of branching bonds $\check{b}$ and continuous in the amount of monomer units $\bar{k}$, is more appropriate. One obtains a system of one dimensional partial differential equations for the number density $\hat{n}$ (the accent $\hat{}$ indicates that a variable belongs to a mixed continuous-discrete equation). This also results in a triangular domain $\{\bar{k} \in \mathbb{R}, \check{b} \in \mathbb{N}_0 : \bar{k} \geq 1 \wedge \bar{k} - 1 \geq \check{b}\}$ (see Figure 2.2c).

2.3.3 Population Balance Equation for a linear polymer

If one assumed that the polymer is almost linear and the effect of branching bonds can be neglected, one obtains a one dimensional PBE. This assumption has been validated for soluble starch by Ho et al.

[48]. The resulting equation is easier to solve. Again one obtains a set of ODEs for a discrete PBE for the number concentration $\breve{n}$ which now depends only on the amount of monomer units $\breve{k} \geq 1$. Or if one assumes the polymer to be continuous, one obtains a one dimensional PDE for the number concentration $\bar{n}$.

2.4 Production rate

A hydrolysis of one bond of a polymer results in the creation of two smaller polymers which corresponds to binary breakage in the PBM nomenclature [57]. Some experimental results [199] can be well explained by multiple attack of exo-active enzymes which results in the creation of more than two fragments. However, there are currently no mathematical models for the rate of multiple attacks. Therefore, only binary breakage is considered in this work. But multiple fragments can be handled by PBM [57, 200], if the reaction rate is known.
The production rates are only derived for a discretely represented polymer here but the remaining cases are derived in Appendix A.2.

2.4.1 Production rate for a linear polymer

The production rate of a polymer with k monomer units (variables without accents can either be discrete or continuous) is obtained by first finding an expression for the production of the polymer due to attack of an arbitrary enzyme $\bullet$ on a polymer of k' monomer units and then summing up (or integrating) this production rate. The production of polymer k due to attack on k' can be expressed as the product of the hydrolysis rate $D_\bullet(t,k')$ and a normalized non-negative Product Distribution Function (PDF) $\gamma_\bullet(k,k')$ times 2 [57]. This relation is also detailed in Figure 2.1.
The production rate for a discrete polymer can then be expressed as follows

$$\breve{B}_\bullet(t,\breve{k}) = 2 \cdot \sum_{\breve{k}'=\breve{k}}^{\infty} \breve{\gamma}_\bullet(\breve{k},\breve{k}') \cdot \breve{D}_\bullet(t,\breve{k}'). \tag{2.7}$$

The normalization condition for the PDF is

$$1 = \sum_{\breve{k}=1}^{\breve{k}'} \breve{\gamma}_\bullet(\breve{k},\breve{k}'). \tag{2.8}$$

Furthermore, as all mechanisms conserve the amount of monomer units the PDF must be symmetric [57, pp.53]

$$\breve{\gamma}_\bullet(\breve{k},\breve{k}') = \breve{\gamma}_\bullet(\breve{k}'-\breve{k},\breve{k}'). \tag{2.9}$$

This symmetry means that if a polymer with $\breve{k}$ monomer units is produced, the other produced polymer has $\breve{k}'-\breve{k}$ monomer units. Furthermore, physically impossible polymers with $\breve{k}$ cannot be produced

which coupled with symmetry results in

$$\breve{\gamma}_\bullet(\breve{k},\breve{k}') \neq 0 \Rightarrow 1 \leq \breve{k} \leq \breve{k}' - 1. \tag{2.10}$$

One can reformulate the equations for the production rate and the normalizing condition using the above condition

$$\breve{B}_\bullet(t,\breve{k}) = 2 \cdot \sum_{\breve{k}'=\breve{k}+1}^{\infty} \breve{\gamma}_\bullet(\breve{k},\breve{k}') \cdot \breve{D}_\bullet(t,\breve{k}') \tag{2.11}$$

$$1 = \sum_{\breve{k}=1}^{\breve{k}'-1} \breve{\gamma}_\bullet(\breve{k},\breve{k}'). \tag{2.12}$$

2.4.2 Production rate for branched polymers

The production rate for branched polymers is obtained similarly to the linear case. The PDF is now a function of the amount of monomer units k and branching bonds b of the created polymer and the amount of monomer units k' and branching bonds b' of the attacked polymer. The transfer of the production rate and the normalizing condition is straightforward

$$\breve{B}_\bullet(t,\breve{k},\breve{b}) = 2 \cdot \sum_{\breve{k}'=\breve{k}}^{\infty} \sum_{\breve{b}'=\breve{b}}^{\breve{k}'-1} \breve{\gamma}_\bullet(\breve{k},\breve{k}',\breve{b},\breve{b}') \cdot \breve{D}_\bullet(t,\breve{k}',\breve{b}') \tag{2.13}$$

$$1 = \sum_{\breve{k}=1}^{\infty} \sum_{\breve{b}=0}^{\breve{k}-1} \breve{\gamma}_\bullet(\breve{k},\breve{k}',\breve{b},\breve{b}'). \tag{2.14}$$

However, there is difference whether linear or branched bonds are hydrolyzed.

Production rate for hydrolysis of linear bonds Every mechanism conserves the amount of monomer units and the mechanisms that work on linear α-1-4-bonds also conserve the amount of branching bonds. Accordingly, additivity holds: a polymer with $\breve{k}'$ monomer units and $\breve{b}'$ branching bonds decomposes into a polymer with $\breve{k}$ monomer units with $\breve{b}$ branching bonds and a polymer with $\breve{k}' - \breve{k}$ monomer units and $\breve{b}' - \breve{b}$ branching bonds. Thus, the PDF $\breve{\gamma}_\bullet$ must be symmetric, according to the straightforward extension of the reasoning of Ramkrishna [57, pp.53] when applied to the bivariate case.

$$\breve{\gamma}_\bullet(\breve{k},\breve{k}',\breve{b},\breve{b}') = \breve{\gamma}_\bullet(\breve{k}' - \breve{k},\breve{k}',\breve{b}' - \breve{b},\breve{b}'). \tag{2.15}$$

Because physically impossible polymers cannot be created, the fragment distribution function must be zero for the physically impossible polymers with $\breve{k} < 1$ or $\breve{b} > \breve{k} - 1$. The above derived symmetry then implies that the fragment distribution is zero for $\breve{k} > \breve{k}' - 1$ or $\breve{b}' - \breve{b} > \breve{k}' - \breve{k} - 1$. By changing the limits

of summation the production rate can be rewritten

$$\check{B}_\bullet(t,\check{k},\check{b}) = 2 \cdot \sum_{\check{k}'=\check{k}+1}^{\infty} \sum_{\check{b}'=\check{b}}^{\check{k}'-1-\check{k}+\check{b}} \check{\gamma}_\bullet(\check{k},\check{k}',\check{b},\check{b}') \cdot \check{D}_\bullet(t,\check{k}',\check{b}'). \tag{2.16}$$

If one, furthermore, changes the order of summation one obtains the normalizing condition

$$1 = \sum_{\check{b}=0}^{\check{b}'} \sum_{\check{k}=\check{b}+1}^{\check{k}'-1+\check{b}-\check{b}'} \check{\gamma}_\bullet(\check{k},\check{k}',\check{b},\check{b}'). \tag{2.17}$$

In order for the upper limit of the second sum to be larger than the lower limit the condition $\check{k}'-2 \geq \check{b}'$ needs to be fulfilled. By analogy to integration and the non-negativity this is also the necessary condition for attack being able to occur on linear bonds.

Production rate for hydrolysis of branching bonds If a branching bond is hydrolyzed the sum of the amount of branching bonds in the created polymers is one less than in the attacked polymer, but still the amount of monomer units is conserved. Accordingly, a polymer with $\check{k}'$ monomer units and $\check{b}'$ branching bonds decomposes into a polymer with $\check{k}$ monomer units with $\check{b}$ branching bonds and a polymer with $\check{k}'-\check{k}$ monomer units and $\check{b}'-\check{b}-1$ branching bonds. Thus, the PDF has a different symmetry condition:

$$\check{\gamma}_\bullet(\check{k},\check{k}',\check{b},\check{b}') = \check{\gamma}_\bullet(\check{k}'-\check{k},\check{k}',\check{b}'-\check{b}-1,\check{b}'). \tag{2.18}$$

To avoid the production of physically impossible polymers, the PDF must be zero for $\check{k}<1$ and $\check{b}>\check{k}-1$. The symmetry then implies that the fragment distribution function is also zero for $\check{k}>\check{k}'-1$ and $\check{b}'-\check{b}>\check{k}'-\check{k}$. The production rate and normalizing condition are

$$\check{B}_\bullet(t,\check{k},\check{b}) = 2 \cdot \sum_{\check{k}'=\check{k}+1}^{\infty} \sum_{\check{b}'=\check{b}+1}^{\check{k}'-\check{k}+\check{b}} \check{\gamma}_\bullet(\check{k},\check{k}',\check{b},\check{b}') \cdot \check{D}_\bullet(t,\check{k}',\check{b}') \tag{2.19}$$

$$1 = \sum_{\check{b}=0}^{\check{b}'-1} \sum_{\check{k}=\check{b}+1}^{\check{k}'-\check{b}'+\check{b}} \check{\gamma}_\bullet(\check{k},\check{k}',\check{b},\check{b}'). \tag{2.20}$$

The necessary condition for attack on branching bonds is that a branching bond is present: $\check{b}' \geq 1$. If one (closely) compares the normalization condition for hydrolysis of linear and branched bonds, one sees that the upper limits of summation are different which will have an effect in the following section.

2.4.3 Product Distribution Function

The reaction rates for all enzymes are described in Section 2.5. For a complete model specification the PDFs have to be provided. The PDFs strongly vary for the different mechanisms. The different

forms of the PDF are discussed in this section, except for the one derived from the subsite theory (see Section 2.6). The PDFs discussed here are the blue part in Figure 2.1.

Product distribution function for random-chain scission Random-chain scission (RCS) is an abstraction of an important mechanism in depolymerization. It is often used to model thermal [63, 79, 133] and by endo-active enzymes catalyzed [44, 48, 67, 68] degradation of polymers. Here, RCS implies that every linear bond has the same probability of being cleaved. It follows that the PDF is uniform with respect to the product size (i.e., RCS). This behavior implies that the PDF has a constant value for a given polymer size and physically possible fragment polymers:

$$\gamma_{RCS}(k,k',b,b') = f_{RCS}(k',b') \cdot H(k'-1-k) \cdot H(b-b'+k'-1-k) \cdot H(k-1) \cdot H(k-1-b), \tag{2.21}$$

where H is the Heaviside function

$$H(x) = \begin{cases} 1 & x \geq 0 \\ 0 & x < 0 \end{cases}. \tag{2.22}$$

Because the fragment distribution function is normalized (see Equation (2.17)), the value of $f_{RCS}(k',b')$ can be readily obtained for the discretely represented branched polymer:

$$\breve{f}_{RCS}(\breve{k}',\breve{b}') = \frac{1}{(\breve{b}'+1) \cdot (\breve{k}'-\breve{b}'-1)}. \tag{2.23}$$

The linear case can easily be obtained from the branched case as the special case of $\breve{b}' = 0$. For the continuous representation Equations (A.13) and the mixed continuous-discrete representation Equation (A.15) is used

$$\bar{f}_{RCS}(\bar{k}',\bar{b}') = \frac{1}{\bar{b}' \cdot (\bar{k}'-\bar{b}'-2)} \tag{2.24}$$

$$\hat{f}_{RCS}(\bar{k}',\breve{b}') = \frac{1}{(\breve{b}'+1) \cdot (\bar{k}'-\breve{b}'-2)}. \tag{2.25}$$

There is a difference in the PDF for a discretely and continuously represented polymer. However, this difference is only important for polymers with a low amount of branching bonds and with small difference between the amount of monomer units and branching bonds. The birth terms due to RCS for a discretely and continuously represented branched polymer can then be written as follows (see Appendix A.2 for the remaining equations):

$$\breve{B}_{RCS}(t,\breve{k},\breve{b}) = 2 \cdot \sum_{\breve{k}'=\breve{k}+1}^{\infty} \sum_{\breve{b}'=\breve{b}}^{\breve{b}+\breve{k}'-\breve{k}-1} \frac{\breve{D}_{RCS}(t,\breve{k}',\breve{b}')}{(\breve{b}'+1) \cdot (\breve{k}'-\breve{b}'-1)} \tag{2.26}$$

$$\bar{B}_{RCS}(t,\bar{k},\bar{b}) = 2 \cdot \int_{\bar{k}+1}^{\infty} \int_{\bar{b}}^{\bar{b}+\bar{k}'-\bar{k}-1} \frac{\bar{D}_{RCS}(t,\bar{k}',\bar{b}')}{\bar{b}' \cdot (\bar{k}'-\bar{b}'-2)} \, \mathrm{d}\bar{b}' \, \mathrm{d}\bar{k}' \tag{2.27}$$

Product distribution function for random-debranching scission If the enzymes hydrolyzes a random branching bond, one has random scission of branching bonds called Random-debranching scission (RDS). Again, the PDF has a constant value for a given polymer size and physically possible fragment polymers:

$$\gamma_{RDS}(k,k',b,b') = f_{RDS}(k',b') \cdot H(k-1-b) \cdot H(k'-1-k) \cdot H(k-1) \cdot H(b-b'+k'-k). \tag{2.28}$$

Due to normalization (see Equation (2.20)), f_{RDS} is obtained as follows:

$$\breve{f}_{RDS}(\breve{k}',\breve{b}') = \frac{1}{\breve{b}' \cdot (\breve{k}'-\breve{b}')}. \tag{2.29}$$

The birth term due to RDS is as follows:

$$\breve{B}_{RDS}(t,\breve{k},\breve{b}) = 2 \cdot \sum_{\breve{k}'=\breve{k}+1}^{\infty} \sum_{\breve{b}'=\breve{b}+1}^{\breve{b}+\breve{k}'-\breve{k}} \frac{\breve{D}_{RDS}(\breve{k}',\breve{b}',t)}{\breve{b}' \cdot (\breve{k}'-\breve{b}')}. \tag{2.30}$$

Note that the limits of summation and integration are different than those of RCS. Again slightly different PDFs are obtained depending on the representation.

Production distribution function for end-chain scission End-chain scission (ECS) is a common model for thermal [63, 201] and by exo-active enzymes catalyzed [34, 44, 48, 67, 68] degradation. The mechanisms describes that a smaller fragment is released from the end of the attacked polymer. Glucoamylase is generally [48, 147] considered to scissor aways one monomer unit. Whereas β-amylase [34] and β-glucosidase (EC 3.2.1.21) [44, 67, 68] are generally held to scissor away the dimer unit. The mechanisms is abbreviated as $ECS_{\breve{a}}$ where $\breve{a}$ is the amount of monomer units of the released small polymer. If no index is used, the release of monomer unit ($\breve{a}=1$) is meant. The PDF is therefore given as follows

$$\gamma_{ECS,\breve{a}}(k,k',b,b') = \frac{1}{2} \cdot \delta(k',k+\breve{a}) \cdot \delta(b,b') + \frac{1}{2}\delta(k,\breve{a}) \cdot \delta(b,0), \tag{2.31}$$

where for discrete inputs δ is the Kronecker delta[2] and for continuous $\delta(x,y) = \bar{\delta}(x-y)$, where $\bar{\delta}$ is the Dirac delta function. The birth of polymers is given by:

$$\breve{B}_{ECS,\breve{a}}(t,\breve{k},\breve{b}) = \breve{D}_{ECS,\breve{a}}(t,\breve{k}+\breve{a},\breve{b}) + \delta(\breve{k},\breve{a}) \cdot \delta(\breve{b},0) \cdot \sum_{\breve{k}'=1+\breve{a}}^{\infty} \sum_{\breve{b}'=0}^{\breve{k}'-1-\breve{a}} \breve{D}_{ECS}(t,\breve{k}',\breve{b}'). \tag{2.32}$$

[2]The Kronecker delta is defined as $\delta(x,y) = \begin{cases} 1 & x=y \\ 0 & \text{otherwise} \end{cases}$. Normally, it is written as $\delta_{x,y}$. However, in this work this usage would be cumbersome.

Production distribution function for random scission of inner monomer units The result of Subsite Theory (see Section 2.6) can be best explained, if one also considers a mechanisms that only attacks the inner monomer units of a linear polymer and attack those with uniform probability. A monomer unit is counted as an inner monomer unit if it is at least $\check{k}'' - 1$ monomer away from the end. The product distribution and the birth term are

$$\check{\gamma}_{\text{inner},\check{k}''}(\check{k},\check{k}') = \frac{1}{\check{k}' - 2\cdot\check{k}'' + 1} \cdot H(\check{k} - \check{k}'') \cdot H(\check{k}' - \check{k} - \check{k}'') \tag{2.33}$$

$$\check{B}_{\text{inner},\check{k}''}(t,\check{k}) = 2 \cdot \sum_{\check{k}'=\check{k}+\check{k}''}^{\infty} \frac{\check{D}_{\text{inner},\check{k}''}(t,\check{k})}{\check{k}' - 2\cdot\check{k}'' + 1}. \tag{2.34}$$

Product distribution function for random scission of inner chains If random scission of a linear bond of an inner chain is performed, the small polymer has at least $\check{k}''$ monomer units and at least one branching bond. Accordingly, the PDF and birth term are

$$\begin{aligned}\check{\gamma}_{\text{inner},\check{k}''}(\check{k},\check{k}',\check{b},\check{b}') =& H(\check{b}-1)\cdot H(\check{b}'-1-\check{b})\cdot H(\check{k}-\check{k}'')\cdot H(\check{k}'-\check{k}-\check{k}'')\cdot H(\check{k}-1-\check{b}) \\ &\cdot H(\check{k}'-\check{k}-1-\check{b}'+\check{b})\cdot \begin{cases} \frac{1}{(\check{b}'-1)\cdot(\check{k}'-\check{b}'-1)-(\check{k}''-1)\cdot(\check{k}''-2)} & \check{b}' \geq \check{k}'' \\ \frac{1}{(\check{b}'-1)\cdot(\check{k}'-2\cdot\check{k}''+1)} & \check{b}' < \check{k}'' \end{cases}\end{aligned} \tag{2.35}$$

$$\check{B}_{\text{inner},\check{k}''}(t,\check{k},\check{b}) = 2\cdot H(\check{b}-1)\cdot H(\check{k}-\check{k}'')\cdot \sum_{\check{k}'=\check{k}+\check{k}''}^{\infty} \sum_{\check{b}'=\check{b}+1}^{\check{b}+\check{k}'-\check{k}-1} \check{D}_{\text{inner},\check{k}''}(t,\check{k},\check{b})\cdot\check{\gamma}_{\text{inner},\check{k}''}(\check{k},\check{k}',\check{b},\check{b}') \tag{2.36}$$

2.5 Reaction rate

As only Glycosidases are considered the reaction rate on the polymers is the hydrolysis rate. Furthermore, the enzymes themselves undergo a irreversible denaturation reaction.

2.5.1 Michaelis-Menten kinetics

Michaelis and Menten [202] (see [203] for a translation into English and current usage of terminology) have postulated a reaction mechanism that is nowadays generally used for enzymatically catalyzed reactions. It comprises out of the formation of an enzyme-substrate complex that can either decay back into enzyme and substrate or react to products and enzyme. One can formulate this reaction mechanism for the hydrolysis of a polymer $S_{\check{k}',\check{b}'}$, with the concentration $\check{n}$, by the enzyme E.

$$E \;+\; S_{\check{k}',\check{b}'} \underset{k_{-1,\check{k}',\check{b}'}}{\overset{k_{+1,\check{k}',\check{b}'}}{\rightleftarrows}} ES_{\check{k}',\check{b}'} \xrightarrow{k_{cat,\check{k}',\check{b}'}} E \;+\; \textstyle\sum_{\check{k},\check{b}} 2\cdot\check{\gamma}(\check{k}',\check{b}',\check{k},\check{b})\cdot S_{\check{k},\check{b}}$$

Under the assumptions that the enzyme-substrate complex concentration is constant (quasi-steady state) and the enzyme concentration is negligible compared to the substrate concentration one can

obtain the hydrolysis rate

$$\check{D}(t,\check{k}',\check{b}') = \frac{k_{cat,\check{k}',\check{b}'}}{\check{K}_m(\check{k}',\check{b}')} \cdot E_\bullet \cdot \frac{\check{n}(\check{k}',\check{b}')}{1+\frac{\check{n}(\check{k}',\check{b}')}{\check{K}_m(\check{k}',\check{b}')}} \tag{2.37}$$

$$\check{K}_m(\check{k}',\check{b}') = \frac{k_{-1,\check{k}',\check{b}'} + k_{cat,\check{k}',\check{b}'}}{k_{+1,\check{k}',\check{b}'}}, \tag{2.38}$$

where $E_\bullet$ is the total active enzyme concentration. If there is more than one species of polymer presents, one obtains a competitively inhibited Michaelis-Menten kinetics

$$\check{D}(t,\check{k}',\check{b}') = \frac{k_{cat}(\check{k}',\check{b}')}{\check{K}_m(\check{k}',\check{b}')} \cdot E_\bullet \cdot \frac{\check{n}(\check{k}',\check{b}')}{1+\sum_{\check{k},\check{b}} \frac{\check{n}(\check{k},\check{b})}{\check{K}_m(\check{k},\check{b})}}. \tag{2.39}$$

The Michaelis constant $\check{K}_m(\check{k}',\check{b}')$ and the catalytic constant need to be determined which is also shown in Figure 2.1. This is done in Section 2.6. One can already see that the parametrization introduced by Michaelis and Menten [202] is not the most efficient parametrization. It is rather more convenient to define the specificity [204]

$$s_{cat}(\check{k}',\check{b}') = \frac{k_{cat}(\check{k}',\check{b}')}{\check{K}_m(\check{k}',\check{b}')} \tag{2.40}$$

and the inverse of the Michaelis constant

$$I(\check{k}',\check{b}') = \frac{1}{\check{K}_m(\check{k},\check{b})}. \tag{2.41}$$

This allows writing the Michaelis-Menten kinetics as

$$\check{D}(t,\check{k}',\check{b}') = \frac{s_{cat}(\check{k}',\check{b}') \cdot E_\bullet \check{n}(\check{k}',\check{b}')}{1+\sum_{\check{k},\check{b}} \check{n}(\check{k},\check{b}) \cdot \check{I}(\check{k},\check{b})}. \tag{2.42}$$

2.5.2 Simplified validation case

For validation, it is appropriate to start with a simplified model for the reaction. If the polymer concentration is very small compared to the Michaelis constant and the enzymes do not denature, a first order reaction results from Equation (2.42). However, as explained in Section 2.4 the reaction mechanisms have necessary conditions on the cleaved polymer, in order to produce only physically feasible polymer. Therefore, the reaction rates for validation are chosen as

$$D_{RCS/ECS}(t,k,b) = C_{RCS/ECS} \cdot H(k-2-b) \cdot n(t,k,b) \tag{2.43}$$

$$D_{RDS}(t,k,b) = C_{RDS} \cdot H(b-1) \cdot n(t,k,b). \tag{2.44}$$

This reaction rate is linear in the amount of polymers.

2.5.3 Equilibrium Model

The Michaelis-Menten kinetics includes denaturation and inactivation of enzymes by using the active amount of enzymes in the model without providing a model for it. The Equilibrium Model proposed by Daniel et al. [205] for non-polymeric reactions and validated by Daniel and Danson [206] for several enzymes including several Glucosidase enzymes (exoactive enzymes) provides a model for the enzyme denaturation rate and amount of inactive enzyme. For α-amylase (endoactive enzyme) the mechanism described by the Equilibrium Model has also been observed [207]. The extension to distributed polymers is quite straightforward and is given in this section. Therefore, it is appropriate to use this mechanism. The studied depolymerization scheme then features temperature dependent denaturation kinetics and an inactivation equilibrium:

$$\begin{array}{ccccc} E_{\bullet,den} & & & & \\ \uparrow k_{\bullet,inact} & & & & \\ E_{\bullet,in} & & & & \\ k_{\bullet,-3} \downarrow \uparrow k_{\bullet,+3} & & & & \\ E_{\bullet,act} & + & S(\breve{k}',\breve{b}') \underset{k_{\bullet,-1}(\breve{k}',\breve{b}')}{\overset{k_{\bullet,+1}(\breve{k}',\breve{b}')}{\rightleftarrows}} [E_{\bullet,act}S(\breve{k}',\breve{b}')] \xrightarrow{k_{\bullet,cat}(\breve{k}',\breve{b}')} & E_{\bullet,act} & + \sum_{\breve{k},\breve{b}} 2\cdot\breve{\gamma}(\breve{k}',\breve{k},\breve{b}',\breve{b})\cdot S(\breve{k},\breve{b}) \end{array}$$

The mechanism postulates that the active free enzyme $E_{\bullet,act}$ can either bind a polymer to form an enzyme-polymer complex $[E_{\bullet,act}S_i]$ or be inactivated to the enzyme form $E_{\bullet,inact}$. This inactive form can either fold back to the active form or it can be unfolded irreversibly into the denatured form $E_{\bullet,den}$. The polymer bound in the enzyme-polymer complex can either be released or it is hydrolyzed into two smaller polymers. Note that in the following the notation and equations from Daniel and Danson [208] are used which are extended to a polymeric substrate.

Reaction rate

As the mechanisms is similar to the Michaelis-Menten mechanisms one takes the same assumptions to obtain

$$\breve{D}_\bullet(t,\breve{k}',\breve{b}') = \frac{\breve{s}_{\bullet,cat}(\breve{k}',\breve{b}')\cdot E_\bullet(t)\cdot\breve{n}(t,\breve{k}',\breve{b}')}{1+K_{\bullet,eq}+\sum_{\breve{k},\breve{b}}\breve{n}(t,\breve{k},\breve{b})\cdot\breve{I}_\bullet(\breve{k},\breve{b})} \tag{2.45}$$

$$K_{\bullet,eq} = \frac{k_{\bullet,+3}}{k_{\bullet,-3}} = \frac{E_{\bullet,in}}{E_{\bullet,act}} \tag{2.46}$$

$$\breve{I}_\bullet(\breve{k},\breve{b}) = \frac{k_{\bullet,+1}(\breve{k}',\breve{b}')}{k_{\bullet,-1}(\breve{k}',\breve{b}')+k_{\bullet,cat}(\breve{k}',\breve{b}')} \tag{2.47}$$

$$\frac{\mathrm{d}E_\bullet}{\mathrm{d}t} = -\frac{\breve{k}_{\bullet,inact}\cdot E_\bullet(t)\cdot K_{\bullet,eq}}{1+K_{\bullet,eq}+\sum_{\breve{k},\breve{b}}\breve{n}(t,\breve{k},\breve{b})\cdot\breve{I}_\bullet(\breve{k},\breve{b})}. \tag{2.48}$$

If the denaturation rate is very high, the equation for the denaturation rate poses a numerical problem because the system of equations become stiff. However, by considering the evolution of the logarithm of the enzyme concentration one can remedy this stiffness. Furthermore, this also removes the problem that the enzyme concentration can become negative due to rounding issues

$$\frac{\mathrm{d}\log(E_\bullet)}{\mathrm{d}t} = -\frac{\breve{k}_{\bullet,inact}\cdot K_{\bullet,eq}}{1+K_{\bullet,eq}+\sum_{\breve{k},\breve{b}}\breve{n}(t,\breve{k},\breve{b})\cdot \breve{I}_\bullet(\breve{k},\breve{b})}. \tag{2.49}$$

This equation for the denaturation rate is a part of the model (see Fig. 2.1).

Temperature dependence

The essence of a potentially optimal temperature profile is the strong dependence of the enzymatic process on temperature. Accordingly, this has to be modeled which is called Equilibrium Model in Figure 2.1. The ratio of $E_{\bullet,in}$ to $E_{\bullet,act}$ is

$$\frac{E_{\bullet,in}}{E_{\bullet,act}} = K_{\bullet,eq} = \exp\left(\frac{\Delta H_{\bullet,eq}}{R}\cdot\left(\frac{1}{T_{\bullet,eq}}-\frac{1}{T}\right)\right), \tag{2.50}$$

where $\Delta H_{\bullet,eq}$ is the enthalpy difference between the active and inactive enzyme form, T the absolute temperature, R is the universal gas constant, and $T_{\bullet,eq}$ is defined as the temperature where the active and reversible inactive form have equal concentrations ($K_{\bullet,eq}(T_{\bullet,eq}) = 1$). The Michaelis constant is assumed to follow an Arrhenius temperature dependence

$$I_{\bullet,i} = I_{\bullet,i}(T_{ref})\cdot\exp\left(\frac{\Delta H_m}{R}\cdot\left(\frac{1}{T_{ref}}-\frac{1}{T}\right)\right), \tag{2.51}$$

where $K_{\bullet,m,i}(T_{ref})$ is the Michaelis constant of a polymer of chain length i at the reference temperature T_{ref} and ΔH_m is the enthalpy of substrate binding. The rate constant of inactivation is

$$k_{\bullet,inact} = \frac{k_B\cdot T}{h}\cdot\exp\left(-\frac{\Delta G^{\ddagger}_{\bullet,inact}}{R\cdot T}\right), \tag{2.52}$$

where k_B is the Boltzmann constant, h is Planck's constant, and $\Delta G^{\ddagger}_{\bullet,inact}$ the activation energy of the inactivation step. The catalytic constant for a polymer of chain length i is

$$k_{\bullet,cat} = k_{\bullet,cat,i}(T_{ref})\cdot\frac{T}{T_{ref}}\cdot\exp\left(-\frac{\Delta G^{\ddagger}_{\bullet,cat}}{R}\cdot\left(\frac{1}{T}-\frac{1}{T_{ref}}\right)\right), \tag{2.53}$$

where $\Delta G^{\ddagger}_{\bullet,cat}$ is the activation energy of the hydrolysis. This leads to

$$s_{\bullet,cat} = s_{\bullet,cat,i}(T_{ref})\cdot\frac{T}{T_{ref}}\cdot\exp\left(\frac{\Delta H_m-\Delta G^{\ddagger}_{\bullet,cat}}{R}\cdot\left(\frac{1}{T}-\frac{1}{T_{ref}}\right)\right). \tag{2.54}$$

The temperature dependencies given by the above rate or equilibrium equations yield a reaction rate that first increases for increasing temperature. However, the equilibrium shifts to the inactivated form of the enzyme, which causes the reaction rate to decrease above a critical temperature. Furthermore, the denaturation rate increases with temperature due the equilibrium shift and the increase in the denaturation constant.

2.6 Subsite Theory

One approach to describe the hydrolysis of linear short-chained glycosidic connected polymers is the Subsite Theory. Development was started in the 60s [209] to explain the strong dependence of Michaelis constant and maximal reaction rate on the chain length of the polymers. Furthermore, it was developed to explain preferential scission. It has been applied successfully to endo-active [210–212] as well as exo-active [28, 213, 214] enzymes. All of the mentioned studies also estimated the parameters for their specific enzymes. First the theory is reviewed for linear polymers and then extended to branched polymer. Refer to Figure 2.1 to see what this model provides.

2.6.1 Linear polymer

The Subsite Theory [28] postulates that the active site of an enzyme consists of several subsites, which are responsible for binding the substrate, and one catalytic site which is responsible for hydrolyzing the bond. This is consistent with visualization of 3D structures of enzymes [212]. Each monomer unit can only bind to one subsite and each subsite can only bind one monomer unit. This binding is reversible.

Definitions and assumptions

For ease of discussion, the subsites are numbered (note that other numberings are sometimes used in literature): The first subsite gets the number 1. There are $\check{z}$ subsites and the catalytic center lies between subsite $\check{z}_-$ and $\check{z}_- + 1$. The number of subsites above the catalytic center defines $\check{z}_+$. Furthermore, the monomer units of the polymer are indexed with the reducing end having the number 1 and the non-reducing end assigned to the number $\check{k}'$. $\check{s}$ is defined as the index of the monomer unit which occupies the subsite 1.
The polymer has to occupy contiguous subsites. This means that, if subsite 3 and 5 are occupied, subsite 4 needs to be occupied. Furthermore, the polymer is oriented in such a way that the index of the monomer unit decreases with the subsite number. This means that if monomer unit 7 occupies subsite 3 then monomer unit 8 occupies subsite 2 and not 4. Additionally, the polymer cannot leave the active site of the enzyme. This means that, if monomer unit 2 occupies subsite 3, subsite 2 can only be empty if the polymer has only two monomer units [28].

Reaction mechanism

All this assumptions together allow the formulation of the reaction mechanism:

$$E \;+\; S_{\check{s},\check{k}'} \underset{k_{-1,\check{s},\check{k}'}}{\overset{k_{+1,\check{s},\check{k}'}}{\rightleftarrows}} ES_{\check{s},\check{k}'} \xrightarrow{k_{+2,\check{s},\check{k}'}} E \;+\; S_{\check{k}'-\check{k}} \;+\; S_{\check{k}}$$

For each polymer many bindings are possible. Precisely, the binding modes $\check{s} \in [1, \check{z} + \check{k}' - 1]$ are possible. Furthermore, because the bond at the catalytic center is hydrolyzed one can specify $\check{k} = \check{s} - \check{z}_- - 1$. It follows trivially that the catalytic constants is only different from zero if the catalytic center is occupied. This is the case if $\check{s} \in [\check{z}_{-1} + 1, \check{z}_- + \check{k} - 1]$.

Hydrolysis rate

The reaction mechanism describes a reaction of Michaelis-Menten type. Accordingly, each binding mode can be described with the following equation, if quasi-steady state is assumed and the enzyme concentration is sufficiently low

$$D_{\check{s},\check{k}'} = (k_{+2,\check{s},\check{k}'} \cdot I_{\check{s},\check{k}'}) \frac{E_\bullet \cdot \check{n}(\check{k})}{1 + \check{n}(\check{k}) \cdot \sum_{i=1}^{\check{k}'+\check{z}-1} I_{i,\check{k}'}} \tag{2.55}$$

$$I_{i,\check{k}'} = \frac{k_{+1,\check{s},\check{k}'}}{k_{-1,\check{s},\check{k}'} + k_{+2,\check{s},\check{k}'}}. \tag{2.56}$$

This equation for each mode is quite inconvenient and one desires one equation for each amount of monomer unit. By summing up the hydrolysis over all productive modes one obtains this equation which is of Michaelis-Menten type:

$$D(\check{k}') = \frac{\check{s}_{cat}(\check{k}') \cdot \check{n}(\check{k}) \cdot E_\bullet}{1 + \check{n}(\check{k}) \cdot \check{I}(\check{k}')} \tag{2.57}$$

$$\check{I}(\check{k}') = \sum_{\check{s}=1}^{\check{k}'+\check{z}-1} \check{I}_{\check{s},\check{k}'} \tag{2.58}$$

$$\check{s}_{cat}(\check{k}') = k_{cat}(\check{k}') \cdot \check{I}(\check{k}') = \sum_{\check{s}=\check{z}_-+1}^{\check{k}'+\check{z}_- -1} k_{+2,\check{s},\check{k}'} \cdot I_{\check{s},\check{k}'}. \tag{2.59}$$

Microscopic constants

In the Subsite Theory it is assumed that the subsites do not further interact with each other. The association constant $\check{K}'_{\check{s},\check{k}'}$, which describes how strongly a polymer with $\check{k}'$ monomer units binds to the

enzyme in position $\check{s}$, is then given by

$$\Delta G_{\text{mixing}} + \sum_{i=\check{s}-\check{k}'+1}^{\check{s}} \Delta G_i = -R \cdot T \cdot \ln(\check{K}'_{\check{s},\check{k}'}), \tag{2.60}$$

where the cratic free energy of mixing ΔG_{mixing} is the contribution of the solvent to the binding energy

$$\Delta G_{\text{mixing}} = R \cdot T \cdot \ln 55.51, \tag{2.61}$$

where $x = 55.51$ is a physical constant of water [215, ch.5]. The unitary free energy of binding ΔG_i is the contribution of the binding of the polymer to subsite i to the binding energy. This contribution is zero for imaginary subsites ($i < 0$ or $i > \check{z}_+ + \check{z}_-$). Under the assumption that the hydrolysis of the bond is much slower than the binding of the polymer (assumption of fast equilibrium) the Michealis constant for each binding mode $K_{m,\check{s},\check{k}'}$ is equal to the inverse of the association constant for this binding mode. An alternative way of stating this is to say that the inverse of the Michaelis constant for each binding mode $\check{I}_{\check{s},\check{k}'}$ is equal to the association constant for this binding mode $\check{K}'_{\check{s},\check{k}'}$

$$\check{K}'_{\check{s},\check{k}'} \approx \check{I}_{\check{s},\check{k}'}. \tag{2.62}$$

In the standard Subsite Theory $k_{+2,\check{s},\check{k}'}$ would be only temperature dependent and the equation above would be fully specified. However, some authors [125, 216] have found that the Subsite Theory cannot describe the hydrolysis by all enzymes. They have introduced an *ad hoc* strain to allow for interaction between subsites. It is assumed that the binding of a substrate monomer unit lowers the activation-energy barrier by a constant amount. This constant amount ΔG_a is called the acceleration factor.

$$\check{k}_{+2,\check{s},\check{k}'} = \begin{cases} C(T) \cdot \exp\left(\sum_{i=\check{s}-\check{k}'+1}^{\check{s}} \frac{\Delta G_a}{R \cdot T} \cdot H(i-1) \cdot H(\check{z}_+ + \check{z}_- - i)\right) & \check{z}_- + 1 \leq \check{s} \leq \check{z}_- + \check{k}' - 1 \\ 0 & \text{otherwise} \end{cases} \tag{2.63}$$

The proportionality factor C is a product of the temperature dependent catalytic constant and the time and temperature dependent concentration of active enzyme. Both of which can be described using the Equilibrium Model. If the acceleration factor is set to zero, the standard Subsite Theory is obtained again. Nevertheless, the specificity of the enzyme can be computed.

Product distribution function

If the polymer of length $\check{k}'$ is hydrolyzed while in position $\check{k} + \check{z}_- + 1$, two polymers one with $\check{k}$ monomer units and another with $\check{k}' - \check{k}$ monomer units are produced. The polymer of length $\check{k}$ is also produced from position $\check{k}' - \check{k} + \check{z}_- + 1$. By summing up the production rate due to this two positions and division by the total production rate, the PDF is obtained

$$\check{\gamma}(\check{k}, \check{k}') = \frac{1}{2 \cdot \check{s}_{cat}(\check{k}')} \cdot \left(\check{k}_{+2,\check{k}+\check{z}_-+1,\check{k}'} \cdot \check{I}_{\check{k}+\check{z}_-+1,\check{k}'} + \check{k}_{+2,\check{k}'-\check{k}+\check{z}_-+1,\check{k}'} \cdot \check{I}_{\check{k}'-\check{k}+\check{z}_-+1,\check{k}'}\right). \tag{2.64}$$

Simplification for sufficiently large polymer

For polymers with more monomer units than there are subsites one can simplify the equations because the binding modes that occupy all bindings sites have the same affinity $\breve{K}'_{int}$ and the same catalytic constant $\breve{k}_{+2,\max}$

$$\breve{K}'_{int} = \exp\left(-\frac{\Delta G_{\text{mixing}}}{R\cdot T} - \frac{\sum_{i=1}^{\breve{z}_+ + \breve{z}_-}\Delta G_i}{R\cdot T}\right) \approx \breve{I}_{int} \tag{2.65}$$

$$\breve{k}_{+2,\max} = C\cdot\exp\left(\frac{(\breve{z}_+ + \breve{z}_-)\cdot\Delta G_a}{R\cdot T}\right) \tag{2.66}$$

$$\breve{I}(\breve{k}') = (\breve{k}' - \breve{z})\cdot\breve{I}_{int} + \sum_{\breve{s}=1}^{2\cdot\breve{z}-1}\breve{K}'_{\breve{s},\breve{z}} \tag{2.67}$$

$$\frac{\breve{k}_{cat}(\breve{k}')}{\breve{K}_m(\breve{k}')} = \breve{k}_{+2,\max}\cdot(\breve{k}' - \breve{z})\cdot\breve{K}'_{int} + \sum_{\breve{s}=\breve{z}_{-1}+1}^{\breve{z}+\breve{z}_- -1}\breve{k}_{+2,\breve{s},\breve{z}}\cdot\breve{I}_{\breve{s},\breve{z}}. \tag{2.68}$$

If the polymer has more than $2\cdot\max(\breve{z}_-,\breve{z}_+)$ monomer units, the product distribution can be expressed as a weighted sum of ECS and random scission on inner monomers

$$\begin{aligned}\breve{\gamma}(\breve{k},\breve{k}') = \frac{1}{\breve{s}_{cat}(\breve{k}')}\Bigg[&\breve{k}_{+2,\max}\cdot\breve{I}_{int}\cdot(\breve{k}' - 2\cdot\max(\breve{z}_-,\breve{z}_+)+1)\cdot\breve{\gamma}_{\text{inner},\max(\breve{z}_-,\breve{z}_+)}(\breve{k},\breve{k}') \\ &+ \sum_{\breve{k}''=1}^{\max(\breve{z}_-,\breve{z}_+)-1}\frac{\breve{k}_{+2,\breve{k}''+\breve{z}_-,\breve{z}}\breve{I}_{\breve{k}''+\breve{z}_-,\breve{z}} + \breve{k}_{+2,\breve{z}_++2\cdot\breve{z}_- -\breve{k}'',\breve{z}}\breve{I}_{\breve{z}_++2\cdot\breve{z}_- -\breve{k}'',\breve{z}}}{2}\cdot\breve{\gamma}_{ECS,\breve{k}''}(\breve{k},\breve{k}')\Bigg]\end{aligned} \tag{2.69}$$

Parameter estimation

The estimation of the binding energies ΔG_i, the acceleration factor ΔG_a, and the proportionality constant C between catalytic constant and the reaction rate was studied by Allen and Thoma [216] who found that given the likelihood of cleavage of a bond, Michealis constants, and the maximal reaction rates the parameters could be well estimated. The likelihood of cleavage of a bond can be obtained by letting the enzyme cleave a radioactive labeled polymer of a certain chain length for a short time followed by chromatography separation of the products [217]. The Michaelis constants and catalytic rates are obtained by letting the enzymes act for a short time on a polymer of a certain chain length and measuring the increase in polymer concentration. By performing repeated experiments at different concentration one can then apply the standard Lineweaver-Burk method to obtain the Michealis constant and the maximal reaction rate from the initial reaction rate [217].

2.6.2 Extension to branched polymer

Marchal et al. [33] have extended the Subsite Theory for α-amylase to amlyopectin. However, their model required a detailed structure of amylopectin, which was created using a Monte Carlo algorithm

[189], and had to be solved using a kinetic Monte Carlo (kMC) technique. This model was found to have to satisfactory agreement with experimental data by Marchal et al. [33] and Besselink et al. [32]. Because the detailed polymer structure is not available using PBM, the model has to be adapted. A schematic drawing of this model is shown in Figure 2.3.

Monte Carlo model

The model postulated by Marchal et al. [33] assumes that the binding of the enzyme to the polymer is not influenced by the branching bonds. Thereby, they neglect effects of the tertiary structure of the polymer and different length and orientations of branching bonds. However, it has been experimentally observed that α-amylase cannot attack close to a branching bond and the hydrolysis rate decreases close to a branching bond [218]. The model handles this by multiplying the catalytic constant with an inhibition factor k_{br} between 0 and 1. Only branching bonds removed less than 4 glucose units from the catalytic center can inhibit the hydrolysis. Branching bonds that are further away, have a inhibition factor of 1. An exponential relation between the inhibition and the distance y to the branching bond is assumed

$$k_{br}(\check{y}) = \begin{cases} \min(1, \exp(b \cdot \check{y}) - 1) & \check{y} \leq 4 \\ 1 & \check{y} > 4. \end{cases} . \tag{2.70}$$

$b \in [0, \ln(2)]$ is a parameter that describes the strength of inhibition. Marchal et al. [33] tried several values of this parameters and choose the value which resulted in the best fit to experimental data. The index T indicated which type of inhibition is considered. There are three types of inhibition:

I Inhibition on a newly started side chain due to the branching bond starting the chain.

II Inhibition on any other branching bond towards the reducing end.

III Inhibition on any other branching bond towards the non-reducing end.

The catalytic constant is multiplied with the inhibition factor due to each inhibition.

Modeling the structure of starch

The chosen population balance model does not have the ability to represent the chain length distribution. Therefore, it is assumed that every chain has the average chain length $\bar{c} = \frac{\check{k}}{2 \cdot \check{b}+1}$. As the PBM does not provide the detailed structure, one does not know whether an arbitrary chosen end-chain has started at the last branching point. Accordingly, one does not know which inhibition to select. Here, it is assumed that every end-chain has started newly and can be described with inhibition I. This also neglects the one end-chain carrying the reducing end. However, this can be included, but is not thought to be necessary because it is only one chain.

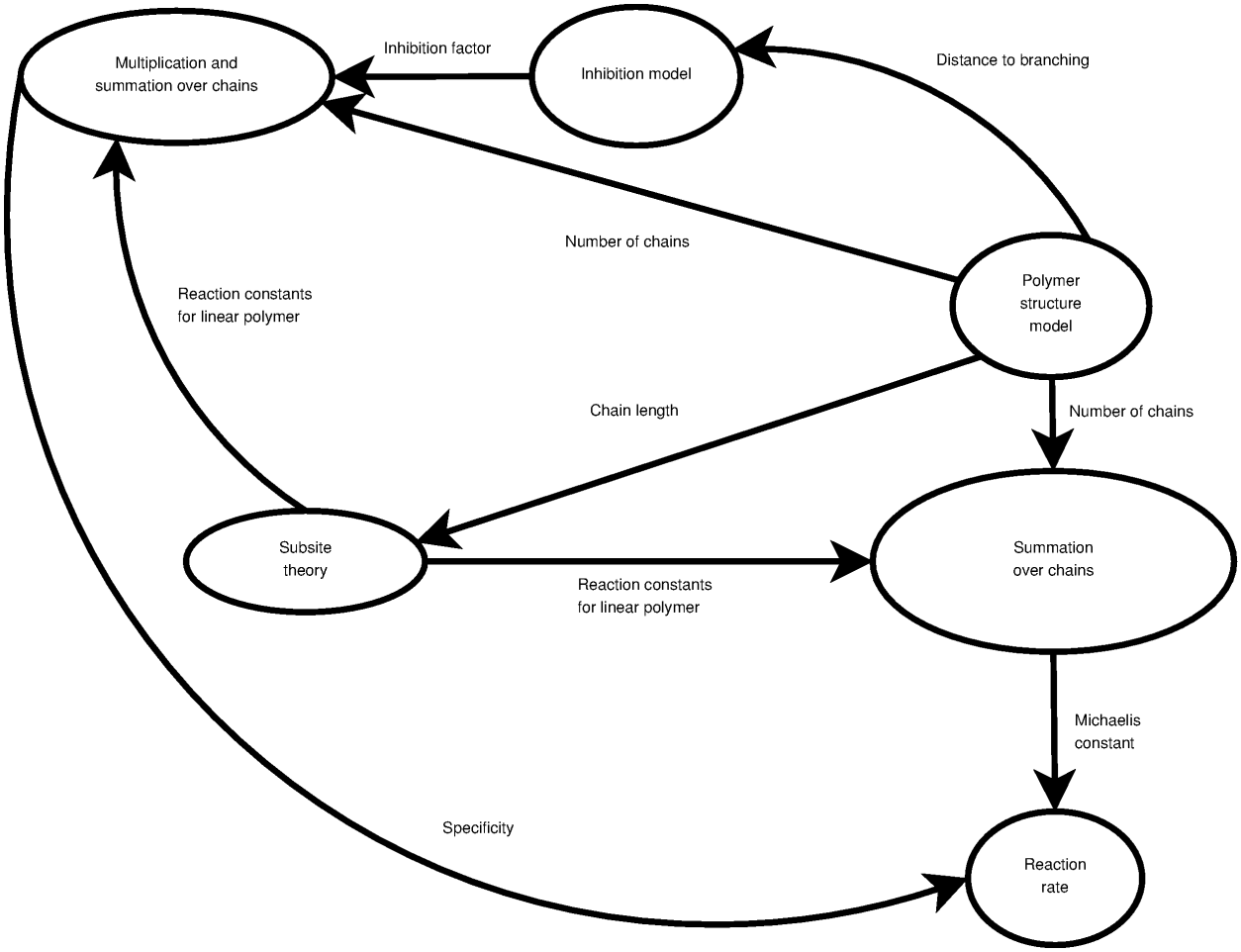

Figure 2.3: Schematic drawing of the model for branched polymer. The arrows indicated with information is provided.

Hydrolysis of branched polymer

If the hydrolysis of the bond is much slower than the binding and unbinding of the polymer, the inverse of the Michaelis parameter $\check{I}(\check{k},\check{b})$ can be obtained by summing up the affinities

$$\check{I}(\check{k},\check{b}) = (\check{b}+2)\cdot\check{I}_{\text{end}}(\bar{c}) + (\check{b}-1)\cdot\check{I}_{\text{inner}}(\bar{c}), \tag{2.71}$$

where $\check{I}_{\text{end}}$ is the affinity and inverse Michaelis constant of one end chain and $\check{I}_{\text{inner}}$ the affinity and inverse Michaelis constant of one inner chain. The effective specificity $\check{s}_{cat}$

$$\check{s}_{cat}(\check{k},\check{b}) = (\check{b}+2)\cdot\check{s}_{cat,end}(\bar{c}) + (\check{b}-1)\cdot\check{s}_{cat,inner}(\bar{c}), \tag{2.72}$$

where $\check{s}_{cat,end}$ and $\check{s}_{cat,inner}$ are the effective specificities of one end chain and, respectively, one inner chain.

The average chain length is not necessarily an integer, but the Subsite Theory and the extension demand integer amount of monomers. Therefore, all computations demanding integers as input are evaluated at the two neighboring integers and the value is obtained by interpolation between these two values. Accordingly, a function f is evaluated by

$$f(\bar{c}) = (\lceil c\rceil - c)\cdot f(\lfloor c\rfloor) + (c-\lfloor c\rfloor)\cdot f(\lceil c\rceil). \tag{2.73}$$

Hydrolysis of end chains The affinity of an end chain $\check{I}_{\text{end}}$ is obtained by summing up the affinity of unproductive bindings and productive bindings

$$\check{I}_{\text{end}}(\check{c}) = \sum_{i=1}^{\min(\check{z}_+,\check{c})} \check{I}_{\check{z},i} + \sum_{i=1}^{\check{c}} \check{I}_{\check{z},i+\check{z}_+}. \tag{2.74}$$

In this computation it it assumed that every end chain ends on a non-reducing end which implies that the enzyme is always oriented with the subsite with the lowest number towards the end of the chain. Furthermore, it is assumed that there are sufficiently many monomer units after the branching bond that the subsites after the branching bonds are always occupied. The effective specificity of one inner chain is

$$\check{s}_{cat,end}(\bar{c}) = \sum_{i=1}^{\check{c}} k_{br,I}(\check{c}+1-i)\cdot\check{k}_{+2,\check{z},i+\check{z}_+}\cdot\check{I}_{\check{z},i+\check{z}_+}. \tag{2.75}$$

Hydrolysis of inner chains It is assumed that every subsite of the enzyme is occupied during a binding to an inner chain. This assumption leads to an underestimation of the Michaelis constant of the branched polymers. The affinity of each is therefore $\check{I}_{int}$ and the uninhibited catalytic constant $\check{k}_{+2,\max}$. The affinity of one inner chain is then

$$\check{I}_{\text{inner}}(\bar{c}) = \check{I}_{int}\cdot\bar{c}. \tag{2.76}$$

The effective specificity can be easily computed by

$$\check{s}_{cat,inner}(\check{c}) = \check{k}_{+2,\max} \cdot \check{I}_{int} \cdot \sum_{i=1}^{\check{c}} k_{br,II}(i) \cdot k_{br,III}(\check{c}+1-i). \tag{2.77}$$

Product distribution function The enzyme is assumed to perform random scission on the inner chains. It is more likely that more monomer units than belonging to two end chains are scissored aways. Therefore, the assumption of random scission is not strictly speaking correct, but this is neglected here.

Chapter 3

Solving the Population Balance Equation using the Direct Quadrature Method Of Moments

The Population Balance Equation (PBE) formulated in the previous chapter needs to be solved. Because an analytical solution is not possible, the PBE has to be solved numerically. In order for the model to be useful for optimization the solution technique needs to be efficient. A promising candidate for an efficient solution technique is the Direct Quadrature Method of Moments (DQMOM). In this chapter first the theory for the DQMOM is explained. The DQMOM is applied to the depolymerization of linear polymers in order to investigate the appropriateness of the method and to introduce all concepts. Afterwards, the DQMOM is applied to the depolymerization of branched polymer. Last, a short conclusion is drawn.

3.1 Direct Quadrature Method Of Moments

Instead of solving the PBE to obtain the Number Density Function (NDF), the Method Of Moments (MOM) solves the evolution equation for the moments of the NDF. Then with the Quadrature Method of Moments (QMOM) and DQMOM a closure rule is used to reconstruct the NDF from the moments. This approximation of the NDF is then used to compute all terms in the evolution equation for the moments. Here, first the monovariate and then the bivariate DQMOM is explained.

3.1.1 Monovariate Population Balance Equation

Even though all functions can be used to obtain scalar values from a NDF [89], typically monomials of the internal coordinates are used to generate the moments. The moments used in the work are of the form:

$$\bar{\mu}^i(t) = \int_1^\infty \bar{k}^i \bar{n}(t,k)\,\mathrm{d}\bar{k}, \tag{3.1}$$

where $i \in \mathbb{N}_0 : i \leq 2 \cdot N - 1$ is the order of the moment and N is the number of quadrature points. The number of quadrature points is proportional to the quadrature order [106]. Here, two moments have a clear physical meaning: The zeroth order moment ($i = 0$) is the total amount of polymers and the first order moment ($i = 1$) is the total amount of monomer units.
Taking the moments of the PBE Equation (A.2) yields the equation for the evolution of the moments as follows:

$$\frac{\mathrm{d}\bar{\mu}^i}{\mathrm{d}t} = -\bar{\omega}^i_{\sum} + \bar{\alpha}^i_{\sum}, \tag{3.2}$$

where $\bar{\omega}^i_{\sum}$ and $\bar{\alpha}^i_{\sum}$ are the i-th moments of the death and birth term, respectively:

$$\bar{\omega}^i_{\sum} = \int_1^{\infty} \bar{k}^i \cdot \bar{D}_{\sum}(t,\bar{k})\,\mathrm{d}\bar{k} \tag{3.3}$$

$$\bar{\alpha}^i_{\sum} = \int_1^{\infty} \bar{k}^i \cdot \bar{B}_{\sum}(t,\bar{k})\,\mathrm{d}\bar{k}. \tag{3.4}$$

The moments of the death and birth term can, generally, not be expressed as a function of the moments solved for. Thus, the system of Ordinary Differential Equations (ODEs) is not closed. Accordingly, closure is required. QMOM provides closure by using a quadrature rule [90]. This approximates the NDF as a sum of Dirac deltas:

$$\bar{n}(t,\bar{k}) = \sum_{l=1}^{N} \bar{w}_l(t) \cdot \delta(\bar{k} - \bar{k}_l(t)), \tag{3.5}$$

where $\bar{w}_l$ is the weight of the l-th quadrature point and $\bar{k}_l$ is the position (or abscissa) of the l-th quadrature point. To use QMOM or a QMOM derived technique, the PBE needs to be formulated continuously. To show that closure is required and to illustrate QMOM, the simplified validation case (see Section 2.5.2) is considered.

Application to validation case The hydrolysis rates of the validation case can be expressed as the product of a function f and the NDF

$$\bar{D}_{\bullet}(t,\bar{k}) = \bar{f}_{\bullet}(\bar{k}) \cdot \bar{n}(t,\bar{k}). \tag{3.6}$$

Substitution into Equation (3.3) yields

$$\bar{\omega}^i_{\bullet} = \int_1^{\infty} \bar{k}^i \cdot \bar{f}_{\bullet}(\bar{k}) \cdot \bar{n}(t,\bar{k})\,\mathrm{d}\bar{k}. \tag{3.7}$$

Unless the function is constant, $\bar{\omega}^i_{\sum}$ cannot be expressed as a function of $\bar{\mu}^i$. But if one substitutes the QMOM approximation into the NDF, one obtains after some calculations

$$\bar{\omega}^i_\bullet = \int_1^\infty \bar{k}^i \cdot \bar{f}_\bullet(\bar{k}) \cdot \sum_{l=1}^{N} \bar{w}_l(t) \cdot \delta(\bar{k} - \bar{k}_l(t)) \, \mathrm{d}\bar{k} \tag{3.8}$$

$$= \sum_{l=1}^{N} \bar{w}_l(t) \cdot \bar{k}_l^i \cdot f_\bullet(\bar{k}_l) \cdot H(\bar{k}_l - 1). \tag{3.9}$$

Therefore, the moment of the death rate can be computed if the weights and positions of the quadrature points are known. The moments of the birth rate have the following form for the validation case

$$\bar{\alpha}^i_\bullet = 2 \cdot \int_1^\infty \bar{k}^i \int_{\bar{k}+1}^\infty \bar{\gamma}_\bullet(\bar{k}, \bar{k}') \cdot \bar{f}_\bullet(\bar{k}') \cdot \bar{n}_\bullet(t, \bar{k}') \, \mathrm{d}\bar{k}' \mathrm{d}\bar{k}. \tag{3.10}$$

Again using the approximation for the NDF the moments can be simplified

$$\bar{\alpha}^i_\bullet = 2 \cdot \sum_{l=1}^{N} \bar{w}_l(t) \cdot \bar{f}_\bullet(\bar{k}_l) \int_1^{\bar{k}_l - 1} \bar{k}^i \cdot \bar{\gamma}_\bullet(\bar{k}, \bar{k}_l) \, \mathrm{d}\bar{k}. \tag{3.11}$$

This integral can be solved either analytically or numerically.

Quadrature The weights and positions of the quadrature points have to be chosen to satisfy the system of equations defined by

$$\bar{\mu}^i = \sum_{l=1}^{N} \bar{w}_l \cdot \bar{k}_l^i. \tag{3.12}$$

The solution of this system of equation is called quadrature. To avoid the ill-conditioned quadrature, Marchisio and Fox [106] developed DQMOM, which has been successfully applied to several problems [107]. DQMOM has also been shown to be suitable for bivariate [219–221] and breakage [220] problems. The quadrature is avoided by solving the ODEs for the evolution of the weights and position of the quadrature points [106]. Marchisio and Fox [106] suggested writing the evolution equation of the moments as follows:

$$\frac{\mathrm{d}\bar{\mu}^i}{\mathrm{d}t} = \sum_{l=1}^{N} (1-i) \cdot \bar{k}_l^i \cdot \frac{\mathrm{d}\bar{w}_l}{\mathrm{d}t} + i \cdot \bar{k}_l^{i-1} \cdot \frac{\mathrm{d}\bar{w}_l \cdot \bar{k}_l}{\mathrm{d}t}. \tag{3.13}$$

If the variables are written into a vector, this equation can be rewritten as follows

$$\frac{\mathrm{d}\bar{\mu}}{\mathrm{d}t} = \bar{\mathbf{A}}(\bar{\mathbf{k}}) \cdot \begin{bmatrix} \frac{\mathrm{d}\mathbf{w}}{\mathrm{d}t} \\ \frac{\mathrm{d}\mathbf{w} \circ \mathbf{k}}{\mathrm{d}t} \end{bmatrix} \tag{3.14}$$

$$\bar{A}_{i,j}(\bar{\mathbf{k}}) = \begin{cases} (1-i) \cdot \bar{k}_j^i & j \leq N \\ i \cdot \bar{k}_{j-N}^{i-1} & j > N \end{cases} \tag{3.15}$$

The symbol $\circ$ specifies the Hadamard product resulting in the entry-wise multiplication of two vectors. If the weights and position of the quadrature points is known at the initial time, the system of ODEs can be solved using any appropriate numerical solver.

3.1.2 Bivariate Population Balance Equation

The extension to a bivariate PBE is straightforward. The moments are obtained by multiplication with $\bar{k}^i \cdot \bar{b}^j$ and integration over the entire domain

$$\bar{\mu}^{i,j} = \int_1^{\infty} \bar{k}^i \int_0^{\bar{k}-1} \bar{b}^j \cdot \bar{n}(t,\bar{k},\bar{b})\,\mathrm{d}\bar{b}\mathrm{d}\bar{k}. \tag{3.16}$$

The moment with $i = 0$ and $j = 1$ is the total amount of branching bonds. Using the same operation on the PBE (3.28) yields the equation for the evolution of the moments as follows:

$$\frac{\mathrm{d}\bar{\mu}^{i,j}}{\mathrm{d}t} = -\bar{\omega}_{\sum}^{i,j} + \bar{\alpha}_{\sum,\mathrm{I}}^{i,j}. \tag{3.17}$$

where $\bar{\omega}_{\sum}^{i,j}$ and $\bar{\alpha}_{\sum,\mathrm{I}}^{i,j}$ are the moments of the death and birth terms, respectively. The NDF is again expressed as a sum of Dirac deltas

$$\bar{n}(t,\bar{k},\bar{b}) \approx \sum_{l=1}^{N} \bar{w}_l \cdot \delta(\bar{k}-\bar{k}_l) \cdot \delta(\bar{b}-\bar{b}_l). \tag{3.18}$$

For the left hand side of Equation (3.17) Marchisio and Fox [106] suggested writing the evolution equations of the moments as follows:

$$\frac{\mathrm{d}\bar{\mu}^{i,j}}{\mathrm{d}t} = \cdot \sum_{l=1}^{N_\mathrm{I}} \left((1-i-j) \cdot \bar{\bar{k}}_l^i \cdot \bar{\bar{b}}_l^j \cdot \frac{\mathrm{d}\bar{w}_l}{\mathrm{d}t} + i \cdot \bar{k}_l^{i-1} \cdot \bar{b}_l^j \cdot \frac{\mathrm{d}(\bar{\bar{w}}_l \cdot \bar{k}_l)}{\mathrm{d}t} + j \cdot \bar{k}_l^i \cdot \bar{b}_l^{j-1} \cdot \frac{\mathrm{d}(\bar{w}_l \cdot \bar{b}_l)}{\mathrm{d}t} \right). \tag{3.19}$$

If the variables are written into a vector, this equation can be rewritten as follows:

$$\frac{\mathrm{d}\bar{\mu}}{\mathrm{d}t} = \mathbf{A}_I(\bar{\mathbf{k}},\bar{\mathbf{b}}) \cdot \begin{bmatrix} \frac{\mathrm{d}\bar{\mathbf{w}}}{\mathrm{d}t} \\ \frac{\mathrm{d}(\bar{\mathbf{w}} \circ \bar{\mathbf{k}})}{\mathrm{d}t} \\ \frac{\mathrm{d}(\bar{\mathbf{w}} \circ \mathbf{b})}{\mathrm{d}t} \end{bmatrix} \tag{3.20}$$

$$A_{l,f_I} = \begin{cases} (1-i(l)-j(l)) \cdot \bar{k}_f^{i(l)} \bar{b}_f^{j(l)} & f \leq N_\mathrm{I} \\ i(l) \cdot \bar{k}_{f-N_\mathrm{I}}^{i(l)-1} & N_\mathrm{I} < f \leq 2 \cdot N_\mathrm{I} \\ j(l) \cdot \bar{b}_{f-2\cdot N_\mathrm{I}}^{j(l)-1} & 2 \cdot N_\mathrm{I} < f \end{cases}, \tag{3.21}$$

where $\mathbf{A}_I$ is the nonlinear inversion matrix. Fox [222] showed that the stability of DQMOM depends on the selected set of moments. His suggested set of moments is adopted for the cases when 4 and 9 quadrature points are used. The moments are given in Table 3.1. The number of moments is always 3 times the number of quadrature points. Therefore, for the results presented below, the first 3, 6, 9, and

so on moments are used.

Table 3.1: Exponents used to compute the moments corresponding to their quadrature point [2] (With kind permission from Elsevier).

N_I	**i**	**j**	N_I	**i**	**j**
1	0	0	6	4	1
1	1	0	6	3	2
1	0	1	6	2	3
2	0	2	7	1	4
2	1	2	7	5	0
2	2	0	7	0	5
3	2	1	8	5	1
3	3	0	8	1	5
3	0	3	8	4	2
4	1	1	9	2	4
4	3	1	9	5	2
4	1	3	9	2	5
5	2	2			
5	4	0			
5	0	4			

3.2 Direct Quadrature Method of Moment for a divided domain

The assumption of continuity is valid for sufficiently large polymers, but not for small polymers [54]. The degradation of polymer results in an increasingly large amount of small polymer. Accordingly, one cannot justify the continuity assumption for the whole process time. In order to use DQMOM, however, the continuity assumption is required. A division of the domain into subdomains can unify both approaches [223]. In addition, the low molecular weight polymers are represented with a high resolution while still DQMOM can be used for the large polymers. The high resolution of the low molecular weight polymers is beneficial, because their processability and value can depend strongly on their molar mass and degree of branching. For the large polymers, on the other hand, total mass is the main property of interest in industrial practice [143] and can be sufficiently determined at a quite low resolution.

3.2.1 Linear polymer

In Subdomain II the continuity simplification justified by McCoy and Madras [54] is used, whereas in Subdomain III the PBE is discrete (see Figure 3.1). There appears to be no experience in using DQMOM for such a mixed continuous-discrete formulation. However, there have been reports of the

use of the MOM for the mixed continuous-discrete formulation [143].
Subdomain II consists of all polymers with more than $\breve{k}_c$ monomer units. $\breve{k}_c$ is the critical amount of monomer units. It is a numerical parameter that can be set to every natural number. The NDF $\bar{n}(t,\bar{k})$ is thus defined on $\{\bar{k} \in \mathbb{R} : \bar{k} > \breve{k}_c\}$. Subdomain III consist of all polymer with less than $\breve{k}_c$ monomer units. Here, rather than the NDF, the amount of polymers with a discrete amount of monomer units is known. Therefore, to still maintain the NDF, the NDF in this subdomain is represented by a sum of Dirac deltas centered on $\{\breve{k} \in \mathbb{N} : \breve{k} \leq \breve{k}_c\}$.

Population balance equation in Subdomain II

As breakage of polymers only creates smaller polymers, Subdomain II is independent of Subdomain III. Therefore, the PBE remains unchanged:

$$\frac{\partial \bar{n}(t,\bar{k})}{\partial t} = -\bar{D}_{\sum}(t,\bar{k}) + \bar{B}_{\sum,II}(t,\bar{k}), \tag{3.22}$$

where $\bar{B}_{\sum,II}$ is the birth due to hydrolysis on polymers in Subdomain II. However, the definitions of the moments has to be changed, in order to not include Subdomain III. The moments are then

$$\bar{\mu}_{\mathrm{II}}^{i} = \int_{\breve{k}_c}^{\infty} \bar{k}^i \cdot \bar{n}(t,\bar{k})\,\mathrm{d}\bar{k}. \tag{3.23}$$

Integer moments of order up to $2 \cdot N - 1$ are used in this study. The approximation for the number density function is used to compute the terms of the right-hand side of Equation (3.17). The resulting equations are shown in Appendix B.

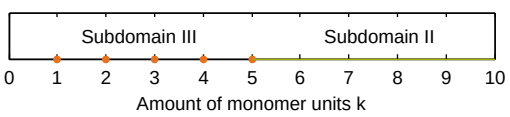

Figure 3.1: The domain and the subdivisions, where $\breve{k}_c = 5$ for illustrative purposes.

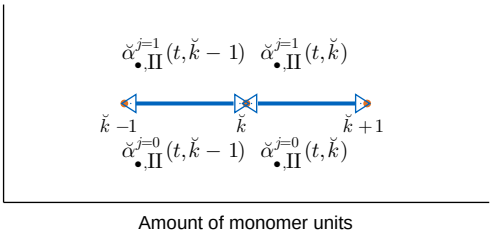

Figure 3.2: Discretization of the birth term in Subdomain III.

Population balance equation in Subdomain III

The hydrolysis of polymers in Subdomain II creates polymer in Subdomain III. The PBE has to be extended by $\breve{B}_{\sum,II}$, which is the birth of polymers due to hydrolysis on polymers in Subdomain II:

$$\frac{\mathrm{d}\breve{n}(t,\breve{k})}{\mathrm{d}t} = -\breve{D}_{\sum}(t,\breve{k}) + \breve{B}_{\sum,\mathrm{III}}(t,\breve{k}) + \breve{B}_{\sum,\mathrm{II}}(t,\breve{k}), \tag{3.24}$$

where $\breve{B}_{\sum,\mathrm{III}}$ is the birth of polymer due to hydrolysis on polymers in Subdomain III. Every reaction $\bullet$ in Subdomain II produces $\bar{B}_{\bullet,\mathrm{II}}$ continuous polymer in Subdomain III. Because Subdomain III is not continuous, this birth has to be discretized in that coordinate to yield $\breve{B}_{\bullet,\mathrm{II}}$. $\breve{B}_{\bullet,\mathrm{II}}$ is only defined for integer values of $\breve{k}$. Kumar and Ramkrishna [112] suggested a method for distributing the birth of particles to adjacent pivots while preserving two arbitrary moments. This method is adopted here to discretize the birth term while preserving two moments of the polymer production rate: The production rate of polymer $\breve{\alpha}^{j=0}_{\bullet,\mathrm{II}}$ and monomer units $\breve{\alpha}^{j=0}_{\bullet,\mathrm{II}}$ in the interval $[\breve{k},\breve{k}+1]$:

$$\breve{\alpha}^{j=0}_{\bullet,\mathrm{II}}(t,\breve{k}) = \int_{\breve{k}}^{\breve{k}+1} \bar{B}_{\bullet,\mathrm{II}}(t,\bar{k}')\,\mathrm{d}\bar{k}' \tag{3.25}$$

$$\breve{\alpha}^{j=1}_{\bullet,\mathrm{II}}(t,\breve{k}) = \int_{\breve{k}}^{\breve{k}+1} \bar{k}' \cdot \bar{B}_{\bullet,\mathrm{II}}(t,\bar{k}')\,\mathrm{d}\bar{k}'. \tag{3.26}$$

Once the total production rate moments over the interval $[\breve{k},\breve{k}+1]$ are known, the polymer generation must be distributed to $\breve{k}$ and $\breve{k}+1$ such that the above computed moments are preserved. Because every point, except the first and last point, belongs to two interval (as shown in Figure 3.2), the contribution due to the intervals $[\breve{k},\breve{k}+1]$ and $[\breve{k}-1,\breve{k}]$ must be added at the point at $\breve{k}$ yielding the equation for $\breve{B}_{\bullet,II}$:

$$\breve{B}_{\bullet,\mathrm{II}}(t,\breve{k}) = (1+\breve{k})\cdot\breve{\alpha}^{j=0}_{\bullet,\mathrm{II}}(t,\breve{k}) - \breve{\alpha}^{j=1}_{\bullet,\mathrm{II}}(t,\breve{k}) + (1-\breve{k})\cdot\breve{\alpha}^{j=0}_{\bullet,\mathrm{II}}(t,\breve{k}-1) + \breve{\alpha}^{j=1}_{\bullet,\mathrm{II}}(t,\breve{k}-1). \tag{3.27}$$

The above introduced discretization of produced amount of polymers in the discrete domain ensures consistency with regard to the zeroth and first order moments due to a mechanism in the continuous domain. The discretization could be modified to preserve any other two moments.

3.2.2 Branched polymer

Figure 3.3 shows a representation of the domain and its division into three subdomains (continuous, continuous-discrete, and discrete). This division is mainly governed by the choice of the critical amount of monomer units $\breve{k}_c$, which can be any natural number. The domain division additionally facilitates a high resolution of the nearly linear polymers that comprise a significant fraction of e.g. starch [10]. However, for the bivariate case the mixed continuous-discrete case has only been investigated by the author [2].

Subdomain I consists of all the polymers with a high amount of monomer units and many branching

bonds. The simplification that the internal coordinates can be considered as continuous quantities is used in this domain. The NDF in Subdomain I is thus represented by $\bar{n}(\bar{k},\bar{b},t)$ on the triangle $\{\bar{k},\bar{b} \in \mathbb{R} | \breve{k}_c < \bar{k} < \infty \wedge \breve{k}_c - 1 < \bar{b} \leq \bar{k} - 1\}$. The polymers within Subdomain II have a lower amount of branching bonds, but the assumption that the amount of monomer units is continuous remains justified. However, the amount of branching bonds in this subdomain is assumed to be discrete. The polymers within this region are therefore only defined on the dashed horizontal lines shown in Figure 3.3. The NDF in Subdomain II is thus represented by $\hat{n}(\bar{k},\breve{b},t)$ on the rectangular set $\{\bar{k} \in \mathbb{R}, \breve{b} \in \mathbb{N}_0 | \breve{k}_c < \bar{k} < \infty \wedge 0 \leq \breve{b} \leq \breve{k}_c - 1\}$. The variables that belong to this subdomain always have the accent mark ˆ. Finally, Subdomain III consists of polymers with a low amount of monomer units and branching bonds. Here, rather than the NDF, the amount of polymers with a discrete amount of monomer units and branching bonds is known. Therefore, to still maintain the NDF, the NDF in this subdomain is represented by a sum of Dirac deltas centered on the integer arguments of the triangular set $\{\breve{k} \in \mathbb{N}, \breve{b} \in \mathbb{N}_0 | 1 \leq \breve{k} \leq \breve{k}_c - 1 \wedge 0 \leq \breve{b} \leq \breve{k} - 1\}$. This approach is equivalent to considering the NDF $\breve{n}(\breve{k},\breve{b},t)$ to be defined only for integer arguments.

Population balance equation in Subdomain I

Subdomain I can be treated quite straightforwardly because the reactions in the other subdomains do not affect the polymers within this subdomain. The PBE for the NDF $\bar{n}$ within Subdomain I is then simply the PBE for the continuous case:

$$\frac{\partial \bar{n}}{\partial t} = -\bar{D}_{\sum} + \bar{B}_{\sum,\mathrm{I}}, \tag{3.28}$$

where $\bar{B}_{\sum,\mathrm{I}}$ is the birth due to hydrolysis on polymers in Subdomain I. In this study, non-dimensional moments are used for Subdomain I, because this approach has been reported to be beneficial for the numerical solution of the problem [219] by improving the condition number of the inversion matrix. The scaling factors $\tilde{w}$, $\tilde{k}$ and $\tilde{b}$ are selected such that the initial zeroth and first order moments are unity at the start of the simulation. The moments for Subdomain I are obtained by multiplication with $\frac{1}{\tilde{w}} \cdot \left(\frac{\bar{k}}{\tilde{k}}\right)^i \cdot \left(\frac{\bar{b}}{\tilde{b}}\right)^j$ and integration over the entire domain

$$\bar{\tilde{\mu}}^{i,j} = \frac{1}{\tilde{w}} \cdot \int_{\breve{k}_c}^{\infty} \left(\frac{\bar{k}}{\tilde{k}}\right)^i \int_{\breve{k}_c - 1}^{\bar{k}-1} \left(\frac{\bar{k}}{\tilde{b}}\right)^j \bar{n} \, \mathrm{d}\bar{b} \, \mathrm{d}\bar{k}. \tag{3.29}$$

Population balance equation in Subdomain II

The PBE for the NDF of polymers $\hat{n}$ within Subdomain II is then as follows:

$$\frac{\partial \hat{n}}{\partial t} = -\hat{D}_{\sum} + \hat{B}_{\sum,\mathrm{I}} + \hat{B}_{\sum,\mathrm{II}}. \tag{3.30}$$

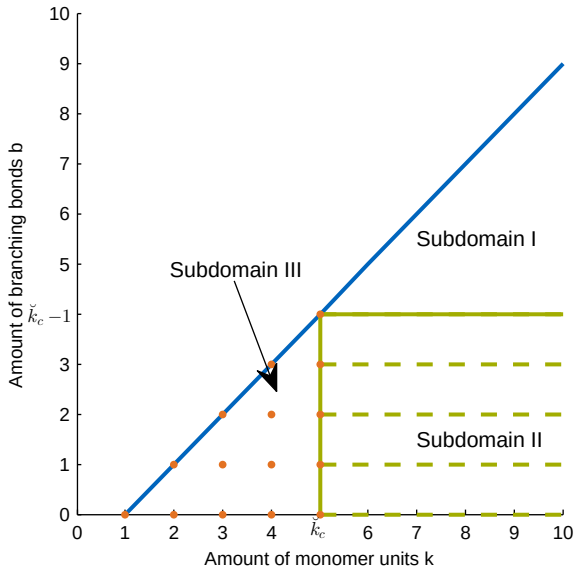

Figure 3.3: The domain and the subdivisions, where $\breve{k}_c = 5$ for illustrative purposes [2] (With kind permission from Elsevier).

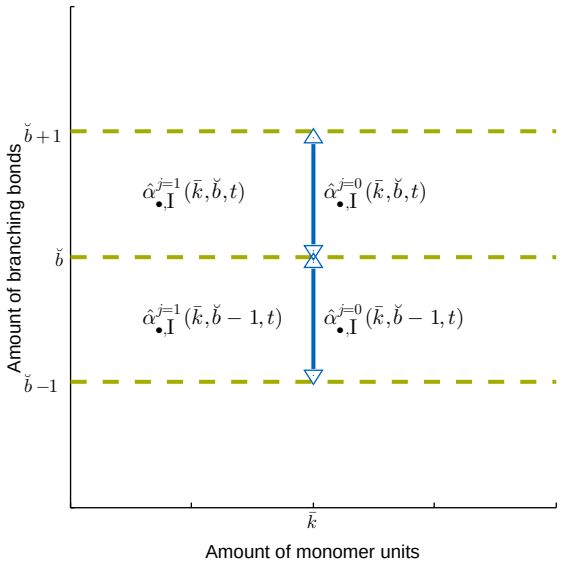

Figure 3.4: Discretization of the birth term in Subdomain II [2] (With kind permission from Elsevier).

In Subdomain II the moments are not non-dimensionalized because non-dimensionalization is not expected to have a benefit. The evolution equation for the moments is as follows:

$$\frac{\mathrm{d}\hat{\mu}^{i\in\mathbb{N}_0}(\breve{b},t)}{\mathrm{d}t} = -\hat{\omega}_{\sum}^{i\in\mathbb{N}_0} + \hat{\alpha}_{\sum,\mathrm{I}}^{i\in\mathbb{N}_0} + \hat{\alpha}_{\sum,\mathrm{II}}^{i\in\mathbb{N}_0}, \tag{3.31}$$

where $\hat{\omega}_{\sum}^{i\in\mathbb{N}_0}$, $\hat{\alpha}_{\sum,\mathrm{I}}^{i\in\mathbb{N}_0}$ and $\hat{\alpha}_{\sum,\mathrm{II}}^{i\in\mathbb{N}_0}$ are the moments of the death and birth terms, respectively.
No reaction in Subdomain III produces any polymer within Subdomain II. However, every reaction $\bullet$ in Subdomain I produces $\bar{B}_{\bullet,\mathrm{I}}$ continuous polymers in Subdomain II. As with production in Subdomain III due to reaction in Subdomain II $\bar{B}_{\bullet,\mathrm{I}}$ needs to be discretized to $\hat{B}_{\bullet,\mathrm{I}}$. However, as the branching bond coordinate is used the production rates of polymer $\hat{\alpha}_{\bullet,\mathrm{I}}^{j=0}$ and branching bonds $\hat{\alpha}_{\bullet,\mathrm{I}}^{j=1}$ in the interval $[\breve{b},\breve{b}+1]$, are used as moments:

$$\hat{\alpha}_{\bullet,\mathrm{I}}^{j=0}(\bar{k},\breve{b},t) = \int_{\breve{b}}^{\breve{b}+1} \bar{B}_{\bullet,\mathrm{I}}(\bar{k},\bar{b}',t)\,\mathrm{d}\bar{b}' \tag{3.32}$$

$$\hat{\alpha}_{\bullet,\mathrm{I}}^{j=1}(\bar{k},\breve{b},t) = \int_{\breve{b}}^{\breve{b}+1} \bar{b}' \cdot \bar{B}_{\bullet,\mathrm{I}}(\bar{k},\bar{b}',t)\,\mathrm{d}\bar{b}'. \tag{3.33}$$

Once the total production rate moments over the interval $[\breve{b},\breve{b}+1]$ are known, the polymer generation must be distributed to $\breve{b}$ and $\breve{b}+1$ such that the above computed moments are preserved. Because every line ($\breve{b} = const$) belongs to two intervals (as shown in Figure 3.4), the contribution due to the

intervals $[\breve{b},\breve{b}+1]$ and $[\breve{b}-1,\breve{b}]$ must be added at the line at $\breve{b}$ yielding the equation for $\hat{B}_{\bullet,\mathrm{I}}$:

$$\hat{B}_{\bullet,\mathrm{I}}(\bar{k},\breve{b},t) = (1+\breve{b})\cdot\hat{\alpha}^{j=0}_{\bullet,\mathrm{I}}(\bar{k},\breve{b},t) - \hat{\alpha}^{j=1}_{\bullet,\mathrm{I}}(\bar{k},\breve{b},t) + (1-\breve{b})\cdot\hat{\alpha}^{j=0}_{\bullet,\mathrm{I}}(\bar{k},\breve{b}-1,t) + \hat{\alpha}^{j=1}_{\bullet,\mathrm{I}}(\bar{k},\breve{b}-1,t). \quad (3.34)$$

Population balance equation in Subdomain III

The PBE within Subdomain III is given as follows:

$$\frac{\partial \breve{n}}{\partial t} = -\breve{D}_{\sum} + \breve{B}_{\sum,\mathrm{I}} + \breve{B}_{\sum,\mathrm{II}} + \breve{B}_{\sum,\mathrm{III}}. \quad (3.35)$$

No scaling is performed in this subdomain because no suitable scaling factor is known. Initially, almost no polymer is in this subdomain, but the depolymerization produces intermediate product in this subdomain. Because of the mechanisms in Subdomain II, $\hat{B}_{\bullet,\mathrm{II}}$ polymers are created in Subdomain III. While already discrete in the amount of branching bonds, the rate must also be discretized in the coordinate for the amount of monomer units. The discretization procedure is equivalent to the one described previously. The two preserved moments are the production rates of polymers $\breve{\alpha}^{i=0}_{\bullet,\mathrm{II}}$ and monomer units $\breve{\alpha}^{i=1}_{\bullet,\mathrm{II}}$ in the interval $[\breve{k},\breve{k}+1]$:

$$\breve{\alpha}^{i=0}_{\bullet,\mathrm{II}}(\breve{k},\breve{b},t) = \int_{\breve{k}}^{\breve{k}+1} \hat{B}_{\bullet,\mathrm{II}}(\bar{k}',\breve{b},t)\,\mathrm{d}\bar{k}' \quad (3.36)$$

$$\breve{\alpha}^{i=1}_{\bullet,\mathrm{II}}(\breve{k},\breve{b},t) = \int_{\breve{k}}^{\breve{k}+1} \bar{k}'\cdot\hat{B}_{\bullet,\mathrm{II}}(\bar{k}',\breve{b},t)\,\mathrm{d}\bar{k}'. \quad (3.37)$$

The discretized birth term is as follows:

$$\breve{B}_{\bullet,\mathrm{II}}(\breve{k},\breve{b},t) = (1+\breve{k})\cdot\breve{\alpha}^{i=0}_{\bullet,\mathrm{II}}(\breve{k},\breve{b},t)\,\&\, - \breve{\alpha}^{i=1}_{\bullet,\mathrm{II}}(\breve{k},\breve{b},t) + (1-\breve{k})\cdot\breve{\alpha}^{i=0}_{\bullet,\mathrm{II}}(\breve{k}-1,\breve{b},t) + \breve{\alpha}^{i=1}_{\bullet,\mathrm{II}}(\breve{k}-1,\breve{b},t). \quad (3.38)$$

A mechanism in Subdomain I causes the birth of $\bar{B}_{\bullet,\mathrm{I}}$ polymers in Subdomain III. This birth term must be discretized in the amount of monomer units and amount of branching bonds. Thus, $\breve{B}_{\bullet,\mathrm{I}}$ is also only defined for the integer values of $\breve{k}$ and $\breve{b}$. Chakraborty and Kumar [224] extended the work of Kumar and Ramkrishna [112] to a bivariate problem. In the present study the discretization is performed using a triangulated Subdomain III, as shown in Figure 3.5. There are two types of elements (L and T) that must be considered. For the discretization of type L elements the method preserved the three moments: production rates of polymers $\breve{\alpha}^{i=0,j=0}_{\bullet,\mathrm{I},L}$, monomer units $\breve{\alpha}^{i=1,j=0}_{\bullet,\mathrm{I},L}$, and branching bonds $\breve{\alpha}^{i=0,j=1}_{\bullet,\mathrm{I},L}$

$$\breve{\alpha}^{i,j}_{\bullet,\mathrm{I},L}(\breve{k},\breve{b},t) = \int_{\breve{k}}^{\breve{k}+1}\int_{\breve{b}}^{\bar{k}'-\breve{k}+\breve{b}} \bar{k}'^{\,i}\cdot\bar{b}'^{\,j}\cdot\bar{B}_{\bullet,\mathrm{I}}(\bar{k}',\bar{b}',t)\,\mathrm{d}\bar{b}'\,\mathrm{d}\bar{k}'. \quad (3.39)$$

The resulting births in the lower left corner, lower right, and upper right corner in Figure 3.5 are $\breve{B}_{\bullet,\mathrm{I},L,ll}(\breve{k},\breve{b},t)$, $\breve{B}_{\bullet,\mathrm{I},L,lr}(\breve{k},\breve{b},t)$, and $\breve{B}_{\bullet,\mathrm{I},L,ur}(\breve{k},\breve{b},t)$, respectively:

$$\breve{B}_{\bullet,\mathrm{I},L,ll}(\breve{k},\breve{b},t) = (1+\breve{k})\cdot\breve{\alpha}^{i=0,j=0}_{\bullet,\mathrm{I},L}(\breve{k},\breve{b},t) - \breve{\alpha}^{i=1,j=0}_{\bullet,\mathrm{I},L}(\breve{k},\breve{b},t) \quad (3.40)$$

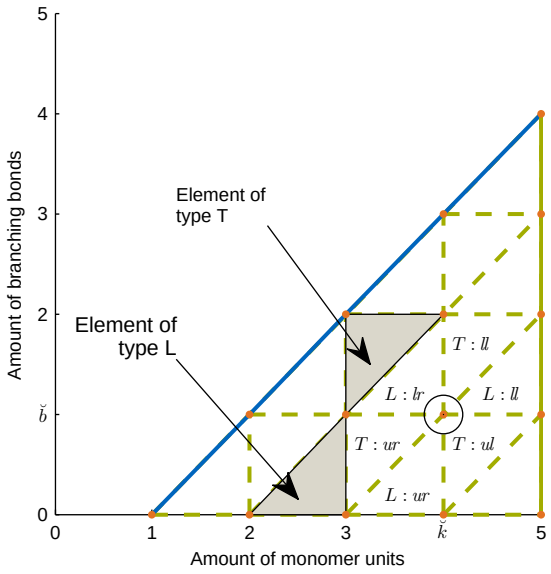

Figure 3.5: Triangulation of Subdomain III and the elements to which the point $(\check{k},\check{b})$ belongs, with the corresponding indices [2] (With kind permission from Elsevier).

$$\check{B}_{\bullet,\mathrm{I},L,lr}(\check{k},\check{b},t) = (\check{b}-\check{k})\cdot \check{\alpha}_{\bullet,\mathrm{I},L}^{i=0,j=0}(\check{k},\check{b},t) + \check{\alpha}_{\bullet,\mathrm{I},L}^{i=1,j=0}(\check{k},\check{b},t) - \check{\alpha}_{\bullet,\mathrm{I},L}^{i=0,j=1}(\check{k},\check{b},t) \tag{3.41}$$

$$\check{B}_{\bullet,\mathrm{I},L,lr}(\check{k},\check{b},t) = -\check{b}\cdot \check{\alpha}_{\bullet,\mathrm{I},L}^{i=0,j=0}(\check{k},\check{b},t) + \check{\alpha}_{\bullet,\mathrm{I},L}^{i=0,j=1}(\check{k},\check{b},t). \tag{3.42}$$

For elements of type T, the same three moments are preserved: production rates of polymers $\check{\alpha}_{\bullet,\mathrm{I},T}^{i=0,j=0}$, monomer units $\check{\alpha}_{\bullet,\mathrm{I},T}^{i=1,j=0}$, and branching bonds $\check{\alpha}_{\bullet,\mathrm{I},T}^{i=0,j=1}$:

$$\check{\alpha}_{\bullet,\mathrm{I},T}^{i,j}(\check{k},\check{b},t) = \int_{\check{k}}^{\check{k}+1}\int_{\bar{k}'-\check{k}+\check{b}}^{\check{b}+1} \bar{k}'^{i}\cdot \bar{b}'^{j}\cdot \bar{B}_{\bullet,\mathrm{I}}(\bar{k}',\bar{b}',t)\,\mathrm{d}\bar{b}'\,\mathrm{d}\bar{k}'. \tag{3.43}$$

The resulting births in the lower left, upper left, and upper right corner are $\check{B}_{\bullet,\mathrm{I},T,ll}(\check{k},\check{b},t)$, $\check{B}_{\bullet,\mathrm{I},T,ul}(\check{k},\check{b},t)$, and $\check{B}_{\bullet,\mathrm{I},T,ur}(\check{k},\check{b},t)$, respectively:

$$\check{B}_{\bullet,\mathrm{I},T,ll}(\check{k},\check{b},t) = (1+\check{b})\cdot \check{\alpha}_{\bullet,\mathrm{I},T}^{i=0,j=0}(\check{k},\check{b},t) - \check{\alpha}_{\bullet,\mathrm{I},T}^{i=0,j=1}(\check{k},\check{b},t) \tag{3.44}$$

$$\check{B}_{\bullet,\mathrm{I},T,ul}(\check{k},\check{b},t) = (\check{k}-\check{b})\cdot \check{\alpha}_{\bullet,\mathrm{I},T}^{i=0,j=0}(\check{k},\check{b},t) - \check{\alpha}_{\bullet,\mathrm{I},T}^{i=1,j=0}(\check{k},\check{b},t) + \check{\alpha}_{\bullet,\mathrm{I},T}^{i=0,j=1}(\check{k},\check{b},t) \tag{3.45}$$

$$\check{B}_{\bullet,\mathrm{I},T,ur}(k,b,t) = -\check{k}\cdot \check{\alpha}_{\bullet,\mathrm{I},T}^{i=0,j=0}(\check{k},\check{b},t) + \check{\alpha}_{\bullet,\mathrm{I},T}^{i=1,j=0}(\check{k},\check{b},t). \tag{3.46}$$

The contributions of each element, that contains point $[\check{k},\check{b}]$, must be summed up. As shown in Figure 3.5, up to six elements may contain the point. Type L elements touch the point with their lower left corner, lower right corner, and upper right corner, whereas type T elements touch the point with their lower left corner, upper left corner, and upper right corner. The total birth $\check{B}_{\bullet,\mathrm{I}}(\check{k},\check{b},t)$ at the point is then

given as follows

$$\begin{aligned}\breve{B}_{\bullet,\mathrm{I}}(\breve{k},\breve{b},t) =& \breve{B}_{\bullet,\mathrm{I},L,ll}(\breve{k},\breve{b},t)+\breve{B}_{\bullet,\mathrm{I},T,ll}(\breve{k},\breve{b},t)+\breve{B}_{\bullet,\mathrm{I},L,ur}(\breve{k}-1,\breve{b}-1,t)\\ &+\breve{B}_{\bullet,\mathrm{I},T,ur}(\breve{k}-1,\breve{b}-1,t)+\breve{B}_{\bullet,\mathrm{I},L,lr}(\breve{k}-1,\breve{b},t)+\breve{B}_{\bullet,\mathrm{I},T,ul}(\breve{k},\breve{b}-1,t).\end{aligned} \tag{3.47}$$

3.3 Numerical implementation

In this section the details of the numerical implementation are provided.

3.3.1 Initial moments

The initial moments are obtained by integration of the initial distribution times the appropriate mononomials numerically using the MATLAB integration `integral2`. The average degree of polymerization is 1000 and the polydispersity is 1.1.

3.3.2 Initial quadrature

Before the time integration of the equations is performed, the initial values for the weights and coordinates of the quadrature points must be calculated from the moments. For the univariate problem there exist efficient algorithms [90, 105, 225] performing this task. For Subdomain II the Chebyshev algorithm described by Upadhyay [105] is used.
However, for the bivariate case with more than one quadrature point, the roots of the following nonlinear system have to be determined:

$$\forall i,j : \sum_{l=1}^{N_\mathrm{I}} \bar{\tilde{w}}_l \cdot \bar{\tilde{k}}_l^i \cdot \bar{\tilde{b}}_l^j - \tilde{\mu}^{i,j} = 0. \tag{3.48}$$

The variables are subject to the constraint that all quadrature points lay within Subdomain I:

$$\forall l \leq N_\mathrm{I} : \bar{\tilde{w}}_l \geq 0, \tilde{b}\cdot\bar{\tilde{b}}_l \geq \breve{k}_c - 1, \tilde{k}\cdot\bar{\tilde{k}}_l \geq \breve{k}_c, \tilde{k}\cdot\bar{\tilde{k}}_l - 1 \geq \tilde{b}\cdot\bar{\tilde{b}}_l \tag{3.49}$$

The existing algorithm [107] cannot handle non-rectangular domains, and thus a suitable brute force algorithm had to be developed for Subdomain I. Starting from an initial guess, the norm of the error between the calculated and the given moments is minimized using the MATLAB® optimizer `lsqnonlin`:

$$\min_{\bar{\tilde{w}}_l,\bar{\tilde{k}}_l,\bar{\tilde{b}}_l} \left\{ \sum_i \sum_j \sum_{l=1}^{N_\mathrm{I}} \left(\frac{\bar{\tilde{w}}_l \cdot \bar{\tilde{k}}_l^i \cdot \bar{\tilde{b}}_l^j}{\tilde{\mu}^{i,j}} - 1 \right)^2 \right\}. \tag{3.50}$$

If the minimizer cannot reduce the error below the desired tolerance of 10^{-6} after 400 iterations, a new initial guess is generated. These steps are repeated until the error is sufficiently small or $10 \cdot N_\mathrm{I}$ initial

guesses have been generated.
The initial guesses are obtained by first assigning uniform random values between 0 and 1 to the weights, then values between $\frac{\check{k}_c}{\tilde{k}}$ and 1 to the amount of monomers coordinate, and finally, values between $\frac{\check{k}_c-1}{\tilde{b}}$ and 1 to the amount of branching bonds using the default random number generator `rand`. If a quadrature point lies outside the valid region, then new random numbers are drawn. A point is considered to be outside the valid region if

$$\bar{\tilde{b}}_l \cdot \tilde{b} > \bar{\tilde{k}}_l \cdot \tilde{k} - 1. \tag{3.51}$$

3.3.3 Solution of the resulting equations with error handling

Starting from the computed initial quadrature points, the resulting system of nonlinear coupled ODEs is integrated in time using the `ode45` integrator in MATLAB® with a relative tolerance of 10^{-5}. Because the problem is not well conditioned, several errors are possible and require handling.
If the inversion matrix becomes numerically singular, the moments in the corresponding step are computed, and the number of quadrature points is decreased until a successful quadrature is realized. If the number of quadrature points reaches zero, the moments are not realizable. If a successful quadrature is obtained, the simulation is continued from this point with the new quadrature. For negative weights or quadrature points outside the valid domain, the same reduction of quadrature points is attempted from the last valid time step.
If a quadrature point of Subdomain I moves into Subdomain II, the quadrature point is transformed to Subdomain II. Using the algorithm to discretize $\bar{B}_{\bullet,\mathrm{I}}$, the quadrature point is distributed to Subdomain II and then the quadrature point is removed from Subdomain I. Similarly, if a quadrature point of Subdomain II moves into Subdomain III, it is transformed to Subdomain III. The disappearance of all quadrature points from Subdomain I does not cause any problem. However, if the number of quadrature points in Subdomain II for a branching becomes zero while there is still a quadrature point above it, the algorithm will fail because any birth due to action on other lines or Subdomain I cannot be added to any quadrature point. To avoid this problem, a quadrature point is added at the arbitrary position $\check{k}_c + 10$ with a small weight of 2^{-1074} when there is no quadrature point at one amount of branching bonds in Subdomain II. The error introduced by this introduction of one quadrature point is negligible and enables the continuation of the computation.
Another issue is the inability of the selected time integrator to guarantee the conservation of positivity of the weights and coordinates of quadrature points. Unfortunately, solvers capable of ensuring positive values are significantly slower than the selected solver. Therefore, if small negative weights or concentrations occur in Subdomain III with an absolute value of less than 10^{-15} occurred, the weights are set to zero and the simulation continues.

Computation time

The computations were performed on a 3.7 GHz 6 cores Intel® E5 processor with more than 128 GB RAM running MATLAB® 2014a. The simulations for the different numerical settings were run in parallel on all cores. The simulation time was measured using the MATLAB® internal stopwatch timer and the measured time was the time required to compute the time evolution of quadrature points given the initial moments.

3.3.4 Validation with Monte Carlo simulations

The completely discrete PBE was solved using a Constant Number Monte Carlo method for Random-chain scission (RCS) and Random-debranching scission (RDS) and a Constant Volume Monte Carlo method for End-chain scission (ECS) [81]. The Constant Volume Monte Carlo was modified to track the ECS product directly. Therefore, no polymer had to be removed after an ECS event, which improved the accuracy of the algorithm. The initial distribution was sampled using the implemented distributions in MATLAB®. When RCS or RDS occurred, $5 \cdot 10^6$ polymers were used. Because ECS is much slower than RCS, only 10^5 polymers were used for pure ECS. Five runs of each simulation were performed.

3.4 Results and Discussion

In the following plots and discussion, nondimensional coordinates are used. The amount of polymer units is nondimensionalized by dividing them with their corresponding initial values. The time is nondimensionalized by multiplying it with $C_{RCS} + C_{RDS} + C_{ECS}$. None of the mechanisms change the amount of monomer units. Thus, this value remains constant and is therefore not shown. In Figures 3.10 - 3.16 the solid curves show the mean value for the Monte Carlo runs. The dashed curves are interpolations between the last two values obtained at a finite time and the end of the simulation.

3.4.1 Monte Carlo technique

The Constant Number Monte Carlo method does not guarantee that moments are conserved. The amount of polymers must be increased until the error is sufficiently small [81]. Here, the errors in the amount of monomer units and amount of branching bonds relative to the initial values were less than 1%. The time at which a certain amount of polymer units was reached also deviated less than 5% from the mean value of all the runs. The results for the Monte Carlo runs can therefore be reasonably used as reference solutions. The average simulation time per run for RCS was more than 6.5 hours, for RDS more than 5.5 hours, for ECS more than 5.5 hours, and for a mixture of RCS and ECS approximately 8 hours. However, the computaton time was dominated by creation of output for comparision and the code could be further optimized. Nevertheless, the computations times using kinetic Monte Carlo (kMC) would be unreasonable for optimal control.

3.4.2 Linear polymer

Grosch et al. [89] showed that typically the accuracy of DQMOM increases as the number of quadrature points increases. However, they also reported that an increase in the number of quadrature points results in a decrease in stability. The dependence of the stability and speed of the algorithm were accordingly studied for different numbers of quadrature points.
The results for RCS on linear polymers are shown in Figures 3.6 and 3.7. The behavior at the initial time and the final state were described well even for low values of $\breve{k}_c$ and N_{II}. However, the quantitative transient behavior deviated quite strongly for low values of $\breve{k}_c$ and N_{II}. The results for mixed continuous-discrete DQMOM converged to the Monte Carlo result as the number of quadrature points and $\breve{k}_c$ increased.
The results for ECS on linear polymers are shown in Figures 3.8 and 3.9. The behavior at the initial time and the final state were described well even for low values of $\breve{k}_c$ and N_{II}. However, the transient behavior is a weak approximation to the real profile. DQMOM returns a non-smooth profile because the approximated NDF is concentrated at a few chain lengths. The profile converges quickly to the exact profile, but with $\breve{k}_c = 20$ only computations with $N_{\text{II}} = 1$ were successful. For describing ECS only the product created by each scission needs to be represented discretely. Accordingly, increasing $\breve{k}_c$ above 2 does not result in improved accuracy, but it decreases numerical stability.

3.4.3 Branched polymer

Variation of the number of quadrature points in Subdomain II

If the number of quadrature points in Subdomain II (N_{II}) was increased to values greater than one, the simulation failed for almost all cases. This result is attributed to the fact that the required time steps were in the order of magnitude of the machine accuracy because the weights of quadrature points in Subdomain II were very small. Therefore, it was necessary for the integrator to take very small time steps to resolve their evolution correctly. All further simulations were performed accordingly with $N_{\text{II}} = 1$.

Variation of the number of quadrature points in Subdomain I and the amount of monomer units for discrete consideration

In the next three sections, the stability, computation cost, and accuracy are discussed for several values of $\breve{k}_c$ and N_{I}. Note that no results were obtained for $N_{\text{I}} = 5$ because the initial quadrature was not possible. This situation may be due to an improper set of moments. Separately, if $\breve{k}_c$ is set to zero, the undivided domain is obtained. In this case, the domain consists only of Subdomain I and the equations for the other subdomains are not used.

End chain scission If ECS was active exclusively, it was only possible to simulate the degradation to the completion for $N_{\text{I}} = 1, 2, 3, 6$. For other N_{I} values, the simulation generally halted at more than 50 % percent conversion, except when $N_{\text{I}} = 9$, for which the simulation stopped much earlier.

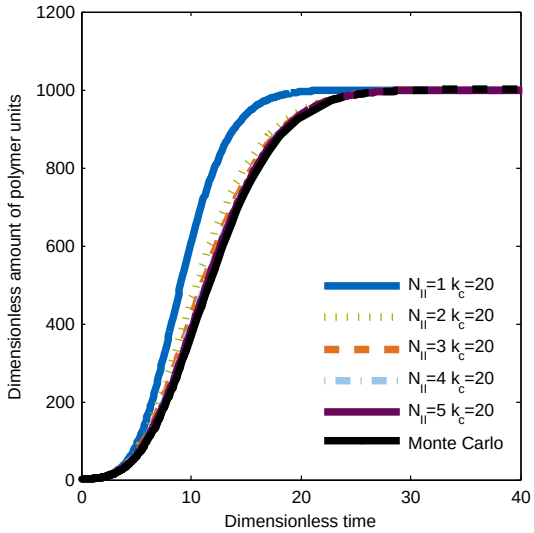

Figure 3.6: Polymer concentration as a function of time for linear polymers attacked by RCS with varying N_{II} [2] (With kind permission from Elsevier).

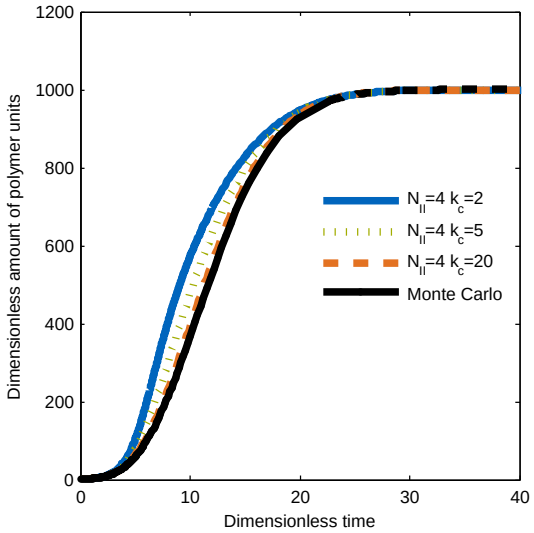

Figure 3.7: Polymer concentration as a function time for linear polymers attacked by RCS with varying $\breve{k}_c$ [2] (With kind permission from Elsevier).

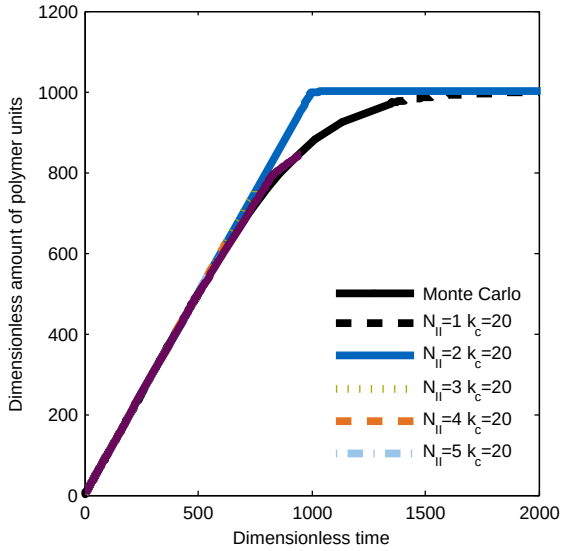

Figure 3.8: Polymer concentration as a function of time for linear polymers attacked by ECS with varying N_{II}.

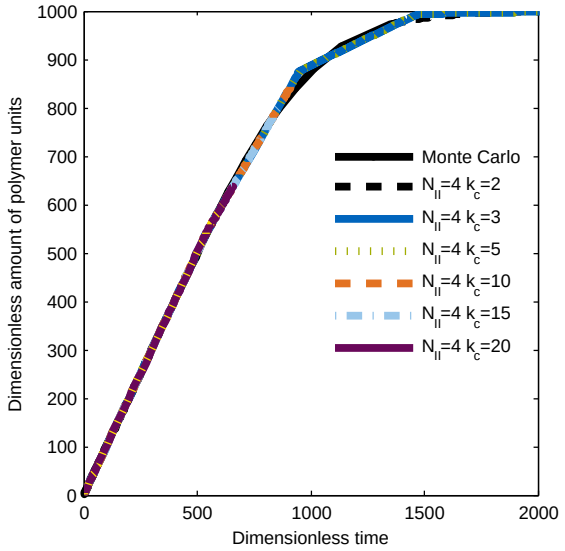

Figure 3.9: Polymer concentration as a function time for linear polymers attacked by ECS with varying $\breve{k}_c$.

For the undivided domain ($\breve{k}_c = 0$) and for $N_\mathrm{I} < 8$, instead of the correct constant rate of increase of the amount of polymer units an exponential increase was obtained at the beginning. However, after some time a constant rate of increase was obtained. Furthermore, the wrong final state was computed. The time taken to obtain a constant rate decreased as the value N_I increased until $N_\mathrm{I} = 8$, for which the correct rate was obtained. In addition, the final state for $N_\mathrm{I} = 6$ was closer to the true solution than that for $N_\mathrm{I} = 3$, but the true value was not obtained. On the other hand, if the domain was divided ($\breve{k}_c = 2$), the correct qualitative behavior was obtained for every N_I (see Figure 3.10) and the final state was predicted within the accuracy of the Monte Carlo results. In addition it was observed that the results converged to the Monte Carlo results with increasing N_I. However, a further increase in $\breve{k}_c$ did not show any further improvement in the results.

The strong benefit of dividing the domain can be explained as follows. If the domain is undivided, the product of ECS (monomer) is created in Subdomain I. Accordingly, the amount of polymer units that can be hydrolyzed is increased erroneously and the reaction rate increases, resulting in an exponential increase rather than a uniform increase. Creation of monomer in Subdomain I forces one quadrature point to describe it. If the monomer is represented by one quadrature point, the amount of polymer units that can be attacked does not increase, and the correct behavior is obtained. In addition, the time taken for one quadrature point to represent the ECS product is reduced with an increase in the number of quadrature points. Therefore, the time taken to predict the right behavior decreases. Furthermore, if the domain is divided, the ECS product is created in the discrete domain and accordingly the reaction is better described.

A further increase in $\breve{k}_c$ does not have any benefit because no intermediate products are created and the initial quantity of the polymer in Subdomain II and III is negligible.

Note that the computation time for the action of ECS (see Table 3.2) grew nearly quadratically with $\breve{k}_c$ for $N_\mathrm{I} = 1$ and 2 because the number of discrete equations is a quadratic function in $\breve{k}_c$. For $N_\mathrm{I} \geq 3$, several computations took unexpectedly longer times and were aborted because they reached the maximum allowed simulation time of 2 hours. These simulations took longer because the problem became very ill-conditioned such the integrator had to take very small time steps to satisfy the tolerance constraints. The computation time also increased with an increase in the value of N_I.

Random chain scission of linear bonds If only the RCS mechanism was active, the simulations were successful for up to $N_\mathrm{I} = 4$ for all values of $\breve{k}_c$, except for $N_\mathrm{I} = 4$ and $\breve{k}_c = 9$. This simulation failed because the integrator had to take very small steps, which resulted in an unacceptably high simulation time. Results for $N_\mathrm{I} > 4$ could only be obtained in very few cases.

Notably, the results obtained with the DQMOM and the Monte Carlo simulations deviated quite strongly, although the same qualitative behavior was obtained (see Figures 3.11 and 3.12). For low values of $\breve{k}_c$ not even the final state was predicted correctly (see Figure 3.11). The final state did, however, converge to the Monte Carlo solution with increasing $\breve{k}_c$. In addition, while the value for the final state approached the true solution very slowly with increasing N_I, the transient behavior approached the Monte Carlo result rapidly as the value of N_I increased (see Figure 3.12). The accuracy increased as the value

of N_I increased because larger polymers are better described using more quadrature points. On the other hand, the increase in accuracy as the value of $\breve{k}_c$ increased can be attributed to a more accurate description of the degradation of small polymers, which are created as intermediate products because the assumption of continuity is not made for them and their resolution is higher. The representation of the intermediate product is important because a significant percentage of the monomer units are within Subdomain II and III after a short time. Therefore, a higher resolution for low molecular weight polymers yields a smaller error.

As an example of the concentration of a low molecular weight polymer, the number concentration of the dimer without a branching bond is shown in Figure 3.13. The concentration first increases as the dimer is formed. At a certain point in time, however, the dimer is degraded into monomers as rapidly as it is formed. Subsequently, the dimer concentration decreases. Interestingly, the profile for these polymers was correct qualitatively in the DQMOM simulations, whereas it was quantitatively wrong . However, as the value of $\breve{k}_c$ increase, the concentration approached the Monte Carlo result. Here, the approach for N_I was very slow.

In addition, the simulation time increased with increasing N_I (see Table 3.2). Furthermore, dividing the domain first increased the computation time significantly because it enabled a quadrature point to leave the domain at a certain time and determining that point in time is computationally expensive. However, the computation time decreased with a further increase in $\breve{k}_c$ because the quadrature point left the domain more rapidly. Subsequently, the computation time increased again because the number of equations to be solved is a quadratic function of $\breve{k}_c$. The table shows that the simulations with $\breve{k}_c = 10$ were always faster than the Monte Carlo simulations.

Random debranching scission If only RDS was active, the simulations were successful for up to $N_\mathrm{I} = 4$ for all values of $\breve{k}_c$, except for two cases. Those two cases failed because of negative weights in the continuous-discrete region. Values of N_I greater than 5 only succeeded for three cases. But those cases only succeeded because the number of quadrature points was decreased almost immediately to values < 4 (see the discussion of error handling in Section 3.3.3).

The amount of polymer units deviated quite strongly from the Monte Carlo result for the undivided domain (see Figure 3.15), whereas for the divided domain, convergence to the Monte Carlo results was observed. Notably, an increase in the value of N_I (see Figure 3.14) from 1 to 2 decreased the deviation considerably, but further increase only had a small influence on the results. In addition, the results for the amount of monomers (see Figure 3.16) deviated quite strongly from the Monte Carlo results at low values of $\breve{k}_c$ and N_I, but approached the Monte Carlo results as both $\breve{k}_c$ and N_I increased.

Furthermore, the simulation time (see Table 3.2) increased quite significantly for the undivided domain as N_I increased. This behavior can be explained by the approach of the value of the $\bar{b}$ coordinate of one quadrature point to 1. If $\bar{b} > 1$, the polymer represented by the quadrature point was attacked and $\bar{b}$ was decreased. If $\bar{b} < 1$, the polymer represented by the quadrature point could not be attacked. Because the other quadrature point(s) still produced polymers with an average value for $\bar{b} > 1$, the value for $\bar{b}$ of the quadrature point increased again. This process was repeated several times. Because the change

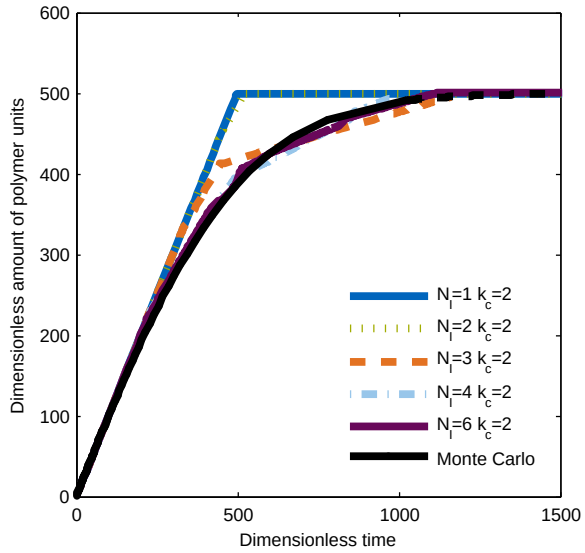

Figure 3.10: Comparison of the amount of polymers generated due to ECS for various numbers of quadrature points N_l with $\breve{k}_c = 2$ [2] (With kind permission from Elsevier).

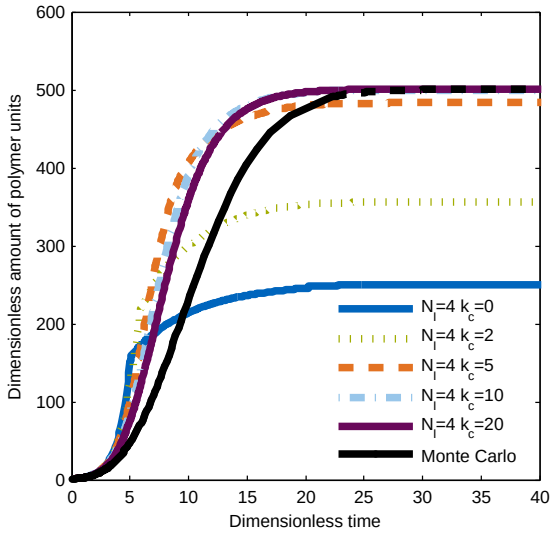

Figure 3.11: Comparison of the amount of polymers generated due to RCS for several values of $\breve{k}_c$ with $N_\mathrm{l} = 4$ [2] (With kind permission from Elsevier).

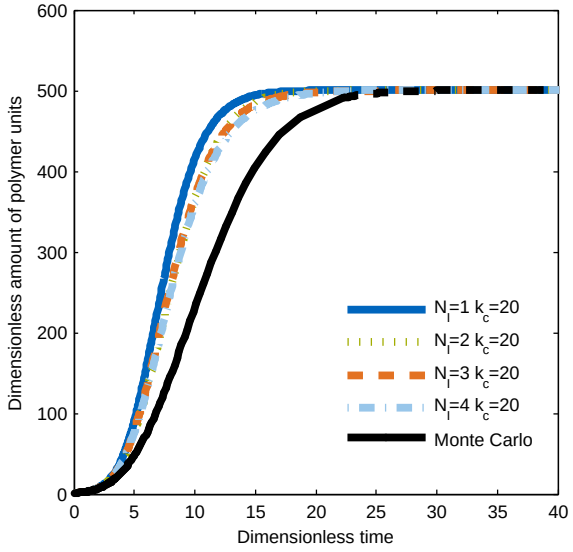

Figure 3.12: Comparison of the amount of polymers generated due to RCS for several values of N_l with $\breve{k}_c = 20$ [2] (With kind permission from Elsevier).

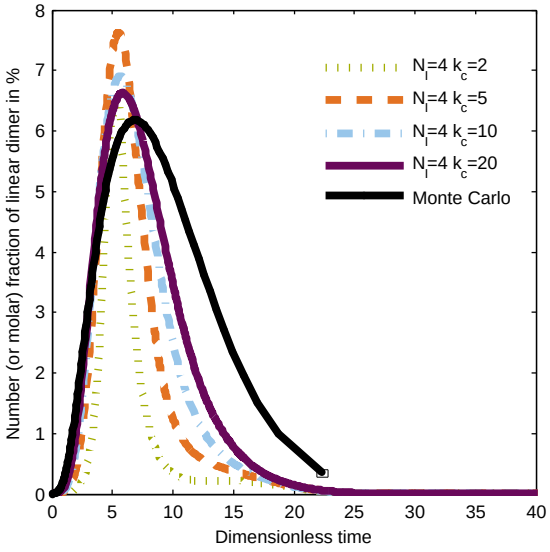

Figure 3.13: Number (or molar) fraction of the dimer without a branching bond subjected to RCS for several values of $\breve{k}_c$ with $N_\mathrm{l} = 4$ [2] (With kind permission from Elsevier).

Table 3.2: Computation time in seconds [2] (With kind permission from Elsevier).

	RCS				RDS				ECS			
$\breve{k}_c$	$N_\mathrm{l}=1$	2	3	4	1	2	3	4	1	2	3	4
1	0.4	92.4	100.8	5695	0.4	386.3	379.9	500.2	0.4	0.6	1.1	113.9
2	1.9	319.3	652.6	7200^*	1.3	1.8	2.8	3.6	0.6	1.0	7200^*	32.9
3	2.5	290.6	296.6	7200^*	1.9	2.6	3.0	4.1	1.0	1.5	2.3	7200^*
4	3.2	256.2	268.0	7200^*	2.2	2.9	3.9	5.1	1.8	2.5	3.4	942.4
5	4.4	235.0	208.7	1051	3.1	3.5	4.7	9.6	2.2	3.2	3.7	7200^*
6	4.8	243.2	954.5	923.0	3.4	5.5	5.8	6.9	3.2	3.9	7200^*	3360
7	6.1	296.2	285.0	7200^*	4.8	5.9	7.7	9.3	3.4	4.6	5.1	3003
8	8.0	315.3	319.7	1162	6.4	7.2	7.8	38.2	4.6	5.6	8.0	6130
9	9.2	378.7	356.0	2173	7.8	10.0	11.4	13.7	5.2	7.4	9.2	21.4
10	11.8	424.6	424.6	2970	9.4	10.5	12.8	14.3	7.0	7.5	11.8	36.5

* Simulation aborted.

in the time derivatives was large, the time step size decreased to very small values. Consequently, this process required a lot of computational effort. However, the computation time for two or more quadrature points strongly decreased when a subdomain was introduced because the values of the $\bar{b}$ coordinates of the quadrature points were always > 1, and thus a discontinuity in the reaction rate could not occur. On the other hand, a further increase in $\breve{k}_c$ led to a nearly quadratic increase in the simulation time because the number of discrete equations increased quadratically with $\breve{k}_c$.

Simultaneous random chain and end chain scissions When both RCS and ECS occurred simultaneously with the same reaction constant, RCS was the dominant process. RCS created polymers that could be attacked, whereas ECS only released one monomer unit. The numerical behavior was also dominated by RCS. Therefore if RCS is described well, the whole process is described well. Therefore, showing the results obtained under these conditions is not necessary because they do not provide any further insights.

3.5 Conclusion and outlook

In this chapter a novel method for describing the depolymerization of a branched polymer using Direct Quadrature Method of Moments (DQMOM) in a mixed continuous-discrete formulation was described. The new method increased the accuracy of the simulation for all the mechanisms considered. More accurate results could be obtained by increasing the number of quadrature points or the amount of monomer units to be considered discretely. However, doing so, strongly increased the simulation time to levels not acceptable for model-based control and optimization. Furthermore, stability problem occurred at high number of quadrature points or $\breve{k}_c$.

In particular, the discrete consideration of the monomer produced by End-chain scission (ECS) in-

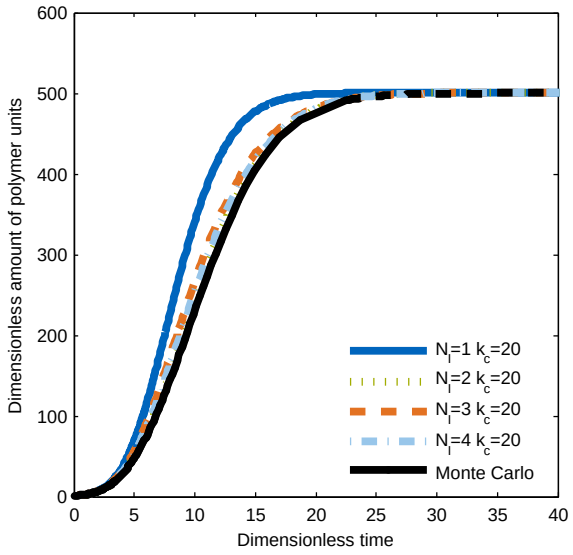

Figure 3.14: Polymer concentration as a function of time for RDS with varying N_{l} [2] (With kind permission from Elsevier).

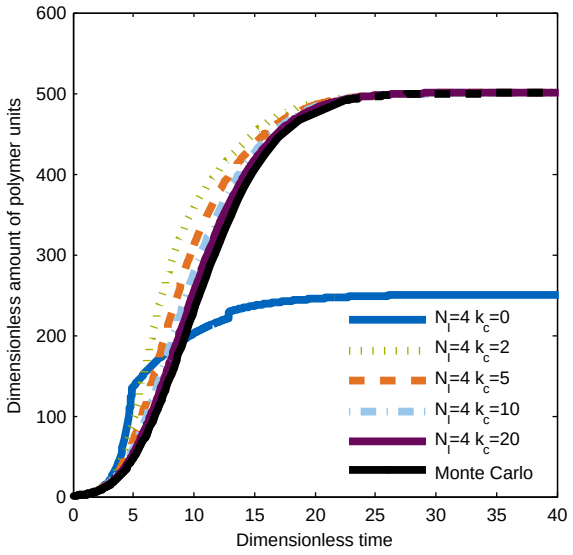

Figure 3.15: Polymer concentration as a function of time for RDS with varying $\breve{k}_c$ [2] (With kind permission from Elsevier).

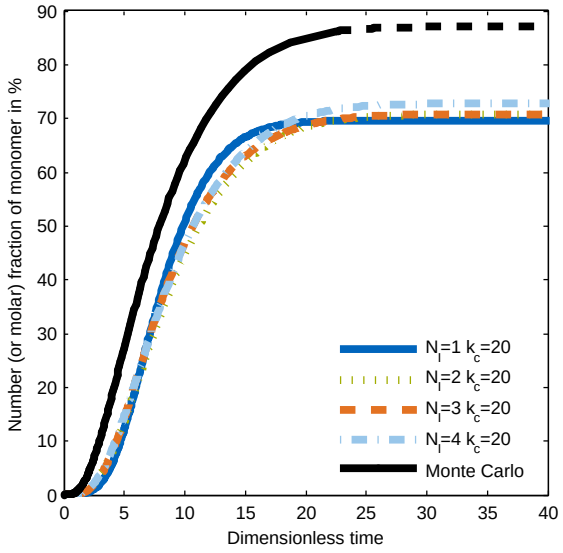

Figure 3.16: Number (or molar) fraction of monomer in % as a function of time generated via RDS with varying N_{l} [2] (With kind permission from Elsevier).

creased the accuracy. Thus, the division of the computational domain was beneficial for removing highly localized phenomena that are known to cause problems using Quadrature Method of Moments (QMOM) techniques [89]. The division of the domain also removed the discontinuity in the reaction rate of Random-chain scission (RCS), which helped reduce the required computational effort. It is postulated that removing discontinuities from the reaction rates used in DQMOM will also be beneficial for other scenarios. Simulations of ECS or similar mechanisms (e.g. preferred attack close to the chain end [216]) must consider the end chain products discretely.

On the other hand, the accuracy of the description of RCS was not acceptable. This problem is not related to the domain decomposition developed in this study but it is a limitation of either DQMOM or the continuity approximation. If it is due to the continuity approximation, one should try to implement a Method Of Moments (MOM) without using the continuity assumption. This has never been done before. The underlying theory of QMOM is based on continuity and, therefore, application to a discrete formulation will be difficult. If the problem is due to a deficiency of DQMOM, other moment-based methods for solving bivariate Population Balance Equations (PBEs), such as the Conditional Quadrature Method of Moments [226], the Sectional Quadrature Method of Moments [108], and the Differential Maximum Entropy Method [111], should be evaluated in future works. If any method is suitable to describe the validation problem considered here, it should be applied to more complicated cases where the reaction rate depends on the characterizing variables.

This domain decomposition algorithm developed in this Chapter can also be extended to other problems besides depolymerization. It can be used when the underlying PBE is discrete. Furthermore, the benefit is expected to be the greatest when very large values of the internal coordinates appear together with very small values. This algorithm then allows a very fine resolution of very small values of the internal coordinate. However, the algorithm can only be successfully applied if the method used to simulate the evolution of Subdomain I has a sufficient accuracy and is validated.

Chapter 4

Solving the Population Balance Equation using a Method of Classes

Besides the Method Of Moments (MOM) Methods Of Classes (CMs), also called sectional methods, are commonly used to solve Population Balance Equations (PBEs). In this chapter the theory behind these sectional methods is reviewed and adapted to a discrete PBE. The implementation is described and then the algorithm is validated by comparison to kinetic Monte Carlo (kMC) results. Afterwards, the model proposed in Chapter 2 is solved and compared to literature data. Last, a short conclusion is drawn.

4.1 Theory

CMs were first formulated in a general form by Kumar and Ramkrishna [112, 113, 114] in an influential series of papers. Previous works, e.g. [227], were only formulated for specific meshes. For simplicity, the methods are explained first for the monovariate case and then extended to the bivariate case.

4.1.1 Method of Classes for a monovariate Population Balance Equation

All CMs first divide the computational domain $[k_{m,\min}, k_{m,\max}]$, where the index m stands for mesh, into elements, called bins or classes. The borders of the i-th elements are $[\bar{k}_{m,i}, \bar{k}_{m,i+1}]$ where $\bar{k}_{m,1} = k_{\min}$ and $\bar{k}_{m,N+1} = k_{m,\max}$ with N being the number of elements. Then the Number Density Function (NDF) in the bin is expressed by one particular value $\bar{k}_i$ ($\bar{k}_{m,i} < \bar{k}_i < \bar{k}_{m,i+1}$), the pivot. This result in the approximation of the NDF by a sum of Dirac deltas

$$\bar{n}(t,\bar{k}) \approx \sum_{i=1}^{N} \bar{w}_i \cdot \delta(\bar{k} - \bar{k}_i). \tag{4.1}$$

The equations for the time evolution of the weights and the pivots should result in a good approximation of the time evolution of the NDF. CMs can be grouped into two families that obtain this equations in a

different manner:

Moving pivot

The Moving Pivot technique was invented by Kumar and Ramkrishna [113]. In this method the position of the Dirac delta is variable. This allows good representation of growth [113, 114]. However, numerical problems were reported in solving breakage [228] and also encountered in preliminary work performed by Mr. Spaunhorst and me. Furthermore, twice as many equations as with Fixed Pivot technique (FP) based methods need to be solved. A derivative was applied to enzymatic catalyzed depolymerization by Lebaz et al. [138], but the results did not converge to the exact solution. Accordingly, using this method is not seen as a promising solution strategy.

Fixed pivot and derivatives

The Fixed Pivot technique (FP) was proposed by Kumar and Ramkrishna [112]. In this method the positions of the Dirac deltas are constant. Besides increased numerical stability, often computations can be performed prior to solving the system of Ordinary Differential Equations (ODEs) (offline) which increases computational efficiency. However, this comes at the price of having only one degree of freedom per bin which necessitates using a heuristical approach to close the equations. The FP and all of its derivative demand that at least two arbitrary moments are preserved. In this study, the zeroth and first order moments are chosen because they have a clear physical interpretation. Kostoglou [229] extended a FP derivative to preserve more than two moments and the extension can be easily transfered to the FP. As only two moments have a clear physical meaning this extension is not needed here.

If one would demand that one sectional moment per bin is preserved, one would obtain a method that preserves one moment and describes the behavior in each bin well. The l-th order sectional moment is obtained by multiplication of the NDF with an arbitrary function (here 1 or k) and then integration from $\bar{k}_{m,l}$ to $\bar{k}_{m,l+1}$. This yields the form of the moment as follows:

$$\bar{\mu}_l^i = \int_{\bar{k}_{m,l}}^{\bar{k}_{m,l+1}} \bar{k}^i \cdot \bar{n}(t,\bar{k})\,\mathrm{d}\bar{k}. \tag{4.2}$$

The equation for the time evolution of the zeroth and first order sectional moment can be easily obtained

$$\frac{\mathrm{d}\bar{\mu}_l^0}{\mathrm{d}t} = -\int_{\bar{k}_{m,l}}^{\bar{k}_{m,l+1}} \bar{D}_{\sum}(t,\bar{k})\,\mathrm{d}\bar{k} + \int_{\bar{k}_{m,l}}^{\bar{k}_{m,l+1}} \bar{B}_{\sum}(t,\bar{k})\,\mathrm{d}\bar{k} = -\bar{\omega}_{\sum,l}^0(t) + \bar{\alpha}_{\sum,l}^0(t) \tag{4.3}$$

$$\frac{\mathrm{d}\bar{\mu}_l^1}{\mathrm{d}t} = -\int_{\bar{k}_{m,l}}^{\bar{k}_{m,l+1}} \bar{k}\cdot\bar{D}_{\sum}(t,\bar{k})\,\mathrm{d}\bar{k} + \int_{\bar{k}_{m,l}}^{\bar{k}_{m,l+1}} \bar{k}\cdot\bar{B}_{\sum}(t,\bar{k})\,\mathrm{d}\bar{k} = -\bar{\omega}_{\sum,l}^1(t) + \bar{\alpha}_{\sum,l}^1(t). \tag{4.4}$$

Moments of the death and birth term If the approximation of the NDF is substituted into the above equations, one can compute the moments. The zeroth order moment of the death term for the simplified

linear validation case (see Section 2.5.2) can easily be computed as

$$\bar{\omega}^0_{RCS/ECS,l} = \begin{cases} C_{RCS/ECS} \cdot w_l & k_l \geq 2 \\ 0 & \text{otherwise} \end{cases} . \tag{4.5}$$

If the reaction rate is computed with the equilibrium model, one obtains

$$\bar{\omega}^0_{\bullet,l} = \frac{s_{\bullet,cat}(k_l) \cdot E_\bullet \cdot w_l}{1 + K_{\bullet,eq} + \sum_{i=1}^{N} w_i \cdot I_\bullet(k_i)}. \tag{4.6}$$

For most death rates, including all rates considered in this work, the first order moment can be expressed as

$$\bar{\omega}^1_{\bullet,l}(t) = \bar{k}_l \cdot \bar{\omega}^0_{\bullet,l}(t). \tag{4.7}$$

Furthermore, using Equation (A.8) for the birth rate, allows expressing the moments of the birth rate as

$$\bar{\alpha}^0_l(t) = \sum_{j=1}^{N} \bar{\omega}^0_j(t) \cdot 2 \cdot \int_{\bar{k}_{m,l}}^{\bar{k}_{m,l+1}} \bar{\gamma}(\bar{k}, \bar{k}_j) \cdot H(\bar{k}_j - \bar{k} - 1)\, \mathrm{d}\bar{k} \tag{4.8}$$

$$\bar{\alpha}^1_l(t) = \sum_{j=1}^{N} \bar{\omega}^0_j(t) \cdot 2 \cdot \int_{\bar{k}_{m,l}}^{\bar{k}_{m,l+1}} \bar{k} \cdot \bar{\gamma}(\bar{k}, \bar{k}_j) \cdot H(\bar{k}_j - \bar{k} - 1)\, \mathrm{d}\bar{k}. \tag{4.9}$$

One can identify the j-th order sectional moments of birth occurring in the l-th bin due to hydrolysis in bin j $\bar{\alpha}^i_{l,j}$

$$\bar{\alpha}^i_{l,j} = \bar{\omega}^0_j \cdot 2 \cdot \int_{\bar{k}_{m,l}}^{\bar{k}_{m,l+1}} \bar{k}^i \cdot \bar{\gamma}(\bar{k}, \bar{k}_j) \cdot H(\bar{k}_j - \bar{k} - 1)\, \mathrm{d}\bar{k}. \tag{4.10}$$

Because the product distribution function is time-invariant in this work, one can extract a matrix that allows computation of the birth moments from the death rate

$$\bar{M}^i_{\bullet,l,j} = 2 \cdot \int_{\bar{k}_{m,l}}^{\bar{k}_{m,l+1}} \bar{k}^j \cdot \bar{\gamma}(\bar{k}, \bar{k}_j) \cdot H(\bar{k}_j - \bar{k} - 1)\, \mathrm{d}\bar{k} \tag{4.11}$$

$$\bar{\alpha}^j_\bullet(t) = \bar{\mathbf{M}}^j_\bullet \cdot \bar{\omega}^0_\bullet(t). \tag{4.12}$$

Evolution of the Number Density Function If the approximation to the NDF is substituted into the left side, one obtains

$$\frac{\mathrm{d}\bar{\mu}^0_l}{\mathrm{d}t} = \sum_{i=1}^{N} \int_{\bar{k}_{m,l}}^{\bar{k}_{m,l+1}} \delta(\bar{k} - \bar{k}_i)\, \mathrm{d}\bar{k} \cdot \frac{\mathrm{d}\bar{w}_i}{\mathrm{d}t} = \frac{\mathrm{d}\bar{w}_l}{\mathrm{d}t}. \tag{4.13}$$

This is an equation for the evolution of the weights. However, only by chance would the first order moment be conserved. In order to also satisfy preservation of a second moment, FPs demand that a second moment is preserved. The preservation of the second moment is guaranteed if also the second

sectional moment is preserved. Again substitution of the NDF into the left side yields

$$\frac{\mathrm{d}\bar{\mu}_l^1}{\mathrm{d}t} = \sum_{i=1}^{N} \int_{\bar{k}_{m,l}}^{\bar{k}_{m,l+1}} \bar{k} \cdot \delta(\bar{k} - \bar{k}_i)\, \mathrm{d}\bar{k} \cdot \frac{\mathrm{d}\bar{w}_i}{\mathrm{d}t} = \bar{k}_l \cdot \frac{\mathrm{d}\bar{w}_l}{\mathrm{d}t}. \tag{4.14}$$

If $-\bar{\omega}_l^1(t) + \bar{\alpha}_l^1(t)$ cannot be expressed as $\bar{k}_l \cdot (-\bar{\omega}_l^0(t) + \bar{\alpha}_l^0(t))$, application of the simple rule presented in Equation (4.13) would not preserve both moments and, accordingly, the amount of monomer units would not be constant. Accordingly, the sectional moments of the death rate are preserved if the change of the l-th weight is equal to the l-th sectional zeroth moment of the death rate plus a contribution due to the birth rate. The contribution due to the birth rate should be positive to guarantee positivity of the NDF.

Cell Average Technique Kumar et al. [230] proposed the Cell Average Technique (CAT) as an improved form of FP. In a later work [231] they proved that CAT has better convergence properties than FP. In another work of this group [232] it was shown that for the test cases considered CAT was more accurate than FP. Furthermore, Singh et al. [233] found that for the aggregation problems considered in their work CAT was more accurate than FP. Mostafaei et al. [234] proposed a similar but computational more efficient method. However, as this method has not been extended to bivariate cases as CAT has been [235], this method is not used.

With the CAT the contribution to the pivots are set such that the zeroth and first order sectional moment of the birth term are preserved. The contribution due to production in the i-th bin on the j-th pivot $\psi_{i,j}$ are

$$\psi_{i,j} = \begin{cases} \frac{\bar{\alpha}_i^0 \cdot \bar{k}_{j+1} - \bar{\alpha}_i^1}{\bar{k}_{j+1} - \bar{k}_j} & i = j \text{ and } \bar{\alpha}_i^1 > \bar{\alpha}_i^0 \cdot \bar{k}_j \\ \frac{\bar{\alpha}_i^1 - \bar{\alpha}_i^0 \cdot \bar{k}_{j-1}}{\bar{k}_j - \bar{k}_{j-1}} & i = j \text{ and } \bar{\alpha}_i^1 \leq \bar{\alpha}_i^0 \cdot \bar{k}_j \\ \frac{\bar{\alpha}_i^1 - \bar{\alpha}_i^0 \cdot \bar{k}_j}{\bar{k}_{j+1} - \bar{k}_j} & i = j+1 \text{ and } \bar{\alpha}_i^1 > \bar{\alpha}_i^0 \cdot \bar{k}_j \\ \frac{\bar{\alpha}_i^0 \cdot \bar{k}_j - \bar{\alpha}_i^1}{\bar{k}_j - \bar{k}_{j-1}} & i = j-1 \text{ and } \bar{\alpha}_i^1 \leq \bar{\alpha}_i^0 \cdot \bar{k}_j \\ 0 & \text{otherwise} \end{cases}. \tag{4.15}$$

Fixed Pivot Technique Instead of assigning the moment of the total birth rate, FP assign the i-th order sectional moments of birth in bin l due to hydrolysis in bin j $\bar{\alpha}_{l,j}^i$. This results in the equation for the contribution due to the i-th pivot via the l-th bin on the j-th pivot $\psi_{i,l,j}$

$$\psi_{i,l,j} = \begin{cases} \frac{\bar{\alpha}_{l,i}^0 \cdot \bar{k}_{j+1} - \bar{\alpha}_{l,i}^1}{\bar{k}_{j+1} - \bar{k}_j} & l = j \text{ and } \bar{\alpha}_{l,i}^1 > \bar{\alpha}_{l,i}^0 \cdot \bar{k}_j \\ \frac{\bar{\alpha}_{l,i}^1 - \bar{\alpha}_{l,i}^0 \cdot \bar{k}_{j-1}}{\bar{k}_j - \bar{k}_{j-1}} & l = j \text{ and } \bar{\alpha}_{l,i}^1 \leq \bar{\alpha}_{l,i}^0 \cdot \bar{k}_j \\ \frac{\bar{\alpha}_{l,i}^1 - \bar{\alpha}_{l,i}^0 \cdot \bar{k}_j}{\bar{k}_{j+1} - \bar{k}_j} & l = j+1 \text{ and } \bar{\alpha}_{l,i}^1 > \bar{\alpha}_{l,i}^0 \cdot \bar{k}_j \\ \frac{\bar{\alpha}_{l,i}^0 \cdot \bar{k}_j - \bar{\alpha}_{l,i}^1}{\bar{k}_j - \bar{k}_{j-1}} & l = j-1 \text{ and } \bar{\alpha}_{l,i}^1 \leq \bar{\alpha}_{l,i}^0 \cdot \bar{k}_j \\ 0 & \text{otherwise} \end{cases}. \tag{4.16}$$

This has the advantage that, if $\bar{\gamma}$ is not a function of time, the time intensive computations can be performed prior to the actual simulation and the result collected in a matrix P. An equation linear in the zeroth order moment of the hydrolysis rate results

$$\frac{\mathrm{d}\bar{\mathbf{w}}}{\mathrm{d}t} = \sum (\mathbf{P}_\bullet(\bar{\mathbf{k}}) - \mathbf{I})\bar{\omega}_\bullet^0(t, \bar{\mathbf{w}}, \bar{\mathbf{k}}). \tag{4.17}$$

4.1.2 Fixed Pivot based techniques for a bivariate Population Balance Equation

Again first the computational domain is divided into elements. The shape of those elements can be arbitrary. The NDF is again expressed by one particular value within this element. This results in the approximation:

$$\bar{n} \approx \sum_{i=1}^{N} \bar{w}_i \cdot \delta(\bar{k} - \bar{k}_i) \cdot \delta(\bar{b} - \bar{b}_i). \tag{4.18}$$

The sectional moments can also be easily extended

$$\bar{\mu}_l^{i,j} = \int_{E_l} \bar{k}^i \cdot \bar{b}^j \cdot \bar{n}(t, \bar{k}, \bar{b}) \, \mathrm{d}\bar{b}\mathrm{d}\bar{k}, \tag{4.19}$$

where E_l is the l-th element. The evolution equation of the moments is

$$\frac{\mathrm{d}\bar{\mu}_l^{i,j}}{\mathrm{d}t} = -\int_{E_l} \bar{D}_\sum(t, \bar{k}, \bar{b}) \, \mathrm{d}\bar{b}\mathrm{d}\bar{k} + \int_{E_l} \bar{B}_\sum(t, \bar{k}, \bar{b}) \, \mathrm{d}\bar{b}\mathrm{d}\bar{k} = -\bar{\omega}_{\bullet,l}^{i,j}(t) + \bar{\alpha}_{\bullet,l}^{i,j}(t). \tag{4.20}$$

All moments can again be expressed as a linear product of the zeroth order moment of the death term and a time-independent multiplicator

$$\bar{\omega}_{\bullet,l}^{i,j}(t) = \bar{k}_l^i \cdot \bar{b}_l^j \bar{\omega}_{\bullet,l}^{0,0}(t) \tag{4.21}$$

$$\bar{\alpha}_{\bullet,l}^{i,j}(t) = \bar{\mathbf{M}}_\bullet^{i,j} \bar{\omega}_\bullet^{0,0}(t). \tag{4.22}$$

Again one wants to preserve more than one moment. However, with more than one dimension selecting the pivots to distribute the birth to is not unique. Kumar et al. [235] have proposed a method of selecting four pivots and preserving three moments. This method requires a regular grid and can not be straightforwardly used for the non rectangular domain encountered in this work. Chakraborty and Kumar [224] have proposed a method of selecting three pivots and preserving three moments which is used in this work. The three moments used in this work are the zeroth order and the two first order moments which correspond to the amount of polymer, monomer units, and branching bonds produced in a bin.

Distributing the birth rate The first step is to find a space filling triangulation of the domain with the pivots as corner points. This can be done using for example Delaunay triangulation [236]. Then it is determined in which element the produced particles lie. This is at the point defined by $\left[\frac{\bar{\alpha}_l^{1,0}}{\bar{\alpha}_l^{0,0}}, \frac{\bar{\alpha}_l^{0,1}}{\bar{\alpha}_l^{0,0}}\right]$. If

the index of the corner points is i, j, and m then the following linear system has to be obtained to find the contribution due to birth in the l-th element to the i-th pivot $\psi_{i,l}$

$$\begin{bmatrix} 1 & 1 & 1 \\ \bar{k}_i & \bar{k}_j & \bar{k}_m \\ \bar{b}_i & \bar{b}_j & \bar{b}_m \end{bmatrix} \cdot \begin{bmatrix} \tilde{\psi}_{i,l} \\ \tilde{\psi}_{j,l} \\ \tilde{\psi}_{m,l} \end{bmatrix} = \begin{bmatrix} 1 \\ \frac{\bar{\alpha}_l^{1,0}}{\bar{\alpha}_l^{0,0}} \\ \frac{\bar{\alpha}_l^{0,1}}{\bar{\alpha}_l^{0,0}} \end{bmatrix} \tag{4.23}$$
$$\psi_{\bullet,l} = \tilde{\psi}_{\bullet,l} \cdot \bar{\alpha}_l^{0,0}.$$

The methods was described for CAT here, but was originally developed for FP and can be easily converted back by substituting the moments of the birth rate to due a specific pivot in this bin. Again with the FP one can - for time independent Product Distribution Functions (PDFs) - perform most computations prior to solving the system of ODEs and collect the results in a matrix. This results in

$$\frac{\mathrm{d}\bar{\mathbf{w}}}{\mathrm{d}t} = \sum (\mathbf{P}_\bullet(\bar{\mathbf{k}}, \bar{\mathbf{b}}) - \mathbf{I}) \bar{\omega}_\bullet^{0,0}(t, \bar{\mathbf{w}}, \bar{\mathbf{k}}, \bar{\mathbf{b}}). \tag{4.24}$$

4.2 Extension to a discrete Population Balance Equation

Polymers are built from discrete monomer units. One can assume for large polymers that the PBE is continuous [54]. However, this assumption is not valid in the whole domain, as already discussed in the preceding chapter. Therefore, it is desirable to use FP or CAT for a discrete PBE. The definition of the sectional moments has to be changed from integration to summation. For the monovariate case

$$\breve{\mu}_l^i = \sum_{\breve{k}=\breve{k}_{m,l}}^{\breve{k}_{m,l+1}} \breve{k}^i \cdot \breve{n}(t, \breve{k}). \tag{4.25}$$

Choosing the borders to be discrete is difficult with commonly used meshes. Therefore, the borders are discretized. The left border is $\breve{k}_{m,l} = \lfloor \bar{k}_{m,l} + 1 \rfloor$ and the right border $\breve{k}_{m,l} = \lfloor \bar{k}_{m,l} \rfloor$. This prevents double counting and guarantees that for all $\breve{k}$ in element l: $\bar{k}_{m,l} < \breve{k} \leq \bar{k}_{m,l+1}$. The definition of the sectional moments is changed:

$$\breve{\mu}_l^i = \sum_{\breve{k}=\lfloor \bar{k}_{m,l}+1 \rfloor}^{\lfloor \bar{k}_{m,l+1} \rfloor} \breve{k}^i \cdot \breve{n}(t, \breve{k}). \tag{4.26}$$

For the bivariate case discretizing the borders is more complicated. In this work only rectangular and triangular elements are used. Simplifying the problem is that the triangular elements do not have a left neighbor. The sectional moments are defined for a rectangular element $[\bar{k}_{m,l}, \bar{k}_{m,l+1}] x [\bar{b}_{m,l}, \bar{b}_{m,l+1}]$

$$\breve{\mu}_l^{i,j} = \sum_{\breve{k}=\lfloor \bar{k}_{m,l}+1 \rfloor}^{\lfloor \bar{k}_{m,l+1} \rfloor} \sum_{\breve{b}=\lfloor \bar{b}_{m,l}+1 \rfloor}^{\lfloor \bar{b}_{m,l+1} \rfloor} \breve{k}^i \cdot \breve{b}^j \cdot \breve{n}(t, \breve{k}, \breve{b}). \tag{4.27}$$

For a triangular element $\breve{k},\breve{b} \in \mathbb{N}_0 : \lfloor \bar{k}_{m,l}+1 \rfloor \leq \bar{k} \leq \lfloor \bar{k}_{m,l+1} \rfloor, \lfloor \bar{b}_{m,l}+1 \rfloor \leq \breve{b} \leq \breve{k}-1$

$$\breve{\mu}_l^{i,j} = \sum_{\breve{k}=\lfloor \bar{k}_{m,l}+1 \rfloor}^{\lfloor \bar{k}_{m,l+1} \rfloor} \sum_{\breve{b}=\lfloor \bar{b}_{m,l}+1 \rfloor}^{\breve{k}-1} \breve{k}^i \cdot \breve{b}^j \cdot \breve{n}(t,\breve{k},\breve{b}). \tag{4.28}$$

Furthermore, one needs to substitute the Dirac deltas in the approximation of the NDF by Kronecker deltas which requires pivot at integer values. The pivot is almost always taken to be in the middle of the element which would not be at an integer value. This problem is solved by simply rounding. For the monovariate case

$$\breve{k}_l = \text{round}(\bar{k}_{m,l}, \bar{k}_{m,l+1}) \tag{4.29}$$

$$\breve{n}(t,\breve{k}) \approx \sum_{i=1}^{N} \bar{w}_i \cdot \breve{\delta}_{\breve{k}_l,\breve{k}} \tag{4.30}$$

Not having pivots on the boundary line $k-1=b$ could introduce problems and, accordingly, pivots are forced to be on this lines. This leads to

$$\breve{k}_l = \text{round}(\bar{k}_{m,l}, \bar{k}_{m,l+1}) \tag{4.31}$$

$$\breve{b}_l = \text{round}(\bar{b}_{m,l}, \bar{b}_{m,l+1}) \tag{4.32}$$

$$\breve{n}(t,\breve{k}) \approx \sum_{i=1}^{N} \bar{w}_i \cdot \breve{\delta}_{\breve{k}_l,\breve{k}} \cdot \breve{\delta}_{\breve{b}_l,\breve{b}}. \tag{4.33}$$

The moments can again be expressed by a linear product of the zeroth order moment of the death term and a time-independent multiplicator.

4.3 Implementation

In this section the details of the numerical implementation are described.

4.3.1 Meshing

The division of the computational domain into elements is required for applying any sectional technique. A mesh is good if a high accuracy is obtained at a moderate computational cost.

Linear polymer

Here, the meshing strategy proposed by Ho et al. [127] is used. The mesh is visualized in Figure 4.1a. Ho et al. [127] proposed a mesh divided in three parts: The first part up to $\breve{k}_c$ has exactly represented polymers. It is important to know the products (monomer and small oligomers) precisely. Therefore, the equations describing those oligomers are solved directly without using any class method. The second

part starts with a bin size of 1 and each bin increases in size by 1. The third part has a geometric mesh. This means that the width of element $l+1$ is equal to the width of element l times the growth factor. In order to not have any jumps in the mesh size increase it is demanded that the first increase of the geometric mesh is the equal to the increase of the linear mesh. The meshing is continued until a specified amount of monomer units is within the meshed area.

Branched polymer

Several authors have studied how to best set up a multi-dimensional grid [224, 237]. However, nobody has studied breakage or depolymerization in great detail. Here a simple meshing strategy is used. This strategy is visualized in Figure 4.1b The meshing strategy for the linear mesh is used for both coordinates with the same parameters, except that the exactly represented branching bonds start from 0 and go up to $\breve{k}_c - 1$ and that the maximal amount of branching bonds is set such that almost no polymer has a greater amount of branching bonds than the maximal amount. This results in one completely exact region, one region in which the class method is only used in the amount of monomer unit, and the largest region where the class method is used for both coordinates. This domain has rectangular and triangular elements. After this meshing is done, the elements above a specified amount of branching bonds, which is chosen to be sufficiently large, are cut away.

4.3.2 Computations prior to the solution of the Ordinary Differential Equations

The matrix describing the birth term for the Fixed Pivot technique and the initial condition can be evaluated prior to solving the ODEs.

Distributing the birth term

For all pivots with less than or equal to $\breve{k}_c$ monomer units no distribution is necessary. And for all pivots with less than or equal to $\breve{k}_c - 1$ branching bonds the equations have already been provided in Equations (4.15) and (4.16). For the remaining pivots a space filling Delaunay triangulation using the MATLAB function `delaunay` is used. Then the MATLAB algorithm `triangulation` is used to identify the element in which the birth occurs and also to provide already the distribution to each corner. This algorithm, however, returns small negative values if the birth occurs close to the boundary of the elements. In this case the birth is shifted onto the boundary and the distribution of the birth is performed using the 1D algorithm. For CAT and FP the same algorithm is used. However, using CAT the distribution of the birth term has to computed with every evaluation of the hydrolysis rate.

Initial condition

As the first step in initialization the amount of polymers, monomer units, and branching bonds in each bin is obtained. Then using the algorithm to distribute the birth term, which has been described just

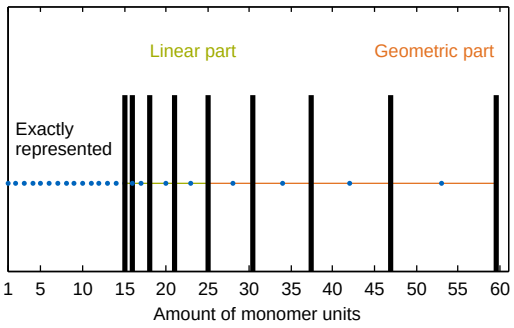

(a) The mesh for a linear polymer with $\check{k}_c = 15$. In green the linear part of the mesh and in orange the geometric part.

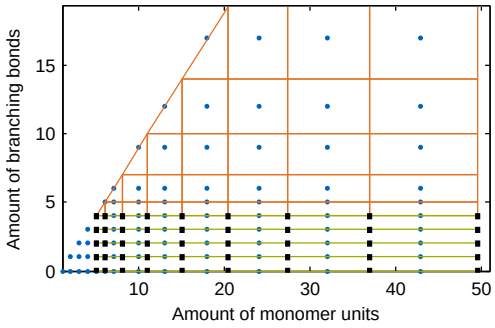

(b) The mesh for a branched polymer with $\check{k}_c = 5$ and maximal 10 branching bonds. In green the exact representation in the amount of branching bonds and in orange the approximation for both coordinates.

Figure 4.1: The growth factor is $1.\overline{3}$. The maximal amount of monomer units is 55. The blue dots represent the pivots and the black bars are separators between the bins.

before this, this is distributed to the bins. This guarantees that the amount of polymers, monomer units, and branching bonds is computed to values close to the machine precision. By just assigning the amount of polymer units to each pivot, the amount of monomer units would not be obtained with a high accuracy with a coarse mesh.

For a small amount of monomer units and linear polymers the required moments can be obtained by just evaluating the initial distribution in each point in a reasonable time (<10 minutes). However, for branched polymer the computational time and memory requirement scales quadratically with the amount of monomer units. This would lead to requiring days with large branched polymer. Therefore, for such large systems the initial distribution in monomer directions is approximated as a Gamma distribution for more than 1×10^5 monomer units and in branching bond direction with a normal distribution for more than 1×10^5 branching bonds. Then instead of evaluating at every point and summation, this can be replaced by a numerical integration with the MATLAB integrator `integral2`.

Normalization

The polymer concentration is low which would cause numerical problems. Furthermore, large polymers have more monomer units than small polymers and should, therefore, be weighted more strongly in decisions about the step size. For FP this can be implemented easily offline. However, for CAT parts of the computations would have to be performed online, because of the non-linear nature of the distribution of the birth term. Therefore, only normalization with the polymer concentration is performed

Normalization for the Fixed Pivot technique In order to satisfy this requirements, the initial amount at each pivot is normalized by multiplication with the amount of monomer units of the pivot and division

by the total initial concentration

$$\tilde{w}_l = \frac{w_l}{\sum_{i=1}^{N} w_i(t=0) \cdot k_l}. \tag{4.34}$$

Accordingly, the inverse of the Michaelis constants needs to be normalized as well

$$\tilde{I}(k_l, b_l) = \tilde{I}_l = \frac{I_l}{k_l} \cdot \sum_{i=1}^{N} w_i(t=0) \cdot k_i. \tag{4.35}$$

Furthermore, the matrices relating the zeroth order moment of the death term to the other moments need to be normalized

$$\tilde{\mathbf{M}}_{\bullet}^{i,j} = \begin{pmatrix} k_1 & 0 & \cdots & \\ 0 & k_2 & 0 & \cdots \\ \vdots & & \ddots & \vdots \\ 0 & \cdots & 0 & k_N \end{pmatrix} \cdot \mathbf{M}_{\bullet}^{i,j} \cdot \begin{pmatrix} \frac{1}{k_1} & 0 & \cdots & \\ 0 & \frac{1}{k_2} & 0 & \cdots \\ \vdots & & \ddots & \vdots \\ 0 & \cdots & 0 & \frac{1}{k_N} \end{pmatrix}. \tag{4.36}$$

This leads to a normalized distribution matrix $\mathbf{P}$

$$\tilde{\mathbf{P}}_{\bullet} = \begin{pmatrix} k_1 & 0 & \cdots & \\ 0 & k_2 & 0 & \cdots \\ \vdots & & \ddots & \vdots \\ 0 & \cdots & 0 & k_N \end{pmatrix} \cdot \mathbf{P}_{\bullet} \cdot \begin{pmatrix} \frac{1}{k_1} & 0 & \cdots & \\ 0 & \frac{1}{k_2} & 0 & \cdots \\ \vdots & & \ddots & \vdots \\ 0 & \cdots & 0 & \frac{1}{k_N} \end{pmatrix}. \tag{4.37}$$

Normalization for the Cell Average technique The initial amount of polymer at each pivot is normalized by division with the total initial number concentration

$$\tilde{w}_l = \frac{w_l}{\sum_{i=1}^{N} w_i(t=0)}. \tag{4.38}$$

Only the inverse of the Michealis constants needs to be normalized as well

$$\tilde{I}(k_l, b_l) = \tilde{I}_l = \frac{I_l}{k_l} \cdot \sum_{i=1}^{N} w_i(t=0). \tag{4.39}$$

4.3.3 Solving the system of Ordinary Differential Equations

The resulting system of ODEs is solved using the MATLAB solver `ode45` with a relative and absolute tolerance of 1×10^{-6} demanding that the polymer concentration is positive. If due to rounding errors a negative value occurs, it is set to zero.

4.4 Validation

As no prior work has investigated the use of CMs to describe the depolymerization of a branched polymer a validation study has been performed. In this section the enzyme concentrations stays constant and no enzyme becomes inactivated. This means that $K_{eq} = 0$ and the denaturation rates are also zero. In this chapter the computations for the CMs were performed on a computer with 4 Intel Core i5-2500 @3.30 GHz processors with 8 GB RAM running MATLAB® 2013b. The computations were run on all cores at the same time. The times were measured using the internal stopwatch of MATLAB. The computation time for FP was even for $\breve{k}_c = 20$ and a growth factor of 1.02 less than one minute and for most cases studied much less. However, the Monte Carlo results were obtained on a 3.7 GHz 6 cores Intel® E5 processor with more than 128 GB RAM running MATLAB® 2014a, where the kMC runs were executed in parallel. The computation times of the CM and kMC can therefore not be compared.
The solid curves labeled Monte Carlo or MC are lines through the means of the kMC results. The dashed curves are interpolations between the last two values obtained at a finite time and the end of the simulation. Around some Monte Carlo results lines or rectangles are visible. This is the bounding box for the kMC results.

4.4.1 Linear validation case for branched polymer

First the depolymerization of polymer by a hydrolysis rate linear in the NDF and with the three limiting cases for depolymerization processes (Random-chain scission (RCS), Random-debranching scission (RDS), and End-chain scission (ECS)) was investigated. This are the same cases investigated with the Direct Quadrature Method of Moments (DQMOM) in the preceding chapter. All the parameters stayed the same and the same kMC results were used.
The initial distribution was continuous, whereas the solved PBE was discrete. Therefore, for the rectangular and triangular bins instead of obtaining the amount of polymer, monomer units, and branching bonds by summation they were obtained by integration. For the remaining part the algorithm developed in the preceding Chapter to distributed the birth term was adopted.

Agreement of the Fixed Pivot Technique results with Monte Carlo results

In Figures 4.2, 4.3, 4.4, and 4.5 the dimensionless amount of polymer is shown over dimensionless time. For pure RCS and RDS the agreement between the results obtained by FP and kMC is very good for all grids with a growth factor of less than or equal to 1.5 with $\breve{k}_c = 2$.
If only ECS is active, the qualitative agreement is good, but the quantitative agreement is worse than for the other mechanisms. However, with increasing fineness of the mesh the results converge to the kMC solution. The error is acceptable for a mesh with a growth factor of less than or equal to 1.02. Ho et al. [127] have investigated the numerical solution of a depolymerization process with pure ECS using FP. They found that numerical diffusion occurs when an ECS dominated process is solved using FP. Therefore, very fine meshes were required to obtain accurate solutions. The results not shown here

(the degree of branching and the amount of monomer, dimer, and trimer) agreed with the kMC results within the same accuracy as the total polymer amount.
For an equal mixture of RCS and RDS, shown in Figure 4.5, the agreement is significantly worse than with either pure RCS or pure RDS. The results converge towards the kMC results. However, there is even for the finest mesh a deviation between the two methods. As with all other mechanisms increasing $\breve{k}_c$ above 2 did only improve the results slightly. This bad performance of FP for the mixture is surprising as the results for the pure mechanisms look very good. If one compares the results for the amount of linear polymer excluding the monomer, which is shown in Figure 4.6, one can see that for pure RCS and a mixture of RCS and RDS the results agree very well. However, for pure RDS the FP results in a lower amount of linear polymers than the kMC even for the fine mesh used here. The amount of polymers with only branching bonds - the limit dextrines for RCS and ECS - which is shown in Figure 4.7, is well reproduced by FP for RDS. But the results for RCS and the mixture of both mechanisms show a deviation. No clear explanation, why the results for the enzyme mixture are worse than for the pure enzymes, can be offered. It is postulated that the hard switch in the reaction rate causes small deviations to become larger. Accordingly, it should be studied whether the description of molar mass and branching density dependent reaction rates can be well described using the FP. However, one should note that the branching density was 0.5 in this validation case, whereas experimental values are around 0.05 [185]. The production of limit dextrines, which likely causes the deviation in RCS should therefore be smaller. Furthermore, any debranching mechanism will be less important for less highly branched polymers. Such a high branching density was chosen to test a limiting case for the algorithm.
The results for a mixture of ECS and RCS were very good and the deviation was smaller than the mean of the deviations of pure ECS and pure RCS separately. As this process is dominated by RCS it is not surprising that the error is dominated by RCS as well. An equal mixture of all enzymes had a slightly smaller deviation than the mixture of RCS and RDS which can be explained by the well described mechanism of ECS also being active.

Computation time

The computation times for the cases discussed above are presented in Tables 4.1 and 4.2. One can see that increasing $\breve{k}_c$ and the fineness of the mesh increases the computational effort. However, the computation time was for all cases discussed above in the order of seconds. For all mechanisms, except ECS, the computation time can be described as a quadratic function with mechanism dependent parameters of the number of pivots .

Comparison between the Fixed Pivot Technique and the Cell Average Technique

The deviation between the kMC results and the CAT results was approximately the same as between FP and kMC. No difference was visible. This appears to be a contradiction to the better convergence properties proved by Kumar and Warnecke [231]. However, the better convergence properties were

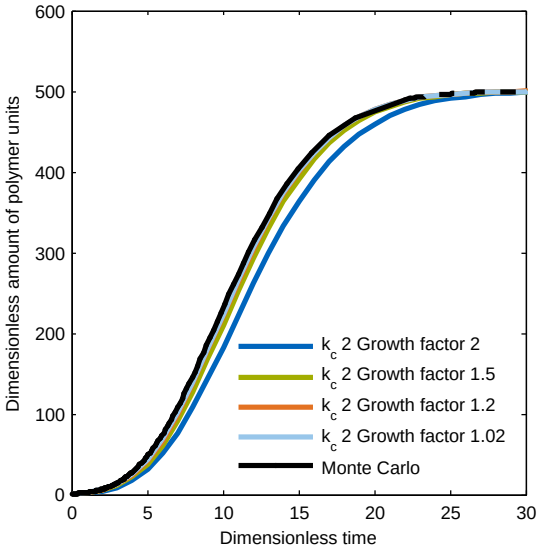

Figure 4.2: Amount of polymer for the validation case of branched polymer for RCS.

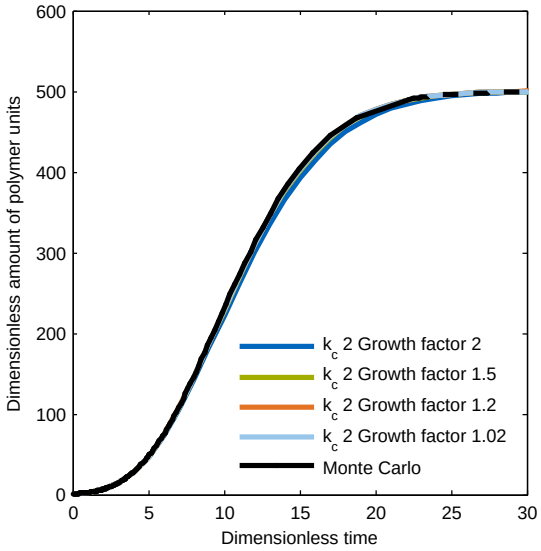

Figure 4.3: Amount of polymer for the validation case of branched polymer for RDS.

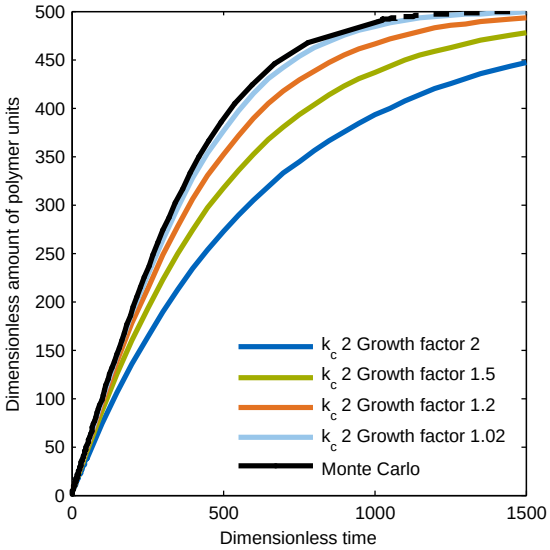

Figure 4.4: Amount of polymer for the validation case of branched polymer for ECS.

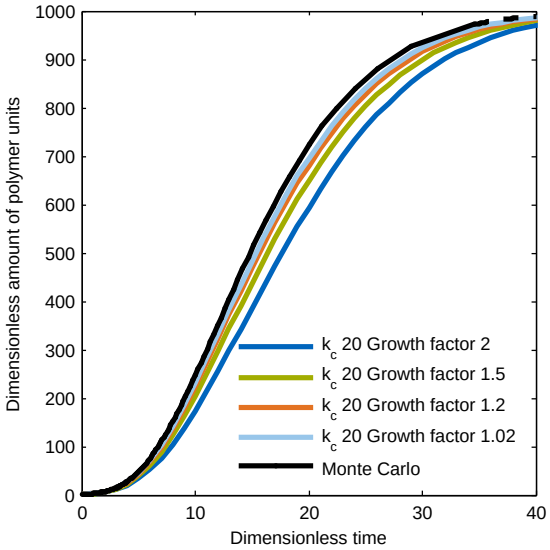

Figure 4.5: Amount of polymer for the validation case of branched polymer for an equal mixture of RCS and RDS.

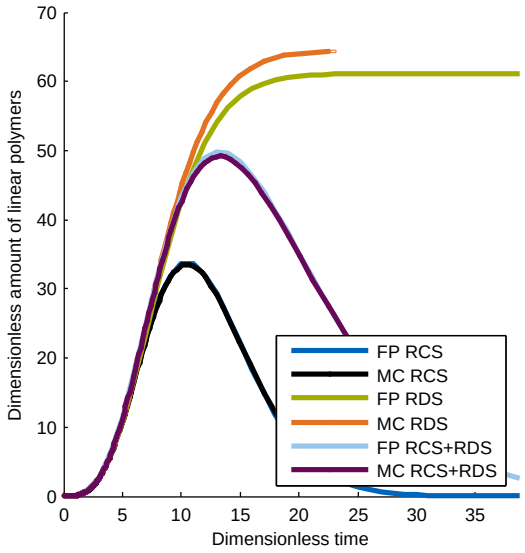

Figure 4.6: Amount of linear polymer excluding the monomer for the validation case of branched polymer for three cases with a growth factor of 1.02 and $\breve{k}_c = 20$.

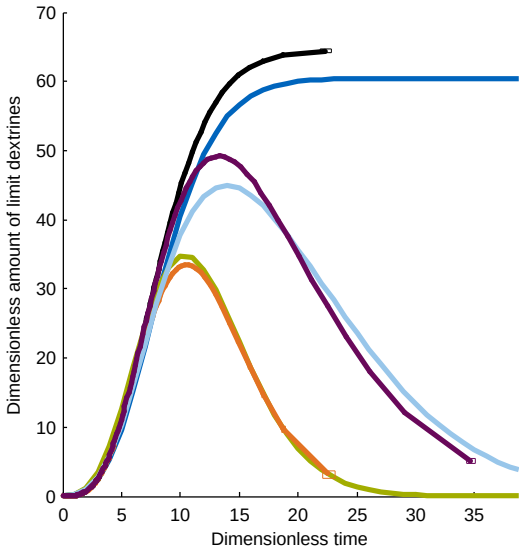

Figure 4.7: Amount of polymer with only branching bonds for the validation case of branched polymer for three cases with a growth factor of 1.02 and $\breve{k}_c = 20$.

Table 4.1: Computation times in seconds for the Fixed Pivot technique at $\breve{k}_c = 2$.

Growth rate	2	1.5	1.2	1.1	1.05	1.02
Pure RCS	0.22	0.16	0.18	0.37	0.82	1.67
Pure ECS	0.52	0.59	0.58	0.67	0.81	1.09
Pure RDS	0.14	0.14	0.17	0.38	0.82	1.62
Equal mixture of RCS and RDS	0.17	0.18	0.25	0.72	1.66	3.23

Table 4.2: Computation times in seconds for the Fixed Pivot technique at a growth factor of 1.1.

$\breve{k}_c$	2	5	10	20
Pure RCS	0.37	0.44	0.57	1.06
Pure ECS	0.67	0.96	1.40	1.65
Pure RDS	0.38	0.43	0.62	0.92
Equal mixture of RCS and RDS	0.72	0.93	1.29	2.27

neither proved for geometric meshes nor for bivariate cases. CAT took at least 4 times and up to ~140 times as long as FP to solve. The faster computation can be explained by CAT having to perform the computation for the birth distribution online whereas for FP those can be performed offline. Furthermore, the code used for the FP was optimized slightly more. However, as the main computational effort for CAT is the distribution of the birth term, optimization of the CAT is expected to only change the numbers slightly.

4.4.2 Validation for linear polymer

In the preceding section it could not be determined whether the FP is suitable for reactions rates which are a function of the molar mass. Accordingly, a case with a linear polymer being depolymerized by a single enzyme (BLA-F) described by the subsite theory is investigated. The enzymes has $\check{z}_- = 6$ and $\check{z}_+ = 2$ subsites and an acceleration factor ΔG_a of 0. The binding energies are provided in Table 4.3. The subsite map is evaluated at $20\,^\circ\mathrm{C}$. Initially the polymer has an average degree of polymerization of 1000 and a polydispersity of 1.1. The initial mass concentration is $3\,\mathrm{g\,l^{-1}}$. The maximal amount of monomer units is set to 3000 which is sufficiently large that almost no polymers are above this value. Due to limitations of the implementation, the minimal value of $\check{k}_c$ was 12 which was also the value chosen here. The implementation cannot handle values of $\check{k}_c$ less than $2 \cdot \max(\check{z}_-, \check{z}_+)$ because only above this value can the PDF expressed with Equation (2.69). However, one can implement this without any difficulties. This was not regarded as necessary in this work because the computational effort was already sufficiently low.

Table 4.3: Used binding energies in $\mathrm{kJ\,mol^{-1}}$.

Subsite	1	2	3	4	5	6	7	8	9	10
BAA [a]	-4.48	-10.21	-0.67	-4.23	-9.54	13.81	-14.39	-7.2	-4.02	5.27
BLA-F [b]	-4.60	-10.04	0	-2.51	-10.04	12.97	0	-1.2		

[a] Ref: [32] originally from Allen and Thoma [217]
[b] Ref: [238]

Monte Carlo results

Four kMC runs with 1×10^5 particles using a Constant Number approach were performed to obtain a reference solution. The amount of monomer units was constant within 1 %. However, after a short time the time at which a certain number concentration was reached differed by more than 10 %. The results can, therefore, used a reference solution, but the deviation from a solution obtained by a CM to the reference solution cannot be quantified.

Agreement between the Fixed Pivot Technique and the Monte Carlo results

The total polymer concentration for a very coarse mesh with a growth factor of 2 and a very fine mesh with a growth of 1.01 is shown in Figure 4.8 both with $\breve{k}_c$ set to the minimal value of 12. For both meshes do the FP and kMC results agree almost perfectly. Increasing $\breve{k}_c$ did, therefore, not reduce the error. In Figure 4.9 the concentration of the 4 smallest polymers is shown with $\breve{k}_c = 12$ and a growth factor of 1.1. It is very difficult to tell the FP and kMC results apart because FP is so accurate. One can therefore conclude that FP is able to handle very well hydrolysis rates which depend on the amount of monomer units.

Comparison between the Fixed Pivot Technique and the Cell Average Technique

The results with the CAT were as accurate, but took longer to compute. Again this is partially due to the birth term distribution and to the further optimization of FP. Additionally, during computation FP does not differentiate between pivots in the different domains, whereas CAT has to do so. This additional bookkeeping slows CAT down. One can, therefore, conclude that the CAT is a worse method than FP for solving depolymerization processes. Further on, only FP is used.

4.4.3 Validation for a branched polymer

One should also investigate, how well the FP can solve the model proposed in Chapter 2 to described the depolymerization of branched starch. Accordingly, the depolymerization of branched starch by a single enzyme described by the subsite theory was investigated here. The parameters from the linear case studied in the subsection before were used. Additionally, a mean degree of branching of 0.05, a maximal amount of branching bonds of 450, and inhibition constants $b_I = 0.3$, $b_{II} = 0.1$, and $b_{III} = 0.1$ were used.

Monte Carlo results

Six kMC runs with 5×10^5 particles using a Constant Number approach were performed to obtain a reference solution. This large number of particles was necessary because the error was otherwise not acceptable. The amount of monomer units was constant within 2 % and the amount of branching was constant within 4 %.

Agreement with Monte Carlo technique results

The total amount of polymer is shown in Figure 4.10. One can see that the amount of polymer agrees quite well with the kMC results even for a very coarse mesh with a growth factor of 2 and $\breve{k}_c = 12$. Increasing $\breve{k}_c$ from 12 to 50 decreases the deviation only by a tiny bit. The decrease of the growth factor from 2 to 1.1 causes the FP results to be almost indistinguishable from the mean of the kMC results. A further refinement of the mesh changed the results only slightly.

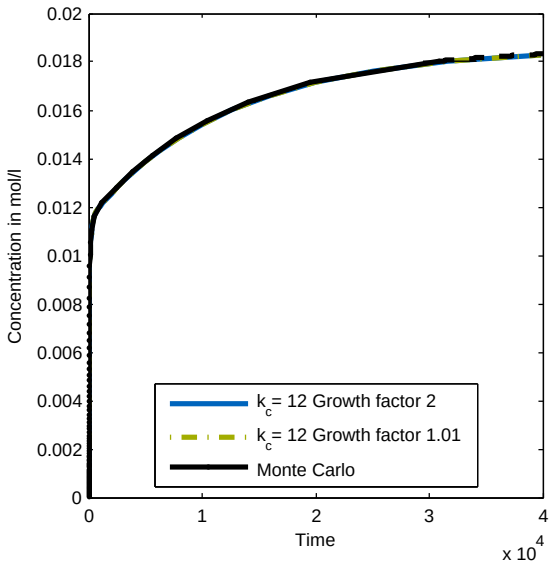

Figure 4.8: Concentration of polymer for the validation case of linear polymer with an enzyme described by the subsite theory for several growth factors.

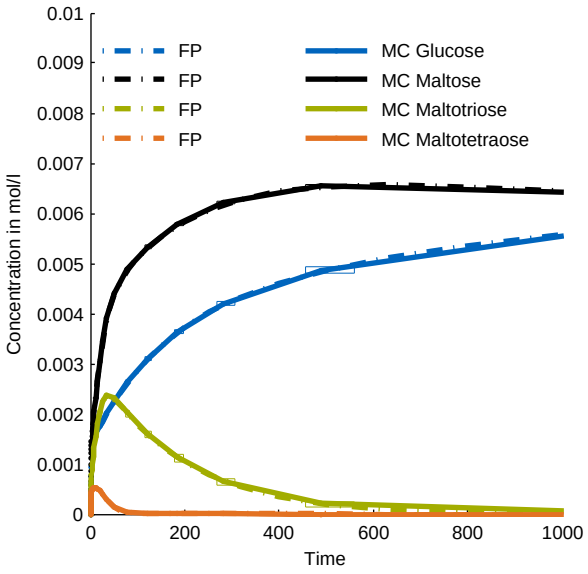

Figure 4.9: Concentration of monomer and some oligomers for the validation case of linear polymer with an enzyme described by the subsite theory for $\breve{k}_c = 12$ and a growth factor of 1.1.

The concentration of a few small oligomers is shown in Figure 4.11. Except for the dimer the agreement between kMC and FP is excellent and even for the dimer the agreement is very good. The degradation of branched polymer with a realistic branching density by an enzyme described by the subsite theory can be described well using FP.

Computation times

The computation times for the branched validation case is shown in Table 4.4. If one compares the computation times to the ones obtained for the simpler validation case, one can see that this computation takes significantly longer. If one compares the amount of polymer for the simple validation case and this one, one can see that the dynamics of the process is qualitatively different. The fast initial rise and the slower rise at the end would - even with a time step control - require more time steps than the constantly declining rise. This suggest that using a solver for stiff ODEs would be beneficial. However, the large number of equations (~1000) makes using them inefficient. One can again correlate the computation time with the square of the pivot numbers.

4.5 Validation of the Population Balance Model

Besselink et al. [32] have investigated the depolymerization of branched starch by α-amylase by a kMC simulation and experimental measurements. This data is used to perform a first validation of the

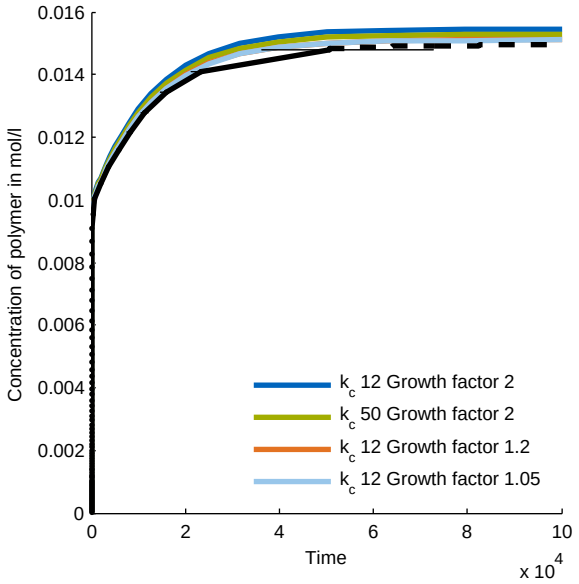

Figure 4.10: Concentration of polymer for the validation case of branched polymer with an enzyme described by the subsite theory for several growth factors and two different values of $\breve{k}_c$.

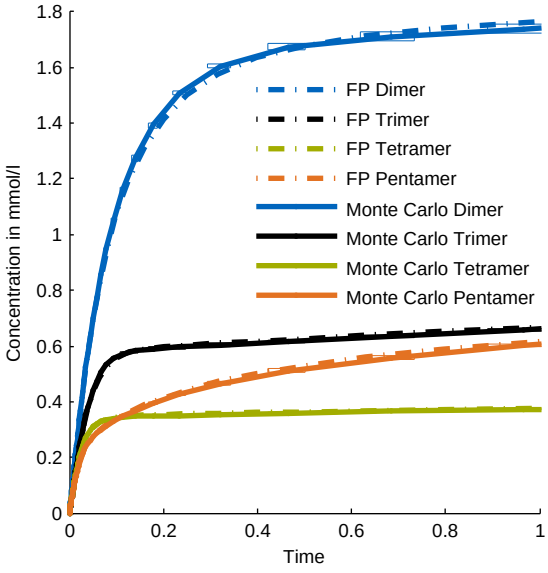

Figure 4.11: Concentration of some oligomers for the validation case of branched polymer with an enzyme described by the subsite theory for $\breve{k}_c = 12$ and a growth factor of 1.1.

Table 4.4: Computation times in seconds for the Fixed Pivot technique.

Growth rate	2	1.5	1.2	1.1	1.05	1.02	1.01
$\breve{k}_c = 12$	5.64	12.13	9.84	27.15	77.07	79.85	211.74
$\breve{k}_c = 50$	15.41	35.88	183.97	153.90	346.97	649.60	848.34

Population Balance Model (PBM) for branched starch proposed in Chapter 2. The kMC simulations were performed without using a PBE. Instead they constructed polymers using a stochastic algorithm [189] and used rules [33] to simulate their hydrolysis.

4.5.1 Parameters

Two enzymes were investigated by Besselink et al. [32]. Here the results are compared for the enzyme BAA, because this enzyme had better agreement between experiment and simulation. The subsite map was estimated by Allen and Thoma [217] and is provided in Table 4.3. All remaining parameters are given in Table 4.5. Besselink et al. [32] used the inhibition factor estimated by Marchal et al. [33]. The experiments were conducted at $50\,^{\circ}\mathrm{C}$ and an initial concentration of $100\,\mathrm{g\,l^{-1}}$.
The approach used by Besselink et al. [32] does not consider the branched polymer to be distributed in the total amount of monomer units. Instead each polymer has a distribution of chain lengths [1]. However, the model developed in this work can consider the polymer to be distributed in the total amount of monomer units and branching bonds but not in the chain length. The measured value of the mean molar mass by weight and polydispersity of waxy wheat starch measured by Rolland-Sabate et al. [184] were used. A mean degree of branching 5 %, which is reasonable [32, 184], was used. For amlyose the average degree of polymerization measured by Hanashiro and Takeda [183] was used. The polydispersity was choosen such that the 10 % and 90 % cutoff agreed with the data measured in the same paper.
The mesh parameter were chosen based on the prior validation study. The maximal amount of monomer units and branching bonds were chosen such that almost no polymer was above it.
Besselink et al. [32] did compute the factor to convert from computational to experimental time. However, it was not provided in the paper. Therefore, the same algorithm to do the conversion was used: The scaling factor was chosen such that the deviation between the simulated and measured dextrose equivalent for the first two experimental time points was minimal. This is equivalent to having the same slope in the initial almost linear region.

4.5.2 Results

Besselink et al. [32] used the Dextrose Equivalent (DE) to compare simulation and experiment. It is computed here as

$$DE = 100 \cdot \frac{(M_{H_2O} + M_{Glu}) \cdot \sum_i \breve{w}_i}{\sum_i \breve{w}_i \cdot (M_{H_2O} + \breve{k}_i \cdot M_{Glu})}. \tag{4.40}$$

Furthermore, the mass fraction was used. The mass fraction x_j of the j-th pivot is

$$x_j = 100 \cdot \frac{(M_{H_2O} + M_{Glu} \cdot \breve{k}_j) \cdot \breve{w}_j}{\sum_i \breve{w}_i \cdot (M_{H_2O} + \breve{k}_i \cdot M_{Glu})}. \tag{4.41}$$

[1] Here, a chain is defined as the amount of linearly connected monomer units starting from a branching bond [10].

Table 4.5: Parameters used to compare the developed Population Balance Model to data from Besselink et al. [32].

Parameter	Symbol	Value
Subsites below the catalytic center[a]	$\breve{z}_-$	6
Subsites above the catalytic center[a]	$\breve{z}_+$	4
Acceleration factor[d]	ΔG_a	$1.55\,\mathrm{kJ\,mol^{-1}}$
Molar mass of water[a]	M_{H_20}	$18.02\,\mathrm{g\,mol^{-1}}$
Molar mass of anhydro-glucose[a]	M_{Glu}	$162.14\,\mathrm{g\,mol^{-1}}$
Inhibition by chain starting branching bond[b]	b_I	0.1
Inhibition by branching bond towards the reducing end[b]	b_{II}	0.2
Inhibition by branching bond towards the non-reducing end[b]	b_{III}	0.4
Temperature[c]	T	$50\,^\circ\mathrm{C}$
Initial concentration of starch[c]		$100\,\mathrm{g\,l^{-1}}$
Mass percentage of starch as amylopectin[c]		75 %
Mean molar mass by weight of amylopectin[e]		$2.27 \times 10^8\,\mathrm{g\,mol^{-1}}$
Polydispersity of amylopectin[e]		1.13
Mean degree of branching of amylopectin[c]		5 %
Average polymerization degree of amylose[f]		1220
90 cutoff of amylose[f]		3130
10 cutoff of amylose[f]		190
Mesh growth factor		1.1
Amount of exactly represented monomer units	$\breve{k}_c$	14
Maximal amount of monomer units		4.20×10^6
Maximal amount of branching bonds		2.12×10^5

[a] Ref: Besselink et al. [32] originally from Allen and Thoma [217]
[b] Ref: Besselink et al. [32] originally from Marchal et al. [33]
[c] Ref: Besselink et al. [32]
[d] Ref: Allen and Thoma [217]
[e] Ref: Rolland-Sabate et al. [184]
[f] Ref: Hanashiro and Takeda [183]

The Dextrose Equivalent is plotted over time in Figure 4.12. There is good qualitative agreement between kMC results and the PBE results. The difference between the two methods can be either attributed to the assumptions made in deriving the PBE model or the to different initial conditions. However, the agreement between the experimental and the PBE results is slightly better than for kMC results. The mass fraction of the monomer and the linear trimer is plotted in Figure 4.13. One can see that the overprediction of Maltotriose is greater for the PBE model than for the kMC results. Furthermore, the underprediction of the glucose is also sightly worse. The total mass fraction of the heptamers and hexamers (both branched and linear) is shown in Figure 4.14. The agreement between experimental data and PBE model is better than for the kMC results.

4.6 Conclusion and outlook

In this chapter the Fixed Pivot technique (FP) and Cell Average Technique (CAT) were adapted to a discrete Population Balance Equation (PBE). For several test cases the results of FP and CAT were compared with kinetic Monte Carlo (kMC) simulations based on the PBE. Both methods were found to have comparable accuracy but FP was found to be significantly faster. Therefore, FP should be used to describe depolymerization processes of the kind studied in this work.
It was found that End-chain scission (ECS) is solved with a significant error, unless very fine meshes were used. This has already been reported by Ho et al. [48]. For Random-chain scission (RCS) and Random-debranching scission (RDS) alone the solution of the products and the amount of polymers were found to be in excellent agreement for quite coarse meshes. However, the combination of those two mechanisms resulted in a deviation which did only slowly disappear with increasing mesh fineness. For linear polymer the dependence of the reaction rate on the chain length and the complicated Product Distribution Function (PDF) predicted by the subsite theory did not pose any issues. However, no rigorous convergence study was performed. Also for the branched polymer using the reaction rate and the PDF of the subsite model developed in Chapter 2 did not pose any problems, but rather the agreement between kMC and FP was excellent.
For one case the results of the model developed in Chapter 2 were compared to literature data. The agreement between FP data and experimental data was slightly better than between the kMC results and the experimental data. There was a significant deviation between the FP results and the kMC results. This does not allow a definite statement on the validity of the developed PBE. But the results raise confidence that a Population Balance Model (PBM) approach can be used to describe this process. One could validate the PBM by comparison with either experiments or kMC simulations. If experimental validation is chosen, the initial state and the parameters of the enzymes need to be determined. The effort for experimental validation is high but would result in a model able to describe reality. If validation by kMC simulation is chosen, further simulations need to be performed, because not all input data for the PBE model was provided by Besselink et al. [32]. Because the initial conditions do not necessarily agree, one cannot state whether the deviations between the kMC and the PBE results

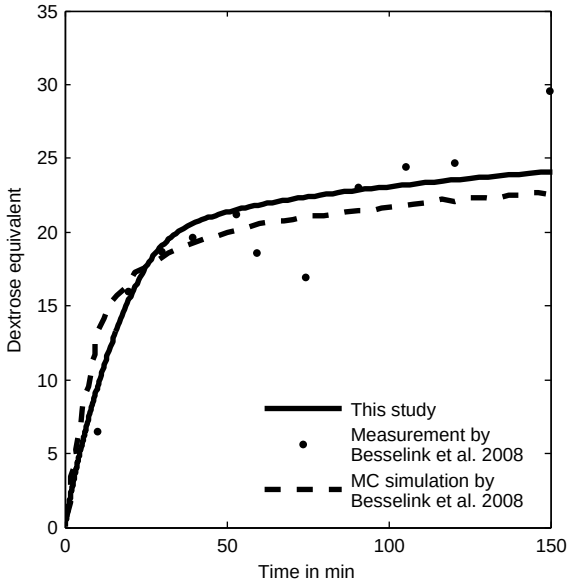

Figure 4.12: Dextrose equivalent over time.

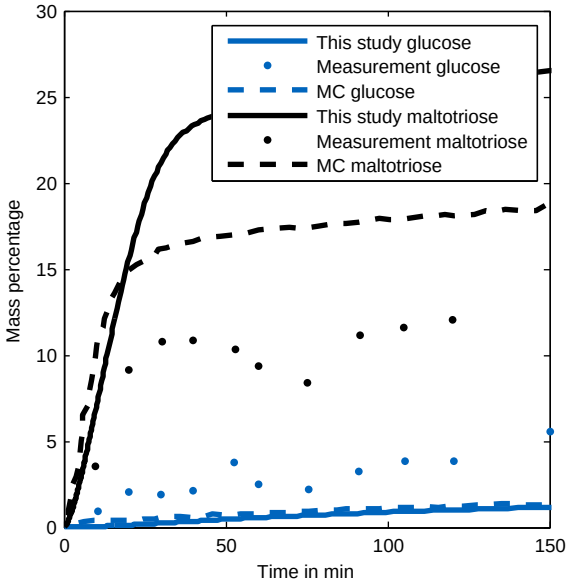

Figure 4.13: Mass fraction of the monomer (glucose) and linear trimer (maltotriose) over time.

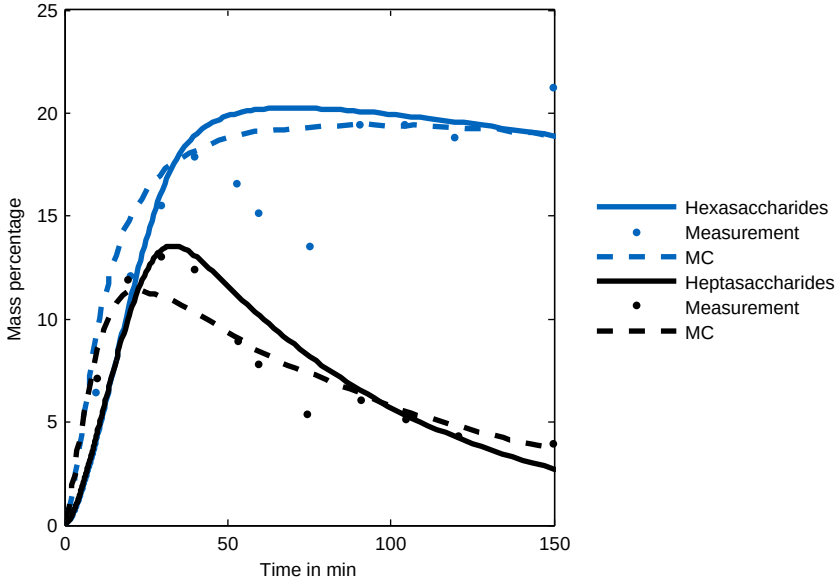

Figure 4.14: Mass fraction of all heptamers and all hexamers over time.

are due to invalid assumptions or different starting conditions. One should therefore implement the model used by Besselink et al. [32] and for example extract the branching distribution directely from the structures generated by the kMC algorithm.
It was found that increasing the exactly represented region increased the computation time by a significant amount but only had a minor benefit for the accuracy. The simulations times and the accuracy of FP are acceptable for usage in optimal control which is therefore performed in the following chapter.

Chapter 5

Optimal control

Here, first the necessary conditions for optimality are derived for one specific case. Then possible numerical techniques to solve optimal control problems are reviewed and the implemented algorithm is described. The algorithm is applied to a case study and the effect of branching is investigated. Last, a short conclusion is drawn.

5.1 Necessary conditions for optimality

In this work an optimal profile in time is desired and, therefore, the necessary conditions are derived for such a profile. The necessary conditions are required input for an indirect solver.

5.1.1 Problem statement

The optimality conditions are derived for a system of Ordinary Differential Equations (ODEs) because this approach requires the smallest number of assumptions. The problem is then given in the form

$$\frac{\mathrm{d}\mathbf{n}}{\mathrm{d}t} = \mathrm{f}_n(t, \mathbf{n}, \mathbf{E}, T) \tag{5.1}$$

$$\frac{\mathrm{d}\mathbf{E}}{\mathrm{d}t} = \mathrm{f}_E(t, \mathbf{n}, \mathbf{E}, T) \tag{5.2}$$

$$\frac{\mathrm{d}T}{\mathrm{d}t} = u \tag{5.3}$$

$$\mathbf{n}(t=0) = \mathbf{n}_0 \tag{5.4}$$

$$\mathbf{E}(t=0) = \mathbf{E}_0 \tag{5.5}$$

$$T(t=0) = T_0, \tag{5.6}$$

where u is the rate of temperature change, T_0 is the initial temperature, $\mathbf{E}_0$ is the initial concentration of the enzymes, and $\mathbf{n}_0$ is the initial distribution. This system of ODEs is solved until the final time t_f. The temperature and the initial temperature should be within a certain range $T \in [T_{\min}, T_{\max}]$ where a hard limit for $T_{\min}$ are the freezing point and for $T_{\max}$ is the boiling point. For ease of discussion this

condition is neglected in deriving the necessary conditions here but it is included in the algorithm used to compute the optimal profiles.

Control variables

In this section it is assumed that the initial temperature and the initial concentration of enzymes can be varied freely. Not for all cases considered in this chapter will the initial enzyme concentration be allowed to vary freely. The initial enzyme concentration cannot be negative $\mathbf{E}_0 \geq 0$. Furthermore, the rate of temperature change will be allowed to vary freely within the interval $[u_{\min}, u_{\max}]$. The reaction duration t_f is not a control variable. However, it is allowed to vary freely.

Objective functional

The purpose of optimal control is to optimize something with regard to an objective. The objective is a maximization of profit (minimization of costs) and is quantified by an objective functional. This objective functional takes the control variable functions as the input and returns a scalar value as the output. Given that enzymes cost money and also heating up or cooling down the starting material costs money one should include those in the objective functional. This is done by the function $f_i(T_0, \mathbf{E}_0)$. Operating the reactor also costs money, therefore the reaction duration t_f should be included in the cost. Furthermore, depending on the final state of the distribution the reaction product might have more or less values. This is included in the objective functional by the function $f_f(t_f, \mathbf{n}(t = t_f))$. The cost of heating up or cooling down the reactor is taken into account by the Lagrange function $L(u(t))$ which needs to be integrated over the whole reaction duration. Summing up of the objectives leads to an objective functional of Bolza type [148]:

$$J(u, T_0, \mathbf{E}_0, t_f) = f_i(T_0, \mathbf{E}_0) + f_f(t_f, \mathbf{n}(t = t_f)) + \int_0^{t_f} L(u(t))\,\mathrm{d}t. \tag{5.7}$$

Final condition

It might be desirable to operate the reactor at such conditions that the final distribution fulfills a condition. For example, one might require the reactor to have certain yield. This can be expressed by demanding

$$g(\mathbf{n}(t = t_f)) = 0, \tag{5.8}$$

where g is a problem specific function.
In conclusion, it is desired to find the optimal profile of the rate of temperature change, the optimal initial temperature, the optimal concentration of enzymes, and the optimal reaction duration such that an objective functional is minimized. The states have to follow a system of ODEs and be within a certain range. Furthermore, some states have to fulfill a condition at the final time.

5.1.2 Derivation

In order to solve the problem, all the conditions have to collected into the objective functional which is achieved by the use of Lagrangian multipliers [148].

$$\begin{aligned} J =& f_i(T_0, \mathbf{E}_0) + f_f(t_f, \mathbf{n}(t=t_f)) + \Psi_g \cdot g(\mathbf{n}(t=t_f)) + \underline{\mu}_E \cdot \mathbf{E}_0 \\ &+ \int_0^{t_f} L(u(t)) + \underline{\Psi}_n \cdot (\mathrm{f}_n - \dot{\mathbf{n}}) + \underline{\Psi}_E \cdot (\mathrm{f}_E - \dot{\mathbf{E}}) + \Psi_T \cdot (u - \dot{T}) + \mu_{\min} \cdot (u - u_{\min}) + \mu_{\max} \cdot (u_{\max} - u)\, \mathrm{d}t. \end{aligned} \tag{5.9}$$

With a suitably defined Hamiltonian H the equation can be written more elegantly

$$H = L + \underline{\Psi}_n \cdot \mathrm{f}_n + \underline{\Psi}_E \cdot \mathrm{f}_E + \Psi_T \cdot u + \mu_{\min} \cdot (u - u_{\min}) + \mu_{\max} \cdot (u_{\max} - u) \tag{5.10}$$

$$\begin{aligned} J =& f_i(T_0, \mathbf{E}_0) + f_f(t_f, \mathbf{n}(t=t_f), T(t=t_f)) + \Psi_g \cdot g(\mathbf{n}(t=t_f)) + \underline{\mu}_E \cdot \mathbf{E}_0 \\ &+ \int_0^{t_f} H(t, u, \mathbf{n}, \mathbf{E}, T, \underline{\Psi}_n, \underline{\Psi}_E, \Psi_T, \mu_{\min}, \mu_{\max})\, \mathrm{d}t \\ &- \int_0^{t_f} \underline{\Psi}_n \cdot \dot{\mathbf{n}} + \underline{\Psi}_E \cdot \dot{\mathbf{E}} + \Psi_T \cdot \dot{T}\, \mathrm{d}t. \end{aligned} \tag{5.11}$$

This equation can be rewritten using integration by parts [188]

$$\begin{aligned} J =& f_i(T_0, \mathbf{E}_0) - \underline{\Psi}_n(t=0) \cdot \mathbf{n}(t=0) + (\underline{\mu}_E - \underline{\Psi}_E(t=0)) \cdot \mathbf{E}(t=0) - \Psi_T(t=0) \cdot T(t=0) \\ &+ f_f(t_f, \mathbf{n}(t=t_f), T(t=t_f)) + \underline{\Psi}_n(t=t_f) \cdot \mathbf{n}(t=t_f) + \underline{\Psi}_E(t=t_f) \cdot \mathbf{E}(t=t_f) \\ &+ \Psi_T(t=t_f) \cdot T(t=t_f) + \Psi_g \cdot g(\mathbf{n}(t=t_f)) + \int_0^{t_f} H(t, u, \mathbf{n}, \underline{\Psi}_n, \underline{\Psi}_E, \Psi_T, \mu_{\min}, \mu_{\max})\, \mathrm{d}t \\ &- \int_0^{t_f} \dot{\underline{\Psi}}_n \cdot \mathbf{n} + \dot{\underline{\Psi}}_E \cdot \mathbf{E} + \dot{\Psi}_T \cdot T\, \mathrm{d}t. \end{aligned} \tag{5.12}$$

Calculus of variations

The necessary condition for a function to have an optimum is that the first derivative is zero [148]. In order to transfer this definition to optimal control calculus of variations (see e.g. [148, 150, 239]) is used. In order to transform the functional into a function the functions are expressed as the sum of the optimal function * and the product of an arbitrary fixed function $\tilde{}$ and a scalar ε:

$$u(t) = u^*(t) + \varepsilon \cdot \tilde{u}(t) \tag{5.13}$$

$$\mathbf{n}(t) = \mathbf{n}^*(t) + \varepsilon \cdot \tilde{\mathbf{n}}(t) \tag{5.14}$$

$$\tilde{\mathbf{n}}(t=0) = 0 \tag{5.15}$$

$$\mathbf{E}(t) = \mathbf{E}^*(t) + \varepsilon \cdot \tilde{\mathbf{E}}(t) \tag{5.16}$$

$$T(t) = T^*(t) + \varepsilon \cdot \tilde{T}(t) \tag{5.17}$$

This allow expressing, the functional as a scalar function Φ

$$\begin{aligned}
\Phi(\varepsilon) =& f_i(T(t=0)^* + \varepsilon\cdot\tilde{T}(t=0), \mathbf{E}^*(t=0) + \varepsilon\cdot\tilde{\mathbf{E}}(t=0)) \\
&- \underline{\Psi}_n(t=0)\cdot\mathbf{n}^*(t=0) + (\underline{\mu}_E - \underline{\Psi}_E(t=0))\cdot(\mathbf{E}^*(t=0) + \varepsilon\cdot\tilde{\mathbf{E}}(t=0)) - \Psi_T(t=0)\cdot(T^*(t=0) + \tilde{T}(t=0)) \\
&+ f_f(t_f, \mathbf{n}^*(t=t_f) + \varepsilon\cdot\tilde{\mathbf{n}}(t=t_f), T^*(t=t_f) + \varepsilon\cdot\tilde{T}(t=t_f)) \\
&+ \underline{\Psi}_n(t=t_f)\cdot(\mathbf{n}^*(t=t_f) + \varepsilon\tilde{\mathbf{n}}(t=t_f)) + \underline{\Psi}_E(t=t_f)\cdot(\mathbf{E}^*(t=t_f) + \varepsilon\cdot\tilde{\mathbf{E}}(t=t_f)) \\
&+ \Psi_T(t=t_f)\cdot(T^*(t=t_f) + \varepsilon\cdot\tilde{T}(t=t_f)) + \Psi_g\cdot g(\mathbf{n}^*(t=t_f) + \varepsilon\cdot\tilde{\mathbf{n}}(t=t_f)) \\
&+ \int_0^{t_f} H(t, u^* + \varepsilon\cdot\tilde{u}, \mathbf{n}^* + \varepsilon\tilde{\mathbf{n}}, \underline{\Psi}_n, \underline{\Psi}_E, \Psi_T, \mu_{\min}, \mu_{\max})\,\mathrm{d}t \\
&- \int_0^{t_f} \dot{\underline{\Psi}}_n\cdot(\mathbf{n}^* + \varepsilon\cdot\tilde{\mathbf{n}}) + \dot{\underline{\Psi}}_E\cdot(\mathbf{E}^* + \varepsilon\cdot\tilde{\mathbf{E}}) + \dot{\Psi}_T\cdot(T^* + \varepsilon\cdot\tilde{T})\,\mathrm{d}t. \qquad (5.18)
\end{aligned}$$

The necessary condition for an optimal point is then that the derivative with respect to ε at $\varepsilon = 0$ is zero

$$\begin{aligned}
\left.\frac{\partial\Phi}{\partial\varepsilon}\right|_{\varepsilon=0} =& \frac{\partial f_i(T_0^*, \mathbf{E}_0^*)}{\partial T_0^*}\cdot\tilde{T}(t=0) + \frac{\partial f_i(T_0^*, \mathbf{E}_0^*)}{\partial \mathbf{E}_0^*}\cdot\tilde{\mathbf{E}}(t=0) \\
&+ (\underline{\mu}_E - \underline{\Psi}_E(t=0))\cdot\tilde{\mathbf{E}}(t=0) - \Psi_T(t=0)\cdot\tilde{T}(t=0) \\
&+ \frac{\partial f_f(t_f, \mathbf{n}^*(t=t_f), T^*(t=t_f))}{\partial\mathbf{n}}\cdot\tilde{\mathbf{n}}(t=t_f) + \frac{\partial f_f(t_f, \mathbf{n}^*(t=t_f), T^*(t=t_f))}{\partial T}\cdot\tilde{T}(t=t_f) \\
&+ \underline{\Psi}_n(t=t_f)\cdot\tilde{\mathbf{n}}(t=t_f) + \underline{\Psi}_E(t=t_f)\cdot\tilde{\mathbf{E}}(t=t_f) \\
&+ \Psi_T(t=t_f)\cdot\tilde{T}(t=t_f) + \Psi_g\cdot\frac{\partial g(\mathbf{n}^*(t=t_f))}{\partial\mathbf{n}}\cdot\tilde{\mathbf{n}}(t=t_f) \\
&+ \int_0^{t_f}\frac{\partial H(t, u^*, \mathbf{n}^*, \underline{\Psi}_n, \underline{\Psi}_E, \Psi_T, \mu_{\min}, \mu_{\max})}{\partial u}\tilde{u}\,\mathrm{d}t \\
&+ \int_0^{t_f}\left(\frac{\partial H(t, u^*, \mathbf{n}^*, \underline{\Psi}_n, \underline{\Psi}_E, \Psi_T, \mu_{\min}, \mu_{\max})}{\partial\mathbf{n}} - \dot{\underline{\Psi}}_n\right)\tilde{\mathbf{n}}\,\mathrm{d}t \\
&+ \int_0^{t_f}\left(\frac{\partial H(t, u^*, \mathbf{n}^*, \underline{\Psi}_n, \underline{\Psi}_E, \Psi_T, \mu_{\min}, \mu_{\max})}{\partial\mathbf{E}} - \dot{\underline{\Psi}}_E\right)\tilde{\mathbf{E}}\,\mathrm{d}t \\
&+ \int_0^{t_f}\left(\frac{\partial H(t, u^*, \mathbf{n}^*, \underline{\Psi}_n, \underline{\Psi}_E, \Psi_T, \mu_{\min}, \mu_{\max})}{\partial T} - \dot{\underline{\Psi}}_T\right)\tilde{\mathbf{T}}\,\mathrm{d}t
\end{aligned}$$

Because the functions with the accent $\tilde{}$ are arbitrary, every term multiplied with such a function has to be zero in order for the functions * to be optimal. This is the fundamental lemma of the calculus of variations [148]. This leads to the necessary conditions for optimality:

$$\underline{\Psi}_E(t=0) - \underline{\mu}_E = \frac{\partial f_i}{\partial\mathbf{E}_0} \qquad (5.19)$$

$$\Psi_T(t=0) = \frac{\partial f_i}{\partial T_0} \qquad (5.20)$$

$$\underline{\Psi}_n(t=t_f) = -\frac{\partial f_n}{\partial\mathbf{n}} - \Psi_g\cdot\frac{\partial g}{\partial\mathbf{n}} \qquad (5.21)$$

$$\underline{\Psi}_E(t=t_f) = \mathbf{0} \qquad (5.22)$$

$$\Psi_T(t=t_f) = -\frac{\partial f_n}{\partial T} \tag{5.23}$$

$$g(\mathbf{n}(t=t_f)) = 0 \tag{5.24}$$

$$\frac{\partial H}{\partial u} = 0 \tag{5.25}$$

$$\underline{\dot{\Psi}}_n = \frac{\partial H}{\partial \mathbf{n}} \tag{5.26}$$

$$\underline{\dot{\Psi}}_E = \frac{\partial H}{\partial \mathbf{E}} \tag{5.27}$$

$$\dot{\Psi}_T = \frac{\partial H}{\partial T} \tag{5.28}$$

$$u \geq u_{\min} \tag{5.29}$$

$$u \leq u_{\max} \tag{5.30}$$

$$\mu_{\min} \geq 0 \tag{5.31}$$

$$\mu_{\max} \geq 0 \tag{5.32}$$

$$\mathbf{E}_0 \geq 0 \tag{5.33}$$

$$\underline{\mu}_E \geq 0 \tag{5.34}$$

Note that if L is not a function of u the solution would have a singular arc [148] and the necessary conditions for optimality would have to be changed.

Final time

The above stated conditions are valid for every value of the reaction duration. However, in order for t_f to be optimal the derivative of the objective function with respect to t_f must be zero

$$\frac{\mathrm{d}J}{\mathrm{d}t} = 0. \tag{5.35}$$

This is equivalent to taking the derivative of Equation (5.11). If one used the chain rule and the rule about derivatives of parameter integrals [188], one obtains this derivative as

$$\frac{\partial f_f}{t_f} + \dot{\mathbf{n}}(t=t_f) \cdot \left(\frac{\partial f_f}{\partial \mathbf{n}} + \Psi_g \cdot \frac{\partial g}{\partial \mathbf{n}} - \underline{\Psi}_n(t=t_f) \right) - \underline{\Psi}_E(t=t_f) \cdot \dot{\mathbf{E}}(t=t_f) + \dot{T}(t=t_f) \cdot \left(\frac{\partial f_f}{\partial T} - \Psi_T(t=t_f) \right)$$
$$+ H(t_f, u(t=t_f), \mathbf{n}(t=t_f), \mathbf{E}(t=t_f), T(t=t_f), \underline{\Psi}_n(t=t_f), \underline{\Psi}_E, \Psi_T, \mu_{\min}, \mu_{\max}) = 0 \tag{5.36}$$

5.2 Algorithm

Both approaches (continuous and discrete) to the Population Balance Equation (PBE) introduce problems for optimal control. If the PBE is assumed to be continuous, one needs to solve a Partial Differential Equation (PDE) with an integral term. Even though there is some work on optimal control of PDEs

[239], I have not found any theoretical approaches to optimal control of PDEs with an integral term. If the PBE is assumed to be discrete, the resulting system of ODEs cannot be solved directly, but rather one has to use a numerical technique (see Chapter 4). To the best of my knowledge nobody has made any investigation one how optimal control combines with the Fixed Pivot technique (FP). It is therefore assumed that the result of optimal control of the approximated ODE system is also optimal for the exact system. This is likely to be valid because the results of FP and the kinetic Monte Carlo (kMC) reference solution result agree very well with each other.
The PBE is solved using the FP as presented in Chapter 4. The optimal control algorithm is explained in this subsection.

Parametrization or discretization of the optimal control problem

The optimal control problem is solved using a direct single shooting approach [176]. Here, this means that the optimal rate of change of temperature profile is approximated by a piecewise constant function. Additionally, the optimal starting temperature is found. This reduces the infinite dimensional optimal control problem to a finite dimensional one. The temperature change rate is bounded between $0\,\mathrm{K}/\mathrm{min}$, which implies that the temperature does not decrease, and $0.1\,\mathrm{K}/\mathrm{min}$ which is much lower than the rate of temperature change of $1\,\mathrm{K}/\mathrm{min}$ commonly used in the mashing process [14]. The low value of the maximal temperature change rate guarantees that the process can be implemented on a large scale. Furthermore, the maximal temperature change rate is not reached in any case discussed in this study.
A successive refinement approach for computing the optimal control similar to the one developed by [175] is used here. For simplicity, first only the algorithm for the fixed time problem, where the yield is maximized and the reaction time is fixed at a preset value, is explained. Starting from an initial guess of $40\,^{\circ}\mathrm{C}$ the optimal isothermal profile is found. Then, using the optimal isothermal temperature as the initial guess, the next step extends the profile to a simple constant temperature change rate over the complete fixed time. Subsequently, the time intervals are bisected in each loop to increase the resolution of the temperature change rate profile, always using the previous profile as the initial guess to improve the speed and robustness of the algorithm. In all shown cases, the domain is bisected 6 times (up to 64 intervals). An example for this routine is shown in Figure 5.2b.
If the reaction time is minimized at a fixed yield and enzyme concentration, the reaction time is always set to reach the desired yield. The first bisection is performed for the interval starting at $t = 0$ and the time required to reach the desired yield for the linear profile. For the further bisections, these times are kept constant.
If a trade-off between the reaction time t_f and any other variable is performed, the t_f is determined by the optimizer as an additional optimization variable. In this case the interval borders shift with t_f such that the intervals have equal length and that the last interval ends at t_f.

Solving the discrete optimal control problem

An efficient optimizer requires gradients and the Hessian matrix. The gradients are computed using Internal Numerical Differentiation with a forward finite difference with the square root of the machine precision as the step size (1.4901×10^{-8}) [177] in a code written by me. The Hessian is computed using forward finite difference for the derivative with the fourth root of the machine precision as the step size (1.2207×10^{-4}). Computation of the derivatives by solving the system of ODEs for the derivative of the states with respect to the control as done in other works [175, 240] is too computationally expensive here due to the large size of the system (up to approximately 1000 equations). Furthermore, computing the Hessian at every time step is also computationally expensive, therefore it is updated using the BFGS algorithm [241].
At the starting point, the function value, derivative, and Hessian are computed, then the direction and step length that minimizes the quadratic approximation to the objective function is found using the MATLAB® solver `quadprog`. Afterwards, a line search based on bisection and parabolic approximation is performed to find the length of the step in the previously computed direction. If the length of the step is larger than 1×10^{-6}, the step is accepted and the derivative and function value is updated. This iteration is performed until the decrease in the function value is less than the tolerance of 1×10^{-9}. If the step length of the quadratic programming step is smaller than the tolerance, a steepest descent step with a line search is performed. The Hessian is then reinitialized to an unity matrix times the step length of the previous steepest descent step.

5.3 Problem specification

In order for the problem to be specified the objective functional and the parameters need to be specified.

5.3.1 Objective function

Many criteria may be selected for which an optimal temperature profile could be found. The general objective functional (see Eq (5.7)) can handle most of them. The cost of heating the starting material and the reactor was neglected. The reaction time and amount of added enzymes should be minimized while maximizing the yield Φ of the product. The following functional formalizes these criteria:

$$J = \underbrace{-t_f \cdot \mathrm{M.U.\,h^{-1}} + C_1 \cdot \phi}_{f_f} \underbrace{-C_2 \cdot \frac{\tilde{E}_{RCS}(t=0) + \tilde{E}_{ECS}(t=0)}{2}}_{f_i} \tag{5.37}$$

The weighting factors C_1 in Monetary Units (M.U.) and C_2 in M.U. convert yield ϕ and normalized enzyme concentration into the profit J expressed in M.U.. If no other value is stated, $C_1 = 6\,\mathrm{M.U.}$ and $C_3 = 96\,\mathrm{M.U.}$. In this study, the yield ϕ is defined as the amount of monomer units present as free monomers and dimers at the final time divided by the total initial amount of monomers, which is a similar definition to the one used by Ouyang et al. [17]

$$\phi = \frac{n_1(t_f) + 2 \cdot n_2(t_f)}{\sum_{i=1}^{k_{\max}} i \cdot n_i(t=0)} \cdot 100\%. \tag{5.38}$$

$\tilde{E}_{RCS}(t=0)$ and $\tilde{E}_{ECS}(t=0)$ are the initial concentrations of the Random-chain scission (RCS) and End-chain scission (ECS) performing enzymes divided by the initial concentration of enzyme necessary to cut the percentage of bonds specified in the case definition. The concentration of the enzyme can be varied in some cases to obtain a more economical process. Furthermore, in all cases the temperature can be varied freely.

If C_1 and C_2 are set to arbitrary positive values and the initial enzymes concentrations, the reactor operation time, and the temperature profile are optimized simultaneously, one obtains the optimal operating conditions. However, for ease of discussion, four simpler objectives are investigated in this work:

Maximizing yield in fixed time with fixed enzyme concentration

If the reaction time of the process is fixed, e.g. due to limitations of the up- or downstream processes, one might be interested in finding a temperature profile that enables the highest possible yield. Thereby, the profit is maximized. By fixing the final time t_f as well as the enzyme concentration to be constant ($\tilde{E}_{RCS}(t=0) = \tilde{E}_{ECS}(t=0) = 1$), the benefit of temperature profile optimization alone can be studied.

Minimizing reaction time with a fixed yield and enzyme concentration

A certain yield might be required but the reaction time t_f of the process can be varied. Then it is desirable to find a temperature profile which minimizes the reaction time. In this case, the enzyme concentration is again kept constant ($\tilde{E}_{RCS}(t=0) = \tilde{E}_{ECS}(t=0) = 1$). By specifying a desired yield Φ_{des}, the time optimal problem (i.e., the shortest possible processing time) is formulated. If the yield is fixed, the function g is given as $\Phi(t_f) - \Phi_{des}$.

Trade-off between reaction time and yield with fixed enzyme concentration

A longer reaction time allows higher yield. But in order to handle the same amount of starting material in a given time the reactor needs to be larger or there must be more reactors which increases the capital costs. For this case, the enzyme concentration is kept constant ($\tilde{E}_{RCS}(t=0) = \tilde{E}_{ECS}(t=0) = 1$). By setting C_1 to an arbitrary positive value the goal of maximizing profit for a specified enzyme dosage is realized. C_1 indicates how much the product is worth, e.g. a value of $C_1 = 6\,\text{M.U.}$ means that a one percent increase in yield justifies an increase of reactor occupation by six hours.

Trade-off between reaction time and enzyme concentration at a fixed yield

Increasing the enzyme concentration allows one to reach a fixed yield in shorter time. However, due to the increased cost of enzymes this might make the process less economically viable. By setting C_2 to an

arbitrary positive value, and specifying a desired yield, the profit at this yield is maximized. C_2 indicates the cost of the enzyme, e.g. a value of $C_2 = 96\,\text{M.U.}$ means that the initial enzyme concentration needed to cut the desired percentage of bonds costs as much as operating the reactor for four days. This optimization can be performed either by keeping the ratio between E_{RCS} and E_{ECS} constant (Constant enzyme mixture composition), in which case only the amount of enzyme cocktail is optimized, or by letting the optimizer find the best ratio (Optimizing the enzyme mixture composition), in which case the enzyme mixture is also optimized. Both problems might be encountered in industrial practice depending on whether one uses a mixture of enzymes or two pure enzymes.

5.3.2 Parameters

Ho et al. [48] have experimentally validated a Population Balance Model (PBM) of enzymatically catalyzed depolymerization of linear and soluble starch at isothermal conditions. The enzymes were described by a simplified version of the Subsite Theory. The Michaelis constant was computed by the Subsite Theory, but the catalytic constant was approximated by a ramp function. Furthermore, they assumed that the single enzyme performed ECS. In another paper [49] they performed simulations that suggest that the presence of a RCS performing enzyme is beneficial for the conversion. As this model is able to describe experimental data an analog model was used. Later on a study to investigate the effects of using the product distribution predicted by the Subsite Theory and the effect of branching is performed.

Base case

The model used in this study takes temperature effects into account by using the equations derived with the Equilibrium model. Both the catalytic constant and the Michaelis constant are computed using the Subsite Theory but instead of using the Product Distribution Function (PDF) derived using the Subsite Theory the simplified extreme cases of RCS and ECS are used. The values of the parameters of the base case are provided in Table 5.1 and 5.2. Each initial enzyme concentration is chosen such that at a temperature of $50\,^{\circ}\text{C}$ during a reaction time of $24\,\text{hrs}$ the single enzyme cuts 5% of the bonds.

Parameter study

The amount of bonds cut is not taken from a literature reference. It is therefore desirable to study the effect of the amount of enzymes on the optimal temperature profile and process performance. Accordingly, the case "Doubled RCS activity" with twice as many bonds cut by RCS and "Doubled ECS activity" with twice as many bonds cut by ECS were considered. As with all other cases, the other parameters are kept constant at the value of the base case.
In order to study the influence of the equilibrium temperature, two additional cases were considered. In the case "Equal equilibrium temperature" both equilibrium temperature are set to $67.8\,^{\circ}\text{C}$, and in the case "Switched equilibrium temperature" $T_{RCS,eq}$ is set to the base case value of $T_{ECS,eq}$ and vice versa

Table 5.1: Parameters of the base case [3] (With kind permission from Springer).

Name	**Symbol**	**Value**	**Unit**
Mass concentration[a]		38.4	$\mathrm{g\,l^{-1}}$
Mean amount of monomer units[a]		160	
Polydispersity[a]		1.325	
Maximal amount of monomer units[a]	$\breve{k}_{\max}$	878	
Enthalpic change associated with enzyme folding RCS[c]	$\Delta H_{eq,RCS}$	192	$\mathrm{kJ\,mol^{-1}}$
Activation energy of hydrolysis RCS[c]	$\Delta G^{\dagger}_{cat,RCS}$	6.9	$\mathrm{kJ\,mol^{-1}}$
Activation energy of irreversible inactivation RCS[c]	$\Delta G^{\dagger}_{inact,RCS}$	105	$\mathrm{kJ\,mol^{-1}}$
Equilibrium temperature of RCS[c]	$T_{eq,RCS}$	90	°C
Position of the catalytic center of RCS	$\breve{z}_{-}$	6	
Enthalpic change associated with enzyme folding ECS[e]	$\Delta H_{eq,ECS}$	225	$\mathrm{kJ\,mol^{-1}}$
Activation energy of hydrolysis ECS[e]	$\Delta G^{\dagger}_{cat,ECS}$	64	$\mathrm{kJ\,mol^{-1}}$
Activation energy of irreversible inactivation ECS[e]	$\Delta G^{\dagger}_{inact,ECS}$	96	$\mathrm{kJ\,mol^{-1}}$
Equilibrium temperature of ECS[e]	$T_{eq,ECS}$	67.8	°C
Position of the catalytic center of ECS	$\breve{z}_{-}$	2	
Reference temperature	T_{ref}	30	°C

[a] Ref: [48]
[b] Ref: [238]
[c] Estimated from [207]
[d] Ref: [28]
[e] Ref: [242]

Table 5.2: Subsite binding energies in $\mathrm{kJ\,mol^{-1}}$ from Ho et al. [49].

Enzyme	1	2	3	4	5	6	7	8
Random-chain scission	4.6	10.0	0	2.5	10.0	-13.0	0	5.0
End-chain scission	-Inf	0	20.3	6.7	1.8	0.9	0.5	0.4

for ECS.
As starting material quality varies in a real process, the effect of variation is investigated. In the case "Sweet potato starch" the values (a mean amount of monomer units of 4100, a maximal amount of monomer units of 22496, and a polydispersity of 1.324) provided by Ho et al. [48] for sweet potato starch are used.

Effect of the Product Distribution Function and branching

Ho et al. [48, 49] used a simplified PDF instead of using the PDF derived using the Subsite Theory. Using the parameters of the base case including the initial enzyme concentration, the effect of using the more realistic but also more complicated PDF computed using the Subsite Theory is investigated.
In order to investigate the effect of branching on optimal control the optimal temperature profile maximizing the yield in fixed time is computed for a branched polymer. The average branching density is taken to be 5 % and all parameters, including the initial enzyme concentration, of the base case are used. Additionally, a maximal amount of branchings of 88 is used which is sufficiently large to have almost no polymer above this value. In order to include the effect of branchings on the reaction rate, the reaction rate derived by the extension of the Subsite Theory to a branched polymer is used. To stay consistent also the PDF derived using this extension is used.

5.3.3 Numerical parameters and settings

For the case using the simplified PDF a very fine mesh with a growth factor of 1.01 and $\breve{k}_c = 20$ was used. These were the values proposed by Ho et al. [48]. Also normalization was only done with respect to the initial polymer concentration as with the Cell Average Technique (CAT) because for the small polymer considered here further normalization was not necessary.
The case with the more realistic PDF and the branched cased used a fine mesh with a growth rate of 1.1 and $\breve{k}_c = 12$. Also normalization with the pivot position was performed. The choice of normalization does not have an effect for the small polymer investigated in this study though.

5.4 Results and Discussion

First the results for the parameter study are discussed. Followed by the presentation of the effect of using a different PDF and including the effect of branching are discussed.

5.4.1 Isothermal operation

Among other information Figure 5.1 shows the yield of the base setting at isothermal processing versus time. If one compares the yield obtained at the optimal isothermal temperature $51.9\,^{\circ}\mathrm{C}$ for maximizing yield within the specified processing time of $7\,\mathrm{d}$ with the yield at a $2.5\,^{\circ}\mathrm{C}$ higher temperature, one can see that the higher temperature initially leads to a higher hydrolysis rate. But the increased denaturation

causes the hydrolysis rate to reduce at later times. This leads to a lower final yield. The yield of both enzymes acting together is greater than the yield obtained by summing up the yield obtained from simulations using either one or the other enzymes separately at the optimal isothermal temperature. This is a clear indication that the synergy due to multi-enzymatic degradation plays a major role in this system.

5.4.2 Maximizing yield in fixed time with fixed enzyme concentration

Figure 5.1 shows the yield over time for some selected cases. First the increase of yield for the optimal linear profile is discussed. The corresponding temperature profile is shown in Figure 5.2 b). At first the lower temperatures of the optimal linear profile result in a low hydrolysis rate but also in a low enzyme denaturation rate. Therefore, at a later time more enzyme is present. This enzyme is then activated by the higher temperature compared to the optimal isothermal temperature at later times which results in a increased hydrolysis efficiency. The final yield, therefore, increases by 4.73 percentage points to 48.38%. It has to be noted that the mean temperature of the optimal linear profile is not the optimal isothermal temperature but rather a higher temperature.

The maximal obtainable yield after $7\,\mathrm{d}$ for an isothermal reactor with the parameters of the base case and with sweet potato starch is presented in Figure 5.2 a) for several levels of resolution of the optimized temperature profile. For the base case the maximal yield at the optimal isothermal temperature of $51.9\,^{\circ}\mathrm{C}$ is 43.65%. Note that this temperature is below $T_{RCS,eq}$ and $T_{ECS,eq}$ given in Table 5.1. The short reaction time coupled with a relatively low enzyme amount results in this low yield. Introducing the first profile resolution refinement increases the yield by only 0.006 percentage points. The next refinement increases the yield further by 0.32 percentage points to 48.71%. The benefit decreases upon further refinement of the temperature profile, e.g. the increase from 32 to 64 intervals (the fully refined profile) only increases the yield by 0.01 percentage points to 48.93%. However, using 64 intervals (the fully refined profile) instead of the optimal linear profile increases the yield by 0.55 percentage points in total. In all investigated cases (not shown) the first refinement only brought a tiny benefit. The second refinement then increased the profit more strongly and the effect leveled off for further refinements.

5.4.3 Minimizing reaction time with a fixed yield and enzyme concentration

Here, a high yield of 90% is demanded. The base case requires $435.6\,\mathrm{hrs}$ at optimal isothermal operation to reach this yield. Using the optimal linear profile reduces this by 6.14% and the fully refined profile results in a reduction of 7.63%. The processing of sweet potato starch takes slightly longer ($451.7\,\mathrm{hrs}$), but the optimization potential for the optimal linear and fully refined profile increases to 8.09% and 10.31%, respectively. If the activity of RCS or ECS is doubled, the required times reduces to $387.0\,\mathrm{hrs}$ and $198.3\,\mathrm{hrs}$, respectively. The reduction using the optimal linear profile were 3.99% and 7.92% and for the fully refined profile 5.60% and 9.20%. If the equilibrium temperature of the two enzymes were switched, the required time at isothermal operation reduces to $200.1\,\mathrm{hrs}$. This can be explained by ECS having a higher optimal isothermal temperature and therefore contributing more towards the hydrolysis.

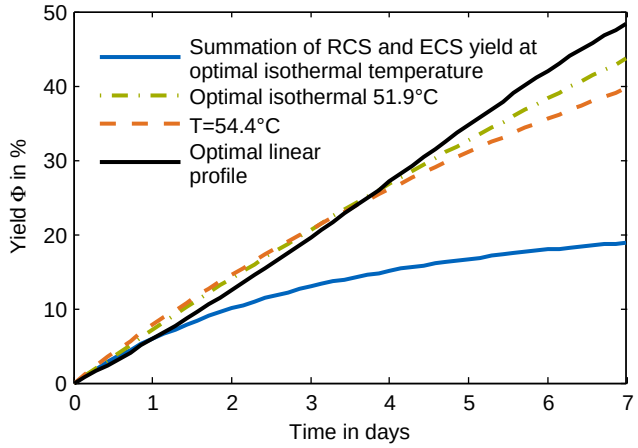

Figure 5.1: The yield over time at several times for the base case at the summation of the yield curves of the pure enzymes, the optimal linear temperature profile, the optimal isothermal temperature, and a 2.5 °C higher temperature.

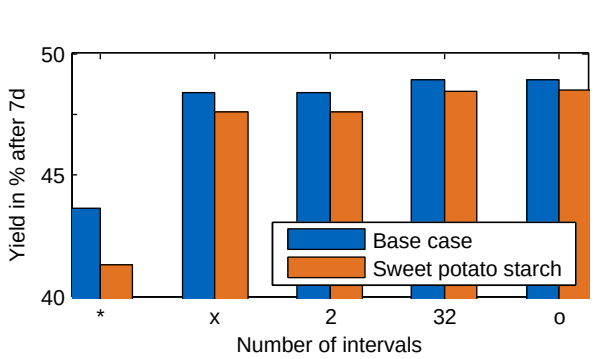

(a) Final yield: * Optimal isothermal temperature, x Optimal linear profile, o Fully refined.

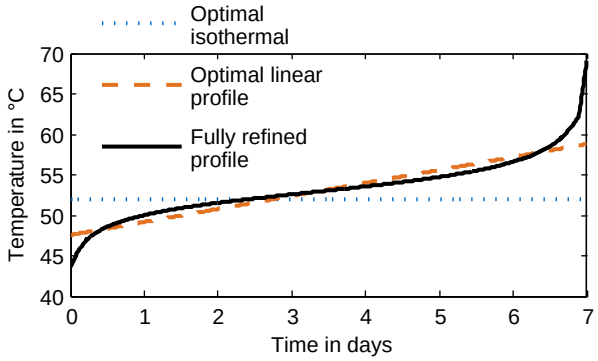

(b) Temperature profile of the base case.

Figure 5.2: Yield after 7 d for several refinements and the corresponding optimal temperature profile.

The reductions for this case were 15.29% for the optimal linear profile and 16% for the fully refined profile. Both enzyme having the same equilibrium temperature of the ECS enzyme results in a required time of 436.7 hrs which is almost the same as for the base case. Surprisingly, the reductions were also similar with 6.21% and 7.68%. The high reduction using the optimal linear profile or even the fully refined profile is surprising because previous studies [20] focused on pauses at - here almost equal - optimal isothermal temperatures of the enzymes.
Further cases, not shown here, suggest that the behavior observed in this study is likely to be not very dependent on specific parameter values. Even without denaturation it is desirable to operate at non-isothermal conditions. However, then the maximum reduction in the reaction time is approximately 0.4%, which is much smaller than for denaturating enzymes.
In Figure 5.3 the temperature profiles are shown for several cases with a desired yield of 90%. One can see that the fully refined temperature profile is strongly non-linear, even though a linear profile is a good approximation. The temperature profiles are all different from each other and there appears to be no simple correlation between them. Therefore, no general guideline on how to choose an optimal temperature profile can be given. Rather optimal control as described in this study should be performed. However, the optimal linear profile always realizes most of the saving potential. I cannot offer any sound explanation why the linear profile is such a good approximation.

5.4.4 Trade-off between reaction time and yield with fixed enzyme concentration

If the default value of product ($C_1 = 6$ M.U.) is used, a yield of 75.97% is optimal for isothermal operation. This yield takes 335.61 hrs to reach and results in profit of 120.21 M.U.. Using the optimal linear temperature profile a yield of 76.25% is obtained. This higher yield is reached in a shorter time of 308.49 hrs which results in a higher profit of 149.03 M.U.. The fully refined temperature profile had a yield of 77.08% which takes 309.12 hrs to reach and results in a profit of 153.39 M.U.. The overall profit can therefore be increased using optimal control.
If the product had a higher market value $C_1 = 12$ M.U., a higher yield of 93.06% is favorable. This takes 467.59 hrs to reach and delivered a profit of 649.13 M.U.. Using the optimal linear profile the yield slightly reduces to 92.6% in a shorter time of 436.65 hrs which results in a greater profit of 674.52 M.U.. The fully refined profile slightly increases the yield to 92.82% with a lower time of 432.66 hrs and a greater profit of 681.19 M.U..

5.4.5 Trade-off between reaction time and enzyme concentration at a fixed yield

Here, an equivalent enzyme cost C_2 of 96 M.U. is used. The results of the optimization are shown in Table 5.3.

Trade-off between reaction time and enzyme mixture at constant enzyme mixture composition
One can see that the reactor runs significantly faster than the one without the optimized enzyme amount. This is because of the usage of additional enzyme. However, the total cost is much lower

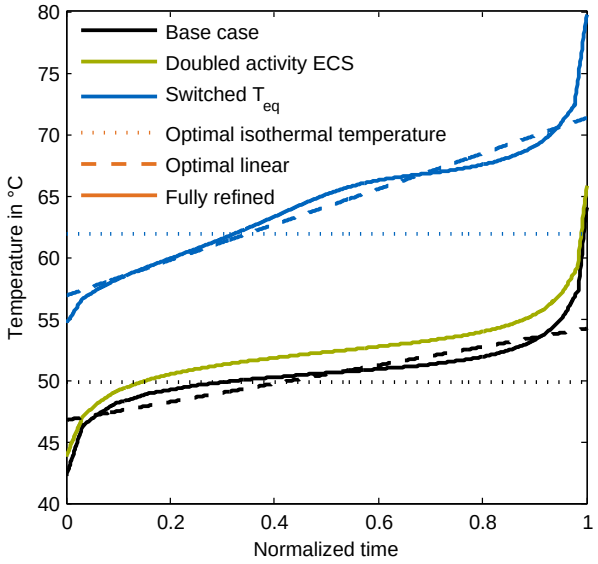

Figure 5.3: The fully refined temperature profile to obtain a desired yield in the shortest time over the normalized time for several cases.

than the one obtained for the original enzyme amount. An interesting result is that the enzyme amount and the reaction time reduce with using the optimal linear temperature profile. This results in a decrease of the cost due to reactor occupation and due to enzyme. Further on, no trend of the enzyme amount increasing or decreasing is visible. The cost reduction due to enzyme amount optimization is much larger than the cost reduction due to temperature profile optimization.
The small variation in the optimal enzyme amount was the motivation to try a simpler strategy. First the enzyme amount is optimized together with temperature for isothermal operation. Then the temperature profile is optimized at the fixed enzyme amount optimal for isothermal operation. One can see that for the optimal linear temperature profile almost all of the saving potential is realized using this simplified strategy.

Optimizing the enzyme mixture composition For the isothermal case, the reaction is faster with less enzymes than the optimization at constant enzyme mixture composition. Using the optimal linear temperature profile results in a greater cost reduction than for the enzyme amount optimization alone. The enzyme composition and amount change only slightly. Further refinement reduces the cost even further and one can see that enzyme mixture amount and composition changes only slightly. The cost reduction due to enzyme mixture optimization is much larger than the cost reduction due to temperature profile optimization.
Again a simpler strategy is pursued. First the enzyme amount and mixture composition is optimized for isothermal operation. Then the temperature profile is optimized at this fixed enzyme amount and mixture composition. One can see that almost all of the saving potential is realized. However, a simultaneous optimization of temperature profile and enzyme mixture is always better by a small margin.

Table 5.3: Cost and profit in M.U. for trade-off between reaction time and enzyme concentration at a fixed yield of 90%.

	Optimal isothermal	**Optimal linear**	**Fully refined**
	Without optimization of enzyme mixture amount or composition		
Total profit	8.44	35.18	41.66
	With enzyme amount optimization but constant enzyme mixture composition		
Cost due to reactor operation	168.63	163.28	161.19
Cost due to enzymes	207.5	201.72	201.68
Total profit	163.87	175.01	177.12
	Without optimization of enzyme mixture amount and composition at isothermal operation already optimized for enzyme amount		
Cost due to reactor operation	168.63	157.67	155.23
Total profit	163.87	174.83	177.27
	With optimization of the enzyme mixture amount and composition		
Cost due to reactor operation	143.03	136.89	135.14
Cost due to RCS	26.08	24.37	24.63
Cost due to ECS	148.23	142.57	142.76
Total profit	222.65	236.17	237.47
	Without optimization of enzyme mixture amount or composition at isothermal operation already optimized for enzyme mixture amount and composition		
Cost due to reactor operation	143.03	129.87	128.39
Total profit	222.65	235.82	237.30

5.4.6 Necessity for optimization

In Figure 5.4 the yield is shown for several temperature change rates at fixed average temperature. The average temperature is chosen as the optimal isothermal temperature. As already mentioned, the optimal linear temperature profile is not centered on the optimal isothermal temperature. However, finding the temperature on which the optimal linear profile is centered would be experimentally very difficult. Therefore, this simplified strategy is used here. One can see that the yield reaches a maximum and then drops strongly off and even falls below the yield for the isothermal process. This implies that just heating the process is not bound to increase the yield. Therefore, just using linear temperature profiles without an enzyme specific optimization is not recommended.

5.4.7 Effect of using the Product Distribution Function derived by Subsite Theory

The yield over temperature at isothermal operation is plotted in Figure 5.5 for the case using the simplified PDF as well as the more realistic PDF predicted by the Subsite Theory. One can see that the yields agree very well with each other. As the enzyme approximated as performing ECS actually does ECS due to the non-finite binding energy this is not very surprising. The small difference can be explained by the fact that the enzyme approximated by RCS does not attack the bonds randomly, but rather has a weak preference for inner bonds of large polymers. The optimal temperature profile maximizing the yield in fixed time, which is shown in Figure 5.6, agrees accordingly also quite well.

5.4.8 Effect of branching bonds

The yield over temperature at isothermal operation is plotted in Figure 5.5 for the linear polymer as well as the branched polymer. It is very surprising that the yield is higher for the branched polymer. The branching bonds should reduce the activity of the endo-active enzyme. And limit dextrines, which cannot be attacked and therefore should decrease the yield, for the attack on end-chains by the exo-active enzyme are possible if branching bonds exist. The contribution of the enzymes to the rate of yield increase over time is shown in Figure 5.7. One can see that the ECS enzyme increases the yield much more than the RCS enzymes. This is due to ECS producing directly monomer and dimer that is counted as product whereas RCS enzyme produces smaller polymer that are still larger than the product. Initially, the rates are higher for the branched polymer because each polymer has more than one end-chain. The enzymes are therefore more likely to create small polymers by each attack. However, if one compares the contribution of the ECS enzyme for the linear and branched polymer, one can see that the rate increases for the branched polymer whereas it decreases for the linear polymer. The rate decreases for the linear polymer because the effect due to denaturation of enzyme and increased product inhibition is larger than the effect from having more attackable polymers due to the action of the RCS enzyme. This should also occur for the branched polymer. However, instead the rate increases up to 80 hrs. This is likely due to each attack of the RCS enzyme on an inner chain creating one end-chains with a reducing end and a non-reducing end. In the model it was assumed that the chain carrying the

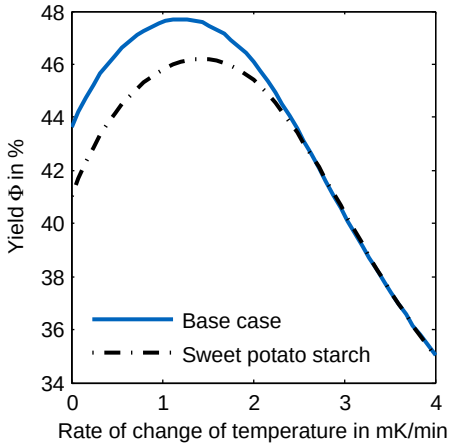

Figure 5.4: The yield over the temperature change rate with fixed average temperature.

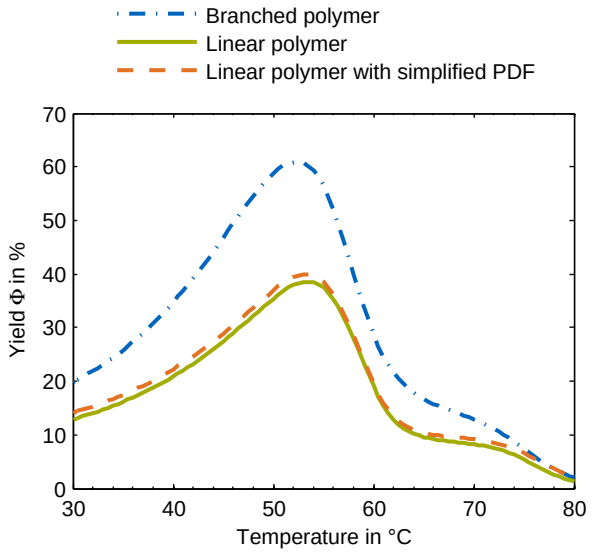

Figure 5.5: The yield of temperature at isothermal operation for the simplified product distribution function, the product distribution function predicted by the Subsite Theory, and the branched polymer.

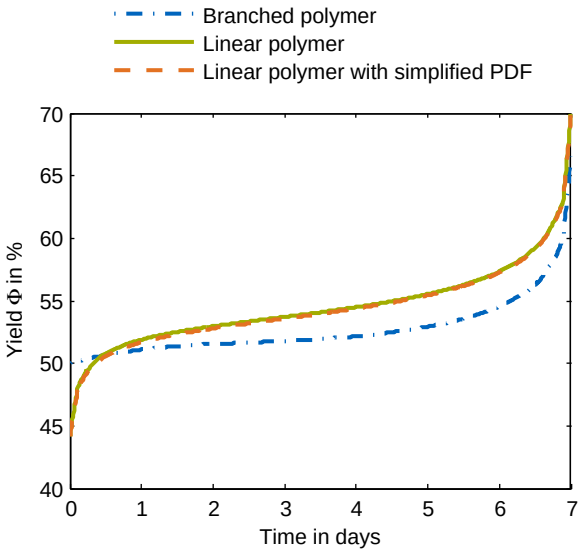

Figure 5.6: The fully refined temperature profile optimal for operating the reactor for 7 d for the simplified product distribution function, the product distribution function predicted by the Subsite Theory, and the branched polymers.

non-reducing end could be handled like a chain carrying a reducing end because it was only one chain out of many chains. However, due to this assumption every attack of RCS increases the amount of ECS attackable chain by 2 instead of by 1. This is a shortcoming of the model which should be redeemed. The validation performed in the preceding chapter did not include an enzyme that performs mainly ECS and therefore did not catch this. However, the increased production of maltotriose, which is another short oligomer, might also be explained by having too many chains with reducing ends.
The temperature profile maximizing conversion computed for the branched polymer is shown in Figure 5.6. This shows that the temperature profile depends on the model used and also that the algorithm is able to deal with branched polymer. No further investigation into the effect of branching on the predicted optimal control profiles was undertaken because the underlying model is not correct.

5.5 Conclusion and outlook

A model-based optimization study of depolymerization described by a population balance approach was performed. The enzyme mixture amount and composition were predicted to have the greatest influence on economic feasibility. But, temperature has also a major influence on process performance. Therefore, those parameters should be optimized. Furthermore, non-isothermal and non-linear temperature profiles have the potential to increase profitability. However, using the optimal linear temperature already realizes much of the saving potential. Even though the optimization problem is non-linear, multi-dimensional, and dependent on the starting material, it could be solved in a simple sequential manner in this study with only a small loss of saving potential.
Model-based optimization of enzyme mixture composition and amount and temperature should be applied to real processes and other biopolymers. This requires including e.g, the dissolution of polymer particles using models such as proposed by Griggs et al. [42], Lebaz et al. [46] or deactivation by irreversible unproductive binding [30]. Furthermore, experimentally obtained parameters are needed. Then there is only a small extra effort for additionally exploiting temperature trajectory optimization. It should be studied whether an (easy-to-implement) linear temperature profile would also be a good approximation for these more realistic cases.
Additionally, the objective functional should be extended to include more cost factors such as the energy consumption due to heating. If required, it can also be extended to include boundary conditions such as a given starting or end temperature. Furthermore, a more sophisticated refinement algorithm, e.g. [240], may be used to speed up computation. Optimal control can also be applied to optimal enzyme dosage [160] and substrate feeding [23].

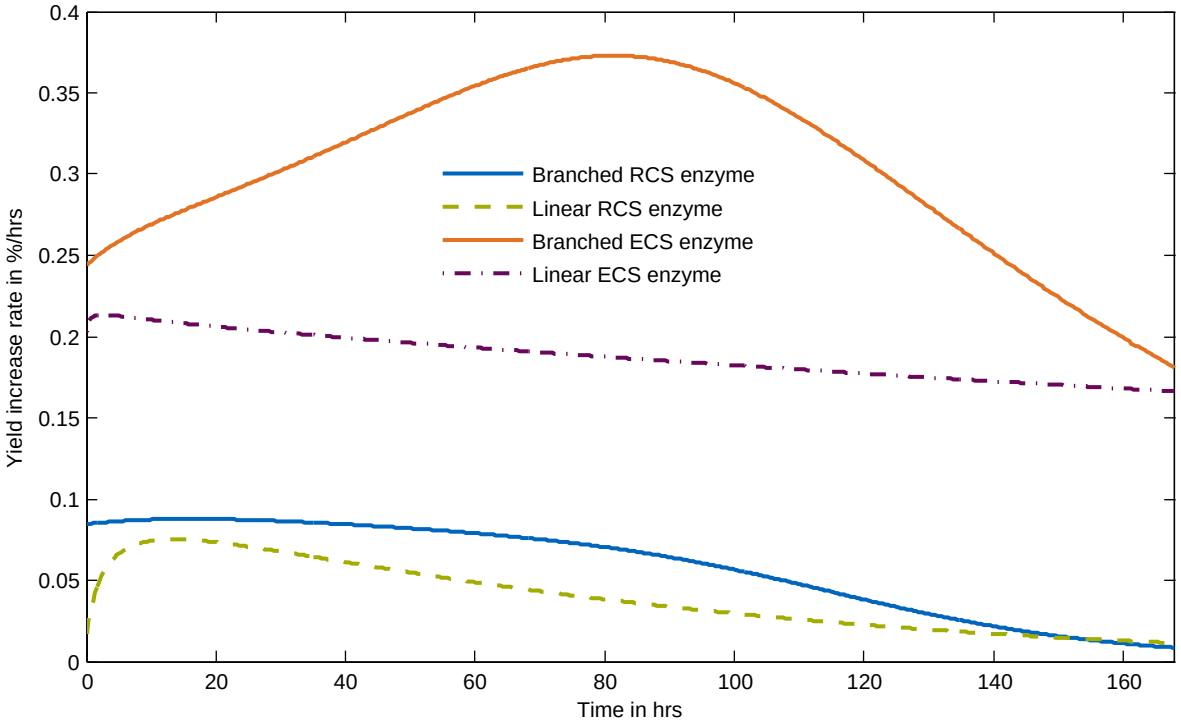

Figure 5.7: Contribution of the enzymes to the rate of yield increase for the branched and linear polymer at the optimal isothermal temperature for conversion of the branched polymer.

Chapter 6

Conclusion and outlook

In this dissertation a Population Balance Model (PBM) to describe the enzymatically catalyzed depolymerization of branched starch was developed. Three techniques (Direct Quadrature Method of Moments (DQMOM), Cell Average Technique (CAT), and Fixed Pivot technique (FP)) to solve such PBMs were adapted to the problem and a convergence study was performed. The adaption for DQMOM made the application of a domain decomposition technique necessary which was the first time such a decomposition was used for non-monovariate problems and with DQMOM. As FP was the best technique an optimal control algorithm was developed using this technique to find the optimal temperature profile.

6.1 Population Balance Model

For several mechanisms (Random-chain scission (RCS), End-chain scission (ECS), and Random-debranching scission (RDS)) the Product Distribution Function (PDF) was derived for the first time for a branched non-crosslinking polymer. This PDFs can be used whenever usage of these mechanisms can be justified. The PBM developed in Chapter 2 is the first model that accounts for the distributed nature of the polymer as well as the temperature dependence of the enzyme. Both effects are described using established and mechanistically sound models (the Subsite Theory [209, 216] and the Equilibrium Model [205]). For the first time a Population Balance Equation (PBE) that extends the Subsite Theory to a branched polymer was developed. Previously, only kinetic Monte Carlo (kMC) solvers could be used [32, 33].
The developed model was tested in Chapter 4 and found to describe experimental data as good as the only other currently available mechanistic model [32]. However, in Chapter 5 the model was found to predict likely false reaction rates for enzymes that perform mainly exo-active attacks. Accordingly, the assumption causing this effect should not be used and the model should be changed. This is not held to be a difficult task. Afterwards, the model should be validated more rigorously by comparison with results obtained using the kMC algorithm proposed by Marchal et al. [33] at precisely defined conditions. Furthermore, one can extract more information from the kMC simulations than just the evolution of the amount of polymers and some species. Rather, one can directly obtain the reaction rate and PDF as a

function of branching density and the amount of monomer units. This information can then be used to validate the PBM. Additionally, one could investigate the PBM separately from a solution technique for the PBE.
The model developed in this work neglects several effects which are relevant to obtaining a truly universal model. Pressure [243], pH-value [243, 244], and ion concentration [243, 245] are known to have an influence on the activity and stability of starch degrading enzymes. If those values vary between or during production runs, then they need to be included in the model. This is possible for a PBM and has been done by Obersteiner [246] for a version of the DQMOM code used in this work. If inhibitors, e.g. cellulose [247], are present, they should also be modeled using an appropriate model (see e.g. [248]).

6.2 Direct Quadrate Method of Moments

In Chapter 3 a modification for the DQMOM to be able to describe depolymerization was proposed. This modification introduced a domain decomposition into a continuous, discrete, and mixed continuous-discrete subdomain. By comparing the results of DQMOM to kMC solutions of the underlying discrete PBE, it was shown that the modification was able to increase the accuracy for all cases considered in this work. However, except for ECS, the accuracy was not acceptable for the branched polymer. For the linear polymer one could find sufficiently high values of the domain decomposition parameter and the number of quadrature points such that the agreement between kMC and DQMOM was acceptable. However, for the branched polymer - even using a highly sophisticated solution technique - the number of quadrature points could not be increased to a level where the agreement was sufficient. This is consistent with Lebaz et al. [67] and Lebaz et al. [46] being able to obtain satisfactory results using DQMOM for describing the depolymerization of linear polymer. Theoretically, one would be able to increase the discrete domain in size until the accuracy would be good. However, the computational effort would not be feasible. Therefore, DQMOM was shown to be unable to handle the depolymerization problem handeled here.
The strong benefit of increasing the discrete domain in size and the good performance of the discretely implemented class methods implies that the continuity assumption is not valid for the depolymerization process. Therefore, one should modify the Method Of Moments (MOM) such that it can be used for a discrete PBE which has never been done before. Furthermore, other MOMs, such as Sectional Quadrature Method of Moments [108] or the Maximum entropy method [111] should be tested, if the continuity assumption is valid, but rather DQMOM is not able to describe the process.

6.3 Methods of Classes

In Chapter 4 two Methods Of Classes (CMs), which have the same principal idea, were implemented in a discrete manner: FP and CAT. Both methods were found to have similar accuracy, but as FP was significantly faster it should be preferred. The faster computation with FP has been reported [230] and

is, therefore, not surprising. The literature on the relative performance of FP and CAT does not allow any conclusions. Some studies found comparable accuracies [233, 249], but theoretical derivations [231] and other computational experiments [231, 235] agree on CAT being superior.
As already mentioned in the literature [48] and similar to other methods [147] a high resolution was required to obtain accurate results for ECS. A case study for a highly branched polymer being attacked by enzymes described using the simplest feasible reaction rates was undertaken. It was found that RCS and RDS together had a much worse agreement with kMC solutions than both mechanisms alone. No clear explanation for this was found. The attack on linear and branched polymer by one enzyme that was described using the subsite theory was represented with a very high precision.
The reason for the bad performance of the combination of RCS and RDS should be investigated in more detail. Also a more rigorous convergence analysis of the algorithm should be undertaken. This study should focus on the behavior for multimodal distributions, larger polymers, and multiple enzymes described by the subsite theory.

6.4 Optimal control

In Chapter 5 an optimal control algorithm for the enzymatic catalyzed depolymerization was described. This algorithm was used for a case study. This case study predicted that there is significant saving potential. Most of this saving potential could be realized using a simple linear profile. Prior studies of optimal control of enzymatically catalyzed depolymerization [16, 23, 159, 250] did not investigate simpler profiles but found significant benefits.
Furthermore, it was found that optimizing the reaction duration and the enzyme mixture composition and amount had potential to increase the feasibility of the process by a significant amount. However, as it was not possible to find a consistent data set for a realistic enzyme cocktails (see [251] for one part of the effort undertaken) the parameters cannot be applied directly to a real process. Therefore, the parameters of one enzyme cocktails should be determined to enable model-based optimization and optimal control. Another shortcoming of the case study was that no cost parameters for a real process were used. By cooperation with an industrial partner the cost parameters should be obtained for one specific process to obtain realistic data for one specific test case. Additionally, the cost of heating the process should be implemented.
It was also shown that the algorithm can be applied to branched polymers. The algorithm can be sped up by using a more sophisticated refinement technique [240]. The algorithm can also be extended to study optimal enzyme dosage [160] and substrate feeding [23].

6.5 Application to cellulose

The most common polymer is cellulose. It is also a biopolymer and homopolymer of glucose [11, 252]. Furthermore, it is also distributed in the amount of monomer units [27]. As it cannot be consumed by

humans and can be grown in locations, where no food stuff can be produced, it does not create a rivalry between the "tank" and the "fork" [11, 252]. Furthermore, it extends the number of plants that can be farmed which would be beneficial to rural areas [5]. Accordingly, there is significant interest in depolymerization of cellulose by enzymes [35, 42, 253, 254] as this polymer can enable the transformation into the bioeconomy.

There have been many studies that focused on modeling the depolymerization of cellulose using PBEs [40–44, 47, 67, 68, 138] besides many other modeling studies [21, 22, 24, 30, 31, 35, 255, 256]. The reaction rate has been modeled without full success using the subsite theory [257]. Furthermore, the deactivation mechanisms is not fully understood [258] and may partially be due to irreversible bindings [255, 259]. Other studies regard thermal deactivation as important [260–263].

If a suitable model is selected, which might need to include both thermal inactivation and irreversible binding, and the effect of the polymer being insoluble, e.g. using the model proposed by Griggs et al. [42], this model can then be used instead of the less mechanistically based simpler model used for optimal control of this process previously [16, 23, 159, 250]. Furthermore, instead of performing experimental optimization [264, 265] one could perform model-based optimal control which would reduce the costs required for optimization. The algorithm developed here can be used to also perform optimal control for cellulose depolymerization. Furthermore, the results gained here in solving a depolymerization PBE can be transferred to cellulose.

Bibliography

[1] C. Kirse and H. Briesen. Population balance model for enzymatic depolymerization of branched starch. In K. V. Gernaey, J. K. Huusom, and R. Gani, editors, *12th International Symposium on Process Systems Engineering and 25th European Symposium on Computer Aided Process Engineering*, volume 37, pages 221–226, 2015.

[2] C. Kirse and H. Briesen. Numerical solution of mixed continuous-discrete population balance models for depolymerization of branched polymers. *Computers & Chemical Engineering*, 73: 154–171, 2015. doi: 10.1016/j.compchemeng.2014.11.008.

[3] C. Kirse and H. Briesen. Temperature profile optimization: Potential for multi-enzymatic biopolymer depolymerization processes. *Bioprocess and Biosystems Engineering*, page Accepted, 2017.

[4] F. C. on Climate Change, Paris agreement. URL `http://unfccc.int/resource/docs/2015/cop21/eng/l09r01.pdf`. Last visited on 2.1.2017.

[5] K. L. Kline, S. Msangi, V. H. Dale, J. Woods, G. M. Souza, P. Osseweijer, J. S. Clancy, J. A. Hilbert, F. X. Johnson, P. C. McDonnell, and H. K. Mugera. Reconciling food security and bioenergy: priorities for action. *GCB Bioenergy*, pages 1–20, 2016. doi: 10.1111/gcbb.12366.

[6] T. M. Mata, A. A. Martins, and N. S. Caetano. Microalgae for biodiesel production and other applications: A review. *Renewable & Sustainable Energy Reviews*, 14(1):217–232, 2010. doi: 10.1016/j.rser.2009.07.020.

[7] J. J. Cheng and G. R. Timilsina. Status and barriers of advanced biofuel technologies: A review. *Renewable Energy*, 36(12):3541–3549, 2011. doi: 10.1016/j.renene.2011.04.031.

[8] K. Kumar, S. Ghosh, I. Angelidaki, S. L. Holdt, D. B. Karakashev, M. A. Morales, and D. Das. Recent developments on biofuels production from microalgae and macroalgae. *Renewable & Sustainable Energy Reviews*, 65:235–249, 2016. doi: 10.1016/j.rser.2016.06.055.

[9] D. Klein-Marcuschamer, P. Oleskowicz-Popiel, B. A. Simmons, and H. W. Blanch. The challenge of enzyme cost in the production of lignocellulosic biofuels. *Biotechnology and Bioengineering*, 109(4):1083–1087, 2012.

[10] S. Pérez and E. Bertoft. The molecular structures of starch components and their contribution to the architecture of starch granules: A comprehensive review. *Starch - Stärke*, 62(8):389–420, 2010. doi: 10.1002/star.201000013.

[11] M. E. Himmel, S.-Y. Ding, D. K. Johnson, W. S. Adney, M. R. Nimlos, J. W. Brady, and T. D. Foust. Biomass recalcitrance: Engineering plants and enzymes for biofuels production. *Science*, 315 (5813):804–807, 2007. doi: 10.1126/science.1137016.

[12] G. W. Huber, S. Iborra, and A. Corma. Synthesis of transportation fuels from biomass: Chemistry, catalysts, and engineering. *Chemical Reviews*, 106(9):4044–4098, 2006. doi: 10.1021/cr068360d.

[13] B. der deutschen Bioethanolwirtschaft, Die deutsche Bioethanolwirtschaft in Zahlen. URL `https://www.bdbe.de/daten/marktdaten-deutschland`. Last visited 01.09.2016.

[14] M. Krottenthaler, W. Back, and M. Zarnkow. *Handbook of Brewing: Processes, Technology, Markets*, chapter Wort Production, pages 207–224. Wiley, Weinheim, 2009.

[15] E. C. Ramirez, D. B. Johnston, A. J. McAloon, and V. Singh. Enzymatic corn wet milling: engineering process and cost model. *Biotechnology for Biofuels*, 2, 2009. doi: 10.1186/1754-6834-2-2.

[16] S. Mutturi and G. Liden. Model- based estimation of optimal temperature profile during simultaneous saccharification and fermentation of arundo donax. *Biotechnology and Bioengineering*, 111(5):866–875, 2014. doi: 10.1002/bit.25165.

[17] J. Ouyang, Z. Li, X. Li, H. Ying, and Q. Yong. Enhanced enzymatic conversion and glucose production via two-step enzymatic hydrolysis of corncob residue from xylo-oligosaccharides producer's waste. *Bioresources*, 4(4):1586–1599, 2009.

[18] D. McElroy and J. Jacobsen. Whats brewing in barley biotechnology. *Bio-Technology*, 13(3): 245–249, 1995. doi: 10.1038/nbt0395-245.

[19] K. Larue, M. Melgar, and V. J. J. Martin. Directed evolution of a fungal beta-glucosidase in saccharomyces cerevisiae. *Biotechnology for Biofuels*, 9, 2016. doi: 10.1186/s13068-016-0470-9.

[20] M. Zarnkow, M. Kessler, W. Back, E. K. Arendt, and M. Gastl. Optimisation of the mashing procedure for 100% malted proso millet (panicum miliaceum l.) as a raw material for gluten-free beverages and beers. *Journal of the Institute of Brewing*, 116(2):141–150, 2010.

[21] M. Wang, L. Han, S. Liu, X. Zhao, J. Yang, S. K. Loh, X. Sun, C. Zhang, and X. Fang. A weibull statistics-based lignocellulose saccharification model and a built-in parameter accurately predict lignocellulose hydrolysis performance. *Biotechnology journal*, 10(9):1424–1433, 2015.

[22] C. M. Galanakis, A. Patsioura, and V. Gekas. Enzyme kinetics modeling as a tool to optimize food industry: A pragmatic approach based on amylolytic enzymes. *Critical Reviews in Food Science and Nutrition*, 55(12):1758–1770, 2015. doi: 10.1080/10408398.2012.725112.

[23] I. D. Cavalcanti-Montano, C. A. Galeano Suarez, U. F. Rodriguez-Zuniga, R. d. L. Camargo Giordano, R. d. C. Giordano, and R. de Sousa Junior. Optimal bioreactor operational policies for the enzymatic hydrolysis of sugarcane bagasse. *Bioenergy Research*, 6(2):776–785, 2013. doi: 10.1007/s12155-013-9294-7.

[24] R. Bezerra and A. Dias. Discrimination among eight modified michaelis-menten kinetics models of cellulose hydrolysis with a large range of substrate/enzyme ratios. *Applied Biochemistry and Biotechnology*, 112(3):173–184, 2004. doi: 10.1385/ABAB:112:3:173.

[25] T. Koljonen, J. J. Hämäläinen, K. Sjöholm, and K. Pietilä. A model for the prediction of fermentable sugar concentrations during mashing. *Journal of Food Engineering*, 26(3):329–350, 1995.

[26] J. Rollings and R. Thompson. Kinetics of enzymatic starch liquefaction - simulation of the high-molecular-weight product distribution kinetics of enzymatic starch liquefaction - simulation of the high-molecular-weight product distribution. *Biotechology and Bioengineering*, 26(12):1475–1484, 1984. doi: 10.1002/bit.260261212.

[27] P. Engel, L. Hein, and A. C. Spiess. Derivatization-free gel permeation chromatography elucidates enzymatic cellulose hydrolysis. *Biotechnology for Biofuels*, 5:77, 2012. doi: 10.1186/1754-6834-5-77.

[28] K. Hiromi. Interpretation of dependency of rate parameters on degree of polymerization of substrate in enzyme-catalyzed reactions - evaluation of subsite affinities of exo-enzyme. *Biochemical and Biophysical Research Communications*, 40(1):1–6, 1970. doi: 10.1016/0006-291X(70)91037-5.

[29] H. Kondo, H. Nakatani, R. Matsuno, and K. Hiromi. Product distribution in amylase-catalyzed hydrolysis of amylose - comparison of experimental results with theoretical predictions. *Journal of Biochemistry*, 87(4):1053–1070, 1980.

[30] P. Bansal, M. Hall, M. J. Realff, J. H. Lee, and A. S. Bommarius. Modeling cellulase kinetics on lignocellulosic substrates. *Biotechnology advances*, 27(6):833–848, 2009.

[31] A. Asztalos, M. Daniels, A. Sethi, T. Shen, P. Langan, A. Redondo, and S. Gnanakaran. A coarse-grained model for synergistic action of multiple enzymes on cellulose. *Biotechnology for Biofuels*, 5, 2012. doi: 10.1186/1754-6834-5-55.

[32] T. Besselink, T. Baks, A. E. M. Janssen, and R. M. Boom. A stochastic model for predicting dextrose equivalent and saccharide composition during hydrolysis of starch by alpha-amylase. *Biotechnology and Bioengineering*, 100(4):684–697, 2008. doi: 10.1002/bit.21799.

[33] L. Marchal, R. Ulijn, C. Gooijer, G. Franke, and J. Tramper. Monte carlo simulation of the α-amylolysis of amylopectin potato starch. 2. α-amylolysis of amylopectin. *Bioprocess and Biosystems Engineering*, 26:123–132, 2003. doi: 10.1007/s00449-003-0342-0.

[34] P. M. Wojciechowski, A. Koziol, and A. Noworyta. Iteration model of starch hydrolysis by amylolytic enzymes. *Biotechnology and Bioengineering*, 75(5):530–539, 2001. doi: 10.1002/bit.10092.

[35] M. Eibinger, T. Zahel, T. Ganner, H. Plank, and B. Nidetzky. Cellular automata modeling depicts degradation of cellulosic material by a cellulase system with single-molecule resolution. *Biotechnology for Biofuels*, 9, 2016. doi: 10.1186/s13068-016-0463-8.

[36] S. Chang, S. Delwiche, and N. Wang. Hydrolysis of wheat starch and its effect on the falling number procedure: Mathematical model. *Biotechnology and Bioengineering*, 79(7):768–775, 2002. doi: 10.1002/bit.10333.

[37] M. Watanabe and F. Kawai. Numerical simulation for enzymatic degradation of poly(vinyl alcohol). *Polymer Degradation And Stability*, 81(3):393–399, 2003. doi: 10.1016/S0141-3910(03)00122-8.

[38] M. Watanabe and F. Kawai. Mathematical modelling and computational analysis of enzymatic degradation of xenobiotic polymers. *Applied Mathematical Modelling*, 30(12):1497–1514, 2006. doi: 10.1016/j.apm.2005.12.011.

[39] M. Watanabe, F. Kawai, S. Tsuboi, S. Nakatsu, and H. Ohara. Study on enzymatic hydrolysis of polylactic acid by endogenous depolymerization model. *Macromolecular Theory and Simulations*, 16(6):619–626, 2007. doi: 10.1002/mats.200700015.

[40] S. A. Hosseini and N. Shah. Modelling enzymatic hydrolysis of cellulose part I: Population balance modelling of hydrolysis by endoglucanase. *Biomass & Bioenergy*, 35(9):3841–3848, 2011. doi: 10.1016/j.biombioe.2011.04.026.

[41] S. A. Hosseini and N. Shah. Enzymatic hydrolysis of cellulose part II: Population balance modelling of hydrolysis by exoglucanase and universal kinetic model. *Biomass & Bioenergy*, 35(9): 3830–3840, 2011. doi: 10.1016/j.biombioe.2011.04.029.

[42] A. J. Griggs, J. J. Stickel, and J. J. Lischeske. A mechanistic model for enzymatic saccharification of cellulose using continuous distribution kinetics I: Depolymerization by EGI and CBHI. *Biotechnology and Bioengineering*, 109(3):665–675, 2012. doi: 10.1002/bit.23355.

[43] A. J. Griggs, J. J. Stickel, and J. J. Lischeske. A mechanistic model for enzymatic saccharification of cellulose using continuous distribution kinetics II: Cooperative enzyme action, solution kinetics, and product inhibition. *Biotechnology and Bioengineering*, 109(3):676–685, 2012. doi: 10.1002/bit.23354.

[44] A. Nag, M. A. Sprague, A. J. Griggs, J. J. Lischeske, J. J. Stickel, A. Mittal, W. Wang, and D. K. Johnson. Parameter determination and validation for a mechanistic model of the enzymatic saccharification of cellulose-I-beta. *Biotechnology Progress*, 31(5):1237–1248, 2015. doi: 10.1002/btpr.2122.

[45] N. Lebaz, A. Cockx, M. Sperandio, and J. Morchain. Reconstruction of a distribution from a finite number of its moments: A comparative study in the case of depolymerization process. *Computers & Chemical Engineering*, 84:326 – 337, 2016. doi: http://dx.doi.org/10.1016/j.compchemeng.2015.09.008.

[46] N. Lebaz, A. Cockx, M. Spérandio, A. Liné, and J. Morchain. Application of the direct quadrature method of moments for the modelling of the enzymatic hydrolysis of cellulose: II. Case of insoluble substrate. *Chemical Engineering Science*, 149:322 – 333, 2016. doi: http://dx.doi.org/10.1016/j.ces.2016.04.029.

[47] M. Huron, D. Hudebine, N. L. Ferreira, and D. Lachenal. Mechanistic modeling of enzymatic hydrolysis of cellulose integrating substrate morphology and cocktail composition. *Biotechnology for Biofuels*, 113(5):1011–1023, 2016. doi: 10.1002/bit.25873.

[48] Y. K. Ho, P. Doshi, H. K. Yeoh, and G. C. Ngoh. Interlinked population balance and cybernetic models for the simultaneous saccharification and fermentation of natural polymers. *Biotechology and Bioengineering*, 112(10):2084–2105, 2015.

[49] Y. K. Ho, P. Doshi, H. K. Yeoh, and G. C. Ngoh. Why are two enzymes better than one for efficient simultaneous saccharification and fermentation (SSF) of natural polymers? Hints from inside and outside a yeast. *Industrial & Engineering Chemistry Research*, 54(42):10228–10244, 2015. doi: 10.1021/acs.iecr.5b01667.

[50] A. D. Randolph. A population balance for countable entities. *The Canadian Journal of Chemical Engineering*, 42(6):280–281, 1964. doi: 10.1002/cjce.5450420612.

[51] H. Hulburt and S. Katz. Some problems in particle technology: A statistical mechanical formulation. *Chemical Engineering Science*, 19(8):555 – 574, 1964. doi: http://dx.doi.org/10.1016/0009-2509(64)85047-8.

[52] M. von Smoluchowski. Drei Vorträge über Diffusion, Brownsche Molekularbewegung und Koagulation von Kolloidteilchen. *Physikalische Zeitschrift*, 17:557–599, 1916.

[53] F. Sporleder, Z. Borka, J. Solsvik, and H. A. Jakobsen. On the population balance equation. *Reviews in Chemical Engineering*, 28(2-3):149–169, 2012. doi: 10.1515/revce-2011-0013.

[54] B. McCoy and G. Madras. Discrete and continuous models for polymerization and depolymerization. *Chemical Engineering Science*, 56(8):2831–2836, 2001. doi: 10.1016/S0009-2509(00)00516-9.

[55] H. Briesen. Simulation of crystal size and shape by means of a reduced two-dimensional population balance model. *Chemical Engineering Science*, 61(1):104–112, 2006. doi: 10.1016/j.ces.2004.11.062. 2nd International Conference on Population Balance Modelling, Valencia, Spain.

[56] A. D. Randolph and M. A. Larson. *Theory of Particulate Processes*. Academic Press, 1971.

[57] D. Ramkrishna. *Population Balances*. Academic Press, London, 2000.

[58] D. Ramkrishna and M. R. Singh. Population balance modeling: Current status and future prospects. In J. Prausnitz, M. Doherty, and R. Segalman, editors, *Annual Review of Chemical and Biochemical Engineering*, volume 5, pages 123–146. Annual Reviews, Palo Alto, U.S.A., 2014. ISBN 978-0-8243-5205-9. doi: 10.1146/annurev-chembioeng-060713-040241.

[59] S. Kumar and H. Briesen. Population balances in the league of mass, momentum, and energy balances. *Chemical Engineering Science*, 70:1–3, 2012. doi: 10.1016/j.ces.2011.12.025.

[60] S. Katz and G. Saidel. Moments of size distribution in radical polymerization. *AIChE Journal*, 13 (2):319–&, 1967. doi: 10.1002/aic.690130223.

[61] W. Ray. Mathematical modeling of polymerization reactors. *Journal of Macromolecular Science - Reviews in Macromolecular Chemistry and Physics*, C 8(1):1–&, 1972.

[62] P. Iedema, M. Wulkow, and H. Hoefsloot. Modeling molecular weight and degree of branching distribution of low-density polyethylene. *Macromolecules*, 33(19):7173–7184, 2000. doi: 10.1021/ma991711o.

[63] B. McCoy and G. Madras. Degradation kinetics of polymers in solution: Dynamics of molecular weight distributions. *AIChE Journal*, 43(3):802–810, 1997. doi: 10.1002/aic.690430325.

[64] J. Yoon, H. Jin, I. Chin, C. Kim, and M. Kim. Theoretical prediction of weight loss and molecular weight during random chain scission degradation of polymers. *Polymer*, 38(14):3573–3579, 1997. doi: 10.1016/S0032-3861(96)00921-4.

[65] B. McCoy. Distribution kinetics for temperature-programmed pyrolysis. *Industrial & Engineering Chemistry Research*, 38(12):4531–4537, 1999. doi: 10.1021/ie990462p.

[66] P. D. Iedema. Predicting MWD and branching distribution of terminally branched polymers undergoing random scission. *Macromolecular Theory and Simulations*, 21(3):166–186, 2012. doi: 10.1002/mats.201100094.

[67] N. Lebaz, A. Cockx, M. Spérandio, A. Liné, and J. Morchain. Application of the direct quadrature method of moments for the modelling of the enzymatic hydrolysis of cellulose: I. Case of soluble substrate. *Chemical Engineering Science*, 149:306 – 321, 2016. doi: http://dx.doi.org/10.1016/j.ces.2016.04.018.

[68] H. Niu, N. Shah, and C. Kontoravdi. Modelling of amorphous cellulose depolymerisation by cellulases, parametric studies and optimisation. *Biochemical Engineering Journal*, 105(B):455–472, 2016. doi: 10.1016/j.bej.2015.10.017.

[69] T. Bak and K. Bak. The viscosity of degrading polymer solutions. *ACTA Chemica Scandinavica*, 13(10):1997–2008, 1959. doi: 10.3891/acta.chem.scand.13-1997.

[70] A. D. Randolph. Effect of crystal breakage on crystal size distribution in a mixed suspension crystallizer. *Industrial & Engineering Chemistry Fundamentals*, 8(1):58–63, 1969. doi: 10.1021/i160029a010.

[71] R. Ziff. Kinetics of polymerization. *Journal of Statistical Physics*, 23(2):241–263, 1980. doi: 10.1007/BF01012594.

[72] M. Falkovitz and L. Segel. Some analytic results concerning the accuracy of the continuous approximation in a polymerization problem. *SIAM Journ an Applied Mathematics*, 42(3):542–548, 1982. doi: 10.1137/0142038.

[73] R. Ziff and E. McGrady. Kinetics of polymer degradation. *Macromolecules*, 19(10):2513–2519, 1986. doi: 10.1021/ma00164a010.

[74] J. Staggs. Modelling random scission of linear polymers. *Polymer Degradation And Stability*, 76 (1):37–44, 2002. doi: 10.1016/S0141-3910(01)00263-4.

[75] A. Hasseine, A. Bellagoun, and H. J. Bart. Analytical solution of the droplet breakup equation by the adomian decomposition method. *Applied Mathematics and Computation*, 218(5):2249–2258, 2011. doi: 10.1016/j.amc.2011.07.041.

[76] N. Metropolis and S. Ulam. The Monte Carlo method. *Journal of the American Statistical Association*, 44(247):335–341, 1949.

[77] Sokal. *Monte Carlo Methods in statistical mechanics*. New York University, 1996. LectureNotes.

[78] D. T. Gillespie. Stochastic simulation of chemical kinetics. *Annual Review of Physical Chemistry*, 58:35–55, 2007. doi: 10.1146/annurev.physchem.58.032806.104637.

[79] H. Tobita. Random degradation of branched polymers .1. Star polymers. *Macromolecules*, 29(8): 3000–3009, 1996. doi: 10.1021/ma950971c.

[80] M. Smith and T. Matsoukas. Constant-number monte carlo simulation of population balances. *Chemical Engineering Science*, 53(9):1777–1786, 1998. doi: 10.1016/S0009-2509(98)00045-1.

[81] Y. Lin, K. Lee, and T. Matsoukas. Solution of the population balance equation using constant-number Monte Carlo. *Chemical Engineering Science*, 57(12):2241–2252, 2002. doi: 10.1016/S0009-2509(02)00114-8.

[82] *COMSOL Multiphysics Reference Manual*, 5.0 edition, 2014.

[83] M. Nicmanis and M. Hounslow. Finite-element methods for steady-state population balance equations. *AIChE Journal*, 44(10):2258–2272, 1998. doi: 10.1002/aic.690441015.

[84] J. Solsvik and H. A. Jakobsen. Spectral solution of the breakage-coalescence population balance equation picard and newton iteration methods. *Applied Mathematical Modelling*, 40(3):1741–1753, 2016. doi: 10.1016/j.apm.2015.08.022.

[85] A. I. Roussos and C. Kiparissides. A bivariate population balance model for the microbial production of poly(3-hydroxybutyrate). *Chemical Engineering Science*, 70:45–53, 2012. doi: 10.1016/j.ces.2011.07.049. 4th International Conference on Population Balance Modeling (PBM).

[86] J. Barrett and N. Webb. A comparison of some approximate methods for solving the aerosol general dynamic equation. *Journal of Aerosol Science*, 29(1-2):31–39, 1998. doi: 10.1016/S0021-8502(97)00455-2.

[87] M. Wulkow, A. Gerstlauer, and U. Nieken. Modeling and simulation of crystallization processes using parsival. *Chemical Engineering Science*, 56(7):2575–2588, 2001. doi: 10.1016/S0009-2509(00)00432-2. Joint Meeting of the 14th International Symposium on Industrial Crystallisation/5th International Symposium on Crystal Growth of Organic Materials, Cambridge, England.

[88] P. Iedema, S. Grcev, and H. Hoefsloot. Molecular weight distribution modeling of radical polymerization in a CSTR with long chain branching through transfer to polymer and terminal double bond (TDB) propagation. *Macromolecules*, 36(2):458–476, 2003. doi: 10.1021/ma020900v.

[89] R. Grosch, H. Briesen, W. Marquardt, and M. Wulkow. Generalization and numerical investigation of QMOM . *AIChE Journal*, 53(1):207–227, 2007. doi: 10.1002/aic.11041.

[90] R. McGraw. Description of aerosol dynamics by the quadrature method of moments. *Aerosol Science & Technology*, 27(2):255–265, 1997. doi: 10.1080/02786829708965471.

[91] F. Santos, J. Favero, and P. Lage. Solution of the population balance equation by the direct dual quadrature method of generalized moments. *Chemical Engineering Science*, 101:663 – 673, 2013. doi: http://dx.doi.org/10.1016/j.ces.2013.07.025.

[92] D. Wright, R. McGraw, and D. Rosner. Bivariate extension of the quadrature method of moments for modeling simultaneous coagulation and sintering of particle populations. *Journal of Colloid and Interface Science*, 236(2):242–251, 2001. doi: 10.1006/jcis.2000.7409.

[93] R. Ziff. An explicit solution to a discrete fragmentation model. *Journal of Physics A: Mathematical and General*, 25(9):2569–2576, 1992. doi: 10.1088/0305-4470/25/9/027.

[94] S. Ponnuswamy, S. Shah, and C. Kiparissides. Computer optimal-control of batch polymerization reactors. *Industrial & Engineering Chemistry Research*, 26(11):2229–2236, 1987. doi: 10.1021/ie00071a010.

[95] M. Yu, J. Lin, and T. Chan. A new moment method for solving the coagulation equation for particles in brownian motion. *Aerosol Science & Technology*, 42(9):705–713, 2008. doi: 10.1080/02786820802232972.

[96] M. Yu, Y. Liu, J. Lin, and M. Seipenbusch. Generalized TEMOM scheme for solving the population balance equation. *Aerosol Science and Technology*, 49(11):1021–1036, 2015. doi: 10.1080/02786826.2015.1093598.

[97] M. Frenklach and S. Harris. Aerosol dynamics modeling using the method of moments. *Journal of Colloid and Interface Science*, 118(1):252–261, 1987. doi: 10.1016/0021-9797(87)90454-1.

[98] K. Mehta and G. Madras. Dynamics of molecular weight distributions for polymer scission. *AIChE Journal*, 47(11):2539–2547, 2001. doi: 10.1002/aic.690471116.

[99] M. Kostoglou and A. Karabelas. An assessment of low-order methods for solving the breakage equation. *Powder Technology*, 127(2):116–127, 2002. doi: 10.1016/S0032-5910(02)00110-9.

[100] M. Strumendo and H. Arastoopour. Solution of bivariate population balance equations using the finite size domain complete set of trial functions method of moments (FCMOM). *Industrial & Engineering Chemistry Research*, 48(1):262–273, 2009. doi: 10.1021/ie800272a.

[101] A. Falola, A. Borissova, and X. Z. Wang. Extended method of moment for general population balance models including size dependent growth rate, aggregation and breakage kernels. *Computers & Chemical Engineering*, 56:1–11, 2013. doi: 10.1016/j.compchemeng.2013.04.017.

[102] V. John, I. Angelov, A. A. Oencuel, and D. Thevenin. Techniques for the reconstruction of a distribution from a finite number of its moments. *Chemical Engineering Science*, 62(11):2890–2904, 2007. doi: 10.1016/j.ces.2007.02.041.

[103] W. Gautschi. *Orthogonal Polynomials: Computation and Approximation*. Numerical Mathematics and Scientific Computation. Oxford University Press, Oxford, 1. edition, 2004.

[104] V. John and F. Thein. On the efficiency and robustness of the core routine of the quadrature method of moments (QMOM). *Chemical Engineering Science*, 75:327–333, 2012. doi: 10.1016/j.ces.2012.03.024.

[105] R. R. Upadhyay. Evaluation of the use of the Chebyshev algorithm with the quadrature method of moments for simulating aerosol dynamics. *Journal of Aerosol Science*, 44:11–23, 2012. doi: 10.1016/j.jaerosci.2011.09.005.

[106] D. Marchisio and R. Fox. Solution of population balance equations using the direct quadrature method of moments. *Journal of Aerosol Science*, 36(1):43–73, 2005. doi: 10.1016/j.jaerosci.2004.07.009.

[107] D. L. Marchisio and R. O. Fox. *Computational Models for Polydisperse Particulate and Multiphase Systems*. Cambridge University Press, 2013.

[108] M. M. Attarakih, C. Drumm, and H.-J. Bart. Solution of the population balance equation using the sectional quadrature method of moments (SQMOM). *Chemical Engineering Science*, 64:742–752, 2009. doi: 10.1016/j.ces.2008.05.006. 3rd International Conference on Population Balance Modeling.

[109] C. Yuan, F. Laurent, and R. O. Fox. An extended quadrature method of moments for population balance equations. *Journal of Aerosol Science*, 51:1–23, 2012. doi: 10.1016/j.jaerosci.2012.04.003.

[110] N. Agmon, Y. Alhassid, and R. Levine. Algorithm for finding the distribution of maximal entropy. *Journal of Computational Physics*, 30(2):250–258, 1979. doi: 10.1016/0021-9991(79)90102-5.

[111] M. Attarakih and H.-J. Bart. Solution of the population balance equation using the differential maximum entropy method (DMaxEntM): An application to liquid extraction columns. *Chemical Engineering Science*, 108:123 – 133, 2014. doi: http://dx.doi.org/10.1016/j.ces.2013.12.031.

[112] S. Kumar and D. Ramkrishna. On the solution of population balance equations by discretization .1. A fixed pivot technique. *Chemical Engineering Science*, 51(8):1311–1332, 1996. doi: 10.1016/0009-2509(96)88489-2.

[113] S. Kumar and D. Ramkrishna. On the solution of population balance equations by discretization .2. A moving pivot technique. *Chemical Engineering Science*, 51(8):1333–1342, 1996. doi: 10.1016/0009-2509(95)00355-X.

[114] S. Kumar and D. Ramkrishna. On the solution of population balance equations by discretization - III. Nucleation, growth and aggregation of particles. *Chemical Engineering Science*, 52(24):4659–4679, 1997. doi: 10.1016/S0009-2509(97)00307-2. 1995 AICHE Annual Meeting, Miama Beach, Florida.

[115] C. Sarmoria, M. Asteasuain, and A. Brandolin. Prediction of molecular weight distributions in polymers using probability generating functions. *Canadian Journal of Chemical Engineering*, 90(2):263–273, 2012. doi: 10.1002/cjce.20699.

[116] A. Brandolin and M. Asteasuain. Mathematical modeling of bivariate distributions of polymer properties using 2D probability generating functions. part II: Transformation of population mass balances of polymer processes. *Macromolecular Theory and Simulations*, 22(5):273–308, 2013. doi: 10.1002/mats.201200089.

[117] T. Smagala and B. McCoy. Population balance modeling of polymer branching and hyperbranching. *Chemical Engineering Science*, 61(1):3–17, 2006. doi: 10.1016/j.ces.2004.12.052. 2nd International Conference on Population Balance Modelling, Valencia, Spain.

[118] J. Kumar, G. Kaur, and E. Tsotsas. An accurate and efficient discrete formulation of aggregation population balance equation. *Kinetic and Related Models*, 9(2):373–391, 2016. doi: 10.3934/krm.2016.9.373.

[119] M. Singh, J. Kumar, A. Bueck, and E. Tsotsas. A volume-consistent discrete formulation of aggregation population balance equations. *Mathematical Methods in the Applied Sciences*, 39 (9):2275–2286, 2016. doi: 10.1002/mma.3638.

[120] Y. Lim, J. Le Lann, X. Meyer, X. Joulia, G. Lee, and E. Yoon. On the solution of population balance equations (PBE) with accurate front tracking methods in practical crystallization processes. *Chemical Engineering Science*, 57(17):3715–3732, 2002. doi: 10.1016/S0009-2509(02)00236-1.

[121] R. Dürr and A. Kienle. An efficient method for calculating the moments of multidimensional growth processes in population balance systems. *Canadian Journal of Chemical Engineering*, 92(12): 2088–2097, 2014. doi: 10.1002/cjce.22062.

[122] A. Reinhold and H. Briesen. High dimensional population balances for the growth of faceted crystals: Combining monte carlo integral estimates and the method of characteristics. *Chemical Engineering Science*, 127:220–229, 2015. doi: 10.1010/j.ces.2015.01.035.

[123] A. Majumder, V. Kariwala, S. Ansumali, and A. Rajendran. Entropic lattice boltzmann method for crystallization processes. *Chemical Engineering Science*, 65(13):3928–3936, 2010. doi: 10.1016/j.ces.2010.03.030.

[124] A. Majumder, V. Kariwala, S. Ansumali, and A. Rajendran. Lattice boltzmann method for population balance equations with simultaneous growth, nucleation, aggregation and breakage. *Chemical Engineering Science*, 69(1):316–328, 2012. doi: 10.1016/j.ces.2011.10.051.

[125] E. M. Torgerson, L. C. Brewer, and J. A. Thoma. Subsite mapping of enzymes. use of subsite map to simulate complete time course of hydrolysis of a polymeric substrate. *Archives of Biochemistry and Biophysics*, 196(1):13 – 22, 1979. doi: 10.1016/0003-9861(79)90546-0.

[126] C. Fortunatti, C. Sarmoria, A. Brandolin, and M. Asteasuain. Prediction of the full molecular weight distribution in raft polymerization using probability generating functions. *Computers & Chemical Engineering*, 66:214–220, 2014. doi: 10.1016/j.compchemeng.2014.02.017. 23rd European Symposium on Computer Aided Process Engineering (ESCAPE), Lappeenranta Univ Technol, Lappeenranta, Finland.

[127] Y. K. Ho, P. Doshi, H. K. Yeoh, and G. C. Ngoh. Modeling chain-end scission using the fixed pivot technique. *Chemical Engineering Science*, 116(0):601 – 610, 2014. doi: http://dx.doi.org/10.1016/j.ces.2014.05.035.

[128] R. Ziff and E. McGrady. The kinetics of cluster fragmentation and depolymerisation. *Journal of Physics A: Mathematical and General*, 18(15):3027–3037, 1985. doi: 10.1088/0305-4470/18/15/026.

[129] R. Ziff. New solutions to the fragmentation equation. *Journal of Physics A: Mathematical and General*, 24(12):2821–2828, 1991. doi: 10.1088/0305-4470/24/12/020.

[130] C. in Technology. URL `http://www.cit-wulkow.de/`. Last visited on 2.1.2017.

[131] M. Wulkow. Computer aided modeling of polymer reaction engineering-the status of predici, 1-simulation. *Macromolecular Reaction Engineering*, 2(6):461–494, 2008. doi: 10.1002/mren.200800024.

[132] P. Iedema, C. Willems, G. van Vliet, W. Bunge, S. Mutsers, and H. Hoefsloot. Using molecular weight distributions to determine the kinetics of peroxide-induced degradation of polypropylene. *Chemical Engineering Science*, 56(12):3659–3669, 2001. doi: 10.1016/S0009-2509(01)00054-9.

[133] N. Yaghini and P. D. Iedema. Three-dimensional chain-length-branching-combination points distribution modeling of low density polyethylene in a continuous stirred tank reactor allowing for gelation. *Chemical Engineering Science*, 140:348 – 358, 2016. doi: 10.1016/j.ces.2015.06.027.

[134] P. Seferlis and C. Kiparissides. Prediction of the joint molecular weight-long chain branching distribution in free-radical branched polymerizations. In J. Grievink and J. VanSchijndel, editors, *12th European Symposium on Computer Aided Process Engineering*, volume 10 of *Computer-Aided Chemical Engineering*, pages 961–966, Amsterdam, Netherlands, 2002. European Federat Chem Engn, Working Party Comp Aided Proc Engn, Elsevier. ISBN 0-444-51109-1.

[135] N. Yaghini and P. D. Iedema. Molecular weight/branching distribution modeling of low-density-polyethylene accounting for topological scission and combination termination in continuous stirred tank reactor. *Chemical Engineering Science*, 116(0):144 – 160, 2014. doi: 10.1016/j.ces.2014.04.039.

[136] N. Yaghini and P. D. Iedema. Population balance modeling of full two-dimensional molecular weight and branching distributions for ldpe with topological scission in continuous stirred tank reactor. *Chemical Engineering Science*, 137:556 – 571, 2015. doi: 10.1016/j.ces.2015.06.045.

[137] G. Madras, J. Smith, and B. McCoy. Degradation of poly(methyl methacrylate) in solution. *Industrial & Engineering Chemistry Research*, 35(6):1795–1800, 1996. doi: 10.1021/ie960018b.

[138] N. Lebaz, A. Cockx, M. Sperandio, and J. Morchain. Population balance approach for the modelling of enzymatic hydrolysis of cellulose. *Canadian Journal of Chemical Engineering*, 93(2, SI): 276–284, 2015. doi: 10.1002/cjce.22088.

[139] A. Krallis and C. Kiparissides. Mathematical modeling of the bivariate molecular weight - long chain branching distribution of highly branched polymers. a population balance approach. *Chemical Engineering Science*, 62:5304–5311, 2007. doi: 10.1016/j.ces.2007.03.035. 19th International Symposium on Chemical Reaction Engineering (ISCRE 19).

[140] P. Iedema and H. Hoefsloot. Computing the trivariate chain length/degree of branching/number of combination points distribution for radical polymerization with transfer to polymer and recombination termination. *Macromolecular Theory and Simulations*, 14(8):505–518, 2005. doi: 10.1002/mats.200500038.

[141] G. Saidel and S. Katz. Dynamic analysis of branching in radical polymerization. *Journal of Polymer Science Part A-2 Polymer Physics*, 6(6PA2):1149ff, 1968. doi: 10.1002/pol.1968.160060608.

[142] R. Li and B. McCoy. Crosslinking kinetics: Partitioning according to number of crosslinks. *Macromolecular Theory and Simulations*, 13(3):203–218, 2004. doi: 10.1002/mats.200300033.

[143] T. Kruse, O. Woo, H. Wong, S. Khan, and L. Broadbelt. Mechanistic modeling of polymer degradation: A comprehensive study of polystyrene. *Macromolecules*, 35(20):7830–7844, 2002. doi: 10.1021/ma020490a.

[144] S. E. Levine and L. J. Broadbelt. Detailed mechanistic modeling of high-density polyethylene pyrolysis: Low molecular weight product evolution. *Polymer Degradation and Stability*, 94(5): 810–822, 2009. doi: 10.1016/j.polymdegradstab.2009.01.031.

[145] C. Fortunatti, B. Mato, A. Brandolin, C. Sarmoria, and M. Asteasuain. Optimal operating policies for synthesizing tailor made copolymers. In K. V. Gernaey, J. K. Huusom, and R. Gani, editors, *12th International Symposium on Process Systems Engineering and 25th European Symposium on Computer Aided Process Engineering*, volume 37, pages 803–808, 2015.

[146] I. Kryven and P. D. Iedema. A novel approach to population balance modeling of reactive polymer modification leading to branching. *Macromolecular Theory and Simulations*, 22(2):89–106, 2013. doi: 10.1002/mats.201200048.

[147] J. J. Stickel and A. J. Griggs. Mathematical modeling of chain-end scission using continuous distribution kinetics. *Chemical Engineering Science*, 68(1):656–659, 2012. doi: 10.1016/j.ces.2011.09.028.

[148] M. Papageorgiou, M. Leibold, and M. Buss. *Optimierung: Statische, dynamische, stochastische Verfahren für die Anwendung*. Springer Vieweg, 2012.

[149] A. E. Bryson Jr. and Y.-C. Ho. *Applied Optimal Control*. Taylor & Francis, 1975.

[150] S. R. Upreti. *Optimal Control for Chemical Engineers*. CRC Press, 2013.

[151] J. T. Betts. *Practical Methods for Optimal Control Using Nonlinear Programming*. Society for Industrial and Applied Mathematics, Philadelphia, 2010.

[152] H. H. Goldstine. *A History of the Calculus of Variations from the 17th through the 19th Century*, volume 5. Springer Science & Business Media, 2012.

[153] A. Bryson. Optimal control - 1950 to 1985. *IEEE Control Systems Magazine*, 16(3):26–33, 1996. doi: 10.1109/37.506395.

[154] F. Horn. Optimale Temperatur- und Konzentrationsverläufe. *Chemical Engineering Science*, 14: 77–89, 1961. doi: 10.1016/0009-2509(61)85055-0.

[155] A. Chou, W. Ray, and R. Aris. Simple control policies for reactors with catalyst decay. *Transactions of the Institution of Chemical Engineers and the Chemical Engineer*, 45(4):T153–&, 1967.

[156] R. Jackson. An approach to numerical solution of time-dependent optimisation problems in 2-phase contacting devices. *Transactions of the Institute of Chemical Engineers and the Chemical Engineering*, 45(4):T160–&, 1967.

[157] L. Ho and A. Humphrey. Optimal control of an enzyme reaction subject to enzyme deactivation .1. Batch process. *Biotechnology and Bioengineering*, 12(2):291–311, 1970. doi: 10.1002/bit.260120209.

[158] P. Valencia, S. Flores, M. Pinto, and S. Almonacid. Analysis of the operational strategies for the enzymatic hydrolysis of food proteins in batch reactor. *Journal of Food Engineering*, 176:121 – 127, 2016. doi: http://dx.doi.org/10.1016/j.jfoodeng.2015.10.029. Virtualization of Processes in Food Engineering.

[159] F.-S. Wang, M.-Y. Yang, and M.-L. Chen. Optimal temperature and ph control for a batch simultaneous saccharification and co-fermentation process. *Chemical Engineering Communications*, 202(7):899–910, 2015. doi: 10.1080/00986445.2014.886200.

[160] J. Asenjo, W. Sun, and J. Spencer. Optimal control of batch processes involving simultaneous enzymatic and microbial reactions. *Bioprocess Engineering*, 14(6):323–329, 1996.

[161] S. Sengupta and J. Modak. Optimization of fed-batch bioreactor for immobilized enzyme processes. *Chemical Engineering Science*, 56(11):3315–3325, 2001. doi: 10.1016/S0009-2509(01)00032-X.

[162] M. Brisk and G. Barton. Online optimal-control of catalytic reactors - simplified approach. *Transactions of the Institution of Chemical Engineers*, 56(2):113–119, 1978.

[163] E. F. Camacho, D. R. Ramirez, D. Limon, D. Munoz de la Pena, and T. Alamo. Model predictive control techniques for hybrid systems. *Annual Reviews in Control*, 34(1):21–31, 2010. doi: 10.1016/j.arcontrol.2010.02.002.

[164] H. Eisenschmidt, N. Bajcinca, and K. Sundmacher. Model-based observation and design of crystal shapes via controlled growth-dissolution cycles. In K. V. Gernaey, J. K. Huusom, and R. Gani, editors, *12th International Symposium on Process Systems Engineering and 25th European Symposium on Computer Aided Process Engineering*, volume 37, pages 1673–1678, 2015.

[165] S. J. Yoo, D. H. Jeong, J. H. Kim, and J. M. Lee. Optimization of microalgal photobioreactor system using model predictive control with experimental validation. *Bioprocess and Biosystems Engineering*, 39(8):1235–1246, 2016. doi: 10.1007/s00449-016-1602-0.

[166] P. Schalbart, D. Leducq, and G. Alvarez. Ice-cream storage energy efficiency with model predictive control of a refrigeration system coupled to a PCM tank. *International Journal of Refrigeration - Revue Internationale du Froid*, 52:140–150, 2015. doi: 10.1016/j.ijrefrig.2014.08.001.

[167] S. Rasoulian and L. A. Ricardez-Sandoval. Stochastic nonlinear model predictive control applied to a thin film deposition process under uncertainty. *Chemical Engineering Science*, 140:90 – 103, 2016. doi: 10.1016/j.ces.2015.10.004.

[168] R. Sargent. Optimal control. *Journal of Computational and Applied Mathematics*, 124(1–2):361 – 371, 2000. doi: 10.1016/S0377-0427(00)00418-0. Numerical Analysis 2000. Vol. IV: Optimization and Nonlinear Equations.

[169] A. Arnold. *Variationsrechnung*. TU Wien, 2013.

[170] T. Walder and C. Storey. Numerical solution of an optimal temperature problem. *The Chemical Engineering Journal*, 1(2):120 – 128, 1970. doi: 10.1016/0300-9467(70)85005-5.

[171] S. Szépe and O. Levenspiel. Optimal temperature policies for reactors subject to catalyst deactivation .I. Batch reactor. *Chemical Engineering Science*, 23(8):881–&, 1968. doi: 10.1016/0009-2509(68)80022-3.

[172] I. Grubecki and M. Wojcik. How much of enzyme can be saved in the process with the optimal temperature control? *Journal of Food Engineering*, 116(2):255–259, 2013. doi: 10.1016/j.jfoodeng.2012.12.019.

[173] I. M. Ross and M. Karpenko. A review of pseudospectral optimal control: From theory to flight. *Annual Review in Control*, 36(2):182–197, 2012. doi: 10.1016/j.arcontrol.2012.09.002.

[174] G. Hicks and W. Ray. Approximation methods for optimal control synthesis. *Canadian Journal of Chemical Engineering*, 49(4):522–&, 1971.

[175] C. Goh and K. Teo. Control parametrization - a unified approach to optimal-control problems with general constraints. *Automatica*, 24(1):3–18, 1988. doi: 10.1016/0005-1098(88)90003-9.

[176] H. Sirisena. Computation of optimal controls using a piecewise polynomial parameterization. *IEEE Transactions on Automatic Control*, AC18(4):409–411, 1973. doi: 10.1109/TAC.1973.1100329.

[177] H. Bock. Numerical treatment of inverse problems in chemical reaction kinetics. In K. Ebert, P. Deuflhard, and W. Jäger, editors, *Modelling of Chemical Reaction Systems*, volume 18 of *Springer Series in Chemical Physics*, pages 102–125. Springer, Berlin, 1981. ISBN 978-3-642-68222-3.

[178] F. Einsiedler, A. Schwill-Miedaner, K. Sommer, and J. Hämäläinen. Experimentelle Untersuchungen und Modellierung komplexer biochemischer und technologischer Prozesse am Beispiel des Maischens. *Monatsschrift für Brauwissenschaft*, 51(1/2):11–21, 1998.

[179] S. C. Alcazar-Alay and M. A. Almeida Meireles. Physicochemical properties, modifications and applications of starches from different botanical sources. *Food Science and Technology*, 35(2): 215–236, 2015. doi: 10.1590/1678-457X.6749.

[180] T. Crowley and K. Choi. Optimal control of molecular weight distribution in a batch free radical polymerization process. *Industrial & Engineering Chemistry Research*, 36(9):3676–3684, 1997. doi: 10.1021/ie970076c.

[181] V. Saliakas, C. Chatzidoukas, A. Krallis, D. Meimaroglou, and C. Kiparissides. Dynamic optimization of molecular weight distribution using orthogonal collocation on finite elements and fixed pivot methods: An experimental and theoretical investigation. *Macromolecular Reaction Engineering*, 1(1):119–136, 2007. doi: 10.1002/mren.200600015.

[182] F. G. Meussdoerffer. *A Comprehensive History of Beer Brewing*, pages 1–42. Wiley-VCH Verlag GmbH & Co. KGaA, 2009. ISBN 9783527623488. doi: 10.1002/9783527623488.ch1.

[183] I. Hanashiro and Y. Takeda. Examination of number-average degree of polymerization and molar-based distribution of amylose by fluorescent labeling with 2-aminopyridine. *Carbohydrate Research*, 306(3):421–426, 1998. doi: 10.1016/S0008-6215(97)10075-1.

[184] A. Rolland-Sabate, P. Colonna, M. G. Mendez-Montealvo, and V. Planchot. Branching features of amylopectins and glycogen determined by asymmetrical flow field flow fractionation coupled with multiangle laser light scattering. *Biomacromolecules*, 8(8):2520–2532, 2007. doi: 10.1021/bm070024z.

[185] G. Nilsson, K. Bergquist, U. Nilsson, and L. Gorton. Determination of the degree of branching in normal and amylopectin type potato starch with H-1-NMR spectroscopy - improved resolution

and two-dimensional spectroscopy. *Starch - Stärke*, 48(10):352–357, 1996. doi: 10.1002/star.19960481003.

[186] S. Podzimek. *Light Scattering Size Exclusion Chromatography and Asymmetric Flow Field Flow Fractionation: Powerful Tools for the Charaterization of Polymers, Proteins, and Nanoparticles*. John Wiley & Sons, New Jersey, 2011.

[187] A. Rolland-Sabate, M. G. Mendez-Montealvo, P. Colonna, and V. Planchot. Online determination of structural properties and observation of deviations from power law behavior. *Biomacromolecules*, 9(7):1719–1730, 2008. doi: 10.1021/bm7013119.

[188] G. Merziger, G. Mühlbach, D. Wille, and T. Wirth. *Formeln+Hilfen zur höheren Mathematik*. Binomi Verlag, Springe, 2007.

[189] L. Marchal, J. Zondervan, J. Bergsma, H. Beeftink, and J. Tramper. Monte carlo simulation of the alpha-amylolysis of amylopectin potato starch - part I: modeling of the structure of amylopectin. *Bioprocess and Biosystems Engineering*, 24(3):163–170, 2001. doi: 10.1007/s004490100247.

[190] H. R. Horton, L. A. Moran, K. G. Scrimgeour, M. D. Perry, and J. D. Rawn. *Biochemie - Bafög-Ausgabe*. Pearson, Hallbergmoos, 2013.

[191] E. Commision. URL `http://www.chem.qmul.ac.uk/iubmb/enzyme/EC3/2/1/`. Last visited on 28.12.2016.

[192] V. Rodriguez, E. Alameda, J. Gallegos, A. Requena, and A. Lopez. Enzymatic hydrolysis of soluble starch with an alpha-amylase from bacillus licheniformis. *Biotechnology Progress*, 22(3):718–722, 2006. doi: 10.1021/bp060057a.

[193] G. Muralikrishna and M. Nirmala. Cereal alpha-amylases - an overview. *Carbohydrate Polymers*, 60(2):163–173, 2005. doi: 10.1016/j.carbpol.2004.12.002.

[194] Y. Nakamura, F. Kobayashi, M. Ohnaga, and T. Sawada. Alcohol fermentation of starch by a genetic recombinant yeast hauling glucoamylase activity. *Biotechnology and Bioengineering*, 53(1):21–25, 1997. doi: 10.1002/(SICI)1097-0290(19970105)53:1<21::AID-BIT4>3.0.CO;2-0.

[195] E. Steverson, R. Korus, W. Admassu, and R. Heimsch. Kinetics of the amylase system of saccharomycopsis-fibuliger. *Enzyme and Microbial Technology*, 6(12):549–554, 1984.

[196] R. Summer and D. French. Action of β-amylase on branched oligosaccharides. *Journal of Biological Chemistry*, 222(1):469–477, 1956.

[197] D. Rosner and J. Pyykonen. Bivariate moment simulation of coagulating and sintering nanoparticles in flames. *AIChE Journal*, 48(3):476–491, 2002. doi: 10.1002/aic.690480307.

[198] A. Håkansson, F. Innings, C. Trägårdh, and B. Bergenståhl. A high-pressure homogenization emulsification model-improved emulsifier transport and hydrodynamic coupling. *Chemical Engineering Science*, 91(0):44 – 53, 2013. doi: 10.1016/j.ces.2013.01.011.

[199] J. A. Thoma. Models for depolymerizing enzymes - criteria for discrimination of models. *Carbohydrate Research*, 48(1):85–103, 1976. doi: 10.1016/S0008-6215(00)83517-X.

[200] M. Gil, E. Luciano, and I. Arauzo. Population balance model for biomass milling. *Powder Technology*, 276(0):34 – 44, 2015. doi: http://dx.doi.org/10.1016/j.powtec.2015.01.060.

[201] S. Lin, W. Yu, X. Wang, and C. Zhou. Study on the thermal degradation kinetics of biodegradable poly(propylene carbonate) during melt processing by population balance model and rheology. *Industrial & Engineering Chemistry Research*, 53(48):18411–18419, 2014. doi: 10.1021/ie404049v.

[202] M. Michaelis and L. Menten. Die Kinetik der Invertinwirkung. *Biochemische Zeitschrift*, 49:333–369, 1913.

[203] K. A. Johnson and R. S. Goody. The original Michaelis constant: Translation of the 1913 Michaelis-Menten paper. *Biochemistry*, 50(39):8264–8269, 2011. doi: 10.1021/bi201284u.

[204] A. Cornish-Bowden. *Fundamentals of Enzyme Kinetics*. Wiley-Blackwell, Weinheim, 4 edition, 2014.

[205] R. Daniel, M. Danson, and R. Eisenthal. The temperature optima of enzymes: a new perspective on an old phenomenon. *Trends in Biochemical Sciences*, 26(4):223–225, 2001. doi: 10.1016/S0968-0004(01)01803-5.

[206] R. M. Daniel and M. J. Danson. A new understanding of how temperature affects the catalytic activity of enzymes. *Trends in Biochemical Sciences*, 35(10):584–591, 2010. doi: 10.1016/j.tibs.2010.05.001.

[207] C. Duy and J. Fitter. Thermostability of irreversible unfolding alpha-amylases analyzed by unfolding kinetics. *Journal of Biological Chemistry*, 280(45):37360–37365, 2005. doi: 10.1074/jbc.M507530200.

[208] R. M. Daniel and M. J. Danson. Temperature and the catalytic activity of enzymes: A fresh understanding. *FEBS Letters*, 587(17):2738 – 2743, 2013. doi: http://dx.doi.org/10.1016/j.febslet.2013.06.027. A century of Michaelis - Menten kinetics.

[209] K. Hanson. Enzyme kinetics of short-chain polymer cleavage. *Biochemistry*, 1(5):723–&, 1962. doi: 10.1021/bi00911a001.

[210] J. A. Thoma, C. Brothers, and J. Spradlin. Subsite mapping of enzymes - studies on bacillus-subtilis amylase. *Biochemistry*, 9(8):1768–&, 1970. doi: 10.1021/bi00810a016.

[211] E. Ajandouz, J. Abe, B. Svensson, and G. Marchismouren. Barley malt-alpha-amylase - purification, action pattern, and subsite mapping of isozyme-1 and 2 members of the isozyme-2 subfamily using para-nitrophenylated maltooligosaccharide substrates. *Biochimica et Biophysica Acta*, 1159(2):193–202, 1992. doi: 10.1016/0167-4838(92)90025-9.

[212] X. Robert, R. Haser, H. Mori, B. Svensson, and N. Aghajari. Oligosaccharide binding to barley α-amylase 1. *Journal of Biological Chemistry*, 280(38):32968–32978, 2005. doi: 10.1074/jbc.M505515200.

[213] M. Kato, K. Hiromi, and Y. Morita. Purification and kinetic studies of wheat bran beta-amylase - evaluation of subsite affinities. *Journal of Biochemistry*, 75(3):563–576, 1974.

[214] G. Henriksson, V. Sild, I. Szabo, G. Pettersson, and G. Johansson. Substrate specificity of cellobiose dehydrogenase from phanerochaete chrysosporium. *Biochimica et Biophysica Acta-Protein Structure and Molecular Enzymology*, 1383(1):48–54, 1998. doi: 10.1016/S0167-4838(97)00180-5.

[215] R. W. Gurney. International chemical series. In *Ionic Processes in Solution*. McGraw Hill, 1953.

[216] J. Allen and J. A. Thoma. Subsite mapping of enzymes - depolymerase computer modeling. *Biochemical Journal*, 159(1):105–120, 1976.

[217] J. Allen and J. A. Thoma. Subsite mapping of enzymes - application of depolymerase computer model to 2 alpha-amylases. *Biochemical Journal*, 159(1):121–131, 1976.

[218] M. Abdullah, W. J. Whelan, and B. J. Catley. The action pattern of human salivary alpha-amylase in the vicinity of the branch points of amylopectin. *Carbohydrate Research*, 57:281–289, 1977. doi: 10.1016/S0008-6215(00)81937-0.

[219] R. O. Fox. Bivariate direct quadrature method of moments for coagulation and sintering of particle populations. *Journal of Aerosol Science*, 37(11):1562–1580, 2006. doi: 10.1016/j.jaerosci.2006.03.005.

[220] C. Frances and A. Line. Comminution process modeling based on the monovariate and bivariate direct quadrature method of moments. *AIChE Journal*, 60(5):1621–1631, 2014. doi: 10.1002/aic.14358.

[221] A. Zucca, D. L. Marchisio, M. Vanni, and A. A. Barresi. Validation of bivariate DQMOM for nanoparticle processes simulation. *AIChE Journal*, 53(4):918–931, 2007. doi: 10.1002/aic.11125.

[222] R. O. Fox. Optimal moment sets for multivariate direct quadrature method of moments. *Industrial & Engineering Chemistry Research*, 48(21):9686–9696, 2009. doi: 10.1021/ie801316d.

[223] M. Kostoglou. Mathematical analysis of polymer degradation with chain-end scission. *Chemical Engineering Science*, 55(13):2507–2513, 2000. doi: 10.1016/S0009-2509(99)00471-6.

[224] J. Chakraborty and S. Kumar. A new framework for solution of multidimensional population balance equations. *Chemical Engineering Science*, 62(15):4112–4125, 2007. doi: 10.1016/j.ces.2007.04.049.

[225] R. Sack and A. Donovan. An algorithm for gausssian quadrature given modified moments. *Numerische Mathematik*, 18(5):465–477, 1972.

[226] C. Yuan and R. O. Fox. Conditional quadrature method of moments for kinetic equations. *Journal of Computational Physics*, 230(22):8216–8246, 2011. doi: 10.1016/j.jcp.2011.07.020.

[227] M. Hounslow, R. Ryall, and V. Marshall. A discretized population balance for nucleation, growth, and aggregation. *AIChE Journal*, 34(11):1821–1832, 1988. doi: 10.1002/aic.690341108.

[228] I. Nopens, D. Beheydt, and P. Vanrolleghem. Comparison and pitfalls of different discretised solution methods for population balance models: a simulation study. *Computers & Chemical Engineering*, 29(2):367–377, 2005. doi: 10.1016/j.compchemeng.2004.10.007.

[229] M. Kostoglou. Extended cell average technique for the solution of coagulation equation. *Journal of Colloid and Interface Science*, 306(1):72–81, 2007. doi: 10.1016/j.jcis.2006.10.044.

[230] J. Kumar, M. Peglow, G. Warnecke, S. Heinrich, and L. Morl. Improved accuracy and convergence of discretized population balance for aggregation: The cell average technique. *Chemical Engineering Science*, 61(10):3327–3342, 2006. doi: 10.1016/j.ces.2005.12.014.

[231] J. Kumar and G. Warnecke. Convergence analysis of sectional methods for solving breakage population balance equations-II: the cell average technique. *Numerische Mathematik*, 110(4):539–559, 2008. doi: 10.1007/s00211-008-0173-7.

[232] J. Kumar, M. Peglow, G. Warnecke, and S. Heinrich. An efficient numerical technique for solving population balance equation involving aggregation, breakage, growth and nucleation. *Powder Technology*, 182(1):81–104, 2008. doi: 10.1016/j.powtec.2007.05.028.

[233] M. Singh, D. Ghosh, and J. Kumar. A comparative study of different discretizations for solving bivariate aggregation population balance equation. *Applied Mathematics and Computation*, 234:434–451, 2014. doi: 10.1016/j.amc.2014.02.052.

[234] P. Mostafaei, M. Rajabi-Hamane, and A. Salehpour. A modified cell average technique for the solution of population balance equation. *Journal of Aerosol Science*, 87:111–125, 2015. doi: 10.1016/j.jaerosci.2015.05.012.

[235] J. Kumar, M. Peglow, G. Warnecke, and S. Heinrich. The cell average technique for solving multidimensional aggregation population balance equations. *Computers & Chemical Engineering*, 32(8):1810–1830, 2008. doi: 10.1016/j.compchemeng.2007.10.001.

[236] S.-W. Cheng. *Delanauy Mesh Generation*. Boca Raton, Florida, 2013.

[237] S. S. Chauhan, A. Chiney, and S. Kumar. On the solution of bivariate population balance equations for aggregation: X-discretization of space for expansion and contraction of computational domain. *Chemical Engineering Science*, 70:135–145, 2012. doi: 10.1016/j.ces.2011.10.005. 4th International Conference on Population Balance Modeling (PBM), Berlin, Germany.

[238] S. Iwasa, H. Aoshima, K. Hiromi, and H. Hatano. Subsite affinities of bacterial liquefying alpha-amylase evaluated from rate parameters of linear substrates. *Journal of Biochemistry*, 75(5): 969–978, 1974.

[239] P. Philip. *Optimal Control of Partial Differential Equations*. Lecture Notes LMU, 2013.

[240] F. Assassa and W. Marquardt. Dynamic optimization using adaptive direct multiple shooting. *Computers & Chemical Engineering*, 60:242–259, 2014. doi: 10.1016/j.compchemeng.2013.09.017.

[241] W. H. Press, S. A. Teukolsky, W. T. Vetterling, and B. P. Flannery. *Numerical Recipes: The Art of Scientific Computing*. Cambridge University Press, Cambridge, 3 edition, 2007.

[242] C. K. Lee, R. M. Daniel, C. Shepherd, D. Saul, S. C. Cary, M. J. Danson, R. Eisenthal, and M. E. Peterson. Eurythermalism and the temperature dependence of enzyme activity. *FASEB Journal*, 21(8):1934–1941, 2007. doi: 10.1096/fj.06-7265com.

[243] R. Buckow, U. Weiss, V. Heinz, and D. Knorr. Stability and catalytic activity of alpha-amylase from barley malt at different pressure-temperature conditions. *Biotechnology and Bioengineering*, 97 (1):1–11, 2007. doi: 10.1002/bit.21209.

[244] R. Alberty. Kinetic effects of the ionization of groups in the enzyme molecule. *Journal of Cellular and Comparative Physiology*, 47(1):245–281, 1956. doi: 10.1002/jcp.1030470418.

[245] D. Bush, L. Sticher, R. van Huystee, D. Wagner, and R. Jones. The calcium requirement for stability and enzymatic-activity of 2 isoforms of barley aleurone alpha-amylase. *Journal of Biological Chemistry*, 264(32):19392–19398, 1989.

[246] M. Obersteiner. Simulation des Maischprozesses: Abhängigkeit des enzymatischen Stärkeabbaus von pH-Wert und Ionenkonzentration. Master's thesis, Technische Universität München, Lehrstuhl für Systemverfahrenstechnik, 2014.

[247] S. Dhital, M. J. Gidley, and F. J. Warren. Inhibition of α-amylase activity by cellulose: Kinetic analysis and nutritional implications. *Carbohydrate Polymers*, 123(0):305 – 312, 2015. doi: http://dx.doi.org/10.1016/j.carbpol.2015.01.039.

[248] H. Bisswanger. *Practical Enzymology*. Wiley-Blackwell, Weinheim, 2011.

[249] R. Kumar, J. Kumar, and G. Warnecke. Moment preserving finite volume schemes for solving population balance equations incorporating aggregation, breakage, growth and source terms. *Mathematical Models & Methods in Applied Sciences*, 23(7):1235–1273, 2013. doi: 10.1142/S0218202513500085.

[250] S. Ochoa, J.-U. Repke, and G. Wozny. Integrating real-time optimization and control for optimal operation: Application to the bio-ethanol process. *Biochemical Engineering Journal*, 53(1):18–25, 2010. doi: 10.1016/j.bej.2009.01.005. 10th International Chemical and Biological Engineering Conference - CHEMPOR, Braga, Portugal.

[251] A. Mayerhofer. Parameterschätzung der thermischen Inaktivierung von Malzenzymen für verschiedene Kinetikmodelle in MATLAB. Master's thesis, Technische Universität München, Lehrstuhl für Systemverfahrenstechnik, 2015.

[252] C. E. Wyman. What is (and is not) vital to advancing cellulosic ethanol. *TRENDS in Biotechnology*, 25(4):153–157, 2007. doi: 10.1016/j.tibtech.2007.02.009.

[253] L. Walker and D. Wilson. Enzymatic-hydrolysis of cellulose - an overview. *Bioresource Technology*, 36(1):3–14, 1991. doi: 10.1016/0960-8524(91)90095-2.

[254] M. Coughlan. Enzymatic-hydrolysis of cellulose - an overview. *Bioresource Technology*, 39(2):107–115, 1992. doi: 10.1016/0960-8524(92)90128-K. 4th Workshop on Biotechnology for the Conversion Lignocellulosics, Lund, Sweden.

[255] B. Z. Shang, R. Chang, and J.-W. Chu. Systems-level modeling with molecular resolution elucidates the rate-limiting mechanisms of cellulose decomposition by cellobiohydrolases. *Journal of Biological Chemistry*, 288(40):29081–29089, 2013. doi: 10.1074/jbc.M113.497412.

[256] R. Sousa, Jr., M. L. Carvalho, R. L. C. Giordano, and R. C. Giordano. Recent trends in the modeling of cellulose hydrolysis. *Brazilian Journal of Chemical Engineering*, 28(4):545–564, 2011.

[257] A. Tanaka, C. Nakagawa, K. Kodaira, K. Senoo, and H. Obata. Basic subsite theory assumptions may not be applicable to hydrolysis of cellooligosaccharides by almond beta-glucosidase. *Journal of Bioscience and Bioengineering*, 88(6):664–666, 1999. doi: 10.1016/S1389-1723(00)87097-8.

[258] K.-E. L. Eriksson, R. Blanchette, and P. Ander. *Microbial and enzymatic degradation of wood and wood components*. Springer Science & Business Media, 1990.

[259] T. Eriksson, J. Karlsson, and F. Tjerneld. A model explaining declining rate in hydrolysis of lignocellulose substrates with cellobiohydrolase I (Cel7A) and endoglucanase I (Cel7B) of trichoderma reesei. *Applied Biochemistry and Biotechnology*, 101(1):41–60, 2002. doi: 10.1385/ABAB:101:1:41.

[260] S. Badieyan, D. R. Bevan, and C. Zhang. Study and design of stability in GH5 cellulases. *Biotechnology and Bioengineering*, 109(1):31–44, 2012. doi: 10.1002/bit.23280.

[261] K. Shin, Y. H. Kim, M. Jeya, J.-K. Lee, and Y.-S. Kim. Purification and characterization of a thermostable cellobiohydrolase from fomitopsis pinicola. *Journal of Microbiology and Biotechnology*, 20(12):1681–1688, 2010. doi: 10.4014/jmb.1008.08009.

[262] M. A. Smith, A. Rentmeister, C. D. Snow, T. Wu, M. F. Farrow, F. Mingardon, and F. H. Arnold. A diverse set of family 48 bacterial glycoside hydrolase cellulases created by structure-guided recombination. *FEBS Journal*, 279(24):4453–4465, 2012. doi: 10.1111/febs.12032.

[263] B. Wu, L.-S. Wang, and P.-J. Gao. The combined effects of temperature and assay time on the catalytic ability and stability of 1,4-beta-d-glucan cellobiohydrolase i. *Enzyme and Microbial Technology*, 43(3):237–244, 2008. doi: 10.1016/j.enzmictec.2008.02.014.

[264] I. J. Kim, J. Y. Jung, H. J. Lee, H. S. Park, Y. H. Jung, K. Park, and K. H. Kim. Customized optimization of cellulase mixtures for differently pretreated rice straw. *Bioprocess and Biosystems Engineering*, 38(5):929–937, 2015. doi: 10.1007/s00449-014-1338-7.

[265] A. Ruangmee and C. Sangwichien. Response surface optimization of enzymatic hydrolysis of narrow-leaf cattail for bioethanol production. *Energy Conversion and Management*, 73:381–388, 2013. doi: 10.1016/j.enconman.2013.05.035.

Appendix A

Different formulations of the Population Balance Equation and production rate

A.1 Formulations of the Population Balance Equation

The different formulations of the Population Balance Equation (PBE) are shown here.

A.1.1 Population Balance Equation for a linear polymer

For a linear polymer the discrete PBE defines a system of Ordinary Differential Equations (ODEs):

$$\frac{\mathrm{d}\check{n}(t,\check{k})}{\mathrm{d}t} = -\check{D}_{\sum}(t,\check{k}) + \check{B}_{\sum}(t,\check{k}). \tag{A.1}$$

If the continuity assumption is taken, a Partial Differential Equation (PDE) is obtained

$$\frac{\partial \bar{n}(t,\bar{k})}{\partial t} = -\bar{D}_{\sum}(t,\bar{k}) + \bar{B}_{\sum}(t,\bar{k}). \tag{A.2}$$

A.1.2 Population Balance Equation for a branched polymer

For a branched polymer the discrete PBE defines a system of ODEs:

$$\frac{\mathrm{d}\check{n}(t,\check{k},\check{b})}{\mathrm{d}t} = -\check{D}_{\sum}(t,\check{k},\check{b}) + \check{B}_{\sum}(t,\check{k},\check{b}). \tag{A.3}$$

If the continuity assumption is valid for both coordinates, a two dimensional PDE is obtained

$$\frac{\partial \bar{n}(t,\bar{k},\bar{b})}{\partial t} = -\bar{D}_{\sum}(t,\bar{k},\bar{b}) + \bar{B}_{\sum}(t,\bar{k},\bar{b}). \tag{A.4}$$

If the continuity assumption is only valid for the amount of monomer units, a system of one dimensional PDEs is obtained

$$\frac{\partial \hat{n}(t,\bar{k},\breve{b})}{\partial t} = -\hat{D}_{\sum}(t,\bar{k},\breve{b}) + \hat{B}_{\sum}(t,\bar{k},\breve{b}). \tag{A.5}$$

A.2 Formulations of the production rate

A.2.1 General form for a linear polymer

The necessary condition for attack is always $k' \geq 2$.

Discrete representation The production rate and normalization for a discrete polymer can be expressed as follows

$$\breve{B}_{\bullet}(t,\breve{k}) = 2 \cdot \sum_{\breve{k}'=\breve{k}+1}^{\infty} \breve{\gamma}_{\bullet}(\breve{k},\breve{k}') \cdot \breve{D}_{\bullet}(t,\breve{k}') \tag{A.6}$$

$$1 = \sum_{\breve{k}=1}^{\breve{k}'-1} \breve{\gamma}_{\bullet}(\breve{k},\breve{k}'). \tag{A.7}$$

Continuous representation The symmetry and the deductions are also valid for a continuously represented polymer. Accordingly, one can express the production rate and normalization condition as

$$\breve{B}_{\bullet}(t,\bar{k}) = 2 \cdot \int_{\bar{k}'=\bar{k}+1}^{\infty} \bar{\gamma}_{\bullet}(\bar{k},\bar{k}') \cdot \bar{D}_{\bullet}(t,\bar{k}') \, \mathrm{d}\bar{k}' \tag{A.8}$$

$$1 = \int_{\bar{k}=1}^{\bar{k}'-1} \bar{\gamma}_{\bullet}(\bar{k},\bar{k}') \, \mathrm{d}\bar{k}'. \tag{A.9}$$

A.2.2 General form for a branched polymer for hydrolysis on linear bonds

The necessary condition for attack is always $k' - 2 \geq b'$.

Discrete representation The production rate and normalization conditions have already been derived

$$\breve{B}_{\bullet}(t,\breve{k},\breve{b}) = 2 \cdot \sum_{\breve{k}'=\breve{k}+1}^{\infty} \sum_{\breve{b}'=\breve{b}}^{\breve{k}'-1-\breve{k}+\breve{b}} \breve{\gamma}_{\bullet}(\breve{k},\breve{k}',\breve{b},\breve{b}') \cdot \breve{D}_{\bullet}(t,\breve{k}',\breve{b}') \tag{A.10}$$

$$1 = \sum_{\breve{b}=0}^{\breve{b}'} \sum_{\breve{k}=\breve{b}+1}^{\breve{k}'-1+\breve{b}-\breve{b}'} \breve{\gamma}_{\bullet}(\breve{k},\breve{k}',\breve{b},\breve{b}'). \tag{A.11}$$

Continuous representation The symmetry and the deductions are also valid for a continuously represented polymer. Accordingly, one can express the production rate and normalization condition as

$$\bar{B}_\bullet(t,\bar{k},\bar{b}) = 2\cdot\int_{\bar{k}+1}^{\infty}\int_{\bar{b}}^{\bar{k}'-1-\bar{k}+\bar{b}} \bar{\gamma}_\bullet(\bar{k},\bar{k}',\bar{b},\bar{b}')\cdot\bar{D}_\bullet(t,\bar{k}',\bar{b}')\,\mathrm{d}\bar{b}'\,\mathrm{d}\bar{k}' \tag{A.12}$$

$$1 = \int_0^{\bar{b}}\int_{\bar{b}+1}^{\bar{k}'-1+\bar{b}-\bar{b}'} \bar{\gamma}_\bullet(\bar{k},\bar{k}',\bar{b},\bar{b}')\,\mathrm{d}\bar{k}\,\mathrm{d}\bar{b}. \tag{A.13}$$

Mixed continuous-discrete representation The symmetry and the deductions are also valid for a mixed continuously-discretely represented polymer. Accordingly, one can express the production rate and normalization condition as

$$\hat{B}_\bullet(t,\bar{k},\check{b}) = 2\cdot\sum_{\check{b}'=\check{b}}^{\infty}\int_{\bar{k}+1+\check{b}'-\check{b}}^{\infty} \hat{\gamma}_\bullet(\bar{k},\bar{k}',\check{b},\check{b}')\cdot\hat{D}_\bullet(t,\bar{k}',\check{b}')\,\mathrm{d}\bar{k}' \tag{A.14}$$

$$1 = \sum_{\check{b}=0}^{\check{b}'}\int_{\check{b}+1}^{\bar{k}'-1+\check{b}-\check{b}'} \hat{\gamma}_\bullet(\bar{k},\bar{k}',\check{b},\check{b}')\,\mathrm{d}\bar{k}.. \tag{A.15}$$

A.2.3 General form for a branched polymer for hydrolysis on branching bonds

The necessary condition for attack is always $b' \geq 1$.

Discrete representation The production rate and normalization condition have already been derived

$$\check{B}_\bullet(t,\check{k},\check{b}) = 2\cdot\sum_{\check{k}'=\check{k}+1}^{\infty}\sum_{\check{b}'=\check{b}+1}^{\check{k}'-\check{k}+\check{b}} \check{\gamma}_\bullet(\check{k},\check{k}',\check{b},\check{b}')\cdot\check{D}_\bullet(t,\check{k}',\check{b}') \tag{A.16}$$

$$1 = \sum_{\check{b}=0}^{\check{b}'-1}\sum_{\check{k}=\check{b}+1}^{\check{k}'-\check{b}'+\check{b}} \check{\gamma}_\bullet(\check{k},\check{k}',\check{b},\check{b}'). \tag{A.17}$$

Continuous representation The symmetry and the deductions are also valid for a continuously represented polymer. Accordingly, one can express the production rate and normalization condition as

$$\bar{B}_\bullet(t,\bar{k},\bar{b}) = 2\cdot\int_{\bar{k}+1}^{\infty}\int_{\bar{b}+1}^{\bar{k}'-\bar{k}+\bar{b}} \bar{\gamma}_\bullet(\bar{k},\bar{k}',\bar{b},\bar{b}')\cdot\bar{D}_\bullet(t,\bar{k}',\bar{b}')\,\mathrm{d}\bar{b}'\,\mathrm{d}\bar{k}' \tag{A.18}$$

$$1 = \int_0^{\bar{b}'-1}\int_{\bar{b}+1}^{\bar{k}'-\bar{b}'+\bar{b}} \bar{\gamma}_\bullet(\bar{k},\bar{k}',\bar{b},\bar{b}')\cdot H(\bar{b}-\bar{b}'+\bar{k}'-\bar{k})\,\mathrm{d}\bar{k}\,\mathrm{d}\bar{b}. \tag{A.19}$$

Mixed continuous-discrete representation The symmetry and the deductions are also valid for a continuously represented polymer. Accordingly, one can express the production rate and normalization

condition as

$$\hat{B}_\bullet(t,\bar{k},\breve{b}) = 2\cdot\sum_{\breve{b}'=\breve{b}+1}^{\infty}\int_{\bar{k}+\breve{b}'-\breve{b}}^{\infty}\hat{\gamma}_\bullet(\bar{k},\bar{k}',\breve{b},\breve{b}')\cdot\hat{D}_\bullet(t,\bar{k}',\breve{b}')\,\mathrm{d}\bar{k}' \tag{A.20}$$

$$1 = \sum_{\breve{b}=0}^{\breve{b}'-1}\int_{\breve{b}+1}^{\bar{k}'-\breve{b}'+\breve{b}}\hat{\gamma}_\bullet(\bar{k},\bar{k}',\breve{b},\breve{b}')\,\mathrm{d}\bar{k}. \tag{A.21}$$

A.2.4 Product Distribution Functions for specific mechanism

Random-chain scission Because the fragment distribution function is normalized (see Eqs. (2.12), (A.9), (2.17), (A.13), and (A.15)), the value of $f_{RCS}(k',b')$ for all the cases described priorly can be readily obtained:

$$\breve{f}_{RCS}(\breve{k}') = \frac{1}{\breve{k}'-1} \tag{A.22}$$

$$\bar{f}_{RCS}(\bar{k}') = \frac{1}{\bar{k}'-2} \tag{A.23}$$

$$\bar{f}_{RCS}(\bar{k}',\bar{b}') = \frac{1}{\bar{b}'\cdot(\bar{k}'-\bar{b}'-2)} \tag{A.24}$$

$$\hat{f}_{RCS}(\bar{k}',\breve{b}') = \frac{1}{(\breve{b}'+1)\cdot(\bar{k}'-\breve{b}'-2)} \tag{A.25}$$

$$\breve{f}_{RCS}(\breve{k}',\breve{b}') = \frac{1}{(\breve{b}'+1)\cdot(\breve{k}'-\breve{b}'-1)}. \tag{A.26}$$

The birth terms due to Random-chain scission (RCS) can then be written as follows:

$$\breve{B}_{RCS}(t,\breve{k}) = 2\cdot\sum_{\breve{k}'=\breve{k}+1}^{\infty}\frac{\breve{D}_{RCS}(t,\breve{k}')}{\breve{k}'-1} \tag{A.27}$$

$$\bar{B}_{RCS}(t,\bar{k}) = 2\cdot\int_{\bar{k}+1}^{\infty}\frac{\hat{D}_{RCS}(t,\bar{k}')}{\bar{k}'-2}\,\mathrm{d}\bar{k}' \tag{A.28}$$

$$\breve{B}_{RCS}(t,\breve{k},\breve{b}) = 2\cdot\sum_{\breve{k}'=\breve{k}+1}^{\infty}\sum_{\breve{b}'=\breve{b}}^{\breve{b}+\breve{k}'-\breve{k}-1}\frac{\breve{D}_{RCS}(t,\breve{k}',\breve{b}')}{(\breve{b}'+1)\cdot(\breve{k}'-\breve{b}'-1)} \tag{A.29}$$

$$\hat{B}_{RCS}(t,\bar{k},\breve{b}) = 2\cdot\sum_{\breve{b}'=\breve{b}}^{\infty}\int_{\bar{k}+1+\breve{b}'-\breve{b}}^{\infty}\frac{\hat{D}_{RCS}(t,\bar{k}',\breve{b}')}{(\breve{b}'+1)\cdot(\bar{k}'-\breve{b}'-2)}\,\mathrm{d}\bar{k}' \tag{A.30}$$

Random-debranching scission Due to normalization (see Eqs. (2.20),(A.19), and (A.21)), f_{RDS} is obtained as follows:

$$\bar{f}_{RDS}(\bar{k}',\bar{b}') = \frac{1}{(\bar{b}'-1)\cdot(\bar{k}'-\bar{b}'-1)} \tag{A.31}$$

$$\hat{f}_{RDS}(\bar{k}',\breve{b}') = \frac{1}{\breve{b}' \cdot (\bar{k}' - \breve{b}' - 1)} \tag{A.32}$$

$$\breve{f}_{RDS}(\breve{k}',\breve{b}') = \frac{1}{\breve{b}' \cdot (\breve{k}' - \breve{b}')}. \tag{A.33}$$

The birth terms due to Random-debranching scission (RDS) are as follows:

$$\breve{B}_{RDS}(t,\breve{k},\breve{b}) = 2 \cdot \sum_{\breve{k}'=\breve{k}+1}^{\infty} \sum_{\breve{b}'=\breve{b}+1}^{\breve{b}+\breve{k}'-\breve{k}} \frac{\breve{D}_{RDS}(\breve{k}',\breve{b}',t)}{\breve{b}' \cdot (\breve{k}' - \breve{b}')} \tag{A.34}$$

$$\bar{B}_{RDS}(t,\bar{k},\bar{b}) = 2 \cdot \int_{\bar{k}+1}^{\infty} \int_{\bar{b}+1}^{\bar{b}+\bar{k}'-\bar{k}} \frac{\bar{D}_{RDS}(t,\bar{k}',\bar{b}')}{(\bar{b}'-1) \cdot (\bar{k}' - \bar{b}' - 1)} \,\mathrm{d}\bar{b}' \,\mathrm{d}\bar{k}' \tag{A.35}$$

$$\hat{B}_{RDS}(t,\bar{k},\breve{b}) = 2 \cdot \sum_{\breve{b}'=\breve{b}+1}^{\infty} \int_{\bar{k}+\breve{b}'-\breve{b}}^{\infty} \frac{\hat{D}_{RDS}(t,\bar{k}',\breve{b}')}{\breve{b}' \cdot (\bar{k}' - \breve{b}' - 1)} \,\mathrm{d}\bar{k}'. \tag{A.36}$$

End-chain scission The birth of polymers is given by:

$$\breve{B}_{ECS,\breve{a}}(t,\breve{k}) = \breve{D}_{ECS,\breve{a}}(t,\breve{k}+\breve{a}) + \delta(\breve{k},\breve{a}) \cdot \sum_{\breve{k}'=1+\breve{a}}^{\infty} \breve{D}_{ECS,\breve{a}}(t,\breve{k}') \tag{A.37}$$

$$\bar{B}_{ECS,\breve{a}}(t,\bar{k}) = \bar{D}_{ECS,\breve{a}}(t,\bar{k}+\breve{a}) + \bar{\delta}(\bar{k}-\breve{a}) \cdot \int_{1+\breve{a}}^{\infty} \bar{D}_{ECS,\breve{a}}(t,\bar{k}') \,\mathrm{d}\bar{b}' \,\mathrm{d}\bar{k}' \tag{A.38}$$

$$\breve{B}_{ECS,\breve{a}}(t,\breve{k},\breve{b}) = \breve{D}_{ECS,\breve{a}}(t,\breve{k}+\breve{a},\breve{b}) + \delta(\breve{k},\breve{a}) \cdot \delta(\breve{b},0) \cdot \sum_{\breve{k}'=1+\breve{a}}^{\infty} \sum_{\breve{b}'=0}^{\breve{k}'-1-\breve{a}} \breve{D}_{ECS}(t,\breve{k}',\breve{b}'). \tag{A.39}$$

$$\bar{B}_{ECS,\breve{a}}(t,\bar{k},\bar{b}) = \bar{D}_{ECS,\breve{a}}(t,\bar{k}+\breve{a},\bar{b}) + \bar{\delta}(\bar{k}-\breve{a}) \cdot \bar{\delta}(\bar{b}) \cdot \int_{1+\breve{a}}^{\infty} \int_{0}^{\bar{k}'-1-\breve{a}} \bar{D}_{ECS,\breve{a}}(t,\bar{k}',\bar{b}') \,\mathrm{d}\bar{b}' \,\mathrm{d}\bar{k}' \tag{A.40}$$

$$\hat{B}_{ECS,\breve{a}}(t,\bar{k},\breve{b}) = \hat{D}_{ECS,\breve{a}}(t,\bar{k}+\breve{a},\breve{b}) + \bar{\delta}(\bar{k}-\breve{a}) \cdot \delta(\breve{b},0) \cdot \sum_{\breve{b}'=0}^{\infty} \int_{\breve{b}'+1+\breve{a}}^{\infty} \hat{D}_{ECS,\breve{a}}(t,\bar{k}',\breve{b}') \,\mathrm{d}\bar{k}'. \tag{A.41}$$

A more common, but equivalent form, for the linear discrete case is

$$\breve{B}_{ECS,\breve{a}}(t,\breve{k}) = \breve{D}_{ECS,\breve{a}}(t,\breve{k}+\breve{a}) + \begin{cases} \sum_{\breve{k}'=1+\breve{a}}^{\infty} \breve{D}_{ECS,\breve{a}}(t,\breve{k}') & \breve{a} = \breve{k} \\ 0 & \text{otherwise} \end{cases}. \tag{A.42}$$

Random scission of inner monomer units and inner chains They are only shown discretely because this are only used for the discrete PBEs in this work. Therefore, everything is already provided in the main text.

Appendix B

Closure of the moments

In this chapter the closure rules provided by Direct Quadrature Method of Moments (DQMOM) are used to provide closure to the moments of the birth and death terms.

B.1 Subdomain I

In Equation (3.17), $\bar{\tilde{\alpha}}^{i,j}_{\sum,\mathrm{I}}$ and $\bar{\tilde{\omega}}^{i,j}_{\sum,\mathrm{I}}$ need to be determined. They can be computed as follows:

$$\bar{\tilde{\alpha}}^{i,j}_{\sum,\mathrm{I}} = \bar{\tilde{\alpha}}^{i,j}_{RCS,\mathrm{I}} + \bar{\tilde{\alpha}}^{i,j}_{ECS,\mathrm{I}} + \bar{\tilde{\alpha}}^{i,j}_{RDS,\mathrm{I}} \tag{B.1}$$

$$\bar{\tilde{\omega}}^{i,j}_{\sum,\mathrm{I}} = \bar{\tilde{\omega}}^{i,j}_{RCS,\mathrm{I}} + \bar{\tilde{\omega}}^{i,j}_{ECS,\mathrm{I}} + \bar{\tilde{\omega}}^{i,j}_{RDS,\mathrm{I}}. \tag{B.2}$$

The terms appearing in the equation for $\bar{\tilde{\omega}}^{i,j}_{\sum,\mathrm{I}}$ are the moments of the reaction rate. After closure (see Equations (2.43) and (2.44)), they are as follows:

$$\bar{\tilde{\omega}}^{i,j}_{RCS/ECS} = C_{RCS/ECS} \cdot \sum_{l=1}^{N_\mathrm{I}} \bar{\tilde{w}}_l \cdot \bar{\tilde{k}}_l^{\,i} \cdot \bar{\tilde{b}}_l^{\,j} \cdot H(\tilde{k} \cdot \bar{\tilde{k}}_l - 2 - \tilde{b} \cdot \bar{\tilde{b}}_l) \tag{B.3}$$

$$\bar{\tilde{\omega}}^{i,j}_{RDS} = C_{RDS} \cdot \sum_{l=1}^{N_\mathrm{I}} \bar{\tilde{w}}_l \cdot \bar{\tilde{k}}_l^{\,i} \cdot \bar{\tilde{b}}_l^{\,j} \cdot H(\tilde{b} \cdot \bar{\tilde{b}}_l - 1). \tag{B.4}$$

The terms appearing in the equation for $\bar{\tilde{\alpha}}^{i,j}_{\sum,\mathrm{I}}$ are the moments of the birth terms. After closure (see Equations (2.27), (A.35) and (A.40)), they are:

$$\begin{aligned}
\bar{\tilde{\alpha}}^{i,j}_{RCS,\mathrm{I}} =& 2\cdot C_{RCS}\cdot\frac{1}{j+1}\cdot\sum_{l=1}^{N_\mathrm{I}}\frac{\bar{\tilde{w}}_l\cdot H(\tilde{k}\cdot\bar{\tilde{k}}_l-2-\tilde{b}\cdot\bar{\tilde{b}}_l)}{\bar{\tilde{b}}_l\cdot\left(\bar{\tilde{k}}_l-\frac{\tilde{b}\cdot\bar{\tilde{b}}_l}{\tilde{k}}-\frac{2}{\tilde{k}}\right)}\\
&\cdot\left\{\sum_{f=0}^{i-1}\left[\binom{i}{f}\cdot\left(\frac{\tilde{b}}{\tilde{k}}\right)^{f+1}\cdot\frac{\left(\frac{1}{\tilde{k}}\right)^{i-f}-\left(\bar{\tilde{k}}_l-\frac{\tilde{b}}{\tilde{k}}\cdot\bar{\tilde{b}}_l-\frac{1}{\tilde{k}}\right)^{i-f}}{j+2+f}\cdot\left(\bar{\tilde{b}}_l{}^{j+2+f}-\left(\frac{\breve{k}_c-1}{\tilde{b}}\right)^{j+2+f}\right)\right]\right.\\
&+\frac{1}{i+1}\cdot\left[\bar{\tilde{b}}_l{}^{j+1}\cdot\left(\left(\bar{\tilde{k}}_l-\frac{1}{\tilde{k}}\right)^{i+1}-\left(\frac{\tilde{b}}{\tilde{k}}\cdot\bar{\tilde{b}}_l+\frac{1}{\tilde{k}}\right)^{i+1}\right)\right.\\
&\left.\left.-\left(\frac{\breve{k}_c-1}{\tilde{b}}\right)^{j+1}\cdot\left(\left(\bar{\tilde{k}}_l-\frac{\tilde{b}}{\tilde{k}}\cdot\bar{\tilde{b}}_l+\frac{\breve{k}_c}{\tilde{k}}-\frac{2}{\tilde{k}}\right)^{i+1}-\left(\frac{\breve{k}_c}{\tilde{k}}\right)^{i+1}\right)\right]\right\}
\end{aligned}\tag{B.5}$$

$$\begin{aligned}
\bar{\tilde{\alpha}}^{i,j}_{RDS,\mathrm{I}} =& 2\cdot C_{RDS}\cdot\frac{1}{j+1}\cdot\sum_{l=1}^{N_\mathrm{I}}\frac{\bar{\tilde{w}}_l\cdot H\left(\tilde{b}\cdot\bar{\tilde{b}}_l-1\right)}{\bar{\tilde{b}}_l\cdot\bar{\tilde{k}}_l-\frac{\bar{\tilde{k}}_l}{\tilde{b}}-\frac{\tilde{b}\cdot\bar{\tilde{b}}_l{}^2}{\tilde{k}}+\frac{1}{\tilde{k}\cdot\tilde{b}}}\\
&\cdot\left\{\sum_{f=0}^{i-1}\left[\binom{i}{f}\cdot\left(\frac{\tilde{b}}{\tilde{k}}\right)^{f+1}\cdot\frac{\left(\frac{1}{\tilde{k}}\right)^{i-f}-\left(\bar{\tilde{k}}_l-\frac{\tilde{b}}{\tilde{k}}\cdot\bar{\tilde{b}}_l\right)^{i-f}}{j+2+f}\cdot\left(\left(\bar{\tilde{b}}_l-\frac{1}{\tilde{b}}\right)^{j+2+f}-\left(\frac{\breve{k}_c-1}{\tilde{b}}\right)^{j+2+f}\right)\right]\right.\\
&-\frac{1}{i+1}\cdot\left(\frac{\breve{k}_c-1}{\tilde{b}}\right)^{j+1}\cdot\left(\left(\bar{\tilde{k}}_l-\frac{\tilde{b}}{\tilde{k}}\cdot\bar{\tilde{b}}_l+\frac{\breve{k}_c}{\tilde{k}}-\frac{1}{\tilde{k}}\right)^{i+1}-\left(\frac{\breve{k}_c}{\tilde{k}}\right)^{i+1}\right)\\
&\left.+\frac{1}{i+1}\cdot\left(\bar{\tilde{b}}_l-\frac{1}{\tilde{b}}\right)^{j+1}\cdot\left(\left(\bar{\tilde{k}}_l-\frac{1}{\tilde{k}}\right)^{i+1}-\left(\frac{\tilde{b}}{\tilde{k}}\cdot\bar{\tilde{b}}_l\right)^{i+1}\right)\right\}
\end{aligned}\tag{B.6}$$

$$\bar{\tilde{\alpha}}^{i,j}_{ECS,\mathrm{I}} = C_{ECS}\cdot\sum_{l=1}^{N_\mathrm{I}}\bar{\tilde{w}}_l\cdot H(\tilde{k}\cdot\bar{\tilde{k}}_l-2-\tilde{b}\cdot\bar{\tilde{b}}_l)\cdot\left[\left(\bar{\tilde{k}}_l-\frac{1}{\tilde{k}}\right)^{i}\cdot\left(\bar{\tilde{b}}_l\right)^{j}+(\delta_{\breve{k}_c,0}+\delta_{\breve{k}_c,1})\cdot\delta_{j,0}\cdot\left(\frac{1}{\tilde{k}}\right)^{i}\right],\tag{B.7}$$

where $\delta_{x,y}$ is the Kronecker delta, which equals one if $x=y$ and zero otherwise.

B.2 Contribution of Subdomain I to Subdomain II

In Equation (3.31), $\hat{\alpha}^{i\in\mathbb{N}_0}_{\sum,I}$ must be determined. It is defined as follows:

$$\hat{\alpha}^{i\in\mathbb{N}_0}_{\sum,I}=\hat{\alpha}^{i\in\mathbb{N}_0}_{ECS,I}+\hat{\alpha}^{i\in\mathbb{N}_0}_{RCS,I}+\hat{\alpha}^{i\in\mathbb{N}_0}_{RDS,I}.\tag{B.8}$$

ECS in Subdomain I has no contribution to Subdomain II, therefore:

$$\hat{\alpha}^{i\in\mathbb{N}_0}_{ECS,\mathrm{I}}=0.\tag{B.9}$$

The other two unknown terms are determined using Equation (3.34), where $\hat{B}_{\bullet,\mathrm{I}}$ and $\hat{\alpha}_{\bullet,I}^{j\in\mathbb{N}_0}$ are substituted by $\hat{\alpha}_{\bullet,I}^{i\in\mathbb{N}_0}$ and $\hat{\alpha}_{\bullet,I}^{i,j}$, respectively. The necessary $\hat{\alpha}_{\bullet,I}^{i,j}$ are:

$$\hat{a}_l(\breve{b}) = \tilde{k}\cdot\bar{\tilde{k}}_l - \tilde{b}\cdot\bar{\tilde{b}}_l + \breve{b} - \breve{k}_c \tag{B.10}$$

$$\begin{aligned}\hat{\alpha}_{RCS,\mathrm{I}}^{i,j=0} =& 2\cdot C_{RCS}\cdot\frac{\tilde{w}}{\tilde{k}\cdot\tilde{b}}\cdot\sum_{l=1}^{N_\mathrm{I}}\frac{\bar{\tilde{w}}_l\cdot H(\tilde{k}\cdot\bar{\tilde{k}}_l - 2 - \tilde{b}\cdot\bar{\tilde{b}}_l)}{\bar{\tilde{b}}_l\cdot\left(\bar{\tilde{k}}_l - \frac{\tilde{b}\cdot\bar{\tilde{b}}_l}{\tilde{k}} - \frac{2}{\tilde{k}\cdot\tilde{b}}\right)}\cdot\frac{H(\hat{a}_l(\breve{b}))}{i+1}\\ &\cdot\left\{\frac{1}{i+2}\cdot\left[(\breve{b}+\tilde{k}\cdot\bar{\tilde{k}}_l-\breve{k}_c)^{i+2} - \max\left(\breve{b}+\tilde{k}\cdot\bar{\tilde{k}}_l-\tilde{b}\cdot\bar{\tilde{b}}_l-1,\breve{k}_c\right)^{i+2}\right]\right.\\ &\left.-\breve{k}_c^{i+1}\cdot\left[\breve{b}+1-\max\left(\breve{b},\breve{k}_c+\tilde{b}\cdot\bar{\tilde{b}}_l+1-\tilde{k}\cdot\bar{\tilde{k}}_l\right)\right]\right\}\end{aligned} \tag{B.11}$$

$$\begin{aligned}\hat{\alpha}_{RCS,\mathrm{I}}^{i,j=1} =& 2\cdot C_{RCS}\cdot\frac{\tilde{w}}{\tilde{k}\cdot\tilde{b}}\cdot\sum_{l=1}^{N_\mathrm{I}}\frac{\bar{\tilde{w}}_l\cdot H(\tilde{k}\cdot\bar{\tilde{k}}_l - 2 - \tilde{b}\cdot\bar{\tilde{b}}_l)}{\bar{\tilde{b}}_l\cdot\left(\bar{\tilde{k}}_l - \frac{\tilde{b}\cdot\bar{\tilde{b}}_l}{\tilde{k}} - \frac{2}{\tilde{k}\cdot\tilde{b}}\right)}\cdot\frac{H(\hat{a}_l(\breve{b}))}{i+1}\\ &\cdot\left\{\frac{1}{i+3}\cdot\left[(\breve{b}+\tilde{k}\cdot\bar{\tilde{k}}_l-\breve{k}_c)^{i+3} - \max\left(\breve{b}+\tilde{k}\cdot\bar{\tilde{k}}_l-\tilde{b}\cdot\bar{\tilde{b}}_l-1,\breve{k}_c\right)^{i+3}\right]\right.\\ &-\frac{\tilde{k}\cdot\bar{\tilde{k}}_l-\tilde{b}\cdot\bar{\tilde{b}}_l-1}{i+2}\cdot\left[(\breve{b}+\tilde{k}\cdot\bar{\tilde{k}}_l-\breve{k}_c)^{i+2} - \max\left(\breve{b}+\tilde{k}\cdot\bar{\tilde{k}}_l-\tilde{b}\cdot\bar{\tilde{b}}_l-1,\breve{k}_c\right)^{i+2}\right]\\ &\left.-\frac{\breve{k}_c^{i+1}}{2}\cdot\left[(\breve{b}+1)^2 - \max\left(\breve{b},\breve{k}_c+\tilde{b}\cdot\bar{\tilde{b}}_l+1-\tilde{k}\cdot\bar{\tilde{k}}_l\right)^2\right]\right\}\end{aligned} \tag{B.12}$$

$$\hat{c}_l(\breve{b}) = \min(\breve{b}+1, \tilde{b}\cdot\bar{\tilde{b}}_l - 1) \tag{B.13}$$

$$\hat{d}_l(\breve{b}) = \max(\breve{b}, \breve{k}_c + \tilde{b}\cdot\bar{\tilde{b}}_l - \tilde{k}\cdot\bar{\tilde{k}}_l) \tag{B.14}$$

$$\begin{aligned}\hat{\alpha}_{RDS,\mathrm{I}}^{i,j=0} =& 2\cdot C_{RDS}\cdot\frac{\tilde{w}}{\tilde{k}\cdot\tilde{b}}\sum_{l=1}^{N_\mathrm{I}}\frac{\bar{\tilde{w}}_l\cdot H(\tilde{b}\cdot\bar{\tilde{b}}_l - 1)}{\bar{\tilde{b}}_l\cdot\bar{\tilde{k}}_l - \frac{\bar{\tilde{k}}_l}{\tilde{b}} - \frac{\tilde{b}\cdot\bar{\tilde{b}}_l^{\,2}}{\tilde{k}} + \frac{1}{\tilde{k}\cdot\tilde{b}}}\cdot\frac{H(\hat{c}_l(\breve{b}) - \breve{k}_c + \tilde{k}\cdot\bar{\tilde{k}}_l - \tilde{b}\cdot\bar{\tilde{b}}_l)}{i+1}\\ &\cdot\left\{\frac{1}{i+2}\cdot\left[\left(\hat{c}_l(\breve{b})+\tilde{k}\cdot\bar{\tilde{k}}_l-\tilde{b}\cdot\bar{\tilde{b}}_l\right)^{i+2} - \left(\hat{d}_l(\breve{b})+\tilde{k}\cdot\bar{\tilde{k}}_l-\tilde{b}\cdot\bar{\tilde{b}}_l\right)^{i+2}\right]\right.\\ &\left.-\breve{k}_c^{i+1}\left(\hat{c}_l(\breve{b}) - \hat{d}_l(\breve{b})\right)\right\}\end{aligned} \tag{B.15}$$

$$\begin{aligned}\hat{\alpha}_{RDS,\mathrm{I}}^{i,j=1} =& 2\cdot C_{RDS}\cdot\frac{\tilde{w}}{\tilde{k}\cdot\tilde{b}}\cdot\sum_{l=1}^{N_\mathrm{I}}\frac{\bar{\tilde{w}}_l\cdot H(\tilde{b}\cdot\bar{\tilde{b}}_l - 1)}{\bar{\tilde{b}}_l\cdot\bar{\tilde{k}}_l - \frac{\bar{\tilde{k}}_l}{\tilde{b}} - \frac{\tilde{b}\cdot\bar{\tilde{b}}_l^{\,2}}{\tilde{k}} + \frac{1}{\tilde{k}\cdot\tilde{b}}}\cdot\frac{H(\hat{c}_l(\breve{b}) - \breve{k}_c + \tilde{k}\cdot\bar{\tilde{k}}_l - \tilde{b}\cdot\bar{\tilde{b}}_l)}{i+1}\\ &\left\{\frac{1}{i+3}\cdot\left[\left(\hat{c}_l(\breve{b})+\tilde{k}\cdot\bar{\tilde{k}}_l-\tilde{b}\cdot\bar{\tilde{b}}_l\right)^{i+3} - \left(\hat{d}_l(\breve{b})+\tilde{k}\cdot\bar{\tilde{k}}_l-\tilde{b}\cdot\bar{\tilde{b}}_l\right)^{i+3}\right]\right.\\ &\frac{\tilde{k}\cdot\bar{\tilde{k}}_l-\tilde{b}\cdot\bar{\tilde{b}}_l}{i+2}\cdot\left[\left(\hat{c}_l(\breve{b})+\tilde{k}\cdot\bar{\tilde{k}}_l-\tilde{b}\cdot\bar{\tilde{b}}_l\right)^{i+2} - \left(\hat{d}_l(\breve{b})+\tilde{k}\cdot\bar{\tilde{k}}_l-\tilde{b}\cdot\bar{\tilde{b}}_l\right)^{i+2}\right]\\ &\left.-\frac{\breve{k}_c^{i+1}}{2}\left(\hat{c}_l(\breve{b})^2 - \hat{d}_l(\breve{b})^2\right)\right\}\end{aligned} \tag{B.16}$$

B.3 Subdomain II

In Equation (3.31), $\hat{\omega}_{\sum}^{i\in\mathbb{N}_0}$ must be determined. It is defined as follows:

$$\hat{\omega}_{\sum}^{i\in\mathbb{N}_0} = \hat{\omega}_{ECS}^{i\in\mathbb{N}_0} + \hat{\omega}_{RCS}^{i\in\mathbb{N}_0} + \hat{\omega}_{RDS}^{i\in\mathbb{N}_0}. \tag{B.17}$$

The moments of the reaction rates (see Equations (2.43) and (2.44)) are closed as follows:

$$\hat{\omega}_{RCS/ECS}^{i\in\mathbb{N}_0}(\breve{b},t) = C_{RCS/ECS} \cdot \sum_{l=1}^{N_{\text{II}}} \hat{w}_l \cdot \hat{k}_l^i \cdot H(\hat{k}_l - 2 - \breve{b}) \tag{B.18}$$

$$\hat{\omega}_{RDS}^{i\in\mathbb{N}_0}(\breve{b},t) = C_{RDS} \cdot H(\breve{b}-1) \cdot \sum_{l=1}^{N_{\text{II}}} \hat{w}_l \cdot \hat{k}_l^i. \tag{B.19}$$

Furthermore, in Equation (3.31), $\hat{\alpha}_{\sum,II}^{i\in\mathbb{N}_0}$ must also determined. It is defined as follows:

$$\hat{\alpha}_{\sum,II}^{i\in\mathbb{N}_0} = \hat{\alpha}_{ECS,II}^{i\in\mathbb{N}_0} + \hat{\alpha}_{RCS,II}^{i\in\mathbb{N}_0} + \hat{\alpha}_{RDS,II}^{i\in\mathbb{N}_0}. \tag{B.20}$$

The moments of the birth (see Equations (A.30), (A.41), and (A.36)) can be closed as follows:

$$\begin{aligned}\hat{\alpha}_{RCS,II}^{i\in\mathbb{N}_0} =& 2 \cdot C_{RCS} \cdot \sum_{\breve{b}'=\breve{b}}^{\breve{k}_c-1} \sum_{l=1}^{N_{\text{II}}(\breve{b}')} \frac{\hat{w}_l}{(\breve{b}'+1)\cdot(\hat{k}_l - \breve{b}' - 2)} \cdot H(\hat{k}_l - 2 - \breve{b}') \cdot H\left(\hat{k}_l - \breve{k}_c - 1 + \breve{b} - \breve{b}'\right) \\ & \cdot \frac{(\hat{k}_l - 1 + \breve{b} - \breve{b}')^{i+1} - \breve{k}_c^{i+1}}{i+1}\end{aligned} \tag{B.21}$$

$$\hat{\alpha}_{ECS,II}^{i\in\mathbb{N}_0} = C_{ECS} \cdot \left\{ \sum_{l=1}^{N_{\text{II}}(\breve{b})} \hat{w}_l \cdot H(\hat{k}_l - 2 - \breve{b}) \cdot (\hat{k}_l - 1)^i \cdot H(\hat{k}_l - 1 - \breve{k}_c) \right\} \tag{B.22}$$

$$\hat{\alpha}_{RDS,II}^{i\in\mathbb{N}_0} = 2 \cdot C_{RDS} \cdot \sum_{\breve{b}'=\breve{b}+1}^{\breve{k}_c-1} \sum_{l=1}^{N_{\text{II}}(\breve{b}')} \hat{w}_l \cdot \frac{H(\hat{k}_l - \breve{k}_c - \breve{b}' + \breve{b})}{\breve{b}' \cdot (\hat{k}_l - 1 - \breve{b}')} \cdot \frac{(\hat{k}_l - \breve{b}' + \breve{b})^{i+1} - \breve{k}_c^{i+1}}{i+1}. \tag{B.23}$$

B.4 Contribution of Subdomain I to Subdomain III

To solve Equation (3.35) via Equation (3.47), $\breve{\alpha}_{\bullet,\mathrm{I},T}^{i,j}$ and $\breve{\alpha}_{\bullet,\mathrm{I},L}^{i,j}$ must be known.
The only contribution of ECS in Subdomain I to Subdomain III is through the creation of the monomer, therefore:

$$\breve{\alpha}_{ECS,\mathrm{I},L}^{i=0,j=0} = \breve{\alpha}_{ECS,\mathrm{I},L}^{i=1,j=0} = \delta_{\breve{k},1} \cdot \delta_{\breve{b},0} \cdot C_{ECS} \cdot \tilde{w} \cdot \sum_{l=1}^{N_{\mathrm{I}}} \bar{\tilde{w}}_l \cdot H(\tilde{k} \cdot \bar{\tilde{k}}_l - 2 - \tilde{b} \cdot \bar{\tilde{b}}_l) \tag{B.24}$$

$$\breve{\alpha}_{ECS,\mathrm{I},L}^{i=0,j=1} = \breve{\alpha}_{ECS,\mathrm{I},T}^{i=0,j=0} = \breve{\alpha}_{ECS,\mathrm{I},T}^{i=1,j=0} = \breve{\alpha}_{ECS,\mathrm{I},T}^{i=0,j=1} = 0. \tag{B.25}$$

After closure, the moments of the contribution of RCS in Subdomain I to Subdomain III are as follows:

$$\breve{R}_{RCS,\mathrm{I},l} = 2 \cdot C_{RCS} \cdot \frac{\tilde{w}}{\tilde{k} \cdot \tilde{b}} \cdot \bar{\bar{w}}_l \cdot \frac{H(\tilde{k} \cdot \bar{\bar{k}}_l - 2 - \tilde{b} \cdot \bar{\bar{b}}_l)}{\bar{\bar{b}}_l \cdot (\bar{\bar{k}}_l - \frac{\bar{\bar{b}}_l \cdot \tilde{b}}{\tilde{k}} - \frac{2}{\tilde{k} \cdot \tilde{b}})} \tag{B.26}$$

$$\breve{R}_{RCS,\mathrm{I},L,l} = \breve{R}_{RCS,\mathrm{I},l} \cdot H(\tilde{k} \cdot \bar{\bar{k}}_l - 1 - \tilde{b} \cdot \bar{\bar{b}}_l + \breve{b} - \breve{k}) \tag{B.27}$$

$$\hat{L}_{RCS,\mathrm{I},L,l} = 1 - \min(1, \tilde{k} \cdot \bar{\bar{k}}_l - 1 - \tilde{b} \cdot \bar{\bar{b}}_l + \breve{b} - \breve{k}) \tag{B.28}$$

$$\breve{\alpha}^{i=0,j=0}_{RCS,\mathrm{I},L} = \sum_{l=1}^{N_\mathrm{I}} \frac{1}{2} \cdot \breve{R}_{RCS,\mathrm{I},L,l} \cdot \left(1 - \hat{L}^2_{RCS,\mathrm{I},L,l}\right) \tag{B.29}$$

$$\breve{\alpha}^{i=1,j=0}_{RCS,\mathrm{I},L} = \sum_{l=1}^{N_\mathrm{I}} \breve{R}_{RCS,\mathrm{I},L,l} \cdot \left[\frac{\breve{k}}{2} + \frac{1}{3} - \frac{\hat{L}^2_{RCS,\mathrm{I},L,l}}{2} \cdot \left(\breve{k} + 1 - \frac{\hat{L}_{RCS,\mathrm{I},L,l}}{3}\right)\right] \tag{B.30}$$

$$\breve{\alpha}^{i=0,j=1}_{RCS,\mathrm{I},L} = \sum_{l=1}^{N_\mathrm{I}} \breve{R}_{RCS,\mathrm{I},L,l} \cdot \left[\frac{\breve{b}}{2} + \frac{1}{6} - \frac{\hat{L}^2_{RCS,\mathrm{I},L,l}}{2} \left(\breve{b} + 1 + \frac{\hat{L}_{RCS,\mathrm{I},L,l}}{3}\right)\right] \tag{B.31}$$

$$\hat{L}_{RCS,\mathrm{I},T,l} = \min(1, \tilde{k} \cdot \bar{\bar{k}}_l - \tilde{b} \cdot \bar{\bar{b}}_l + \breve{b} - \breve{k}) \tag{B.32}$$

$$\breve{\alpha}^{i=0,j=0}_{RCS,\mathrm{I},T} = \sum_{l=1}^{N_\mathrm{I}} \breve{R}_{RCS,\mathrm{I}} \cdot H(\hat{L}_{RCS,\mathrm{I},T,l}) \tag{B.33}$$

$$\breve{\alpha}^{i=1,j=0}_{RCS,\mathrm{I},T} = \sum_{l=1}^{N_\mathrm{I}} \breve{R}_{RCS,\mathrm{I},T,l} \cdot \frac{\hat{L}^2_{RCS,\mathrm{I},T,l}}{2} \tag{B.34}$$

$$\breve{\alpha}^{i=0,j=1}_{RCS,\mathrm{I},T,l} = R^{III,\mathrm{I}}_{RCS,B} \cdot \frac{\hat{L}^2_{RCS,\mathrm{I},T,l}}{2} \cdot \left(\breve{k} + \frac{\hat{L}_{RCS,\mathrm{I},T,l}}{3}\right) \tag{B.35}$$

$$\breve{\alpha}^{i=0,j=1}_{RCS,\mathrm{I},T} = \sum_{l=1}^{N_\mathrm{I}} R^{III,\mathrm{I}}_{RCS,\mathrm{I},T,l} \cdot \frac{\hat{L}^2_{RCS,\mathrm{I},T,l}}{2} \cdot \left(\breve{b} + \frac{2 \cdot \hat{L}_{RCS,\mathrm{I},T,l}}{3}\right). \tag{B.36}$$

After closure, the moments of the contribution of RDS in Subdomain I to Subdomain III are as follows:

$$\breve{a}_l = \tilde{k} \cdot \bar{\bar{k}}_l - \tilde{b} \cdot \bar{\bar{b}}_l + \breve{b} - \breve{k} \tag{B.37}$$

$$\breve{d}_l = \min(\breve{k} + 2 - \tilde{k} \cdot \bar{\bar{k}}_l, 0) + \tilde{b} \cdot \bar{\bar{b}}_l - 1 \tag{B.38}$$

$$\breve{R}_{RDS,\mathrm{I}} = 2 \cdot C_{RDS} \cdot \frac{\tilde{w}}{\tilde{k} \cdot \tilde{b}} \tag{B.39}$$

$$\breve{e}_{RDS,l} = \frac{\bar{\bar{w}}_l}{\bar{\bar{k}}_l \cdot \bar{\bar{b}}_l - \frac{\bar{\bar{k}}_l}{\tilde{b}} - \frac{\bar{\bar{b}}^2_l \cdot \tilde{b}}{\tilde{k}} + \frac{1}{\tilde{k} \cdot \tilde{b}}} \tag{B.40}$$

$$\begin{aligned}\breve{\alpha}^{i=0,j=0}_{RDS,\mathrm{I},L} = \breve{R}_{RDS,\mathrm{I}} \sum_{l=1}^{N_\mathrm{I}} \breve{e}_{RDS,l} \cdot \Bigg[& H(\breve{a}_l - 1) \cdot \frac{(\hat{c}(\breve{b}) - \breve{b}) \cdot (2 + \breve{b} - \hat{c}(\breve{b}))}{2} \\ & + (1 - H(\breve{a}_l - 1)) \cdot H(\breve{a}_l) \cdot \left((\breve{d}_l - \breve{b}) \cdot \breve{a}_l + \frac{\hat{c}(\breve{b}) - \breve{d}_l}{2} \cdot (2 + 2 \cdot \breve{b} - \hat{c}(\breve{b}) - \breve{d}_l) \right) \Bigg]\end{aligned} \tag{B.41}$$

$$\begin{aligned}\breve{\alpha}_{RDS,\mathrm{I},L}^{i=1,j=0} =&\breve{R}_{RDS,\mathrm{I}}\sum_{l=1}^{N_\mathrm{I}}\breve{e}_{RDS,l}\cdot\Bigg\{H(\breve{a}_l-1)\cdot\frac{\hat{c}(\breve{b})-\breve{b}}{6}\cdot\left[3\cdot\breve{k}\cdot(2+\breve{b}-\hat{c}(\breve{b}))+3-(\hat{c}(\breve{b})-\breve{b})^2\right]\\&+(1-H(\breve{a}_l-1))\cdot H(\breve{a}_l)\cdot\Bigg[\frac{\breve{d}_l-\breve{b}}{2}\cdot\breve{a}_l\cdot(\breve{a}_l-\breve{b}+\breve{d}_l)+\frac{\hat{c}(\breve{b})-\breve{d}_l}{6}\\&\cdot\left[3\cdot(\breve{k}-\breve{b})\cdot(2\cdot\breve{b}+2-\hat{c}(\breve{b})-\breve{d}_l)+3\cdot(\breve{b}+1)^2-(\hat{c}(\breve{b})+\breve{d}_l)^2+\hat{c}(\breve{b})\cdot\breve{d}_l\right]\Bigg]\Bigg\}\end{aligned}\tag{B.42}$$

$$\begin{aligned}\breve{\alpha}_{RDS,\mathrm{I},L}^{i=0,j=1} =&\breve{R}_{RDS,\mathrm{I}}\sum_{l=1}^{N_\mathrm{I}}\breve{e}_{RDS,l}\cdot\Bigg\{H(\breve{a}_l-1)\cdot\frac{\hat{c}(\breve{b})-\breve{b}}{6}\cdot\left[(3+\breve{b})\cdot(\hat{c}(\breve{b})+\breve{b})-2\cdot\hat{c}(\breve{b})^2\right]\\&+(1-H(\breve{a}_l-1))\cdot H(\breve{a}_l)\cdot\Bigg[\frac{\breve{d}_l-\breve{b}}{2}\cdot\breve{a}_l\cdot(\breve{d}_l+\breve{b})+\frac{\hat{c}(\breve{b})-\breve{d}_l}{6}\\&\cdot\left[3\cdot(1+\breve{b})\cdot(\hat{c}(\breve{b})+\breve{d}_l)-2\cdot(\hat{c}(\breve{b})+\breve{d}_l)^2+2\cdot\hat{c}(\breve{b})\cdot\breve{d}_l\right]\Bigg]\Bigg\}\end{aligned}\tag{B.43}$$

$$\breve{\alpha}_{RDS,\mathrm{I},T}^{i=0,j=0} =\breve{R}_{RDS,\mathrm{I}}\sum_{l=1}^{N_\mathrm{I}}\breve{e}_{RDS,l}\cdot\left[\frac{H(\breve{a}_l)}{2}+(1-H(\breve{a}_l))\cdot H(\breve{a}_l+1)\cdot\frac{(\breve{a}_l+1)^2}{2}\right]\tag{B.44}$$

$$\breve{\alpha}_{RDS,\mathrm{I},T}^{i=1,j=0} =\breve{R}_{RDS,\mathrm{I}}\sum_{l=1}^{N_\mathrm{I}}\breve{e}_{RDS,l}\cdot\left[H(\breve{a}_l)\cdot\left(\frac{\breve{k}}{2}+\frac{1}{6}\right)+(1-H(\breve{a}_l))\cdot H(\breve{a}_l+1)\cdot\frac{(\breve{a}_l+1)^2\cdot(\breve{a}_l+3\cdot\breve{k})}{6}\right]\tag{B.45}$$

$$\begin{aligned}\breve{\alpha}_{RDS,\mathrm{I},T}^{i=0,j=1} =&\sum_{l=1}^{N_\mathrm{I}}\breve{e}_{RDS,l}\\&\cdot\left[H(\breve{a}_l)\cdot\left(\frac{\breve{b}}{2}+\frac{1}{3}\right)+(1-H(\breve{a}_l))\cdot H(\breve{a}_l+1)\cdot\frac{(\breve{a}_l+1)^2\cdot(\breve{k}-\tilde{k}\cdot\bar{\tilde{k}}_l+\tilde{b}\cdot\bar{\tilde{b}}_l+2\cdot\breve{b}+2)}{6}\right].\end{aligned}\tag{B.46}$$

B.5 Contribution of Subdomain II to Subdomain III

To solve Equation (3.35) via Equation (3.38), $\breve{\alpha}_{\bullet,\mathrm{II}}^{i=0}$ and $\breve{\alpha}_{\bullet,\mathrm{II}}^{i=1}$ must be known:

$$\begin{aligned}\breve{\alpha}_{RCS,\mathrm{II}}^{i\in\mathbb{N}_0} =&2\cdot C_{RCS}\cdot\sum_{\breve{b}'=\breve{b}}^{\breve{k}_c-1}\sum_{l=1}^{N_\mathrm{II}(\breve{b}')}\frac{\hat{w}_l}{(\breve{b}'+1)\cdot(\hat{k}_l-\breve{b}'-2)}\cdot H(\hat{k}_l-2-\breve{b}')\\&\cdot H\left(\hat{k}_l-\breve{k}-1+\breve{b}-\breve{b}'\right)\cdot\frac{\min(\hat{k}_l-1+\breve{b}-\breve{b}',\breve{k}+1)^{i+1}-\breve{k}^{i+1}}{i+1}\end{aligned}\tag{B.47}$$

$$\begin{aligned}\breve{\alpha}_{ECS,\mathrm{II}}^{i\in\mathbb{N}_0} =&C_{ECS}\cdot\Bigg\{\sum_{l=1}^{N_\mathrm{II}(\breve{b})}\left[\hat{w}_l\cdot H(\hat{k}_l-2-\breve{b})\cdot(\hat{k}_l-1)^i\cdot H(\hat{k}_l-1-\breve{k})\cdot H(\breve{k}-\hat{k}_l+2)\right]\\&+\delta_{\breve{b},0}\cdot\delta_{\breve{k},1}\cdot\sum_{\breve{b}'=0}^{\breve{k}_c-1}\sum_{l=1}^{N_\mathrm{II}(\breve{b}')}\hat{w}_l\cdot H(\hat{k}_l-2-\breve{b}')\Bigg\}\end{aligned}\tag{B.48}$$

$$\breve{\alpha}_{RDS,\mathrm{II}}^{i\in\mathbb{N}_0} = 2 \cdot C_{RDS} \cdot \sum_{\breve{b}'=\breve{b}+1}^{\breve{k}_c-1} \sum_{l=1}^{N_{\mathrm{II}}(\breve{b}')} \hat{w}_l \cdot \frac{H(\hat{k}_l - \breve{k} - \breve{b}' + \breve{b})}{\breve{b}' \cdot (\hat{k}_l - 1 - \breve{b}')} \cdot \frac{\min(\hat{k}_l - \breve{b}' + \breve{b}, \breve{k} + 1)^{i+1} - \breve{k}^{i+1}}{i+1}. \tag{B.49}$$

Appendix C

Curriculum Vitae

Christoph Kirse

Adress	Jagdstraße 11, 85356 Freising, Germany
Contact	+49 8161 71 3788 , christoph.kirse@tum.de
Birth date and place	17.07.1987, Düsseldorf

Education

09/2012- /2017	Technical University of Munich, Chair of Process Systems Engineering Graduate work towards degree Dr.-Ing.
04/2011- 08/2012	Technische Universität Darmstadt, Department of Mechanical Engineering Master of Science in Mechanical and Process Engineering
10/2006- 03/2011	Technische Universität Darmstadt, Department of Mechanical Engineering Bachelor of Science in Mechanical and Process Engineering
08/1997- 07/2006	Konrad-Adenauer Gymnasium, Langenfeld, Germany Allgemeine Hochschulreife

International experience

07/2008- 06/2009	Indian Institute of Technology Bombay Department of Mechanical Engineering
08/2003- 07/2004	Hempstead High School, Hempstead, Texas, U.S.A